Thermal Alterations of Sharp Force Trauma in Porcine Bone: A Forensic Investigation

Thesis submitted in accordance with the requirements of Liverpool John Moores University for the degree of Doctor in Philosophy

By

Caighley Logan

August 2025

Contents

List of figures Page

List of tables Page

Declaration

I declare that the content of this thesis entitled 'Thermal Alterations to Sharp Force Trauma on Porcine Bone: A Forensic Investigation' is my own work and was carried out at Liverpool John Moores University.

Caighley Logan MSc, BSc (Hons.)

Liverpool John Moores University

2025

Acknowledgments

I would like to give my biggest thanks to Dr Suzzanne McColl, my sole supervisor, for your guidance and support throughout the entirety of my PhD and helping me bring the idea of my research to fruition.

I would like to thank the members of the forensic science department for all your help. Especially to Megan and Tara, for helping me with every lab-based issue I faced and for putting up with the smell.

Special thanks to Dr O'Hara, for answering my many, many questions over the years, even the ones completely out of your remit.

Finally, to my Mum and Tom for the love and support I have received throughout, for listening to the same problems over and over, and to Izzy, for being there every time I needed you.

Thank you all for believing in me, I simply couldn't have done it without you.

Abstract

In recent years, forensic scientists have faced increasing challenges in the interpretation of skeletal remains, particularly those subjected to both thermal and sharp force trauma. According to the Office for National Statistics (ONS), the year ending June 2024 saw 263 fire-related fatalities and 283 sharp force trauma deaths in England and Wales. These figures highlight the need for a standardised approach to analysing skeletal remains, particularly in detecting and interpreting trauma in thermally altered or burned bone, which is essential for establishing cause of death or reconstructing events in potential homicide cases.

This research explores the interactions between thermal alterations and sharp force trauma on porcine skeletal remains, with the aim of improving forensic interpretation in cases where fire has been used to conceal or remove evidence of violent death. Using a variety of porcine bones, as human alternatives, the study subjected specimens to controlled burning, with the use of a muffle furnace, at temperatures ranging from 300°C to 900°C, in increments of 150°C. Burning conditions for more realistic results included, a recreation of a domestic living room fire scenario in a storage container, initiated by a discarded butane cigarette lighter, and an open flame fire in a garden incinerator fuelled by either wood or charcoal, ignited by butane lighter fluid. To assess thermal and trauma-induced alterations, a multi-analytical approach was carried out, incorporating Agilent Attenuated Total Reflectance Fourier Transform Infrared (ATR-FTIR) and a Malvern Panalytical, Epsilon 1 X-Ray Fluorescence (XRF), Keyence 3D Microscope, and Kubtec X-Ray imaging. The techniques highlighted the identification of chemical composition, structural integrity, and morphological changes in both skeletal bone samples, and those with sharp force trauma injuries.

Results revealed that bones exposed to realistic fire scenarios absorbed combustion byproducts not present in control or furnace-burned samples. Trace amounts of elements such as Neodymium, Bromine, and Cerium, linked to flame retardants, lighter fluid, and flint mechanisms, were detected, indicating the potential identification of a fires source attribution in forensic

investigations. Thermally altered samples also resulted in notable increases in bone porosity, loss of mineral and organic content, and colour alterations, all of which may obscure or distort evidence of trauma. The focus on sharp force trauma found analysis of average cut mark volumes, produced by three knife types; smooth-edged blade, serrated steak knife, and serrated bread knife, demonstrated statistically significant differences in morphology based on both the type of weapon ($p=0.001$) and the type of bone involved ($p=0.003$). Following thermal exposure, 61.7% of cut marks were reduced in size, and some were entirely obscured or converted into complete fractures. This finding highlights the risk of underestimating or misidentifying sharp force trauma in thermally altered remains.

This thesis contributes to the field of forensic science by demonstrating the forensic relevance of combining chemical, structural, and morphological analyses to assess trauma in burned skeletal remains. The findings advance the understanding of how fire modifies traumatic signatures and offer methodological improvements for post-mortem trauma analysis in complex forensic scenarios. These insights hold significant implications for forensic anthropology, taphonomy, and medico-legal investigations involving fire-damaged human remains.

Chapter 1

Introduction

1. Introduction

1.1 Overview

This aim of this thesis is to explore the changes to bone, both microscopically and molecularly, when exposed to various temperatures and open fire. This also includes the injuries that can be sustained from sharp instruments, how said injuries may alter due to various temperatures, and how this can be applied to, and influence the forensic analysis of burned skeletal remains. By investigating both heat-induced alterations and sharp force trauma in a controlled, systematic manner, this research seeks to enhance the accuracy of fire analysis, trauma identification and what may or may not be acts of crime. Ultimately, the findings aim to improve the interpretation of skeletal evidence in forensic investigations, offering valuable insights into both the circumstances surrounding death and the condition of the remains. This overall aim will be broken down into three more specified aims: analysing the effects of high temperatures and fire on bone, the effects of sharp force trauma on bone, and finally, the combination of both sharp force trauma and exposure to high temperatures.

1.2. Skeletal System

The skeletal system is a composition of bones, ligaments, cartilage, muscles, nerves and blood vessels to create the complex bony structures within the human body (Bloise, et al. 2022) The system also possesses key functions such as supporting movement, blood-cell formation and mineral homeostasis, each an important aspect in human stability. However, depending on factors such as age, health, lifestyle, or trauma, damage to the skeletal system can result in a lack of function and therefore reduction in the quality of stability (Bloise, et al. 2022).

A clear understanding of the skeletal system is a critical skill regarding many forensic investigations to be able to identify individuals, determine cause of death, and to understand the events surrounding and leading up to death. Identification of an individual can come from the information obtained from a person's skeleton, i.e., age, ethnicity, lifestyle, illness. For example, structures in the skull alongside dental structures can highlight facial features to estimate an

individual's sex/age. This can be differentiated through characteristics such as males having an overall larger and more robust shaped skull than females, whose skull is often smaller and smoother. As for age, this is often estimated by the fusion cranial sutures, flexible joints between cranial sections. Physical impairments may also produce identifying characteristics that can be linked to medical history, e.g. previous injuries or surgical alterations. Additionally, the skeletal system can also allude to cause of death or treatment of the body post-mortem through signs of trauma or illness and disease.

1.2.1 Types of bones and their functions

The natural structure of bone is known as a heterogenous composite material featuring both organic and inorganic materials, this includes such materials as Collagen (Organic) or Hydroxyapatite (inorganic) (Unal, et al. 2021). The adult skeletal system is comprised of 206 - 213 bones, the variation due to differences in number of vertebrae or sesamoid bone depending on the individual. This is broken down into 126 appendicular bones, 74 axial bones and six auditory bones, however, the structure and composition of each bone further categorises into one of five groups: long, short, flat, irregular, or sesamoid, see figure 1.1 (Clarke, 2008).

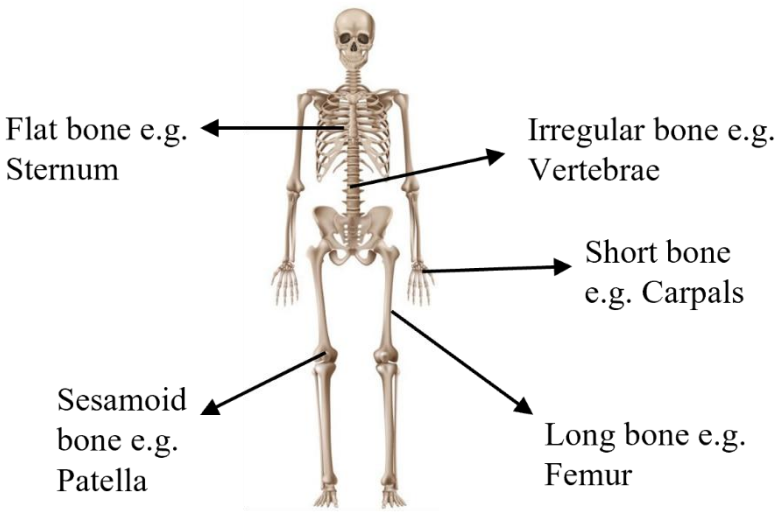

Figure 1: Examples of each type of bone and where it can be found in the skeleton. Copyright free image with labels by author.

Long bones

The long bones of the skeleton are found in the extremities of the body such as the thigh, lower leg, arm, and forearm, and are composed of the rounded epiphysis at the end of the bone above the growth plates, a metaphysis below the growth plates and finally the diaphysis, a hollow shaft in the midst of the bones structure. Both the metaphysis and epiphysis are composed of trabecular/cancellous bone, a porous material composed of both hard and soft tissue (Oftadeh, et al. 2015), with a meshwork-like structure, whereas the diaphysis is composed of a much denser cortical bone, a concentric arrangement of cylindrical structures (Collins, et al. 2019), providing strength and structure (Clarke, 2008).

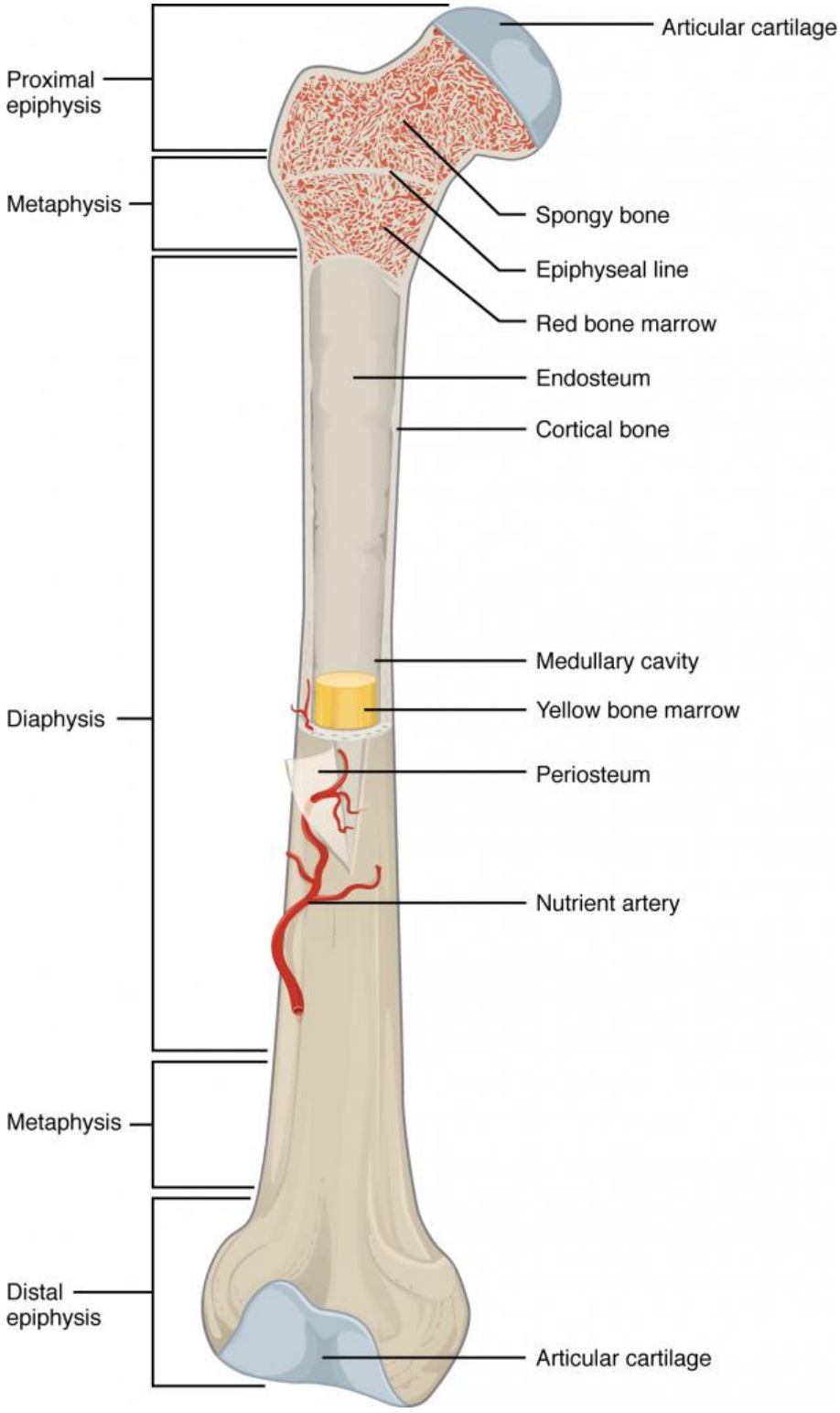

Figure 2: Anatomy of the long bone showing both trabecular and cortical bone types. Trabecular, a porous material in a mesh-like structure, and cortical bone, a concentric arrangement creating a dense structure (Betts, et al. 2022).

Short Bones

Primarily found in the wrist and ankle, the short bones of the skeletal system are composed of a thin layer of cortical bone covering a vast structure of cancellous bone and bone marrow (Grujicic, 2023). Due to their small size, the short bones lack a diaphysis section, and are essentially entirely an epiphysis structure (Brouhard, 2023).

Flat bones

Primarily situated in the skull, mandible, sternum, and ribs (Clarke, 2008). Flat bones are structured with a layer of periosteum, the outer surface of the bone that includes blood vessels and nerves. This is coupled with layers of cortical bone below the periosteum and cancellous bone as the innermost layer (Morrison, 2018). Unlike other types of bone, the flat bones are the sole type to also include 'sutures. Sutures are a fibrous joint, tightly connected by fibrous tissue and occur primarily in the cranium flat bones. However, fusing does not take place until around the age of 20 as the body and brain continues to develop (Morrison, 2018).

Sesamoid Bones

Sesamoid bones are often split into two categories, types A and B, depending on their positioning and attachment. Type A sesamoid bones are often found near a joint and are connected to the joint capsule, for example, the patella. Type B sesamoid includes those that are positioned over a bony surface and are separated by an underlying fluid filled sac known as a bursa, more specifically the peroneus fibularis in the lateral compartment of the leg (Yeung, et al. 2023).

Another notable type of sesamoid bone includes the fibrocartilaginous sesamoid that allows the maintenance of tendon structure and flexibility via cartilage tissue (Yeung, et al. 2023).

Irregular bones

Bones that do not fit the aforementioned categories are often referred to as 'irregular bone'. This type of bone includes those of more complex shapes such as the vertebrae within the spinal cord or facial bones containing sinuses (Clarke, 2008). The irregular bones are structured more primarily

by cancellous bone tissue with a much thinner layer of cortical bone, when compared to the long or short bones (NIH, 2018).

1.2.2 Structure of bones

Bone Tissue

Bone tissue is a viscous, mineralised connective tissue that is vital for various function within the body. This can adapt and modify itself to aid biological processes such as remodelling, and is categorically separated into three groups: Cortical, Cancellous and Subchondral (Angin, et al. 2020)

Cortical

Cortical tissue, also known as compact, is a dense structure that is found on the external surfaces of bone and contributes to the walls along the diaphysis of long bones (Christensen, et al. 2014). This bone tissue surrounds the marrow space and is composed of osteons known as 'Haversian systems', a cylindrical shape that forms a network of branches throughout the structure of the cortical bone (Clarke, 2008). The cortical bone tissue also contains two subcategories: outer periosteal and inner endosteal surfaces. The outer surface is vital for fractional repair and growth, whereas the inner surface provides remodelling aid throughout aging (Clarke, 2008).

Cancellous

Cancellous, trabecular, or spongey bone is less dense than cortical bone and is a honey-comb structured tissue that is primarily found in the epiphysis (NIH, 2023). This type of bone is categorised by the trabeculae plates and much more porous structures than compared to cortical bone.

Membranes

Within the body, a membrane is a thin and flexible layer of tissue that is used to either separate or connect various parts of an organism.

Endosteum

The endosteum is a membrane lining surrounding the bone marrow. The membrane also lines the Haversian canal and other internal cavities within the bone and is comprised of a layer of flattened osteoprogenitor cells and type-III collagen fibres (see Table 1) (Nahian & Chauhan, 2023). Commonly, there are three types of endostea, Cortical, Osteon and Trabecular: Cortical endosteum lines the bone marrow cavity, osteon is primarily found lining osteons that contain blood vessels and nerves whilst finally, the trabecular endosteum lines near the developing part of the bone, the trabecular (Nahian & Chauhan, 2023). The primary function of the endosteum is to provide calcium related homeostasis through transmission of calcium between the bone matrix and blood (Nahian & Chauhan, 2023).

Periosteum

Within the bone, the periosteum is a thin layer of osteogenic and fibroblastic cells located along the periosteal cortex of cortical bone (Lopliez & Markel, 2012). This structure is composed of two layers, the outer firm, and the fibrous layer. The outer firm is composed of collagen fibres that contain arteries, veins, sensory nerves and lymphatic vessels. The inner fibrous layer contains cells such as osteoblasts (Fritz, et al. 2008).

Cartilage

Cartilage is a non-vascular tissue with a primary function of supporting connective tissues throughout the body. It is a flexible tissue that differs from bone and is often split into three categories: Hyaline, Fibrous and Elastic.

Hyaline

Hyaline cartilage is often found in the joints of the body and consists of a collagen matrix that is primarily comprised of glycoproteins, providing a large volume of water within its structure. This characteristic provides the cartilage with a more resilient response to high pressures than other

types of cartilage through a slow diffusion of pressure, i.e., often found in the nose, ribs, joints, vertebrae, and larynx (Eriksson, et al. 2023).

Fibrous

Also known as Fibrocartilage, fibrous cartilage is a dynamic tissue that is primarily found in regions of high pressure and compressive forces (McGonagle & Benjamin, 2015). Composed of Type I collage fibres in large fibre bundles, fibrous cartilage provides support and protection to the intervertebral discs, and intra-articular cartilages of the knee, wrist and mandibular joints (Maynard & Downes, 2019).

Elastic

The most flexible type of cartilage, composed of a dense structure of elastin fibres made of proteoglycans, elastic cartilage provides support to non-load bearing body parts such as ears, nose, and epiglottis (Watkins, et al. 2009). This cartilage can return to its original shape if affected by a strong force of high pressure (Cleveland, 2022).

On a more molecular level, the structure of bones also contains a series of cells that form connective tissue. This is composed of: osteoblasts and osteocytes, osteoclasts, and osteoid cells.

1.2.3 Connective Tissue

Osteoblasts & Osteocytes

The two primary cells within a bone structure that are required are Osteoblasts and Osteocytes. The osteoblasts are mononucleate cubic, round, or flat cells that can synthesise and secrete bone matrix to aid in bone formation. This is achieved through the mineralisation of bone thus regulating the calcium and phosphate ions during structural development (Bassi, et al. 2011). In comparison, osteocytes are flat, almond shaped cells, with a primary function of regulating minerals within the bone structure. Osteocytes are derived from osteoblasts through a series of stages including osteoid-osteocyte, preosteocyte, young osteocyte and mature osteocyte (Franz-Odendaal, et al. 2005).

The process of osteoblast differentiation, figure 3, involves the transformation of a Mesenchymal stem cell to an osteoblast through the activation of master osteogenic transcriptional factors, this stimulates a common osteo-chondroprogenitor cell to become bound therefore becoming a preosteoblast (Ponzetti & Rucci, 2021). Once formed, the osteoblast expresses early osteogenic genes i.e., alkaline phosphatase (ALP) or a branch of collagen (COL1A1) coupled with various markers such as bone sialoprotein (BSP II) to eventually experience one of three pathways: becoming a bone lining cell, apoptosis, or becoming an osteocyte (Ponzetti & Rucci, 2021).

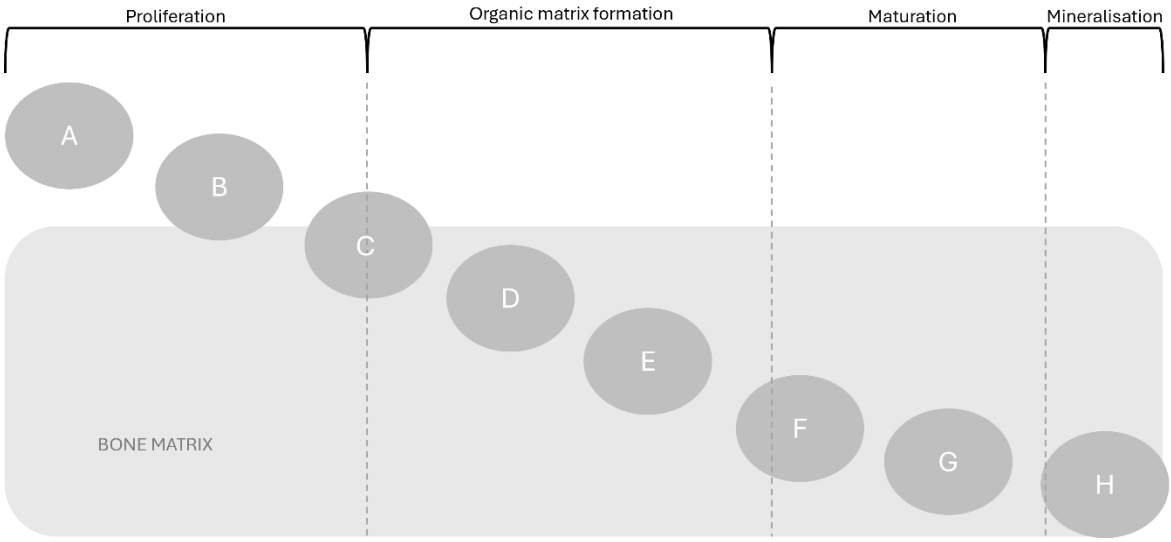

Figure 3: The process of Osteogenesis from preosteoblast to a mature osteocyte. A - a preosteoblast, B - preosteoblastic osteoblast, C - fully formed osteoblast, D - an osteoblastic osteocyte, E - osteoid-osteocyte, F - preosteocyte, G - young osteocyte and finally H – a mature osteocyte (diagram by author) (Franz-Odendaal, et al. 2005)

Osteoclasts

Osteoclasts are multinucleated cells, containing between 2 – 12 nuclei per cell, with the primary function of absorption to repair damaged bone, and is the only cell with the ability to degrade bone also (Parvizi, 2010, Ross, 2011). The function of an osteoclast, figure 4, promotes the remodelling

of the extracellular matrix through the formation of a plasma membrane with the adjacent bone, attaching to the bone with podosomes containing αvβ3 integrin, an integrin with the primary purpose of osteoclast-mediated bone resorption, and other functions of angiogenesis, pathological neovascularisation, and tumour metastasis (Liu, et al. 2008). This dissolves the matrix through enzymatic secretions and enhances the solubility of the minerals ossified tissues (Parvizi, 2010).

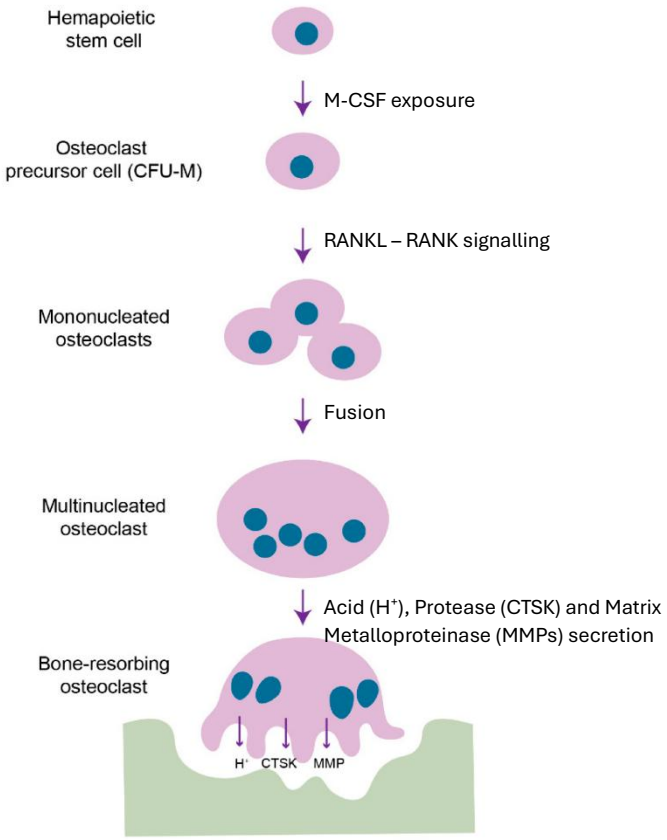

Figure 4: Process of an osteoclast transformation from hematopoietic cell through mononucleated to a multinucleated cell with bone reabsorbing qualities (Some labelling by author) (Kim, et al 2020).

Osteoid

Within the bone, the osteoid is a predominantly active cell, composed of 90% collagen type 1 (Wexler, et al. 2014). Osteoids are produced by the osteoblasts and are eventually transformed into calcified bone through osteogenesis (Bonewald, 2013). The structure of an osteoid contains

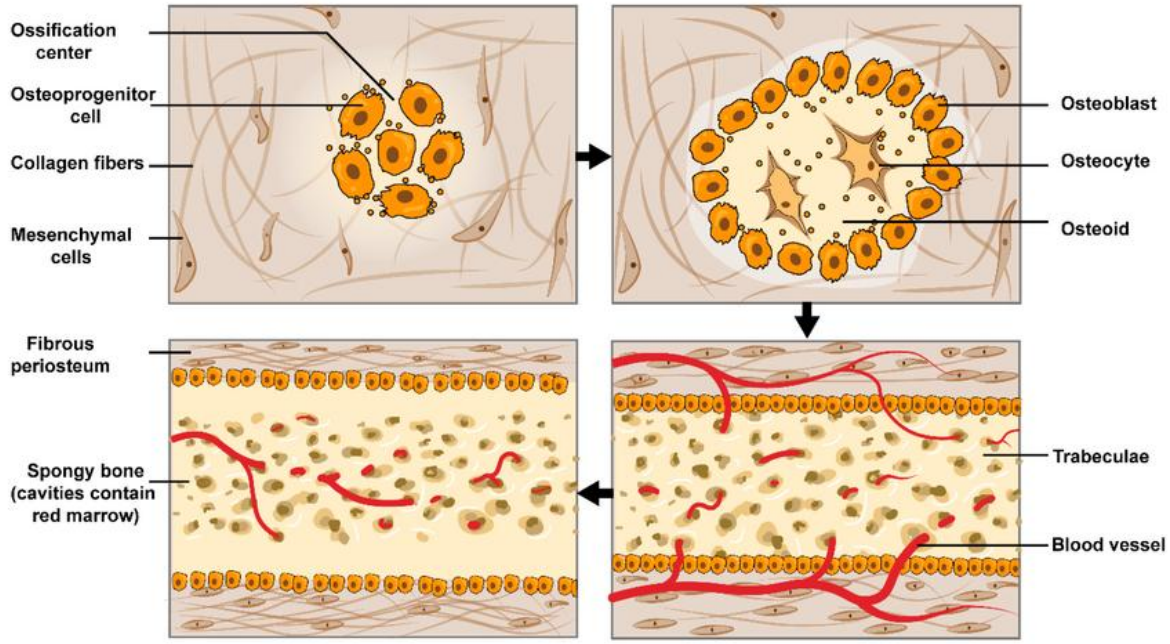

both 'woven' and lamellar bone, with collagen fibrils being positioned randomly in the woven bone thus illustrating the term 'woven' in the area due to their felt-like texture, conversely, a more structured orientation of collagen fibrils is in the lamellar bone providing a more dense and reliable structure. The types can transform from one to the other, i.e., a broken bone may initially repair itself using woven bone prior to the transformation into lamellar bone for its definitive form (Shenoy, et al. 2017).

Figure 5: Molecular anatomy of a bone showing an example of each connective tissue cell: Osteoblast, Osteocyte, Osteoclast and Osteoid (Lin, et al. 2023)

1.2.4 Organic and Inorganic Materials

Organic Materials

Organic materials in bone include fundamental materials such as marrow, collagen, proteoglycans, and glycoproteins. What is known as the organic-inorganic phase ratio of bone can provide vital information of the bone's material quality (Luo & Amromanoh, 2021). The understanding of the organic-inorganic phase ratio has been deemed a fundamental aspect of determining bone quality, as seen in figure 6.

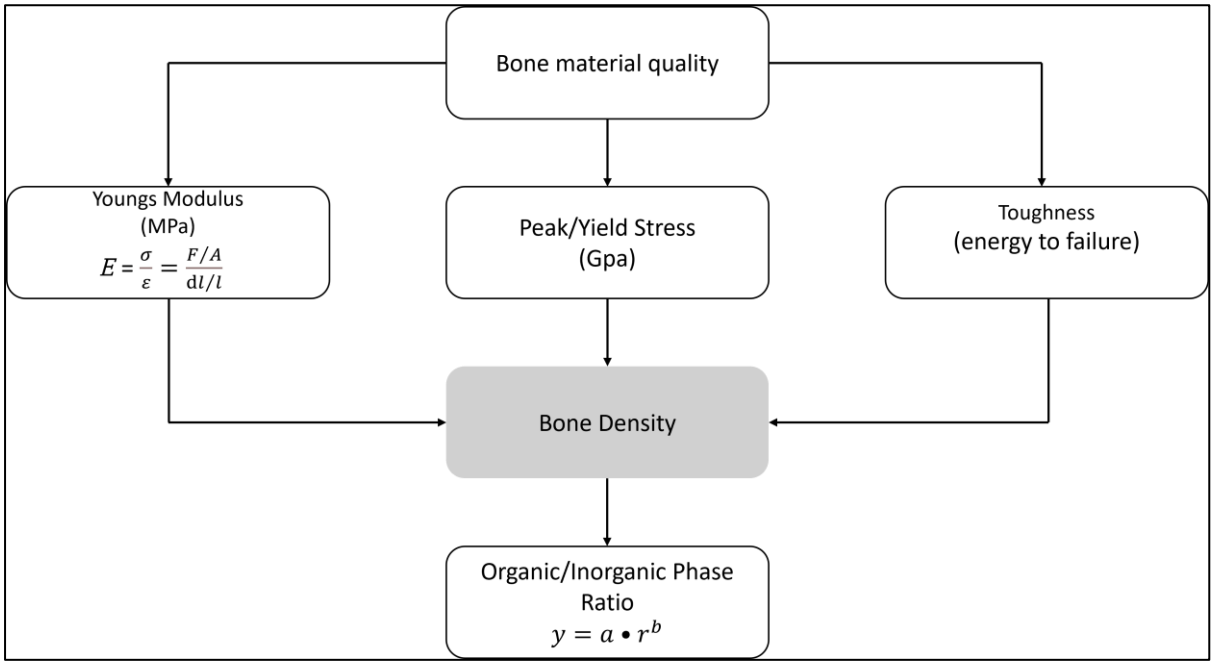

Figure 6: Organic/Inorganic phase ratio (Luo & Amromanoh, 2021).

Youngs modulus refers to the ratio of tensile stress vs tensile strain and is often depicted in the form of an equation, in which, E represents young's modulus, σ refers to tensile stress, ε depicts tensile strain. This is further equated with F/A representing the force applied per unit and finally dl/l referring to the extension per unit length (UoB, 2023):

$$E = \frac{\sigma}{\varepsilon} = \frac{F/A}{\mathrm{d}l/l}$$

Bone Marrow

There are two types of bone marrow: red and yellow. Red bone marrow is often found inside flat bones and the epiphysis of long bones and consists of hematopoietic cells, with a primary function of producing blood cells (Thomas, et al., 2013). Alternatively, yellow bone marrow is commonly found in the diaphysis of long bones and is composed of mainly adipocytes. As an individual ages, the fat within bone marrow increases due to maturation, transforming the completely red bone marrow at birth to an estimated 50% red and yellow by adulthood (Thomas, et al., 2013).

Collagen

Within the bone there are four primary types of collagens (I - V), each type contributes to the extracellular matrix necessary for a bones mechanical support and 'scaffolding' (Lin, et al. 2020).

Type I collagen is the most abundant within the bone, measuring up to 90% of the organic mass and is the primary collagen in skin, ligaments, corneas, and other interstitial connective tissues (Mark, 2006). Type I is composed of 2x Pro-alpha1 (Proa1) chains containing 1464 amino acid residues and Pro-alpha2 (Proa2) subunits containing 1366 amino acid residues (Mark, 2006) in the formation of a triple helical structure including G-X-Y, G referring to glycine and X/Y referring to varying amino acids (Naomi, et al. 2021). Other types of collagen can be seen in table 1.

Table 1: Collagen types and their functions (Fan, et al 2021, Lin, et al. 2020, Garnero, 2015, Mark, 2006)

Collagen Type	Function
II (<5%)	Maintains joint flexibility and resistance to stress and fractures due to its primary location in cartilages (Fan, et al. 2021).
III (<5%)	Often in low levels within bone and cooperate to module type I collagen fibril diameter and fibrillogenesis (Lin, et al. 2020, Garnero, 2015). *Type V also assembles with Type I to form heterofibrils (Mark, 2006).*
V (5%)	

Proteoglycans

Often coupled with glycoproteins, proteoglycans are one of the most abundant proteins within bone. This type of protein is an attachment of a long-chained polysaccharide to core protein molecules such as Keratosulfate ($C_{28}H_{48}N_2O_{32}S_4$) (Zhu, 2002). Proteoglycans can be split into four groups: Intracellular, extracellular, cell surface and pericellular.

Table 2 Various types of proteoglycans, and their functions (Iozzo & Schaefer, 2015)

Type	Proteoglycan	Functions
Intracellular	Serglycin	Retention of effector or inflammatory molecules in various cells including Endothelial cells, for example (De Armas & Podack, 2010).
Extracellular	Hyaluronans	Regulate normal structural and integrity during development. This includes tissue responses to injuries, repairs and regeneration (Garantzotis, 2020)
	Aggrecan	A major proteoglycan in articular cartilage that provides a hydrated gel structure and produces the cartilage with load-bearing qualities (Kiani, et al. 2002).
	Versican	The primary function is forming blood cells (angiogenesis), healing wounds, promoting inflammation and preventing growth of cancerous tumours (Wight, 2002, Wu, et al. 2005)
	Neurocan & Brevican	Neurocan – A chondroitin sulphate proteoglycan that is the dominant inhibitor molecule for axon regeneration in injured nerves (Su, et al. 2017).

		Brevican – A major component of the extracellular matrix of perineuronal nets and suggests a role within the synaptic transmission (Blosa, et al. 2015).
Pericellular	Perlecan	A basement membrane specific heparan sulphate proteoglycan that is vital for regulating diverse cellular processes such as: • Bone formation • Inflammation • Cardiac development • Angiogenesis (Gubbiotti, et al. 2016)
	Agrin	Critical for the formation and regulation of intraneuronal synapses, particularly excitatory synapses in the brain (Daniels, 2013).
	Collagens XVIII & XV	XVIII – essentially an anti-angiogenesis proteoglycan with various functions, such as: • Regulating cell survival • Aiding inflammation (Heljasvaara, et al. 2017) XV – Regulates the growth of axons and contributes towards angiogenesis (Bretaud, et al. 2020)
Cell Surface	Syndecan	Coreceptors with adhesion receptors and also work to perfect signal transfers across extracellular cell surfaces to the cytoskeleton. Initiate signal transfers across multiple intracellular cascades (Hilenski & Griendling, 2013)

CSPG4/NG2	Vital for proliferation of cells, migration, and metastasis. Also important for pericyte centralisation to the endothelial layer whilst promoting interactions with endothelial cells (Schiffer, et al. 2018)
Betaglycan	A transmembrane proteoglycan that is primarily a coreceptor with TGF-β (transforming growth factor B) and one of the predominant proteoglycans for growth factor signalling (Sherbet, 2011)
Phosphacan (RPTPbeta)	Plays a role in the regulation of axon growth, cell migration, and myelination (Faissner, et al. 2013).
Glypican	Bound to the outer surface of the plasma membrane by a glycosylphosphatidylinositol anchor (Filmus, et al. 2008) Glypican is a heparan sulphate proteoglycan that is important for regulating morphogen gradient formation and all growth through the control of Wnt$^{6-8}$ pathway (Li, et al. 2020).

Glycoproteins

Similar to proteoglycans, glycoproteins are one of the most abundant noncollagenous proteins within the bone (Zhu, 2008). Glycoproteins are often split into three types: N-linked, O-linked and nonenzymatic glycosylated glycoproteins (Blanco & Blanco, 2022). Each type of glycoprotein interacts with one another to begin and complete the process of glycosylation, the process in which enzymatic modifications of an organic molecule and protein function, such as interactions with other proteins, occur due to the addition of a glucose molecule (Kattla, et al. 2011, Welsh, et al. 2016). N-linked glycoproteins, also known as amide groups, are protein modifiers and are vital for biological processes such as cell growth, differentiation, programming of cell deaths and cell to cell recognition (Tian & Zhang, 2013). N-linked glycoproteins are often used to identify disease

associated changes within glycoprotein structure and function (Tian & Zhang, 2013). O-linked glycoproteins, hydroxyl groups, are large proteins that represents around 50-80% of the overall mass within glycosylation (Merck, 2023). This type of glycoprotein includes structures such as immunoglobulins or caseins (Gonzalez-Morelo, 2020).

Inorganic materials

As previously mentioned, bone is a complex structure containing bone organic and inorganic materials. Of the inorganic materials the primary structure is Crystalline Hydroxyapatite (Feng, 2009). Other notable inorganic materials include varying levels of magnesium and potassium.

Crystalline hydroxyapatite

Crystalline hydroxyapatite [$Ca_{10}(PO_4)_6(OH)_2$] is an inorganic material within bone that is composed of small plate-like hydroxyapatite crystals (Feng, 2009). It is the crystalline form of calcium phosphate through the binding of calcium chloride ($CaCl_2$) and sodium phosphate (Na_3PO_4) (Palmer & Bonner (2011). The structure of hydroxyapatite in figure 7 involves positively charged calcium ions that are repelled by negatively charged hydroxyl groups and phosphates.

Primarily the function of Hydroxyapatite is to promote healthy and effective bone regeneration. As it is naturally occurring in the bone, the ions involved can be combined to form various structures (Jeong, et al. 2019).

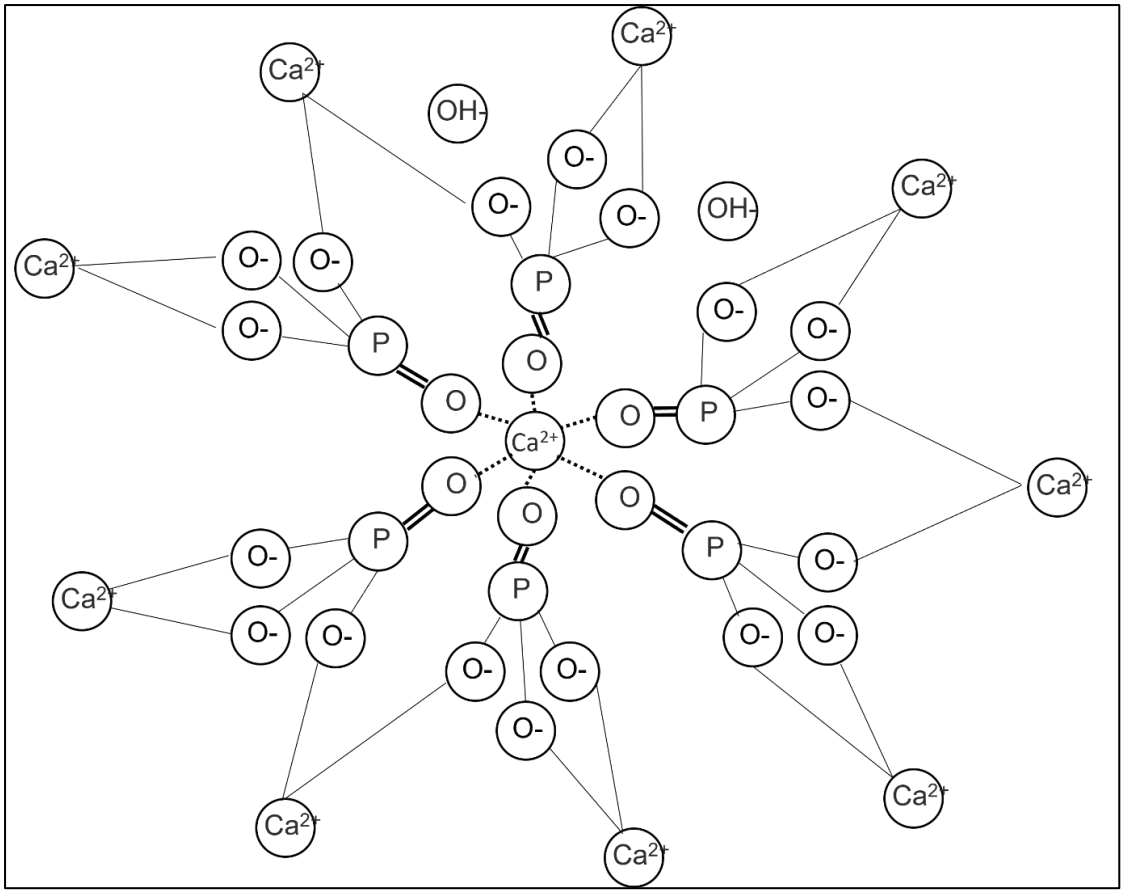

Figure 7: The chemical structure of Hydroxyapatite Crystalline structure (diagram by author) (Panda, et al. 2021).

1.3 Trauma Analysis on bone

Skeletal trauma often occurs as a result of high pressure or impact being applied to an individual, resulting in an alteration to the physical properties inside and outside of the bone.

Skeletal trauma is characterised via many factors, such as, the timing of the injury in relation to the time of death, also the application in which the trauma was applied, i.e., blunt force or sharp force trauma (Christensen, et al. 2014). The timing of the trauma can be split into categories such as, antemortem, perimortem and post-mortem, referring to either before, at the time of or after death (Christensen, et al. 2014).

As for the types of application in which trauma can be applied, this includes Blunt force trauma, sharp force trauma, thermal trauma, firearm trauma, and explosion trauma.

1.3.1 Blunt force

Blunt force injuries occur due to an exposure to a high impact with a blunt object, such as assault, vehicle collisions or a fall from a great height. This type of trauma results in various injuries depending on the specifications of the injury i.e., injuries may result in contusions, abrasions, lacerations, or fractures (Simon, et al. 2023).

Contusion

More commonly known as a 'bone bruise' a skeletal contusion is a commonly occurring injury, particularly for those in highly active careers, such as athletes. Due to the form of impact required to result in a contusion, this injury primarily occurs on joints such as shoulder, Ilium, and knee. The bruise appears due to the high impact causing a rupture in the surrounding capillaries underneath the skins surface (Simon, et al. 2014).

Abrasion

An abrasion to the skeletal system occurs due to the dragging or scraping of a body over an extended period, most abrasions are superficial, only affecting the soft tissue of the body (Tumram, 2020). An abrasion can be used within forensic investigations to identify a potential weapon or mechanism that may have led to the injury, i.e., distinct patterns can be left behind on the body providing visual aids towards finding a potential murder weapon, e.g., a zig-zag pattern of a shoelace or teeth-style pattern of a zip (Simon, et al. 2023).

Laceration

Primarily, a laceration is an injury resulting in a split/cut in the skin or soft tissue, and most commonly occur where bone is more prominent (Byard, 2016). This type of injury is more discernible to that of a sharp force wound, such as a stab wound or cut, due to the lack of serrated edges within the wound, known as 'incisions' (Byard, 2016). More specifically for the skeletal system, a laceration may also be referred to as a splinter or crack depending on the severity of the injury.

Fractures

Blunt force injuries of a significant impact often result in fractures, this is a complete separation of bone, with a broken structure, sometimes coupled with splintering pieces of bone becoming separated. A fractured bone can be split into subcategories depending on the characteristics of the break and the severity of the impact. This includes either complete or incomplete fracture, depending on whether or not the bone is broken entirely or severely cracked. Each subcategory also contains various labels depending on the formation of the break or crack in the bone. See table 3.

Table 3 Types of fractures and descriptions (Muller, et al. 2012).

Complete Fractures	
Oblique Displaced / Compound	Displaced – Broken at an angle with minor displacement. Compound – Broken at an angle with complete separation.
Transverse Open	A horizontal break in the bone, perpendicular to the shape of the bone.
Segmental	A break in two or more places leaving segments of the bone completely separated.
Spiral Open	A break in the bone in a twisted formation, essentially wrapping around the bone causing a separation.
Impacted	A broken bone in three or more places with small pieces of bone separated from the rest.
Incomplete Fractures	
Oblique Nondisplaced	A crack occurs through the entire width of the bone at an angle.
Transverse Nondisplaced/ Displaced (closed)	Nondisplaced – A horizontal crack across the width of the bone. Displaced (closed) – A horizontal crack/minor break without separation of the segments.

Longitudinal fractures	A vertical break that occurs along the length of the bone.
Greenstick	A break along the side of a bone that does not separate, caused by bending or overstretching.

Mortality rates

In forensic trauma analysis, the understanding of statistics is an essential tool for identifying patterns or determining the frequency of the types of trauma/cause of death depending on various factors i.e., location, age range, sex or date. The Office for National Statistics collects a range of economic and social statistics such as population and demographic statistics, government output activities and also statistics on life events i.e., birth rates, marriages and death rates.

Over the past 11 years (2013 – 2023), there has been a significant increase in blunt force trauma mortality rates. As mentioned, blunt force trauma is the result of coming into contact with a blunt object at a high impact and is the leading cause of death by external factors in England and Wales. Between 2013 and 2023, blunt force trauma accounted for over two million deaths. The predominant causes were falls or accidental falls (33%), intentional self-harm by hanging (14%), and transport-related incidents (7%) (ONS). This increase may be due to an increase in the population overall with the elderly more at risk of falling unexpectedly, this may also be due to an increase in various diseases and illnesses that can affect motor skills and general wellbeing resulting in a lack of balance.

The secondary cause of blunt force death, self-harm by hanging, may also be affected by the growth in population. As stated by ONS and The Samaritans, the predominant reason for suicide in the UK is due to mental health issues and social inequality, (Samaritans, 2019). Similarly, the growth of the population may also have an effect on the number of transport accident deaths, as the population growths as will the number of vehicles in use, therefore increasing the chances of a transport vehicle accident, as stated by ONS.

1.3.2 Sharp force

Sharp force, although often received in similar scenarios to or coupled with blunt force trauma, is categorised separately due to the mechanisms of causation resulting in different wounds (Eze and Ojifinni, 2022). Sharp force trauma is often caused by objects or weapons with sharp edges that can result in cutting or other forms of incision. This includes incised wounds, often obtained from objects with sharp edges such as knives or razors and is a long laceration in which the skin is cut with a potential result of fatal bleeding, and stab injuries, a deep penetrating injury that results in the laceration of the epidermis and dermis including damage to the bone (Eze and Ojifinni, 2022). Each of the injuries can influence the skeletal system, as stab or incision wounds may lacerate through the layers of skin and result in cut marks or potential stab wound into the bone. The analysis of cut marks on bones from sharp force trauma has been widely researched within forensics and has found the characteristics of the cut marks can help determine the instrument used (Love, 2019).

Incised wounds

Incisions are injuries resulting from weapons with sharp edges, i.e., knives, blades, broken glass etc. Incisions are primarily surgical injuries, and are often characterised by length and depth, with visual markers such as the edges of the injury providing information to identify the weapon used. An incision injury is often longer than is it deep, due to the cutting motion that is applied to create the injury. Specifications such as length and depth can also contribute to the identification of whether the injury was accidental, nonaccidental or self-inflicted, this can also be dependent on the angle, and hesitancy markers (pauses in the cutting motion) (Eze & Ojifinni, 2022). Specifically for the skeletal system, this type of injury often leaves miniscule marks, if any, on bone. Primarily, small knicks may be found on the bone where the weapon may have perforated each layer of soft tissue and marked the bone.

Stab wounds

A stab wound, produced by items such as serrated or non-serrated knives, or blades, leaves significant changes to the soft tissue in the form of deep incisions, punctures, or clefts, with cut

marks being produced on to the underlying bone (Christensen, et al. 2014). Stab wounds are predominantly found in the abdomen or chest, with some also often located in the head or extremities. cut marks left behind are able to provide details towards what type of weapon may have been used, for example, a serrated edge knife will leave a lagged edge cut mark on the bone whereas a non-serrated knife or sharp blade will leave a smooth cut along the bone.

Chop wound

The appearance of a chop wound, usually the head or neck, can be distinguished from a stab wound due to the high energy force required to create the injury. For the soft tissue, cuts and lacerations are created due to the force of the impact coupled with a weapon with at least one sharpened edge, such as an axe, cleaver, or machete, however, due to the force, this is also accompanied by the appearance of bruising and other abrasions (See 1.4.1.1 for abrasions). The edges of the laceration also differ to a stab wound due to the movement of the weapon, creating a shorten and much deeper laceration with less clean wounds and more chance of a fracture to the underlying bone (Gitto & Arunkumar, 2022). Depending on the instrument used, the underlying bone will result in various types of fractures due to the effectively blunt force from the impact through the layers of soft tissue (See 1.4.1.4 for fractures).

Atypical wounds

Atypical wounds are those that are produced by sharp or pointed items that do not fit the criteria of other categories. Items such as screwdrivers, ice picks or forks, each produce sharp force traumas to soft tissue and potentially through to bone, but however due to their structure, also produce abnormally shaped wounds i.e., a fork will produce three to four circular lacerations in the skin/soft tissue but may also be applied with enough force to penetrate through to the bone leaving similarly shaped marks on the bones surface. This also applies to that of an ice pick or screwdriver, as the amount of force applied can create an injury to the bone in a similar shape to that of the weapon used (Gitto & Arunkumar, 2022).

Mortality rates

In the year ending 2023, around 283 deaths were categorised as a result of sharp force trauma. This includes causes of death as 'intentional self-harm with a sharp object', equating to 44% of all sharp force trauma deaths. A quarter of deaths are the results of assault with a sharp object; this is in conjunction with an overall increase in the amounts knife crime in England and Wales. Between the years 2013 – 2023, there has been a significant increase in the number of crimes involving sharp objects, an overall increase of 66%, with a notable peak in 2020 resulting in over 54,000 sharp force crimes (ONS, 2023). The primary location of sharp object crimes has been found to be London, with around 27% of crimes taking place, this may be due to the high population density in the area.

1.3.3 Thermal Trauma

Thermal trauma to the skeletal system is a result of exposure to high temperatures or fires. This type of trauma can be detrimental to the soft tissue, with some cases resulting in complete loss of soft tissue and organic components. As for the skeletal system, thermal trauma can change the contents of a bones composition such as the mineral levels (See 1.6 for changes to bone due to thermal damage) (see table 4 for thermal changes and descriptions).

Fire

Fires of ranging temperatures and ignition source can cause a myriad of damage to bones. This includes but is not limited to colour change, weight change, density etc (See table 4 for descriptions and 1.6 for further details).

Table 4 Thermal changes to bone with descriptions (Shehata & Krap, 2024).

Changes	D**escription**
Colour change	Ranging from charred black to calcified white depending on the temperature of the fire.
Weight	A significant loss of weight can be determined depending on the type of bone, temperature of fire and length of time the bone burned.

Density	A loss of density occurs due to the reduction of organic materials within the bone, therefore reducing the organic structure of the bone leaving the remainder weak and brittle.
Porosity	An increase in porosity is often observed due to a complete removal of minerals in the bone from the intense heats and high temperatures.
Crystallinity	An observation has found the higher the temperature the larger the crystallinity structures.

Chemical

Chemical burns, from direct contact with hazardous chemicals, primarily affect the outer layers and soft tissues. The type of burn received can be categorised into degrees of severity (Robinson, 2022):

- First-degree burns: A superficial burn that affects the outer layer of the epidermis with little to no permanent damage.
- Second-degree burns: Perforation to the secondary layers of the dermis, resulting in blisters/swelling and the potential for permanent damage in the form of scars.
- Third-degree burns: penetrates the dermis completely and begins to damage underlying soft tissue, this is coupled with permanent nerve damage.
- Fourth-degree burns: A complete penetration of all soft tissue through to the bone, permanent nerve damage, and surface layer damage to the periosteum.

Electrical contact

Electrical injuries can be obtained from a range of voltages, from small shock to fatal electrocutions. Shocks with a strong enough voltage are able to cause muscle spasms that can become out of control with a force strong enough it can result in a broken/fractured bone or dislocated joint (See 1.4.3.1 for fractures) (HSE, 2023).

Mortality rates

In the 10-year gap between 2013 and 2023, there has been a steady decline in the number of deaths due to thermal trauma, however the number are still exceeding 250 per year. Thermal related deaths include exposure to intense heats, flames, smoke and electrical currents. The primary cause of thermal deaths is exposure to smoke, fire and flames, essentially residential/dwelling fires. Initially, thermal related fatalities followed a higher trend in numbers, however, there has been a steady decrease since the year ending 2017. This decrease may be due to the Grenfell Tower fire in London, in which 70 fire-related fatalities were recorded with a further 70 injured. This disaster sparked a focus on the safety and compliance of residential/commercial buildings in regard to fire safety, e.g. The Building Safety Act received royal assent and implements a new regulation guideline for construction (Gerrard, 2022).

1.3.4 Firearm

Firearm trauma categorises injuries sustained from weapons that require a powdered charge to produce a projectile impact, i.e., handguns, rifles, or shotguns (Fowler, et al. 2015). The devices are categorised via the type of firearm, being labelled as either a rifled firearm or smooth-bore firearm (shotguns), however, a recent third category including those of country-made firearms has been accepted due to the increased use in under-developed countries and abnormal projectile impact produced (Shrestha, et al. 2023).

Gunshot wounds

The resulting injury to a ballistic wound can depend on multiple factors, such as, the firearm used, the distance/angle of the firearm, and mass/velocity of the bullet.

Generally, the injuries sustained from a firearm are classified as either penetrating, the bullet enters the body, perforating, the bullet enters and exist the body, re-entry, the bullet enters, exits, and re-enters the body, i.e., through the lower arm and into the torso or grazing, the bullet grazes the skin and does not enter the body (Gitto & Stoppacher, 2021). Further identification of a firearm wound is dependent on the specifications of a gunshot used, see table 5 for various firearms and their injury characteristics (Gitto & Stoppacher, 2021).

Table 5: Identifying characteristics of various firearm injuries (Gitto & Stoppacher, 2021).

Type of firearm	Identifying characteristics
Handgun	• Distance of the handgun can be determined through the presence of secondary effects on the skin, such as, soot deposition, seared skin, stippling (gunpowder tattooing). • A circular/oval entrance wound indicates a close range shot with potential angle, whereas an atypical wound suggests loss of balance during fire. • Wounds create two cavities: permanent and temporary. o Permanent – primary wound caused by the bullet passing through, resulting in tissue damage. o Temporary – stretching of the permanent cavity with progressive pulsations that eventually collapses. • Exit wounds – Perforated skin, no soot deposit, no stippling, similar shape to a stab wound.
Shotgun	• Entrance wounds: the further the distance, the smaller a central defect becomes and instead is replaced by several pellet holes with reduced penetrability. • Some soft tissue damage. • Little to no bone damage, depending on the distance.
Rifle	• High velocity projectile. • Mass tissue destruction. • Fracturing/complete segmentation of underlying bone. • Certain ammunition releases lead fragments, furthering destruction to the soft tissue and bone.

The result of firearm trauma to the skeletal system can result in various types of breaks and fractures, this includes diaphyseal fractures, metaphyseal and epiphyseal fractures, and indirect fractures (See 1.4.1.4 for fractures) (Veenstra, et al. 2022).

Mortality rates

Over the ten-year period 2013 – 2023, there has been a steady decrease on the number of firearm related fatalities in England and Wales. The prime cause of death related to firearm fatalities is that of intended self-harm with a firearm or by firearm discharge, 47% of firearm deaths, more specifically are that of self-harm with an unspecified firearm, this can include modified weapons such as 'sawn-off rifles' and similar. Over the same period, there has been a steady pattern in the levels of crimes involving firearms, taking into account those resulting in no injuries to those with fatalities. Similar to that of sharp force crimes, there predominant location in which the crimes take place is London, with 20% of all firearm crimes taking place (ONS).

1.3.5 Explosions

Primary injuries

Primary injuries sustained from an explosion are mainly caused by the blast passing through a body. Injuries such as this are often specific to 'high order' explosions, those that contain materials to produce a supersonic pressure wave better known as blast wave or shock wave (Jorolemon, et al. 2022). The injuries sustained include blast ear, blast lung, blast brain, blast eye and blast belly (Jorolemon, et al. 2022), also known as barotrauma due to the increased pressure applied to an 'unvented' area within the body (Battisti, et al. 2023).

Table 6: Injuries sustained and their complications due to explosion trauma (Mizutari, 2019, CDC, 2009, Bryden, et al. 2019, Morley, et al. 2013, Jorolemon, et al. 2022).

Injury sustained	Complications

Blast ear	Entire auditory system is compromised and can result in tympanic membrane perforation (TMP), temporary hearing loss, tinnitus, hyperacusis and sensorineural hearing loss (Mizutari, 2019).
Blast lung	Due to the shockwave created by an explosion, this can cause difficulty breathing, wheezing, apnoea, and can lead to intrapulmonary haemorrhage (CDC, 2009).
Blast brain	The increased pressure produced by the explosion can cause translational and rotational acceleration of the brain resulting in various levels of compression and shearing of the brain tissue, this can also cause lacerations, contusions, and subdural haematomas to the skull (Bryden, et al. 2019).
Blast eye	This injury results in a rupturing of the globe, hyphema causing bleeding in the eye, or dislocation of an intraocular lens, each causing blurriness or loss of vision (Morley, et al. 2013).
Blast belly	Increased pressure and shockwave can cause abdominal haemorrhage and perforation to the abdomen and abdominal organs, this can also cause testicular rupture and rectal complications (Jorolemon, et al. 2022).

Secondary Injuries

The primary source of secondary injuries from an explosion is from the debris that is produce from a blast. Depending on the size of a blast, debris can be carried over extended distances with varying levels of force. This also includes explosions with the intent of harm that therefore contain various materials such as nails, metal scraps, screws and other objects that can cause penetrative injuries (Jorolemon, et al. 2022). Primarily, areas of the body that are most subject to secondary injuries are those most commonly exposed, such as head, neck, and extremities with resulting injuries such as lacerations, fractures, amputations, and dislocations (Jorolemon, et al. 2022). Data retrieved

from the Murrah building explosion in Oklahoma City in 1995 found 48% of people received injuries to the head and neck, 45% receive to the face and 35% to the chest (Pepe, et al. 2008).

Tertiary Injuries

A tertiary level injury is sustained when an explosion causes a strong enough blast, a person is displaced through the air coming into contact with surrounding objects, vehicles, or buildings, this also includes injuries sustained from a collapsed building onto a person (Jorolemon, et al. 2022, Pepe, et al. 2008). This level of injury includes both blunt force and sharp force trauma due to the impact when colliding with a building or vehicle thus resulting in fractures, head injuries, spinal injuries, and many other forms of skeletal damage, and whether a sharp debris or structure also causes a penetrating injury (Jorolemon, et al. 2022).

Quaternary Injuries

Quaternary injuries often include injuries to multiple parts of the body due to exposure to resulting fires, smoke/fumes, radiation, and other biological agents produced by the blast, see table 7.

Table 7: Quaternary injuries depicting potential exposures and their resulting symptoms (Jorolemon, et al. 2022, CDC, 2018, Pepe, et al. 2008)

Exposure	Result
Fire	Burns: flash burn inflammation of the cornea), partial burn (damage to first and second layer of skin), full thickness (an extended burn injuring all layers of skin and some layers of subcutaneous tissue), airway (rapid swelling of burned tissue on respiratory airways) (Jorolemon, et al. 2022).
Fumes/Smoke	Inhalation injuries and compromised respiratory system (Jorolemon, et al. 2022).
Radiation	Severity ranging from minor injury to fatal, this will depend on the type, amount, and length of exposure. This includes symptoms such as fatigue,

	nausea, and vomiting, with more severe cases resulting in erythema, seizures, or death (CDC, 2018).
Biological Agents	Various illnesses can be transmitted depending on the agent that has been used, for example an exposure to Anthrax can result in illnesses such as compromised immunity or haemorrhagic bleeds (Jorolemon, et al. 2022).
Environment	Environmental aspects such as area size where the explosion has occurred can increase the severity of other injuries if in an enclosed small space. Other aspects may include surrounding fixtures or building materials such as gravel or other shrapnel/debris (Pepe, et al. 2008)

Quinary

The final category of blast injuries, known as quinary, depicts the injuries caused by incendiary devices. This type of injury is not categorised in the same format as its predecessors due to this type of injury being a result of toxic substances that have either been inhaled or absorbed into the body, for example a vasodilator causing a significant drop in blood pressure can be absorbed/inhaled and does not result in typical injuries expected from a blast (Pepe, et al. 2008).

Mortality rates

In comparison to the previous fatality types, explosion fatalities are much rarer and are often the result of an accidental explosion or targeted attack. Over the course of 2013 – 2023, a total of eight individuals have died from explosion related trauma. The predominant cause being assault with explosive materials, i.e., fireworks or similar being thrown at an individual in an altercation, however, an unprecedented peak in 2019 highlighting the death of four individuals is the result of a terror attack in London specifically London Bridge and Borough Market in which two members of public were killed alongside the attackers.

1.4 Fire Analysis

Fire and Forensics

The necessity of fire investigations in relation to forensic science is an ever-growing specialist field to determine the cause and origin of a fire in a crime scene. Understanding whether a fire has been the act of arson or accidental is a crucial piece of information as the investigation continues. However, this also highlights potential ignition sources, temperatures the fire may have reached and indications as to how the fire may have burned. In the case of fire related fatalities, understanding the fire is also crucial information to understand what may have happened to the individual prior to/during the fire.

In the year ending 2024, there were 263 fire related fatalities in the UK. The fatalities considered various types of residential fires i.e., dwelling or high-rise flats, with the majority of fatalities (77%) being in dwelling fires (GOV.uk). Over an eleven-year period, fire related fatalities have fluctuated per year with 2017 resulting in the highest mortality rate, this is due to the Grenfell Tower Fire, 363 fatalities overall (GOV.uk). Figure 8 outlines fire related fatalities over an 11-year period.

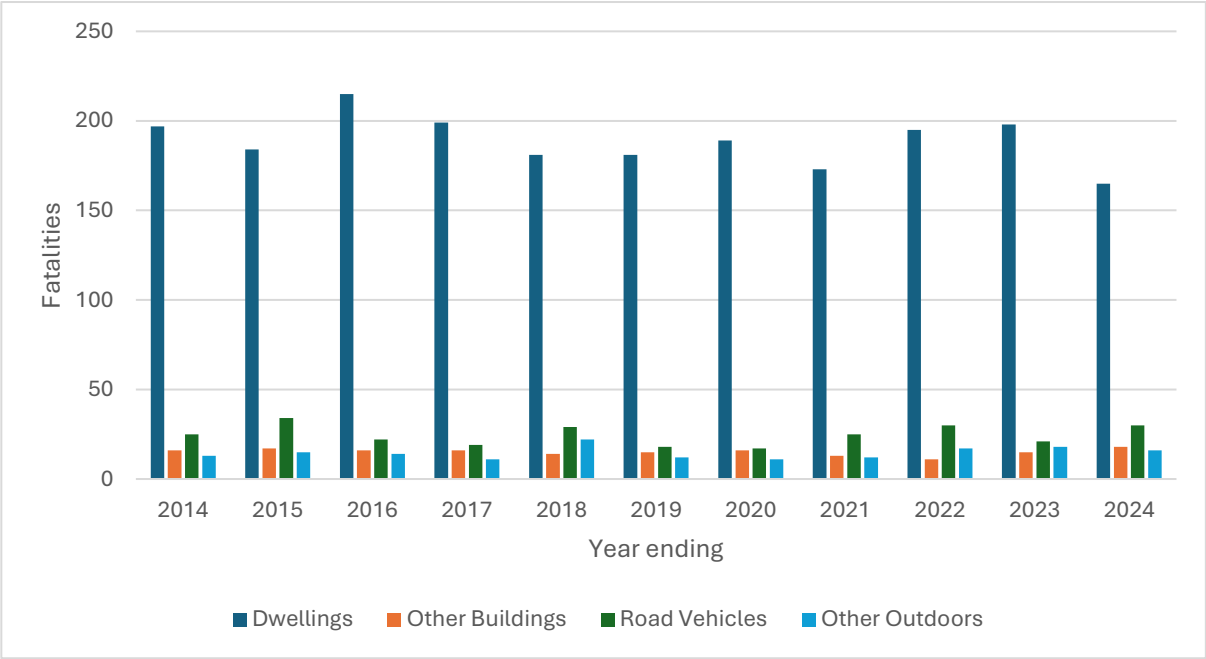

Figure 8: UK GOV statistics showing fire related fatalities over an 11-year period, 2014 – 2024, in England (GOV.uk).

1.4.2 Fire

The process of a fire burning is a chemical reaction between a flammable substance (fuel) coupled with an oxidiser resulting in a mass production of outputs such as light, heat, Carbon Dioxide (CO_2), Carbon Monoxide (CO), and other gasses depending on the fuel source (Blasquez & Thorn, 2010, Coneva & Mullerova, 2018). For a fire to burn, three components are required: Oxygen, Fuel and Heat, this is known as the fire triangle, figure 9. If one component of the triangle is removed the fire cycle will cease, i.e. if a flammable material is stored in an oxygenated atmosphere with no ignition source, a fire will not occur (Chakrabarty, et al. 2016). The flammable/combustible substances within a fire can influence its reaction and burning process, this is categorised into various classes and types.

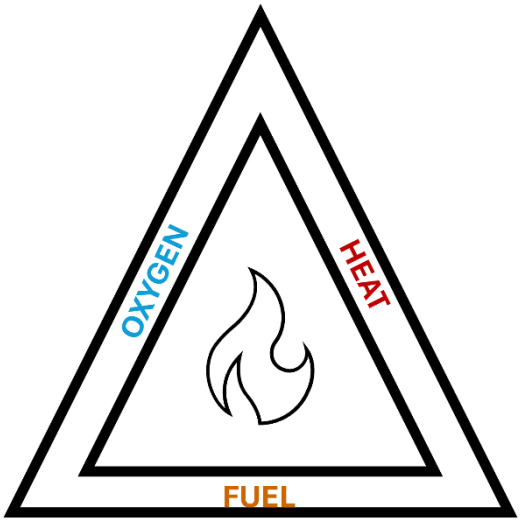

Figure 9: Diagram of the fire triangle with each necessary component, fuel, heat, and oxygen (Diagram by author).

Classes of fire

As mentioned, the reaction of a figure can depend on the fuel source that has been ignited. This fuel source is subcategorised into a 'class' as various fuel sources require different approached when being extinguished, i.e., an electrical fire cannot be extinguished with water. The classes, and further subcategories of types of fire, are split Class A to K and types, see table 8 below (Garche & Brandt, 2022).

Table 8: Classes of fire and associated extinguisher (Muchatuta & Sale, 2007).

Class	Description	Extinguisher
A	Flammable solids e.g. wood, paper, cloth	Water Based / Dry Powder
B	Flammable liquids e.g. Gasoline	CO_2 / Dry Powder
C	Flammable Gasses e.g. Methane	CO_2 / Dry Powder
D	Flammable Metals e.g. Magnesium	
F	Fats/Cooking Oils	
Electrical	Electrical Equipment	Dry Powder

A burning fire can differentiate, primarily depending on the initial ignition source, but also with the addition of surrounding materials. Split into two categories: Slow combustion (smouldering) fire and fast flame fire. A slow combustion fire is a low temperature, flameless form of combustion due to excessive heat to a substance producing large an amount of smoke (Rein, 2009). Different external factors have been found to significantly affect slow combustion fires, resulting in a transition into a flaming fire, this is either via a heated core of a substance furthering the smouldering to the outer parts to eventually be exposed to higher levels of oxygen, resulting in combustion, or secondly as the smouldering begins to produce flammable vapours and what is known as 'glowing spots', each are ignited into a flame fire (Hagen & Meyer, 2021). Fast flaming, whereas are those ignited via flammable sources being exposed to an open flame or heat source, in which the chemical reaction takes place and combustion begins, producing a larger amount of flame and less smoke.

Types of fire

Along with the classes of fire, there are also types of fire based on the way a fire may act, i.e., how it burns, this includes controlled fires, uncontrolled fires, wildfires, and structural building fires. This schematic of fires has been developed in regard to the manufacturing of clothing for firefighters and thus an understanding of the hazards for each type of fire. Controlled fires involve

multiple subcategories of burning, such as cooking fires, melted metals and others that may be caused by a singular combustible source (Song, et al. 2017). Uncontrolled fires refer to a fire that threatens to destroy life, property or natural resources and burns outside of the confines of a firebreak, a prepared space which is designed to prevent a fire from spreading further (NWCG, 2022). Wildfires are an uncontrollable fire in natural environments and are often labelled as such based on their location, for example, bushfires, forest fires or grassfires etc (Becker, 2014). Structural building fires mainly occur in residential, community or commercial based buildings, and hold the greatest amount of variance when considering ignition due to the plethora of flammable items in the aforementioned areas (Song, et al. 2017).

A further categorisation of fire is how it spreads as it burns, this can be due to the ignition source, location or external factors, with types of spread transferring from one to another, see table 9 for descriptions.

Table 9: Ways fire can spread and descriptions (Nishio, et al. 2016)

Type	**How it spreads**
Direct contact	Flames directly come into contact and ignite flammable substances.
Conduction	Heat transfer through direct contact of a heated substance.
Radiation	Heat transfer through electromagnetic waves without direct contact.
Convection	Heat transfer through hot air rising, lowering cooler air and creating a cycle.
Flashover	Secondary to convection, once all cooler air has been replaced with hot, flammable materials are then heated and ignited.
Back Draught	An already flaming fire is exposed to heightened levels of oxygen.

1.5 Understanding the changes to bone through thermal damage

Understanding the changes to bone through thermal damage is crucial in many forensic science investigations. When bones are exposed to high temperatures, they undergo various physical and

chemical alterations that can provide valuable insights into the circumstances surrounding the bones during exposure. Understanding the changes of how heat affects bone structure and composition can aid in identifying the individual, determining characteristics of the fire that occurred, and identifying cause of death. When burned, bones go through four stages of transformation: dehydration, a loss of water and moisture, decomposition, the complete loss of organic components, inversion, changes to the bones chemical structure such as crystallinity, and finally, fusion, the merging or fusing of the remaining structures (Ahlawat, 2021). The different temperatures required for each of the stages to take place can also result in additional changes to bone, this can lead to colour changes, changes to mineral levels, increased porosity, and decreased density. With this, each change can be analysed by a different analytical technique, which when collated, can provide a detailed insight to how the changes have occurred. The analysis techniques often used include Fourier Transform Infrared (FTIR), Scanning Electron Microscopy (SEM), Colorimetric analysis, and X-Ray.

1.5.1 Colour change

As a bone burns, the breakdown of organic materials and mineral structures begins, this results in a change in the colour of the bone from an organic yellow/white through charring to a calcinated white, calcination referring to the process in which bone has lost predominantly all the organic materials and has transformed into a fragile and ceramic-white material (Figueiredo, et al. 2010). The range of colours depends on the temperature the bone has been exposed to, see table 10.

Table 10: The changes in colour of bone through increasing temperatures (Mamede, et al. 2017).

Temperature (°C)	**Colour**
Unheated	Yellow/white
100-300	Black charring
300-500	Black/Grey
500-700	Grey
700-900	Light grey/white

>1000	Calcinated white

The colour of a bone sample can also be affected by factors such as the amount of soft tissue present, the duration of the heat exposure and levels of oxygen present during burning as this can either further or hinder the process of calcination (Marques, et al. 2021).

Colorimetric analysis

To analyse the changes to bone colour, a system referred to as the L*A*B system was found to provide colorimetric values to estimate temperature exposure with an accuracy of over 90%, this study focused on thermally altered colour changes in a variety of human bone samples. The system focuses on Lightness L*, red vs green A*, and yellow vs blue B*, and utilises a DSLR camera and flatbed scanner for imaging (Krap, et al. 2019). For statistical analysis the study used Microsoft Excel and SPSS for Mac to examine the relationship between RGB and L*A*B* parameters through Pearson correlation, or linear correlation. Poorly correlated parameters were plotted in a 2D scatterplot for cluster analysis, with clusters manually identified and thresholds set to create a final model.

The L*A*B* colorimetric system was found to provide high more information on temperature-induce alterations to the colour of bone samples, when compared to the RBG system, and can also advise on a range of temperatures the sample may have been exposed to, along with surrounding materials (Krap, et al. 2019).

1.5.2 Mineral Levels

Collagen

Collagen is one of the most abundant proteins within a bone's organic matrix, and when heated, the loss of collagen essentially removes the organic component of the bone, degrades the quality of protein chains and can result in a much more brittle biomaterial (Gallo, et al. 2021). Once bone has been exposed to intense heat or fire, the organic materials begin to degrade, this included

collagen. Starting at temperatures of 112°C, the organic components of a bone's composition begin to degrade, by temperatures of 300-500°C most of the organic components are lost (Gallo, et al. 2021).

The analysis of changes to mineral levels within burned bone is completed by using ATR-FTIR. The analysis is completed through the measurement of Amide I - III band absorptions and peaks, as this particular method is a reliable approach to optimise the analysis without partial or complete destruction of the sample (Lebon, 2016). The Amide peaks are measured between 1600 – 1200cm^{-1} prior to burning, however once exposed to varying temperatures, the peaks, although remaining within the same measurement, are much smaller and less precise (Legan, et al. 2020). The understanding of the levels of collagen remaining in a burned bone sample can assist in the estimation of temperature the sample has been exposed to, this accompanied by other factors e.g., colour of the sample, other mineral levels or crystallinity size, can help to decipher further information about the temperature reached.

Crystallinity

Alongside the loss of organic materials as a bone is heated, is the loss of some inorganic materials, this includes bioapatite materials known as Hydroxyapatite Crystalline structures, or crystallinity. This change often occurs between the temperatures of 500 - 1100°C and produces large crystal-like structures within the bones structure. Once temperatures have reached upwards of 700°C the crystalline structures undergo fusion in which the bioapatite materials have reached peak growth and combined with surrounding crystals, this also results in a significant increase in porosity, due to the perforated structure of crystalline formations (Gallo, et al. 2021).

Similar to the analysis of collagen, Fourier-transform infrared spectroscopy (FTIR) is also a powerful tool for identifying and characterising changes in the levels of crystallinity in various materials. In the context of bone mineralisation, for example, FTIR can be used to detect shifts in the crystallinity of calcium phosphate ($Ca_3(PO_4)_2$) compounds (Sa, et al. 2023). The FTIR spectrum reveals characteristic absorbance peaks that correspond to various molecular vibrations, including

those of the phosphate ions (PO_4^{3-}) present in the calcium phosphate crystals. By analysing these peaks, it is possible to assess the structural integrity and size of the crystals (Sa, et al. 2023).

As the crystallinity of a material increases, the FTIR absorbance peaks typically become more pronounced and sharper, indicating that the crystal structures are more organised and ordered (Sa, et al. 2023). This suggests that the material has undergone a process of crystallisation, where the individual mineral units have aligned into a more structured form. Conversely, a decrease in crystallinity is associated with broader, less intense peaks, reflecting a more disordered or vague mineral structure.

1.5.3 Future Techniques

Petrography

Primarily focusing on the systematic classification of rocks, petrography is one of the most important analysis techniques within geology and is being introduced as a potential future technique within forensics. The use of petrography can give information about organic and non-organic components that may be found within a sample (Wagner, et al. 2021).

A pilot study was completed in 2020, in which the use of petrography was used for the analysis of heat-induced alterations in bones. The study used samples of porcine bone each burned at varying temperatures from 100 – 1100 degrees Celsius (Carroll, et al. 2020). As expected, the burned samples were found to have increased changes with the higher temperatures of the furnace. As found, the lower temperatures, 100-400 degrees, had little to no effect on the microstructure of the bones sample, higher temperatures such as 500-600 degrees found changes such as the depletion of organic materials and the fusion of hydroxyapatite crystals to increase. This temperature also found microfeatures e.g. porosity, or microcracks, to be identifiable but however were less preserved and deteriorating (Carroll, et al 2020). The samples treated with higher temperature such as 700-900 degrees and more than 1000 degrees, has clear and significant changes to both the organic material and the levels of hydroxyapatite fusion. Those treated with degrees 700-900 lost all organic material and had a clear degeneration of some of the other microscopic features.

Similarly, with those treated with temperatures of 1000 and over, had complete loss of organic material alongside a complete hydroxyapatite fusion (Carroll, et al. 2020). The study concluded the use of Petrography for bone analysis to be a sound and useful new method, particularly when using thin sections of burned bone. However, more so than other studies, there are multiple limitations to this study and its results. One of the primary limitations would be that as this is a plot study, the results must be reproducible to be considered valid and therefore must be revisited. This then leads into the secondary main limitation, time. The process of this study was shown to be very time consuming in producing results thus the reproducibility of the results may also need further work (Carroll, et al. 2020).

1.6 Research aims

The intent for this research is to apply the findings to forensic investigations when analysing burned skeletal remains to determine what may have happened at the scene, how the individual may have died, and any changes that may have occurred post-mortem. In a medicolegal sense, this information is crucial for an ongoing investigation to aid the determination of whether a fire was accidental or arson, whether there has been the act of murder beforehand and what the cause of death to the individual(s) was. This will focus on creating a Standard Operating Procedure for working with burned skeletal remains, with and without sharp force trauma injuries. As this is a relatively new approach and under researched area in forensic investigations, a standardised approach to burned skeletal remains, with or without trauma, is being worked towards. Therefore, this research hopes to provide an analytical approach for the analysis of remains that may be found at the scene of a crime whilst also taking into consideration the potential variations that may occur to said remains. This research may also be used as the beginning of a Standard Operating Procedure when approaching burned skeletal remains analysis.

This research is split into three main aims.

1.6.1 Aim 1: Analyse the effects of high heat and fire on bone

The primary aim of this research is to understand the changes to bone when exposed to high heat and open flame fires. Firstly, a comprehensive understanding of the skeletal system is a necessary starting point to be able to determine the standards and expected controls of bone samples prior to thermal induced alterations.

Once exposed to varying temperatures, the changes to the bone will be analysed to begin to collate expected outcomes for each sample, this will include changes such as:

Structural changes regarding fragility, fractures and surface layer changes.

Colour changes such as calcination, charring, depending on the maximum temperature reached

Microscopic changes such as changes in bone mineral/element levels, micro-fractures, or the size of hydroxyapatite crystalline structures

Differentiation between bone exposed to fire vs. heat exposure i.e. controlled samples vs those in lesser controlled conditions.

This aim also involves a deep analysis of fire and the differences between accidental or arson. Understanding the basics of fire to a more thorough of ignition sources, how fires burn and what can affect it, is necessary when placing samples in a lesser controlled, open flame fire for more realistic results. This understanding is also necessary in a forensic context as this will provide an insight to the changes to the bone and surrounding environment to decipher what has happened at the scene of a crime and what changes to the bone can be expected.

The analysis is completed through a series of analytical techniques, each providing a range of results to be compiled for a comprehensive overview of the changes that can occur to skeletal remains depending on the temperature reached and the type of bone. Agilent Attenuated Total Reflectance Fourier Transform Infrared (ATR-FTIR) is used to collect mineral data to compare the standard levels of mineral in a myriad of bone types to those once heated/burned i.e.,

crystallinity size, collagen levels and amount of Amide I – III. Malvern Panalytical, Epsilon 1 X-Ray Fluorescence (XRF) is used to collate elemental data from the samples to also understand the basis levels of elements within a bone sample but also how the different temperatures and ignition sources may affect the elemental levels in the bone. A Keyence 3D microscope has also been included in the analysis for surface layer imagery at a high magnification, an insight into the bones structure and formation.

Multiple hypotheses can be applied to this research aim, primarily the hypothesis will look to discover if exposure to high heat and fire will cause predictable changes in the bone morphology and microstructure depending on the heat, including colour changes, cracking/fracturing, increased porosity, and changes to chemical levels. Other sub-hypotheses can be applied, such as increasing the temperature will result in a progressively lighter bone colouration, high heat will significantly increase bone fragility and fracture frequency compared to unburned samples, and finally, heat exposure will reduce bone mass and alter the organic and inorganic ratios.

For this research, the null hypothesis: there are no changes to the bones morphology and microstructure when exposed to heat and fire, was rejected. There were noticeable changes to both morphology and microstructure of the bone in the results (section 3.3), accepting the alternative hypothesis: there are predictable changes in bone microstructure and morphology when exposed to heat and fire.

1.6.2 Aim 2: Investigate the effects of sharp force trauma on bone

Secondly, a thorough analysis of the different types of forensic trauma, i.e. Blunt force, Sharp force, Thermal, Firearm, and Explosion trauma. Each type of trauma produces varying injuries depending on the cause of the trauma and the severity in which it was applied. This analysis will provide an educated look into the changes that can occur to bone and what changes can be expected, i.e. cut marks from sharp force.

More specifically for this research, a stronger focus on sharp force trauma will be undertaken considering the different ways in which sharp objects/weapons can affect bones. This will include

a look into the different instruments that can be used to create sharp force trauma injuries and the different injuries that can be created, i.e., stab wounds, chop wounds and incisions.

The primary focus for this aim will be the surface damage that is caused by sharp instruments and to examine the cut mark, depending on the type of bone affected alongside the instrument used. Per cut, the more specific characteristics of each cut mark will also be analysed to differentiate between the instruments used and to decipher if there is a consistency in the results between the type of bone, type of instrument, or an amalgamation of both factors.

Along with the repetition of ATR - FTIR and XRF analysis, 3D microscopy has been used primarily for analysis of the cut marks produced from various instruments, also for a visual understanding of the structure of each type of bone at a high magnification. The use of X-Ray analysis has also been implemented for further visual analysis, specifically for the changes the to surface layers of the bone samples once exposed to the sharp instruments to apply trauma related injuries.

The hypothesis for this research aim considers the idea that sharp force trauma will produce distinct, reproducible cut marks and related characteristics on bone that differ from other forms of trauma. This can also be broken down into sub-hypotheses: Sharp force trauma will produce linear kerfs with well-defined margins, striations, and fracture features indicative of the implement used, the depth and morphology of sharp force lesions will vary according to force applied and blade characteristics, various bones will display different fracture and kerf characteristics depending on their composition.

As seen in the results (section 4.3), regarding the aforementioned hypothesis, there is a clear rejection of the null hypothesis: sharp force trauma will not produce distinct, reproducible cut marks and related characteristics on bone that differ from other forms of trauma. Thus, accepting the alternative hypothesis that the exposure to sharp force trauma will produce predictable, distinct, and reproducible cut marks and related characteristics on bone.

1.6.3 Aim 3: Combine the effects of high heat on bone and how this may affect sharp force trauma injuries

A comprehensive understanding of bone standards, thermal alterations, and sharp force injuries provides a basis for the final research aim of combining thermal / trauma changes to bone to understand the changes in conjunction and what may need to be understood when in a medicolegal setting, i.e. can fire/high heats alter trauma?

This aim is completed by deciphering the patterns that can result from thermal changes to bone and comparing the changes to bone that also have sharp force injuries to decipher what is a result of temperature and what is a result of trauma. This understanding is also an application for identifying trauma in forensic settings to determine injuries that have been sustained ante-, peri-, or post-mortem, and whether further investigations need to be taken in cases of a homicide.

As this research aim is a combination of the two previous aims, the hypothesis for this aim is also a combination, to consider the multiple changes that may occur to the samples. The primary hypothesis for this aim is to determine if the exposure to high heat prior to or following sharp force trauma will significantly alter the appearance, preservation, and interpretability of sharp force trauma features on bone. Further, this hypothesis includes sub-hypotheses for each aspect of the investigation, heat-induced cracking and shrinkage will obscure or mimic sharp force trauma therefore complicating trauma interpretation, burned bone will show reduced kerf clarity and altered fracture propagation compared to unburned bone subjected to sharp force trauma, and finally, the sequence of events, i.e., sharp force trauma before vs. after burning, will result in distinguishable morphological differences in bone trauma patterns. The results regarding this research aim (section 5.3) reject the null hypothesis that the exposure to high heat prior to or following sharp force trauma, will not significantly alter the appearance, preservation, and interpretability of sharp force trauma features on bone. The results show a strong acceptance of the alternative hypothesis that there are predictable changes to the appearance, preservation and interpretability of sharp force trauma features on bone, after being exposed to high heats.

Chapter 2

Materials and Methods

2. Materials and Methods

To achieve the aforementioned aims of this research, a methodology containing multiple steps depending on the sample was created. A schematic of this is shown below (fig.10):

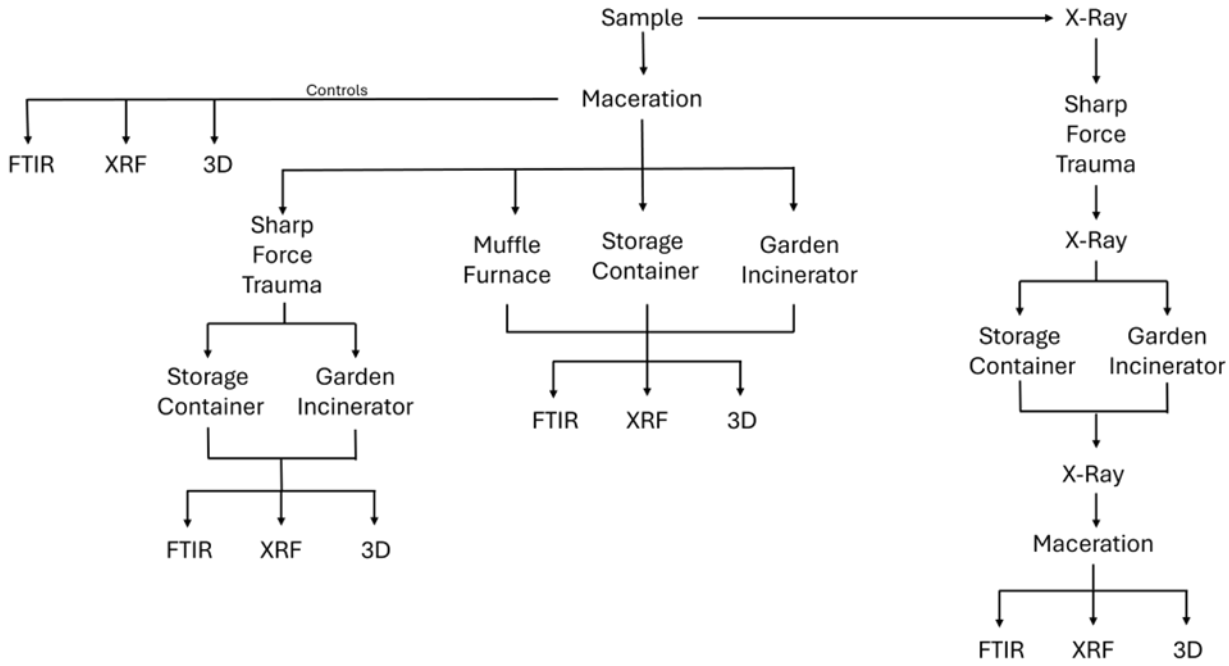

Figure 10: Diagrammatic representation of methodology used throughout (Diagram by author).

2.1 Porcine bone

As this research focuses on a topic that can be applied to forensic investigations, the use of human cadavers would be ideal, however, when working with human samples, many factors must be considered i.e., health profiles, cause of death, ante-mortem medication (Ferner, 2008). With this in consideration and due to the ethical and legal issues surrounding the use of human samples for research in the UK, porcine bone is often favoured instead. When working with animal models there are multiple factors to be taken into account, such as the age of the animal, the quality of the breeding and prior storage conditions (Bonney & Goodman, 2021).

Research has shown there are adequate similarities between the composition of porcine bone when compared to human bone, although there are still significant differences that must be accounted

for, such as elasticity, or hardness in certain limbs depending on whether the samples are infant or adult (Bonney & Goodman, 2021). The use of porcine bone is also often favoured due to the availability and lower expense at which they can be obtained.

This research has used solely porcine bones in place of human bones, locally sourced from an abattoir/butcher. The entirety of this research used 10 of each bone type, including femur, fibula, tibia, vertebrae, scapula, various skull segments, and other smaller bones when using a fleshed 'foot', i.e. carpals/phalanges. With this, and with the lack of human samples, ethical approval was not required for this research.

2.2 Method

The primary approach for this research involved the maceration of samples to work with the bone solely. Some of the samples were simply macerated and analysed with the multiple techniques to gain control data, others were exposed to only heat for a focus on the changes to bone through various heats, whereas the remainder of the samples had trauma applied which was analysed before and after exposure to fire. This provided further information on thermal alterations and how this affects the trauma injuries.

To gain more realistic data for the applied trauma and how the exposure to fire and high heats may affect it, some samples remained fleshed until the heat and trauma had been applied and were defleshed prior to analysis, as the instruments required dry samples only.

2.2.1 Sample preparation

The equipment used for the preparation of the samples included household items such as large boiling pan, sieve and tongs. This equipment was used to boil and simmer the samples and remove unnecessary flesh and soft tissue from the bones, through the process of maceration. The necessity of maceration was taken into consideration when preparing the samples. As fully fleshed samples would have provided more realistic results, some analytical techniques were unable to use with flesh remaining. Therefore, the process was altered to ensure minimal alterations to the bone's integrity and density.

Maceration, also known as Defleshing, is the process of removing the flesh and other soft tissue materials from the bone without damaging the integrity of the bone itself. The process simply involves boiling the sample in a household detergent, more specifically Persil non-bio. This detergent is utilised for its ability to remove and breakdown dirt/grease/stains without added enzymes. This detergent is also able to work consistently in colder temperatures, aiding the removal of flesh from smaller more delicate samples that may not need a higher temperature of water. The protocol followed simply uses 50ml of Persil non-bio per bone <2kg with water to cover the sample entirely. Following this, once removed from the water/detergent, the remaining flesh is gently removed with small scalpels and tweezers. For storage, the samples were frozen at -20°C prevent spoilage or any damage to the integrity of the samples before applying the trauma. This was then followed by the samples defrosting over a minimum of 24 hours depending on the size of the sample. The effects of freezing the samples prior to burning were taken into consideration as this may have affected the quality of the sample, however, this was a necessary preservation method.

2.2.1.1 Burning

When burning the samples, a total of three approaches were used: muffle furnace, garden incinerator and storage container holding an open fire. For each burning method, both garden incinerator and storage container, butane lighter fluid was used, in differing formats. Lighter fluid and a cigarette lighter both composed of primarily butane were chosen for consistency in fuel source and for the flammability of butane.

2.2.2.1.1 Muffle Furnace

A muffle furnace is a device in which samples can be exposed to intense heats without being exposed to direct flames and instead contains an insulated heating chamber (Adejumo & Obasa, 2020). The composition of a muffle furnace prevents the sample from being polluted by ash, gas, or residue of the burning materials as the fuel source, this is due to the separate chambers for both heating and combustion (Adejumo & Obasa, 2020).

For this research, the muffle furnace was used to expose the bone to multiple temperatures, as peak temperatures of fire may vary, in a more controlled environment. The temperatures measured 300°C, 450°C, 600°C, 750°C, and 900°C. The entirety of the burning times were each programmed at three hours, this time was chosen to expose the bone to the maximum temperature chosen for a significant amount of time whilst also factoring in the time taken for the furnace to reach the chosen temperature and cool down.

2.2.1.2.2 Garden incinerator

An incinerator is a furnace made of galvanised steel intended for burning materials or waste (Cheremisinoff & Rosenfeld, 2010). The open chamber with small holes around the base allows for optimised airflow and combustion efficiency, and can withstand temperatures exceeding 850°C.

To create a realistic burning scenario and continue with the use of household items, the initial fuel source used was 'Fire&Flame Heat Logs'. Composed of 100% UK Timber, the logs are made of compressed wood and can light easily with a burn time of approximately one to three hours depending on the amount used. This provides a corresponding approach to burning the samples in the muffle furnace, for comparative analysis of the results.

Similarly, storebought Charcoal was also used as an alternative fuel source, again recreating a realistic burning scenario with household products. 'Pure Lumpwood Charcoal' was purchased due to its ability to reach higher temperatures in a shorter amount of time, when compared to regular charcoal. The product can reach temperatures of >1000°C and can burn for two to three hours, providing a similar maximum temperature and burn time to compare to that of the muffle furnace and garden incinerator. The maximum temperature reached during burning exceeded 600°C and peaked at 625°C.

2.2.1.2.3 Storage Container

The use of a storage container was used to create a realistic living room scenario. The use of this container allowed an intense fire to take place as the flames spread across the 'living room' without

exiting and spreading further than the container itself. The container measured 8.5ft x 8ft x 10ft and was composed of high-strength Corten steel. Corten steel is a non-combustible material that does not burn under normal conditions, i.e. changes often occur due to weathering, or if burned, it has a melting point of 1450-1510°C (Ellobody, 2023). The fire was initiated through the lighting of a butane cigarette lighter and being thrown into the 'room' igniting the surrounding materials. Maximum temperatures reached >600°C, peaking at 623°C.

2.2.2.3 Trauma

The application of sharp force trauma for this research was applied using three different types of knives. Each knife is a commonly found household knife for applications to more realistic scenarios, such as an assault, homicide or form of defence in a household setting. The location of the cut marks in regards to the samples centred around the diaphysis or mid-sections of the samples.

The knives used include a serrated edged knife, more commonly known as a steak knife, a smooth-edged blade, and a large serrated edged knife, known as a bread knife. As for the serrated knives, the smaller serrated knife measured at 124.7mm long and 1.4mm wide, and a 103.3mm handle. The teeth were approximately 1.4mm apart on the serrated side of the knife. The large-serrated knife blade measures at 193.7mm long and 2.6mm wide, with a 115.7mm long handle. The teeth were measured at 6.2mm apart. The blade measured at 129.6m long and 2.1mm wide, including a 117.2mm handle, as this is non-serrated there are no teeth on the blade to measure the distance.

2.2.2 Analysis techniques

2.2.2.1 Attenuated Total Reflectance Fourier Transform Infrared

Attenuated Total Reflectance Fourier Transform Infrared (ATR-FTIR) is an analytical method using on infrared light to determine the molecular composition of a sample. This technique measures the absorbance of said infrared light reflected from the sample using a high-refractive-index crystal (Pasieczna-Patkowska, et al. 2025). ATR-FTIR is a sensitive approach that provides thorough results regarding organic and inorganic materials within bone in the form of spectra,

highlighting the single/double/triple chemical bonds (Mattsson, et al. 2024). This technique can evaluate the changes to mineral levels within a sample's composition, allude to the mineral matrix content, highlight ion levels regarding crystallinity and, determine the levels of collagen and its maturity (Mattsson, et al. 2024). The data is interpreted by comparing the spectrum with reference data to identify unknown compounds and determine their properties.

Particularly for bone minerals, ATR-FTIR has been used extensively to identify substances such as Amides I – III, Phosphate ions, and the current state/size of Hydroxyapatite crystalline structures. Research has found ATR-FTIR to be a valuable technique for analysing the composition and properties of bone (Paschalis, et al. 2011).

The absorptive responses of various minerals, particularly those related to this study, appear in peaks often situated between 1700 and 1000cm^{-1}. Table 11 shows each mineral related to this study and the general regions they appear.

Table 11: Absorptive regions of Hydroxyapatite, Phosphate, and Amides I-III (Kasem et al 2020, Gheisari et al 2015, Hammerli et al 2021).

Mineral	**Absorption (cm^{-1})**
Hydroxyapatite	1100-1100
Phosphate	1150 – 890
Amide I	1650 - 1600
Amide II	1560
Amide III	1100 – 1030

ATR-FTIR was selected for this research due to its demonstrated suitability for analysing heat- and trauma-induced changes in bone at a molecular level. The technique enables the simultaneous evaluation of both organic components, such as collagen and amide structures, and inorganic components, including phosphate and hydroxyapatite, which are known to be significantly affected by thermal exposure and mechanical trauma (Paschalis *et al.*, 2011; Lebon *et al.*, 2016). This dual analytical capability makes ATR-FTIR particularly appropriate for investigating

compositional changes associated with high heat, sharp force trauma, and the combined effects of these processes.

Additionally, ATR-FTIR provides rapid, reproducible, and high-resolution spectral data with minimal sample preparation, reducing the likelihood of sample contamination or physical degradation (Alkhuder, 2022). This advantage is especially relevant when analysing burned bone, which is often brittle and susceptible to fragmentation during handling. The non-destructive nature of ATR-FTIR allows for repeated measurements on the same specimen, facilitating comparative analyses between control, pre-burned, and post-burned samples, as well as improving data reliability and experimental consistency (Lebon *et al.*, 2016).

ATR-FTIR has also been extensively validated within forensic anthropology and bioarchaeology for identifying heat-induced mineral transformations, collagen degradation, and changes in crystallinity and mineral-to-organic ratios (Paschalis *et al.*, 2011; Mattsson *et al.*, 2024). These parameters are critical for interpreting taphonomic processes and assessing the sequence of events affecting skeletal remains. Consequently, ATR-FTIR represents a robust and well-established analytical technique that is well suited to addressing the research aims of this study and enhancing the interpretation of bone alterations resulting from high heat exposure and sharp force trauma.

2.2.2.2 X-Ray

X-ray imaging is one of the most commonly used non-invasive and non-destructive analytical techniques for the examination of skeletal structures. The technique utilises electromagnetic radiation, also referred to as Roentgen rays, operating at wavelengths ranging from approximately 0.01 to 10 nm, allowing X-rays to penetrate bone and produce contrast-based images of internal structures (Fakhlaei *et al.*, 2024).

Extensive research has demonstrated the utility of X-ray imaging in bone analysis due to its relative simplicity, rapid image acquisition, and reproducibility of results. Within a forensic context, X-ray imaging is particularly valuable for the identification and assessment of fractures and skeletal

injuries. This technique enables the detection of trauma patterns, supports interpretations of injury mechanisms, and may contribute to determinations of cause of death depending on the severity and nature of the observed damage. Additionally, X-ray imaging can reveal the presence of foreign objects, such as bullets or explosive fragments, embedded within skeletal remains (Alsulami *et al.*, 2022).

Beyond trauma assessment, X-ray analysis also plays an important role in forensic identification. Radiographic examination can assist in the estimation of biological profiles, including age and sex, and is especially valuable in cases involving mass disasters, multiple fatalities, or significantly decomposed remains where visual identification is not possible (Clemente *et al.*, 2017; Alsulami *et al.*, 2022).

In this study, a Kubtec X-ray system was utilised to obtain high-resolution radiographic images of the bone samples. The system allows for non-invasive, non-destructive imaging with rapid acquisition times and consistent image quality, providing clear visualisation of bone condition and structural integrity while maintaining sample preservation.

X-ray imaging was selected for this research due to its effectiveness in identifying macroscopic and internal structural changes in bone associated with trauma and thermal exposure. The technique enables the visualisation of fractures, internal cracking, and density alterations that may result from sharp force trauma and high heat exposure, providing essential contextual information prior to and alongside more detailed molecular and surface analyses.

The non-destructive nature of X-ray imaging allows for repeated examination of the same samples throughout the analytical process without compromising sample integrity. This is particularly important when working with burned or otherwise fragile skeletal material. Additionally, X-ray imaging serves as a complementary technique to ATR-FTIR, XRF, and 3D microscopy by providing an initial overview of bone condition and trauma presence, thereby supporting a multi-method analytical approach. As such, X-ray imaging represents a robust and appropriate technique

for addressing the research aims of this study and for enhancing the interpretation of trauma and heat-related alterations in skeletal remains.

2.2.2.3 X-Ray Fluorescence

X-ray Fluorescence (XRF) is a non-destructive analytical technique that provides both quantitative and qualitative data on the elemental composition of solid, liquid, or powdered samples (Kohli, 2012). Elemental identification is achieved by irradiating the sample with high-energy X-rays, causing the emission of secondary (fluorescent) X-rays that are characteristic of specific elements. Depending on sample size and concentration, XRF results are commonly reported in parts per million (ppm) (Groarke *et al.*, 2021).

This analytical technique offers a rapid and non-destructive approach, requiring minimal sample preparation and enabling efficient data acquisition. The design of XRF instrumentation also promotes a safe working environment, with negligible risk of sample contamination and minimal exposure risk from X-ray radiation when appropriate laboratory protocols are followed.

Recent research has demonstrated the utility of XRF in the analysis of bone, particularly in cases involving thermal alteration. Studies have shown that the detection of elemental composition using XRF can assist in identifying sharp force trauma in bone both before and after burning, providing insight into trauma presence and potential characteristics of the weapon involved (Rosa *et al.*, 2022).

In this study, XRF analysis was conducted three times on each sample, with mean values calculated to ensure analytical reliability. Powdered bone samples were placed into the instrument and analysed using an *Omnian* analytical scan. Each scan was conducted for a duration of five minutes, producing tabulated results that detail the concentration of each detected element. The raw XRF data are presented in Appendix 1.

XRF was selected for this research due to its effectiveness in identifying and quantifying elemental changes in bone associated with thermal exposure and sharp force trauma. High temperatures are known to alter the elemental composition and distribution within bone, and XRF provides a

reliable means of detecting these changes without causing further damage to the sample. This capability is particularly valuable when analysing burned bone, where fragility and preservation concerns limit the use of more invasive analytical methods.

The non-destructive and rapid nature of XRF allows for repeated analyses of the same sample, facilitating comparative assessments between control, burned, and traumatised specimens. Additionally, XRF complements molecular techniques such as ATR-FTIR by providing elemental-level data, enabling a more comprehensive interpretation of heat-induced and trauma-related alterations in bone. As such, XRF represents a robust and appropriate analytical technique for addressing the research aims of this study and for supporting the identification and interpretation of sharp force trauma in thermally altered skeletal remains.

2.2.2.4 3D Microscopy

A relatively new approach to bone analysis is the use of a Keyence 3D microscope. Three-dimensional microscopy imaging provides both visual and analytical data on a sample while generating a three-dimensional representation of its surface morphology (Fischer *et al.*, 2012). The technique operates by layering multiple two-dimensional images captured at varying focal depths; this process also incorporates images taken by adjacent stereoscopes both in and out of focus to enhance surface texture and topographical detail (Hiraoka *et al.*, 1990).

Within forensic science, the application of 3D microscopy is a comparatively recent development; however, it has been shown to significantly aid investigations, particularly those involving small samples and trace evidence. The analysis of trauma using 3D microscopy allows for the reconstruction and visualisation of sharp force trauma injuries, providing insight into weapon characteristics such as blade edge type (e.g. serrated versus non-serrated) and directionality of force. This approach can also be combined with the examination of suspected weapons to facilitate direct comparison with observed trauma patterns (Baier *et al.*, 2021). Additionally, 3D microscopy has proven valuable in the examination of microscopic trace evidence, including fibres, paint fragments, and soil particles (Carew *et al.*, 2021).

The benefits of using this analytical technique include enhanced image resolution, rapid data acquisition, and a reduction in photobleaching compared to traditional microscopy methods, improving both image quality and analytical efficiency (Fischer *et al.*, 2012).

The Keyence 3D microscope was selected for this research due to its ability to provide high-resolution, non-destructive visualisation of bone surface modifications associated with sharp force trauma and thermal alteration. The technique enables detailed examination of kerf morphology, surface striations, and microfractures in three dimensions, which is essential for accurately characterising trauma features that may be altered or obscured by heat exposure. This level of detail supports the identification and differentiation of trauma types and contributes to the interpretation of weapon characteristics and trauma mechanisms.

Furthermore, the non-contact nature of 3D microscopy is particularly advantageous when analysing fragile or burned bone, as it minimises the risk of further damage during examination. The ability to digitally reconstruct and manipulate three-dimensional models allows for repeated analysis and comparative assessments without compromising sample integrity. Given its established utility in forensic trauma analysis and trace evidence examination, the Keyence 3D microscope represents a robust and appropriate analytical technique for addressing the research aims of this study and for complementing molecular data obtained through ATR-FTIR analysis.

Chapter 3

Thermal alterations to porcine bone

3.1 Introduction

Fire investigation is an increasingly important branch of forensic science, dedicated to determining the cause and origin of fires at crime scenes. A key objective is to establish whether a fire was deliberately set or accidental in nature. This process also provides critical insights into ignition sources; the temperatures reached and burn patterns that reveal how the fire spread. In cases involving fatalities, analysing fire behaviour is vital for reconstructing the sequence of events leading up to or occurring during the incident, which can also help establish the cause of death.

According to the European Fire Safety Alliance, approximately 5,000 people die each year in residential fires, with the number of injuries being about ten times higher (EFSA, 2025). In England and Wales, there were 263 fire-related deaths in the year ending June 2024 (ONS, 2024). Figure 8 (section 1.4.1) shows fluctuations in the number of fire-related fatalities over the past decade.

One of the most widely used methods of classifying fires is based on the type of ignition source. This approach not only identifies where the fire may have begun but also considers factors such as the typical temperature ranges associated with different types of combustion. For example, fires caused by flammable liquids usually burn at higher temperatures than those started by solid fuels like wood or paper (see Table 12). In this study, the samples were exposed to temperatures ranging between 600°C and 625°C, consistent with the combustion of flammable solids.

The classification system also accounts for the interaction between extinguishing agents and certain materials, as inappropriate suppression methods can worsen a fire, for example, applying water to an electrical fire. Therefore, accurate fire categorisation requires understanding both the ignition source and the suitable response materials to manage the incident effectively.

The fire classes are as follows:

Table 12: Classes of fire with their maximum temperatures and examples *(Muchatuta & Sale, 2007, Helmenstine 2024, Babrauskas, 2022).*

Class	Materials	Max temp °C	Examples

A	Flammable solids	600 - 900°C	Paper, Wood, and Cloth
B	Flammable liquids	100 - 450°C	Petrol, Alcohol, and Oil
C	Flammable gasses	1950 - 3100°C	Methane, Propane, and Butane
D	Flammable metals	3000 - 3400°C	Magnesium, Aluminium, and Sodium
F	Fats/Cooking oils	204 - 270°C	Vegetable oil or Sunflower oil
Electrical	Electrical equipment	6200°C	Electric bikes

3.1.1 Changes to burned bone.

The classification of fire holds particular importance when considering the effects of fire on skeletal remains. The temperature and duration of exposure, as well as the materials present during combustion, play a critical role in the extent of alteration to bone (Gallo et al., 2021). High-temperature fires can cause substantial physical and chemical changes, including discoloration, fracturing, and increased fragility (Marques et al., 2018). These alterations can affect the accurate interpretation of trauma, the identification of individuals, and the determination of cause of death.

The nature and severity of bone alterations may also provide valuable insights into the characteristics of the fire itself. For instance, they can indicate the peak temperature reached, the influence of surrounding materials, and the potential ignition source (Logan & McColl, 2024). Table 13 summarises the principal surface changes commonly observed in burned skeletal remains.

Table 13: Descriptions of changes to bone through thermal damage (Marques, et al. 2018).

Changes	**Description**
Colour	The colouring of the bone can often imply the intensity of the temperature it has been exposed to, i.e., various maximum temperatures of a fire can produce significantly different colourations

	to bone samples. Changes from off-white, to a charred grey/black eventually reaching a calcified white (Also seen in Figure 12).
Fracturing/splintering	Lesions to the bones surface structure in the form of a break.
Fragility	An increase in porosity can lead the bone to become much more delicate and fragile. The increasing temperatures can cause the bone to lose mineral levels which can result in a loss of dexterity thus leaving a much weaker sample.
Mineral Levels	Intense temperatures can increase and decrease various minerals within bone, e.g. an increased calcium level can signify the beginning or current stage of calcination (Fig.10).

As for microscopic changes in bone due to temperature, one of the principal changes to signify a fires temperature is the fundamental change to the Hydroxyapatite crystalline structure [$(Ca)_{10}(PO_4)_6(OH)_2$]. The increase of hydroxyl groups, coupled with a loss of water and reduction on carbonate contents, has been found to increase the size of crystallinity structures due to the temperature of the fire. This often occurs when exposed to temperature exceeding 500°C (McKinnon, et al. 2020).

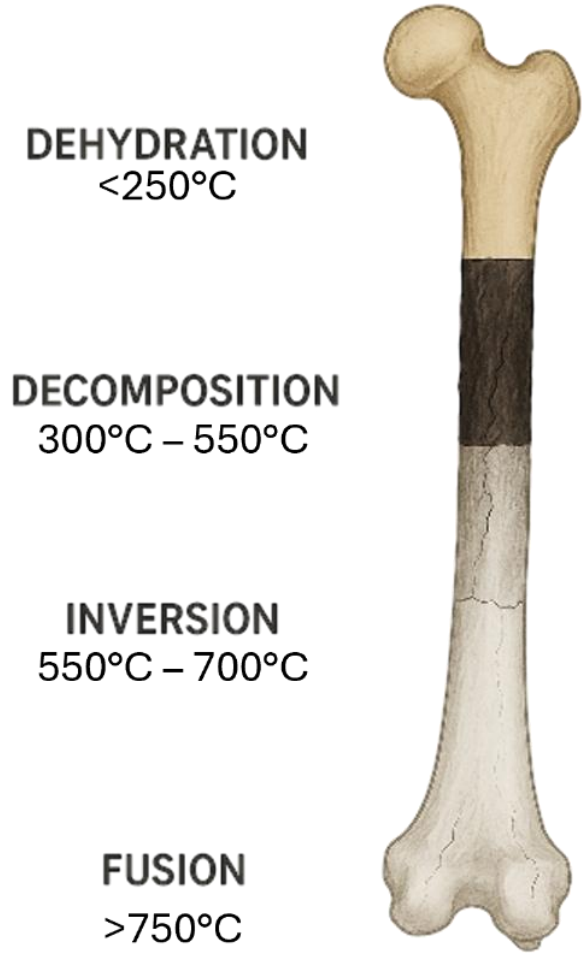

Figure 11 shows the changes to a bones colour, structure, and mineral content due to the temperatures reached during burning, ranging from 250 °C to >1000 °C (Copyright free image labelled by author).

As seen in figure 11, there are various stages a bone will go through depending on the maximum temperature reached. Dehydration refers to the majority, if not complete, loss of moisture within the bone, typically once temperatures reached above 250-300°C. This initiates decomposition, at temperatures of up to 550°C, in which all organic materials breakdown and disintegrate, leading to inversion. Inversion begins at temperatures exceeding 600°C and affects the chemical structures within the bone, i.e., Hydroxyapatite crystalline structures increasing in size and bonding. Finally, Fusion of a burned bone refers to the complete fusion of the remaining structures within the bone,

at temperatures of 700°C and above, producing a more ceramic like product as the bone is now a fragile and calcined white substance (Ahlawat, 2021).

3.1.2 Analysis methods

As for the analysis of the bones, both Agilent Attenuated Total Reflectance Fourier Transform Infrared (ATR-FTIR) and a Malvern Panalytical, Epsilon 1 X-Ray Fluorescence (XRF) were used prior and post burning.

3.1.3 ATR-FTIR analysis

Agilent Attenuated Total Reflectance Fourier Transform Infrared (ATR-FTIR) can evaluate the changes in mineral and matrix content within a bone's composition (Scaggion, et al. 2024). More specifically, the use of ATR-FTIR provides an indication of the mineral content within the samples allowing for the comparison of the results before and after burning. This was completed by using the absorbance setting with parameters set to 4000-400cm^{-1}. Each sample was analysed three times, with a calculated average used for the results. For data interpretation see 2.2.2.1.

3.1.4 XRF analysis

Malvern Panalytical, Epsilon 1 X-Ray Fluorescence focuses on the use of incident x-ray beams exciting secondary wavelengths into solid or powdered samples (Kristo, 2012), See 2.2.2.3 for XRF details. Each sample was analysed three times, with a calculated average used for the results.

3.2 Method

3.2.1 Sample Preparation

Four femurs were prepared by maceration to remove soft tissue (see Section 2.2.1). Samples were stored at –20°C to prevent spoilage and defrosted for at least 24 hours before analysis. Some bones were partially or fully fleshed to simulate realistic burned remains, though fully fleshed samples could not be used in the muffle furnace. For muffle furnace burns, femurs were sectioned into seven smaller diaphyseal samples.

3.2.2 Burning Protocols

Three burning approaches were employed:

Muffle furnace: Samples were exposed to 300°C–900°C in 150°C increments for a total of three hours, including heating and cooling times (peak temperature held <45 min). Six femur samples were burned per session, repeated twice.

Storage container fire: A mock living room setup was ignited using a butane lighter, with two femurs, skull, and ilium samples per burn. Maximum temperatures were ~612°C and 623°C, with burn durations of 6.4–9.5 minutes.

Garden incinerator: Open flames with charcoal and wood as fuels, ignited with butane lighter fluid. Charcoal reached 617°C and wood 625°C, each burn lasting under 20 minutes.

3.2.3 Analysis

Samples were analysed using Agilent ATR-FTIR and Malvern Panalytical Epsilon 1 XRF, each repeated three times. Powdered bone (obtained via mortar and pestle) was used to improve scanning coverage and analytical reliability, though both techniques are non-destructive. Analyses were conducted on samples from each temperature and burn type, with control samples included for comparison (see Sections 2.2.2.1 and 2.2.2.3).

3.3. Results

3.3.1 Colour change

Samples from each temperature in the muffle furnace show a clear pattern of change in colour increase in fragility to the bone samples. Figures 12 – 13 show a multitude of femur samples before and after burning. There is a clear distinction between each set of samples, in both colour and dexterity. The change in colour starts at a charred black/grey through to calcined white, coupled with broken/flaking samples as the temperature increases, showing a decrease in dexterity and increase in fragility.

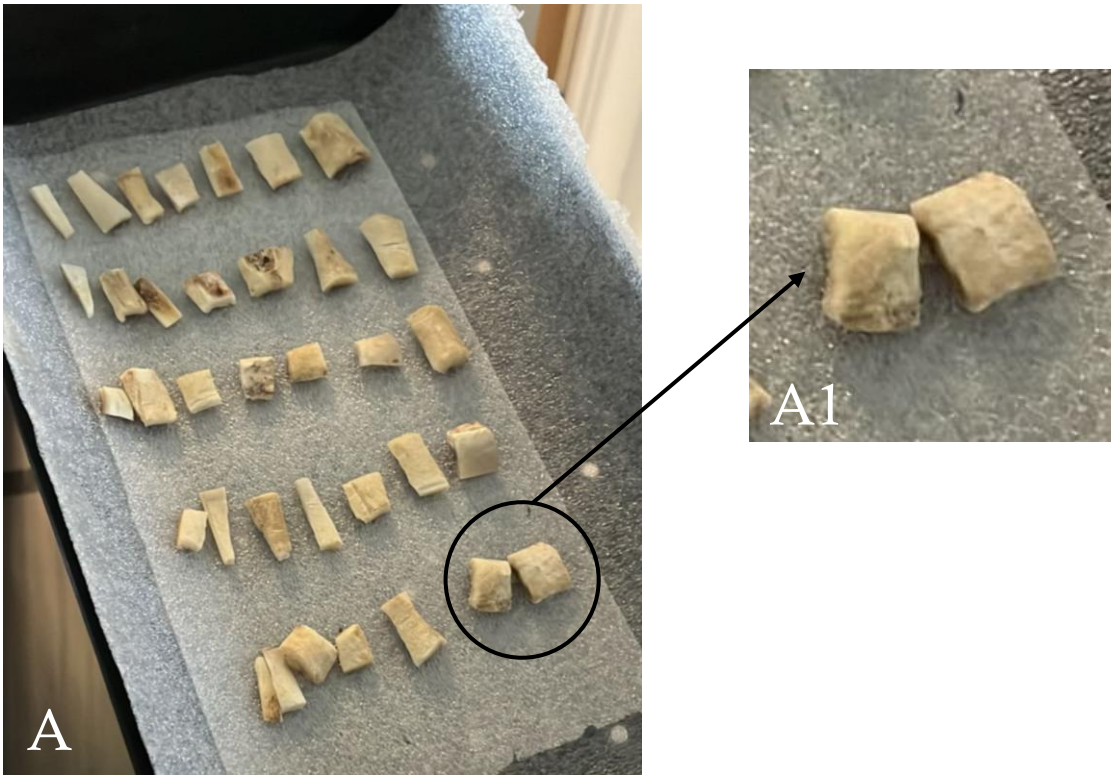

Figure 12: A shows example of femur diaphysis samples prior to being placed in the muffle furnace. A1 shows zoomed in image for clearer example.

Figure 13: Sample selection of femur diaphysis samples representing each temperature used in the muffle furnace, 300°C, 450°C, 600°C, 750°C, and 900°C. Clear distinctions between each temperatures colour and dexterity can be seen, starting at a charred black/grey through to calcined white, coupled with broken/flaking samples. Also shows examples of powdered samples for each temperature, to be used for ATR-FTIR analysis.

3.3.2 ATR-FTIR

Each of the samples were compared, including: the control samples, the samples heated at a range of temperatures from 300° - 900° Celsius in the muffle furnace, samples from both open flame scenarios, burned at 612°C/623°C and samples from both the garden incinerator burns using either wood (625°C) or charcoal (617°C) as an ignition source.

Figure 14 depicts the levels of various chemical components within the control femur sample. This sample contains a clear amalgamation of single, double, and triple bonded compounds, with the inclusion of fingerprinting frequencies. Specifically for the fingerprinting frequencies, at a reading of around 1100cm^{-1} Phosphate group (PO_4^{3-}) can be identified, as to be expected in a bone sample. Similarly another expected sample is read at ~1400cm^{-1}, Carbon Trioxide group (CO_3) an implication of the levels of not only calcium carbonate within the bone but also the -apatite crystals found in hydroxyapatite crystalline structures. Alluding to the organic materials within the sample, Amides I – III can be read at measurement 1680cm^{-1} – 1690cm^{-1}.

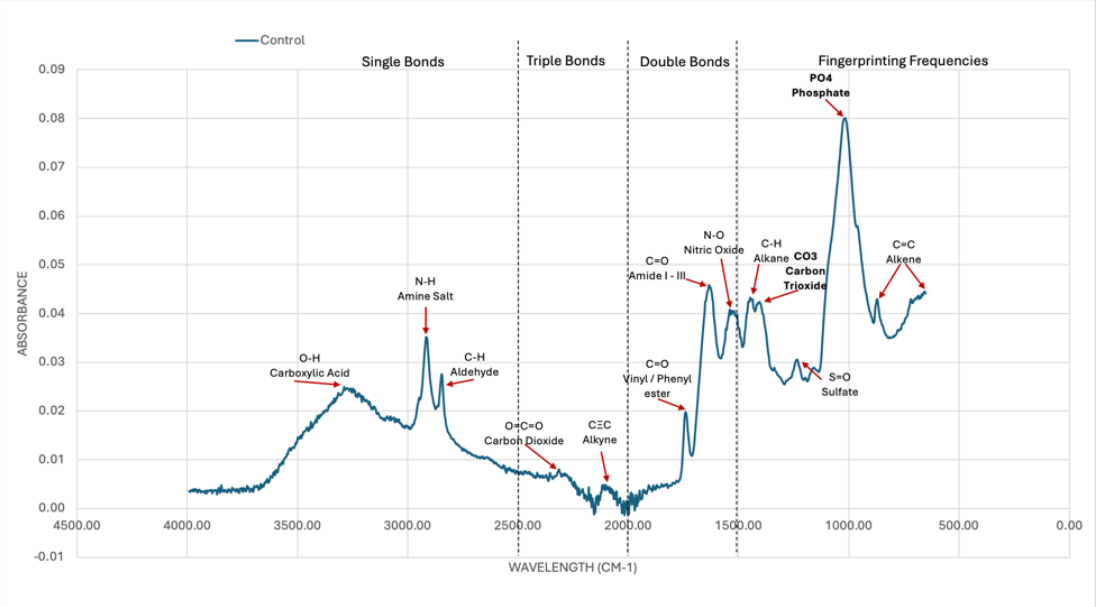

Figure 14: Average ATR-FTIR spectra of the control femur sample with highlighted compounds throughout. Control levels of notable minerals: Amides I-III between 1800 - 1500cm-1, CO3 between 1500 - 1300cm-1, and PO43- at 1100cm-1.

Figure 15 shows the results of the femur samples placed within the muffle furnace at 300°C, 450°C, 600°C, 750°C, and 900°C. In comparison with the control samples, figure 14, there are clear losses of most compounds as the temperatures increase through each sample. The samples heated to 300°C shows a slight but notable decrease in the majority of the various minerals and chemical components e.g. Amide I – III between 1800 - 1500cm^{-1} and CO_3 between 1500 - 1300cm^{-1}. The 450°C samples continue the trend of decreasing components coupled with an increase in the level of PO_4^{3-} at 1400cm^{-1}. For comparison to the samples from the other burning methods, the sample burned at 600°C shows a strong increase in the level of PO_4^{3-} at 1100cm^{-1} alongside a significantly decreased amount of Amides I-III between 1800 - 1500cm^{-1} and CO_3 between 1500 - 1300cm^{-1}. This is due to the depletion of any organic materials, that may have remained in the samples, as the temperature exceeds 500°C, the temperature at which decomposition begins. The strongest increase in PO_4^{3-} is in the 750°C sample, suggesting a potential peak growth in the hydroxyapatite crystalline structures. Finally, the samples burned at 900°C show a slight decline in the level of PO_4^{3-} along with an almost complete loss of all Amides and CO_3.

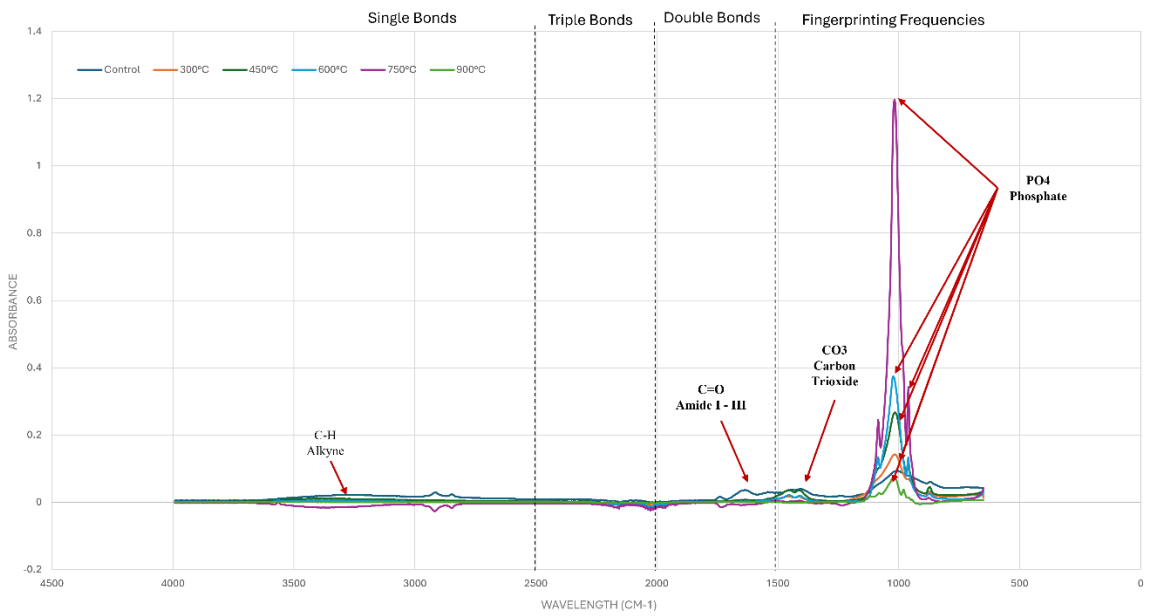

Figure 15 shows Average ATR-FTIR spectra of the femur samples placed in the muffle furnace, comparing the control samples and those burned at 300°C, 450°C, 600°C, 750°C, and 900°C. the sample to 300°C shows a slight increase in PO43- and slight decrease in CO3 du to the initial heating. The 450°C sample shows a trending peak of PO_4^{3-} at 1100cm^{-1} with similar levels of CO_3 to the precious sample at 300°C. There is a slight decrease in Amides I – III between 1500 - 1300cm^{-1}. The sample burned at 600°C shows clear decrease in Amides I-III and CO_3 between 1500 - 1300cm^{-1} but with an increase in PO_4^{3-} at 1100cm^{-1}.750°C shows the strongest peak of PO_4^{3-} at 1100cm^{-1} throughout all of the muffle furnace samples and the lowest level of both and CO_3 between 1500 - 1300cm^{-1} and Amides I-III at 1800 - 1500cm^{-1}. 900°C levels of PO_4^{3-} at 1100cm^{-1} are beginning to reduce due to the high temperature indicating the process of calcination, couples with a complete loss of CO_3 and Amides I-III.

Figure 16 shows a loss, although less significant, of Amides I-III, Phosphate or Carbon Trioxide, due to the temperature. Again, a clear spike in the level of PO_4^{3-} within the sample and loss in the level of CO_3, however not as significant as that lost in the muffle furnace sample. Figure 16 also shows the appearance of smaller vibrations within the sample, a potential for additional compounds that may have been absorbed from the surrounding materials whilst burning, this is assumed to be additional materials due to the lack of presence in other samples. Potential labels for the smaller vibrations between 2500 – 2000 cm^{-1} include CO_2 compounds, possibly due to the output elements as the fire burned, or isocyanate, found between 2275 - 2250cm^{-1}, an essential component in insulation materials and packaging.

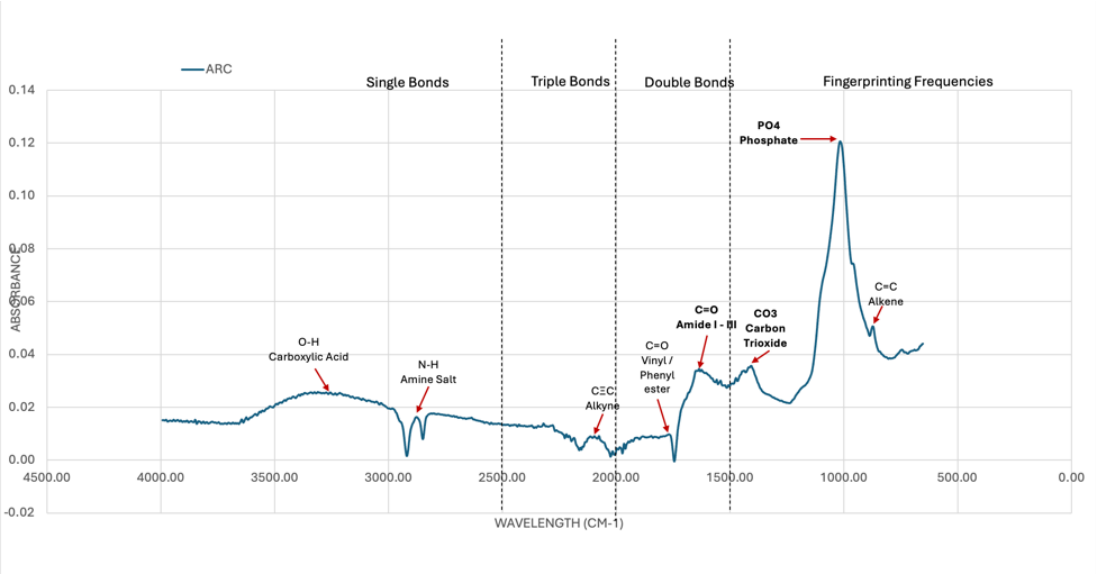

Figure 16: Average ATR-FTIR spectra of the fleshed femur sample placed in the open flame fire and burned at ~612°C. (ARC referring to the Army Reserve Centre in which the fire took place) notable minerals show a continued decrease in Amides I-III and CO3, with a trend towards consistent increase in PO_4^{3-}

Figure 17 shows a consistent depletion of most compounds and other ions due to the high temperature. However, unlike the previous ARC sample, there are significantly less compounds remaining, potentially due to the higher temperature recorded (623°C).

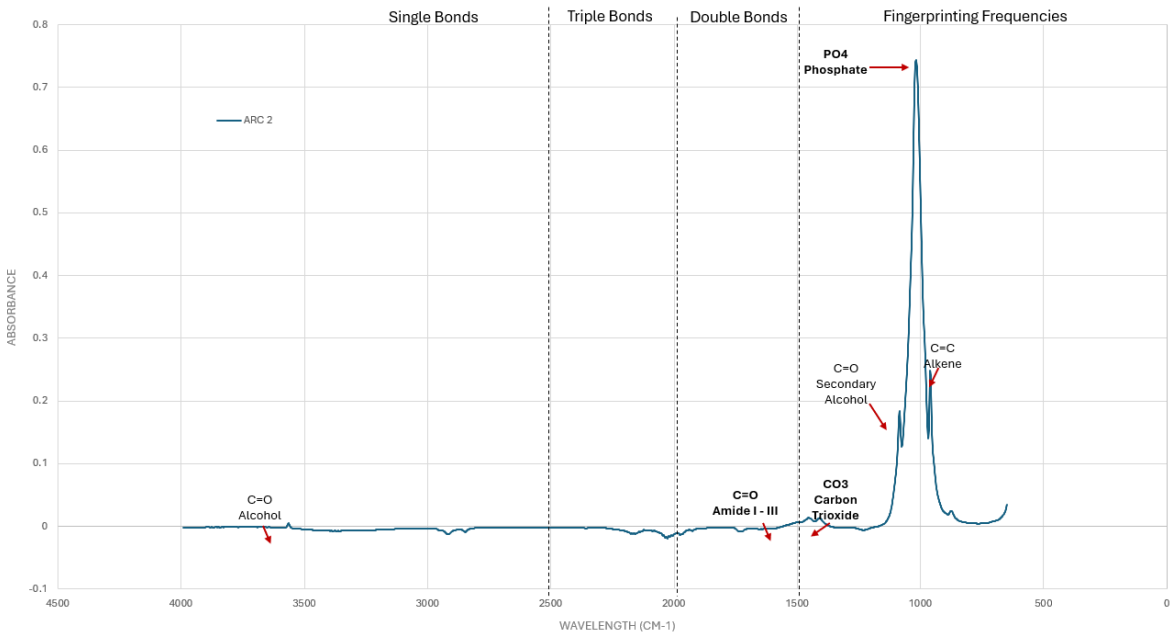

Figure 17: Average ATR-FTIR spectra of the fleshed femur sample placed in the second open flame fire and burned at ~623°C. (ARC referring to the Army Reserve Centre in which the fire took place) showing an almost complete loss of Amide I-III and CO3. This spectra depicts the largest increase in PO_4^{3-} when compared to the results.

The following samples, although similarly femur samples, remained partially fleshed.

Figure 18 shows the sample burned with wood as the ignition source. There is a clear peak representing C-H Alkyne at 3260cm^{-1}, signifying the presence of organic materials and remaining flesh after burning the sample. This is also the case for C-H Alkane recorded at 2850cm^{-1}. Like figures 13 – 15, there is again a clear decrease in the levels of Amides I – III and significant increase in PO_4^3.

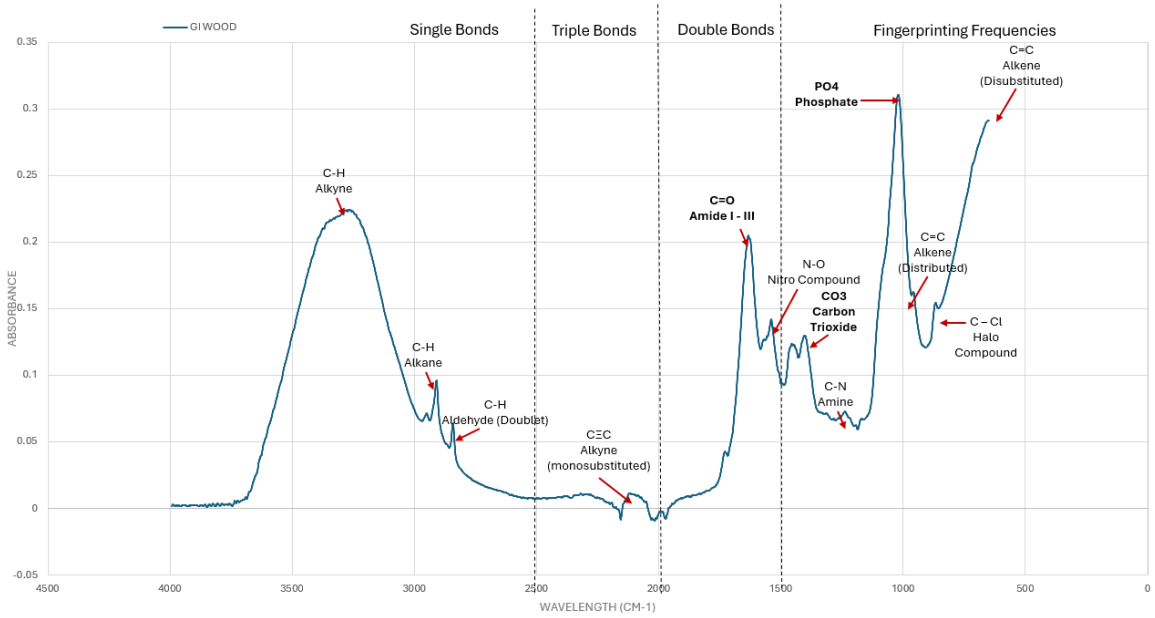

Figure 18 Average ATR-FTIR spectra of the femur sample placed in the Garden incinerator using wood as the ignition source and burned at ~625°C. Remaining flesh is noted through a significant peak in C-H Alkyne at 3260cm^{-1} and C-H Alkane at 2850cm^{-1}.

The sample burned with charcoal as the ignition source, figure 19, shows a similar reaction to that burned with wood. The presence of C-H Alkynes remains stronger than those burned in the muffle furnace or in either ARC. There is a consistent depletion of Amides I – III and increase in PO_4^{3-} with a variance when compared to other burns due to the temperature reached (617°C).

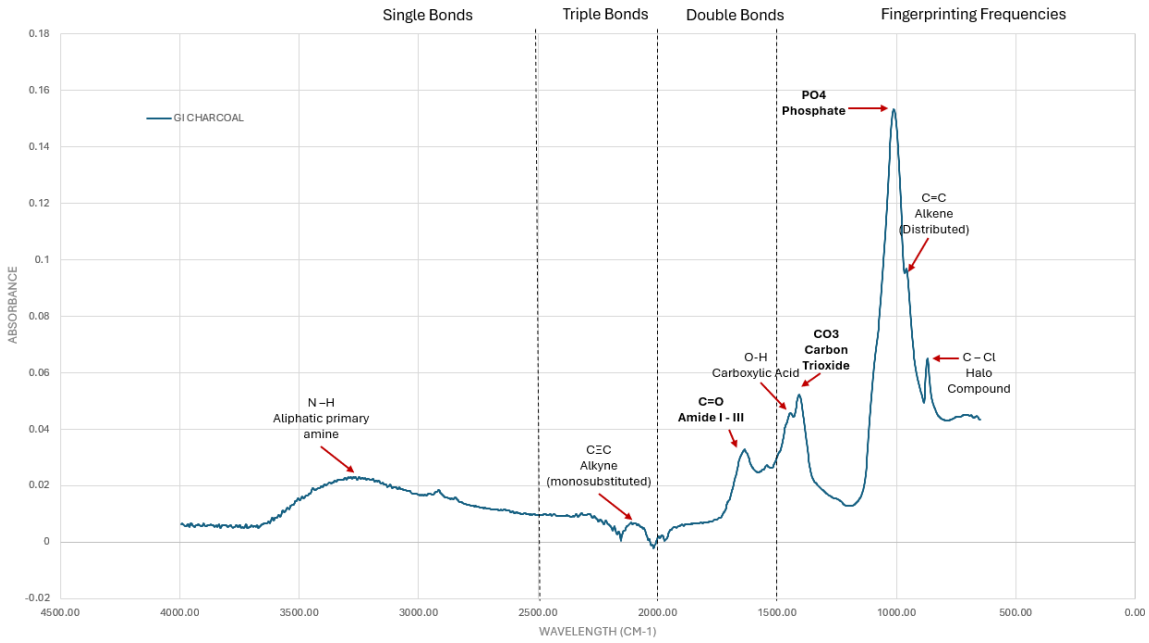

Figure 19: Average ATR-FTIR spectra of the femur sample placed in the Garden incinerator using charcoal as the ignition source and burned at ~617°C. Showing a trend towards a consistent peak in PO_4^{3-}, when compared to other samples, and continued higher level of C-H Alkynes due to presence of some organic materials.

Figure 20 is an accumulation of all samples for comparison.

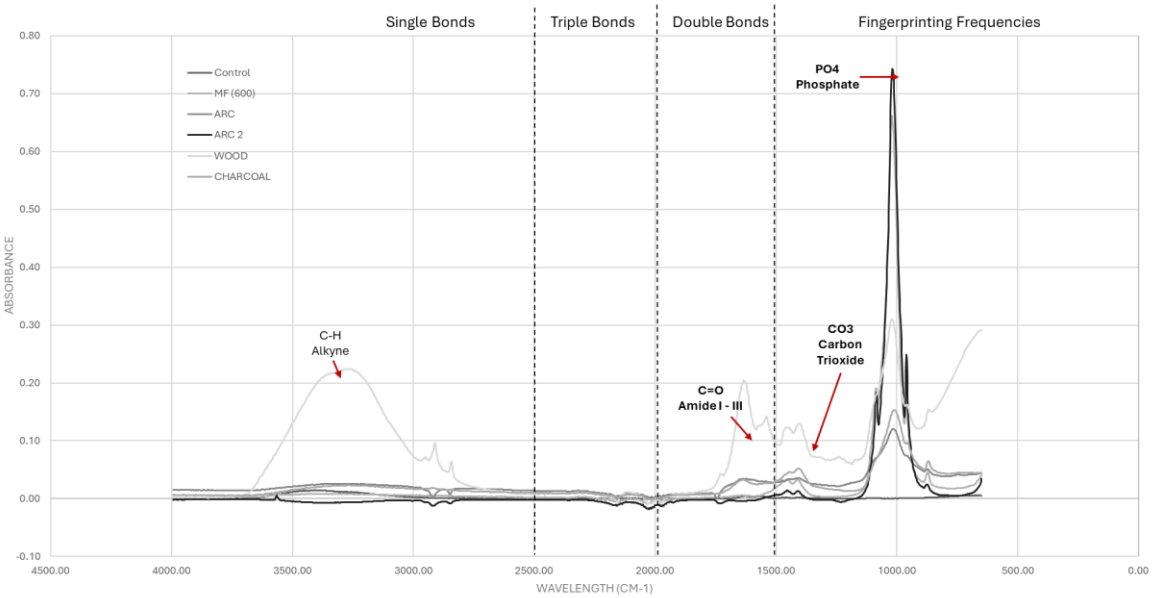

Figure 20: ATR-FTIR spectra of each sample for comparison.

3.3.3 XRF

Table 14 depicts the concentrations of elements within each of the femur samples. There is an expected decrease in the majority of the elements and minerals in the samples, some with a complete loss. Focusing on Calcium, as mentioned in the results of ATR-FTIR, the decreased but remaining volume of calcium within the sample can allude to the start of calcination of the sample. Comparing each sample, there is a loss of calcium from the control to the sample of the muffle furnace, at 600°, with a loss of 2.544%, whereas when comparing the sample with the average result from the open flame fire there is an increase of 0.035%.

Similarly, the levels of Phosphorous (P) show alterations throughout each burning process. Primarily, there is a notable increase in the levels of P when exposed to the direct heat of the muffle furnace, with an increase of 3.975% and a lesser increase of 0.65% in the open flame fire. As for the samples in the garden incinerator, there is an evident increase in the levels of P with an increase of around 7.2% when burned with charcoal, however a notable decrease of 13.62% with wood. Each reading signified a change within the levels and potential size/structure of the crystalline hydroxyapatite components within the sample.

As seen in table 14, Cerium, Neodymium and Bromine are neither present within the control or muffle furnace sample. The readings of each element appear to be present, solely, in the open flame fire and garden incinerator results. Although reading at 0.000% in some cases, trace amounts of the element must be present for the XRF to decipher its presence. Further investigation has found each of the elements mentioned correlate with the ignition source and surroundings used in the open flame fire. Cerium was found to be used in lighter flints, the source of ignition in each of the fires, whilst bromine and neodymium were each related to surrounding materials such as electrical equipment, Neodymium, and fire-resistant materials in soft furnishings, Bromine.

Table 14: XRF readings of element concentration in femur samples from each burning method. See appendix 1 for raw data including all detected elements.

Element	**Control (%)**	**Muffle furnace (%) (600°C)**	**Open flame (%) (612°C)**	**Open flame 2 (%) (623°C)**	**Garden incinerator Wood (%) (625°C)**	**Garden Incinerator Charcoal (%) (617°C)**
Phosphorous (P)	15.238	19.213	15.888	8.520	13.162	16.415
Calcium (Ca)	82.661	80.117	82.696	86.561	81.953	82.619
Cerium (Ce)	N/A	N/A	0.000	N/A	N/A	N/A
Neodymium (Nd)	N/A	N/A	0.000	0.001	0.002	0.002
Bromine (Br)	N/A	N/A	0.030	0.016	0.002	N/A

Tabel 15 shows samples treated in a muffle furnace from 300°C to 900°C in 150°C increments. The results show the phosphorus (P) content increased throughout the temperatures when compared to the control, rising from 14.38% to values between 17.8–18.4% across all temperatures. Calcium (Ca) concentrations ranged from 76.87% in the control to between 80–81% after heating, showing only minor variations across the different temperatures. Trace elements such as cerium (Ce), neodymium (Nd), and bromine (Br) that were previously detected in other burning methods, were not detected in any of the samples.

Table 15: XRF readings of element concentration in femur samples from each temperature in the muffle furnace. See appendix 1 for raw data including all detected elements.

Element	**Control (%)**	**300°C (%)**	**450°C (%)**	**600°C (%)**	**750°C (%)**	**900°C (%)**
Phosphorous (P)	14.383	18.206	17.808	18.428	18.104	18.383
Calcium (Ca)	76.874	80.282	81.436	80.723	81.192	80.605
Cerium (Ce)	N/A	N/A	N/A	N/A	N/A	N/A
Neodymium (Nd)	N/A	N/A	N/A	N/A	N/A	N/A
Bromine (Br)	N/A	N/A	N/A	N/A	N/A	N/A

The results of this study support the hypotheses stated in 1.6.1, therefore rejecting the null hypothesis that the effects of high heats and fire would have no effect on the morphological and macroscopic aspects of the samples. There is also further support of the sub-hypotheses as the results found a clear alteration in the colour of the bone once exposed to high temperatures and will increase the fragility of the bone (fig.13), also supporting the sub-hypothesis that the exposure will alter the organic/inorganic index within the bone samples (fig 14 – 20).

3.4 Discussion

Attenuated Total Reflectance Fourier Transform Infrared Spectroscopy (ATR-FTIR) was used to examine changes in the organic and mineral phases of bone. This method provides valuable information on crystallinity index, carbonate (CO_3) and phosphate (PO_4^{3-}) content, and other mineral changes within the bone matrix (Legan et al., 2020). Thompson et al. (2009) found that

crystallinity varies by bone type and is strongly influenced by temperature, consistent with the results of this study.

Figures 14 – 20 illustrate mineral variations across the samples. A notable reduction in carbonate (CO_3) and other carbon-based absorptions was observed between the control and muffle furnace samples, suggesting that direct heat at 600 °C initiated the decomposition stage of the organic materials. A similar but less pronounced loss of collagen was seen in the ARC sample, likely due to the variable, less controlled conditions of open-flame combustion in the garden incinerator, which reached peak temperatures of approximately 612 °C and 623 °C.

Irregular absorbance patterns appeared in the open-flame samples, potentially indicating additional compounds or trace contaminants absorbed during burning. These may have originated from surrounding materials such as household waste, plastics, or treated fabrics. Such secondary absorptions could offer valuable forensic insights when reconstructing the circumstances of burning.

Comparing figure 16 and 17, revealed a much more significant loss in the secondary burning. This could result from a higher maximum burn temperature, closer proximity to the ignition source, or bone differences, such as density, porosity, or initial mineral composition, that influence thermal degradation rates. The near-complete loss of organic material in figure 17, including collagen, portrayed by absent amide bands, suggests advanced combustion and the onset of calcination. The continuous depletion of CO_3 indicates notable mineral reorganisation consistent with exposure above 600 °C. These observations highlight both environmental and sample-specific variability in post-burn bone characteristics.

Reductions in Amide I, II, and III peaks throughout the figures further confirm collagen loss (Gallo et al., 2021). The amide bands, Amide I (C=O stretch), Amide II (C–N stretching and N–H bending), and Amide III (C–N and N–H stretching with C–Cα stretch), are established markers of collagen in bone (Paschalis et al., 2011). Absorbance in the 1200–1700 cm^{-1} range reflects the

mineral-to-collagen ratio and serves as an indicator of bone mineral density. While ATR-FTIR effectively captures the trends, its interpretation increases when applied alongside other mineral-based techniques (Paschalis et al., 2011).

Finally, ATR-FTIR revealed a substantial increase in PO_4^{3-} content, particularly in the muffle furnace sample (Figure 15), where absorbance rose from 0.08 to 0.65, approximately a 712% increase. This suggests significant growth in hydroxyapatite crystallinity, which intensifies when bone is heated above 500°C (McKinnon et al., 2020). This distinction is forensically relevant as bones burned below 500°C may retain features of fresh remains, whereas higher temperature burns cause more extensive structural changes that require more concentrated analytical approaches.

The detection of cerium (Ce), bromine (Br), and neodymium (Nd) exclusively in the open-flame and garden-incinerator samples, in table 14, indicates that these elements were likely absorbed from nearby materials or introduced via the ignition source, this idea is also furthered when analysing the muffle furnace results in table 15, in which no ignition source was used. In the open-flame scenario, ignition was achieved using a butane cigarette lighter, a highly flammable hydrocarbon alkane (C_4H_{10}) commonly found in residential fires (Murphy, 2006). The presence of cerium, a lanthanide metal, is consistent with its role in mischmetal alloys used in lighter flints, which create sparks to ignite flames (Zhang, et al. 2016). Its absence in the garden-incinerator samples, where a lighter was not used, supports this origin. This represents a novel finding of cerium in burned bone attributable to the ignition source and surrounding materials, with potential forensic applications.

Bromine detected in the open-flame samples likely reflects the presence of brominated flame retardants, commonly incorporated into household furnishings such as sofas (Suzuki, 2009). This occurrence has grown more common due to recent initiatives promoting recycled materials in consumer products (GOV.uk, 2024). Its presence aligns with the residential fire setting used in the experiment, providing a realistic scenario and offering insight into sample placement and materials that were present before the fire. Such findings can be critical in medicolegal investigations for

reconstructing fire origins and understanding the context of the fire and its intent, i.e., accident or arson. While the detection of bromine in burned bone is also a novel observation with possible forensic relevance, further research is required to confirm these associations.

Trace neodymium may originate from small household electronics, such as televisions or other electrical equipment, that frequently use this element in their manufacturing (Royal Society of Chemistry, 2024). Alternatively, Nd could be introduced from the XRF instrument itself, as certain laser-grade glasses in the device contain neodymium. Despite using powdered samples to reduce the chances of contamination, XRF use remains susceptible to analytical variability due to preparation techniques, particle size, and moisture content (Ben et al., 2022). The detection of both bromine and neodymium in the garden-incinerator samples requires further investigation to determine whether they were detected from environmental factors or instrumentation. Given that powdered samples were prepared following XRF guidelines, the detected elements most likely reflect absorption from the ignition source, nearby materials, or the burning container itself.

XRF proved effective for detecting and quantifying elemental changes in burned bone, particularly shifts in calcium and phosphorus concentrations, as seen in tables 14 and 15, but there are also limitations. As a bulk elemental analysis method, XRF lacks the spatial resolution to detect microstructural or localised changes (Latahir et al., 2025). SEM-EDX, though more time-consuming and requiring destructive preparation, offers high-resolution imaging with point-specific elemental data (Rades et al., 2014). This enables detailed examination of surface morphology, detection of micro-cracks, heat damage, and embedded contaminants. Rades et al. (2014) demonstrated the value of SEM-EDX in distinguishing heat-induced diagenetic changes from post-depositional contamination in thermally altered archaeological bone. While XRF is rapid and non-destructive for overall composition analysis, combining it with SEM-EDX would enhance interpretation in cases requiring fine-scale structural or chemical detail.

Incomplete combustion is another factor relevant to these findings. In oxygen-limited conditions, such as extinguished fires, the reaction:

$$\text{Fuel} + O_2 \rightarrow CO + CO_2 + H_2O$$

may stall before full oxidation, causing organic components such as collagen to undergo pyrolysis into smaller hydrocarbons and alkynes (Wang et al., 2021). Depending on burn temperature and duration, the compounds may persist in trace amounts. Incomplete combustion can also partially degrade the bone matrix, reducing density and increasing fragility through mineral loss. From a forensic standpoint, this can obscure molecular markers, complicating DNA recovery and biomolecular analysis (Krap et al., 2019). This is particularly relevant here, as open-flame burns were actively extinguished, whereas garden-incinerator burns ceased more gradually. Further analysis of the subtle ATR-FTIR vibrational features observed in this study may reveal evidence of incomplete combustion.

Chapter 4

Analysis of Sharp Force Trauma on Porcine Bone

Chapter 4: Analysis of Sharp Force Trauma on Porcine Bone

4.1 Introduction

Sharp force trauma is a significant focus in forensic investigations, particularly in cases involving homicide or accidental injury. Understanding the characteristics of sharp force trauma is crucial for accurate interpretation of injured skeletal remains (Waltenberger, et al. 2020).

This study aims to investigate the morphological and histological features of sharp force trauma inflicted on porcine bone. By analysing cut marks under various conditions, with the use of 3D microscopy and X-Ray, we seek to enhance the forensic community's ability to differentiate between trauma types and to understand the implications of such injuries on skeletal remains.

Cause of death can be broadly divided between internal or external factors. Internal causes relate to biological reasons such as disease, cancers and other pathological ailments, whereas external factors are often represented as trauma and relate to externally caused injuries to an individual. Those classed as trauma are further split into categories depending on how the trauma has been applied and the injuries sustained. Types of trauma typically involve blunt, sharp, thermal, and firearm (Eze & Ojifinni, 2022). Each type of trauma is differentiated by its associated injuries, with some further categorised by severity. Blunt force trauma is the result of coming into contact with a blunt or solid item with a certain level of force that can result in a range of injuries depending on the level of impact. This ranges from bruising of the surface layer of skin to fractured/splintering bones beneath the skin, whilst sharp force injuries are the result of contact with sharp edged objects resulting in penetration of the skin, less severe sharp force injuries also include bruising, along with an abrasion of the skin. However, further impact can result in lacerations of the soft tissue and potential fractures to the bone. Firearm injuries are the result of a gunshot wound either grazing the skin or penetrating the skin and causing an internal injury to the soft tissue and bone. As for thermal trauma, similar to other types, the injuries can depend on the severity of the initial trauma i.e., the temperature / fire experienced, and can range from singed/damaged skin to higher degree

burns in which the soft tissue is removed, and bone is affected (Eze & Ojifinni, 2022). See 1.3 for full trauma analysis details.

Further investigations have also determined additional types of trauma including chemical, electrical, radiation explosion, and asphyxia. Chemical trauma categorises injuries due to exposure to toxic substances harmful to humans by either contact or ingestion. Electrical trauma, arguably related to thermal trauma, is the result of contact with electrical currents passing through an individual's body resulting in death, also known as electrocution (Dokov, 2009). Radiation, similar to chemical, is the exposure to harmful substances, however on a much higher scale, as substances include the output of chemical processes such as ionising radiation (Cohen-Jonathan, et al. 1999). Finally, death by asphyxia, similar to blunt trauma, is the result of an inadequate level of oxygen in the body resulting in bodily systems to shut down, this can be the results of hanging, choking, or being crushed by large objects impairing breathing (Houck & Siegel, 2015).

The classification of external causes is essential for public health surveillance, as it aids in identifying patterns and implementing preventive measures. In forensic investigations, accurately determining the cause of death involves a comprehensive analysis of medical history, scene examination, autopsy findings, and toxicological studies. This multidisciplinary approach ensures that all potential factors are considered, leading to a precise and reliable determination of the cause of death.

In many European countries, sharp force trauma is the leading cause of death in a homicide, ranging from 30-40%, for example 27% in Norway and 37% in Sweden (Handlos, et al. 2023). In England and Wales, in 2023, 283 deaths were caused by direct contact of sharp force trauma. This included aspects such as intent of self-harm with a sharp object, which equated to around 44% of all sharp force trauma deaths and is the primary cause of death due to sharp force, or assault by sharp object, such as an aggravated stabbing, which has been recorded at a quarter of all sharp force related fatalities. It was also determined that 74% of knives used in aggravated assaults were a pointed kitchen knife, a commonly found household object (Farrell & Davies, 2025). Figure 21

shows the trend of sharp force trauma deaths by year within England and Wales, in 2013 - 2023 (ONS, 2023).

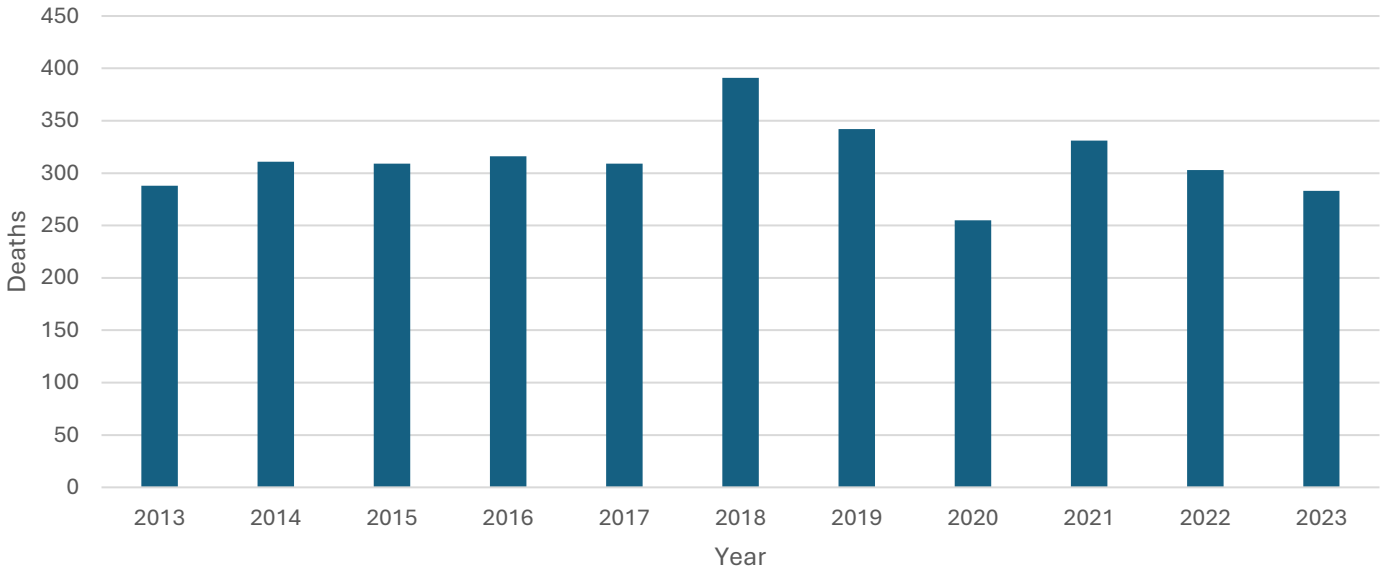

Figure 21: Sharp force trauma fatalities over an 11-year period in England and Wales (ONS Statistics, 2023).

Forensic investigations take multiple steps to identify and determine the cause of death by sharp force trauma, including the thorough analysis of the cut mark itself to determine specifics about the potential weapon used, this is often highlighted through understanding of the kerf.

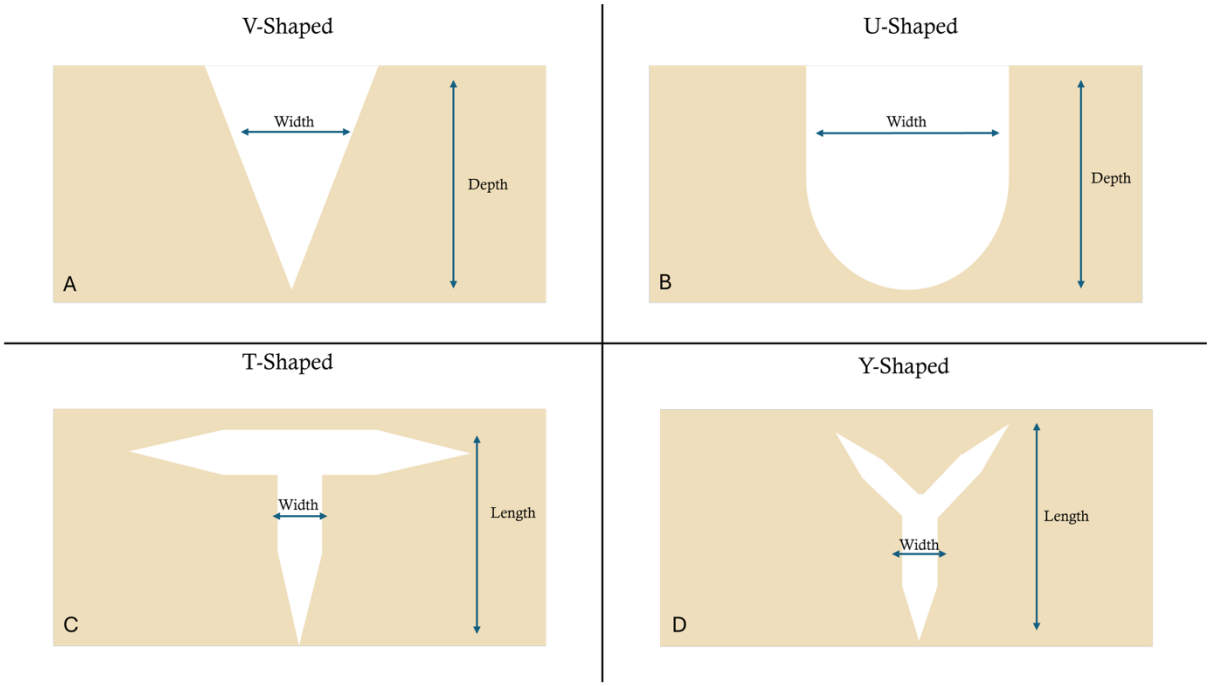

Figure 22 shows the differentiation between a V-shaped (A) and U shaped (B) kerf cut marks. C/D represent the resulting Y-shaped and T shaped surface layer marks depending on the type or knife used, serrated or non-serrated.

A kerf in a bone cut mark refers to the groove or incision left in the bone when it is cut with a tool and is typically V-shaped, U-shaped (Vachirawongsakorn et al., 2021). Certain stab wounds have also shown T-shaped, or Y-shaped incisions on the surface, depending on the type of knife used, serrated or non-serrated (Thompson and Inglis, 2009) (see figure 22). The width and depth of the kerf correspond to the tool's size and the force applied during the cut. Different types of blades leave distinct impressions on bone. For example, serrated knives tend to produce U-shaped kerfs with pronounced striations, while non-serrated knives often leave V-shaped kerfs with smoother walls (Thompson and Inglis, 2009, Ghui, et al. 2023). Kerfs may also exhibit flaking along the edges and striations, which are small scratches that can reveal the motion of the cutting tool (Love, 2019). The angle and characteristics of the kerf, in Table 16, can help forensic experts identify the tool used and determine the cutting technique. Analysing the features of the kerf can provide valuable information in forensic investigations, helping to distinguish between different types of

injuries and offering clues about the method and direction of the cut, alongside characteristics and similarities and differences between weapons (Bailey et al., 2011).

To enhance the accuracy and reliability of kerf analysis, forensic scientists employ advanced imaging techniques. Scanning Electron Microscopy (SEM) is particularly valuable for examining the fine details of kerf walls. SEM allows for the observation of microscopic features such as striations and grooves, which can be indicative of the blade's edge and the manner of cutting. Additionally, three-dimensional imaging methods like Micro-CT scanning provide non-destructive means to analyse kerf characteristics. These techniques enable the visualisation of the kerf's depth and the spatial relationship between the cut and surrounding bone structures, offering a comprehensive view of the injury (Love, 2019).

While kerf analysis provides valuable information, it is most effective when combined with other investigative methods. Forensic anthropologists often correlate kerf characteristics with other evidence, such as the presence of bone fragments, the pattern of injuries, and the context of the scene. By integrating kerf analysis with these factors, investigators can develop a more complete understanding of the events leading to the death.

Table 16: Cut mark characteristics and descriptions provided by McCardle & Stojanovski, 2018.

Characteristic	Description
Flaking	Small pieces become separated from the bones surface resulting in multiple flakes and scarring of the bone.
Feathering	Lateral rising of the bones surface layer in a feathered pattern.
Peeling	Lateral raising or 'peeling' from the bones surface. Also known as an incomplete/hinge fracture.

Micropeeling	The process of 'Peeling' to a scale of <1mm.
Microcurvature	Curving away from the edge of the cut mark at the entry point.
Scoop defect	A concave effect due to the removal of a fragment/wedge of bone during the removal of the weapon from the cut mark.
Exit notch	A fragment/wedge of bone removed from the posterior of the cut mark.
Chattering	Small fragments/chips in the bone break off around the edges of the cut mark.

A recent study has found the characteristics of cut marks and corresponding knives may be differentiated via a flowchart (figure 23); the deciphered traits of the weapon via the cutmark was shown to be a valuable and employable tool when performing cut mark analysis on straight-edged vs serrated knives. However, further work and investigation is needed for differentiation between varying serrated knives. (Ghui, et al. 2023).

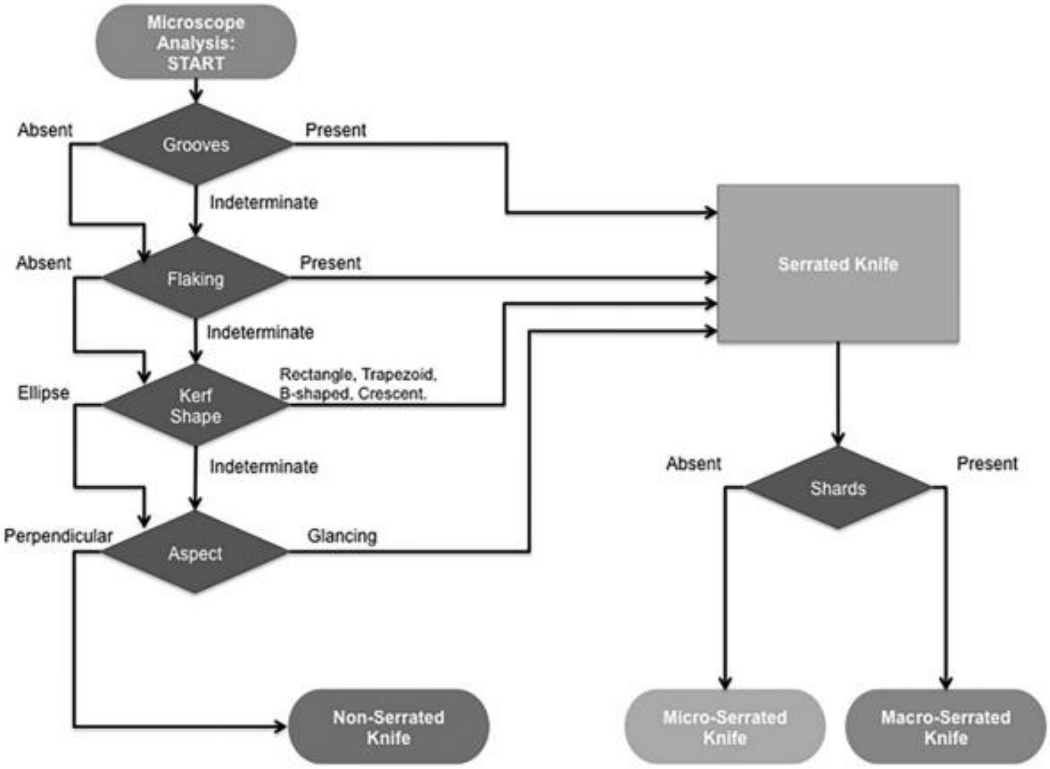

Figure 23: Differentiation of knife type (Ghui, et al. 2023)

4.2 Method

4.2.1 Sample Selection and Preparation

Porcine bone samples were used due to ethical restrictions on human bone and ease of access, sourced from a local butcher. Sample types included two femurs, two scapulae, and two skull segments. Where necessary, maceration was performed using 50 ml of Persil non-bio detergent per bone to remove flesh without damaging the bone (see Section 2.2.1). Remaining tissue was carefully removed with scalpels and tongs. Surface inspection ensured bone integrity, with any damaged samples excluded.

4.2.2 Trauma Application

Three cut marks were applied per sample using three household knives: straight-edged blade, serrated steak knife, and large serrated bread knife (Table 17). Serrated knives were applied with a

pull motion, and the straight-edged blade with a push, one forceful application per cut. Each sample received three cuts from each knife, totalling nine cuts per sample. Blade dimensions are summarised in Table 17.

Images of each knife can be found below, figures 24 - 26.

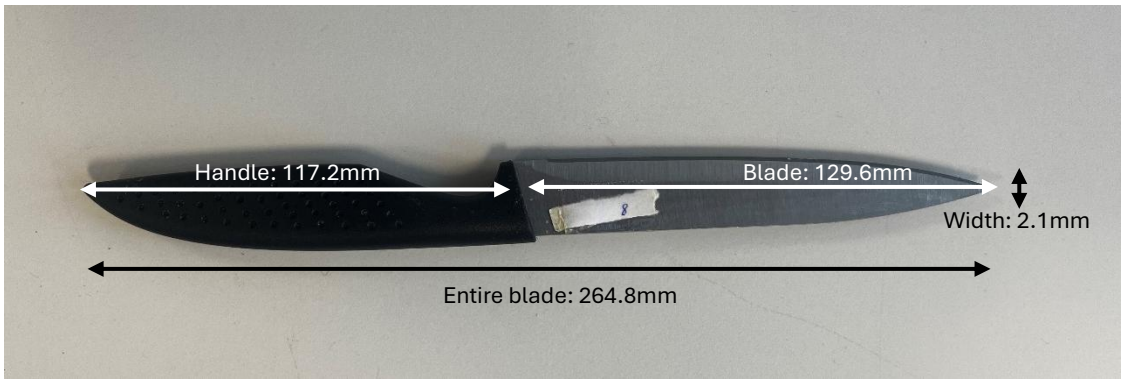

Figure 24: Straight edged blade: 129.6mm long and 2.1mm wide, including a 117.2mm handle, as this is non-serrated there are no teeth on the blade to measure the distance.

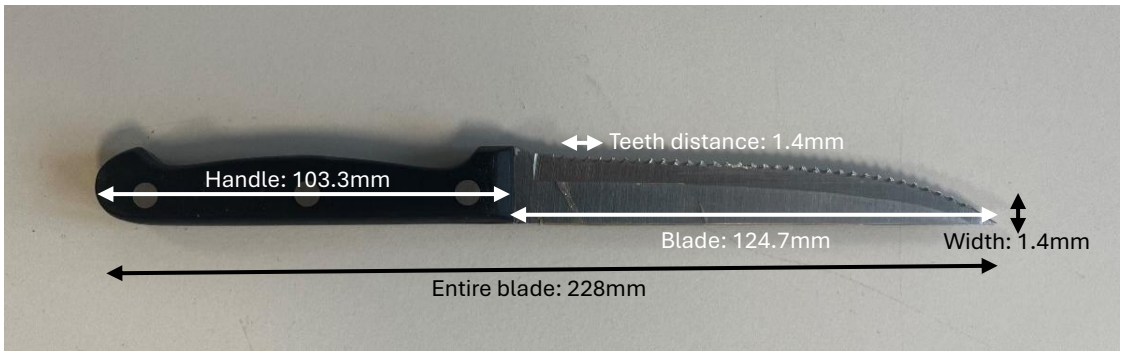

Figure 25: Serrated knife: 124.7mm long and 1.4mm wide, with a 103.3mm handle. The teeth measured approximately 1.4mm apart.

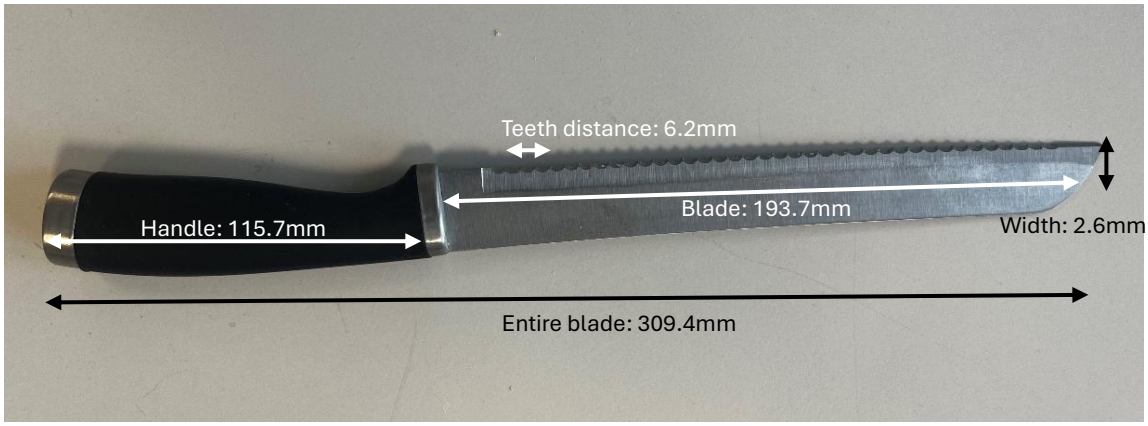

Figure 26: Large, serrated knife: 193.7mm long and 2.6mm wide, with a 115.7mm long handle. The teeth measured at 6.2mm apart.

Table 17: Measurements of each knife used including blade length/width, handle length and distance between teeth (mm).

Smooth edge blade	
Blade length	129.6mm
Blade width	2.1mm
Handle length	117.2mm
Teeth distance	N/A
Serrated steak knife	
Blade length	124.7mm
Blade width	1.4mm
Handle length	103.1mm
Teeth distance	3mm
Large, serrated bread knife	
Blade length	193.7mm
Blade width	2.6mm
Handle length	115.7mm
Teeth distance	6.2mm

4.2.3 Analysis

Cut marks were examined using a Keyence 3D microscope, producing high-resolution images and 3D reconstructions. Maximum magnifications were adjusted according to sample size: femur ×60, skull ×80, scapula ×40. Cut mark volumes were measured three times per cut, with mean values calculated using the formula:

$$V=\pi r^2 h/3$$

where r is half the measured width and h is the height of the cut.

4.3 Results

4.3.1 3D Microscopy

Images of the cut marks show a clear distinction between the types of knives used. Figures 27 - 29 show each of the cut marks with distinct characteristics depending on the knife. Cut marks created by the smooth-edged blade, on average, show more precise cuts with less striations and deviations than when compared to the cuts produced with the serrated and large serrated knives. The cut marks created with the serrated knife show a 'rougher' cut throughout the sample, along with the presence of flaking and feathering along 70.8% the kerf walls. Those created with the large, serrated knife show distinctly deeper cuts from the surface with similar levels of flaking, when compared to the cuts created by the serrated knife. Overall, most samples exhibit examples of flaking or peeling, however, some samples, particularly the cuts created by the large, serrate knife, portray scoop defect characteristics (an example of scoop defect can be seen in Appendix 3 B B). Contrary to this, the cut marks created by the smooth edge blade remained mostly intact with larger, singular examples of flaking, most likely due to the lack of rigidity in the blade providing a smoother cut and therefore less damage.

Figure 27 shows examples of cut marks for each type of knife applied to femur sample. Overall, there is a clear distinction between the cuts produced via either a smooth, serrated or large serrated blade, this is also reflected in the size of the cuts shown in table 18 and the overall averages in tables 21 - 22. The cuts produced by the smooth-edged blade show a much more precise cut with a definitive 'v' shape in the bone with some evidence of flaking/feathering. Cut marks produced by each of the serrated knives show more notable evidence of flaking, and some peeling.

The scapula samples in figure 28 show more depth in the shape of the cut marks for each knife types, when compared to other samples. The cut marks created by the smooth-edged blade continue to show a visible 'v' shape, again with some flaking in the sample. The cut marks produced by the serrated knives show increased levels of flaking and peeling. The serrated knife

cuts also, on average, create much deeper cuts within the scapula, as some samples show evidence of representing a scoop defect/peeling characteristic.

Overall, the skull samples in figure 29 show similarities in each of the cut marks created. The smooth-edged blade shows angled cut marks with little flaking and some evidence of peeling / micro-peeling along the edges of the cuts. Those created by the serrated knives show much deeper cuts, also seen in table 20, with clear evidence of flaking and some scoop defect characteristics in those created by the large, serrated knife

Further images of the cut marks produced can be seen in Appendix 2.

Table 18 shows Femur sample cut mark measurements for each type of knife used.

	Cut mark (μm^3)		
Smooth	322.51 x 262.78	645.97 x 617.91	533.89 x 527.92
Serrated	730.26 x 699.14	925.22 x 521.14	972.45 x 667.14
Large, Serrated	1080.35 x 1092.87	1184.64 x 1169.39	1118.97 x 1109.70

Table 19 shows Scapula sample cut mark measurements for each type of knife used.

	Cut mark (μm^3)		
Smooth	383.03 x 379.14	457.19 x 448.81	669.23 x 510.09
Serrated	602.48 x 564.65	1065.36 x 711.33	969.60 x 763.14
Large, Serrated	1131.17 x 1084.96	674.33 x 561.79	1092.91 x 874.23

Table 20 shows Skull sample cut mark measurements for each type of knife used.

	Cut mark (μm^3)		
Smooth	294.93 x 192.65	948.91 x 841.79	510.41 x 523.71
Serrated	579.21 x 481.11	1331.63 x 1195.11	469.04 x 440.90
Large, Serrated	1494.39 x 1298.85	1030.56 x 762.17	751.82 x 681.69

Table 21 shows the average cut mark for each bone type depending on the type of knife used.

	Femur(μm^3)	**Scapula(μm^3)**	**Skull(μm^3)**
Smooth	3.8×10^7	2.63×10^7	1.51×10^8
Serrated	1.27×10^8	1.51×10^8	2.35×10^8
Large, serrated	3.76×10^8	2.35×10^8	3.57×10^8

Table 22 shows the average volume of each samples cut mark per bone, with all knife types accumulated.

Sample	**Average cut mark (μm^3)**
Femur	$5.19 \text{ X } 10^7$
Scapula	8.78×10^6
Skull	4.70×10^6

Table 23 shows the average volume of each sample per knife type, with all bone types accumulated.

Type of knife	**Average cut mark (μm^3)**
Smooth-edged	8.32×10^7
Serrated	1.67×10^7
Large, Serrated	1.72×10^8

As seen in table 19, the largest average cut mark is found in scapula samples, measuring at $8.78 \times 10^6 \mu m^3$ with the smallest average cut mark measurement in the ilium sample, measuring at $6.72 \times 10^5 \mu m^3$.Further calculations were completed to determine the average in cut mark volume depending on the type of knife used. Table 23 shows the largest cut mark, on average, is created by the large, serrated knife, measuring at 1.72×10^8 μm^3, this is followed by the smooth-edged blade with an average measurement of 8.32×10^7 μm^3 and finally the serrated knife averaging the smallest at 1.67×10^7 μm^3

4.3.2 Statistics

A series of ANOVA tests were conducted to evaluate two hypotheses: (1) whether cut mark volume varies according to bone type, and (2) whether it varies according to knife type. The first ANOVA produced a p-value of 0.003, below the 0.05 significance threshold, indicating a statistically significant effect of bone type on cut mark volume and leading to the rejection of the null hypothesis, the volume of the cut mark is not affected by the type of bone. The second ANOVA yielded a p-value of 0.001, also statistically significant, thereby supporting the rejection of the null hypothesis for knife type i.e., the volume of the cut mark is not affected by the type of knife. However, no significant interaction effect was observed between bone type and knife type. Taken together, these results demonstrate that cut mark volume is significantly influenced by both variables independently, but not by their combined interaction.

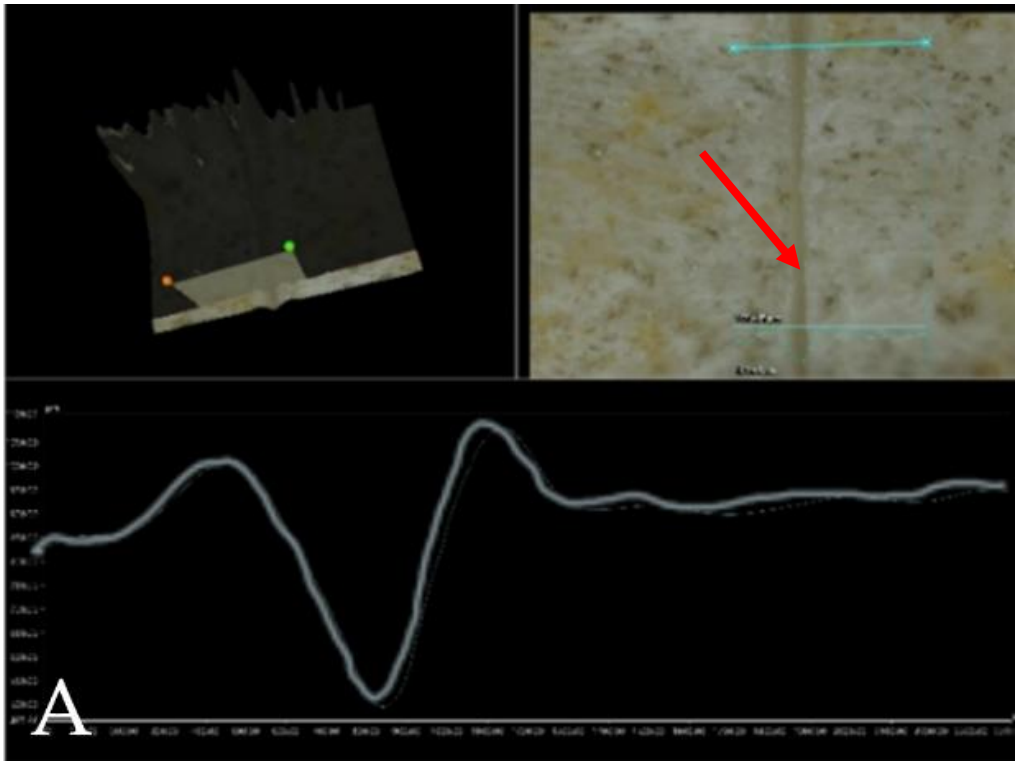
A

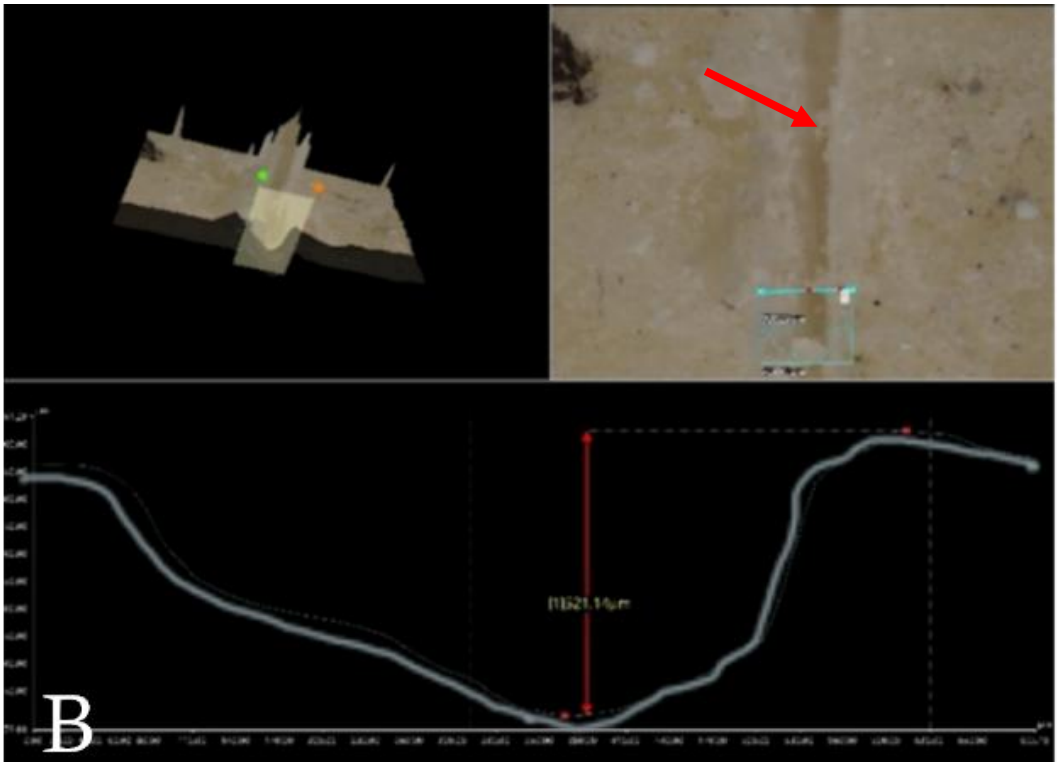
B

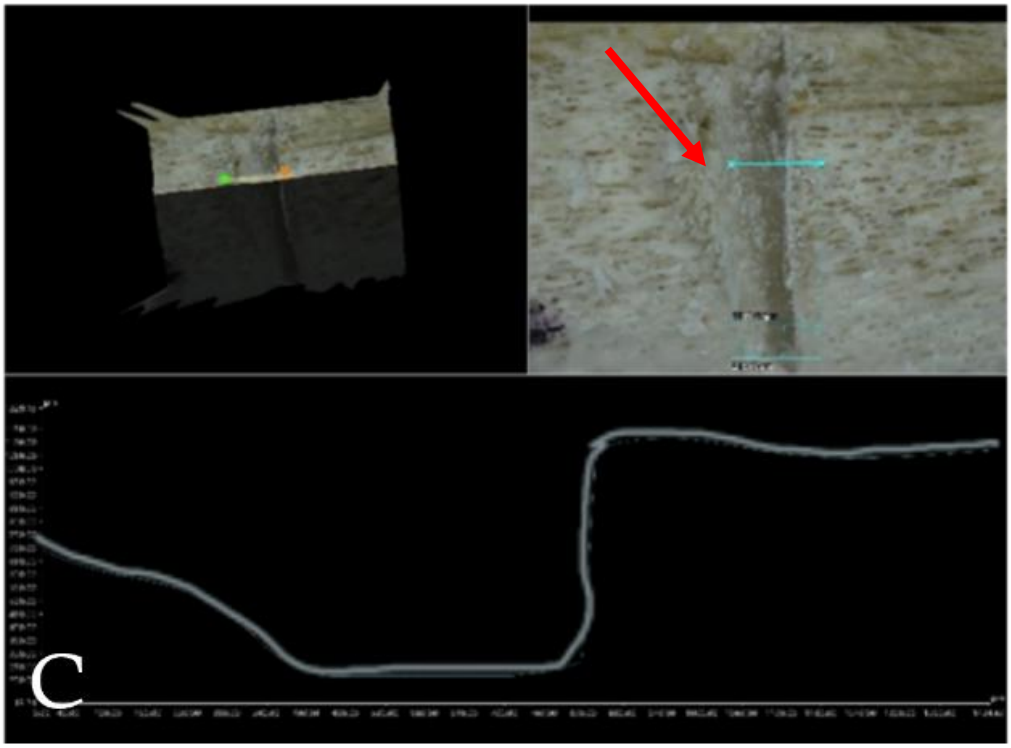

Figure 27 shows examples of cut marks produced on the diaphysis of a femur by a smooth-edged blade (A), serrated knife (B) and large serrated knife (C). A and B show signs of flaking due to the cut mark, whereas C shows signs of feathering along the kerf.

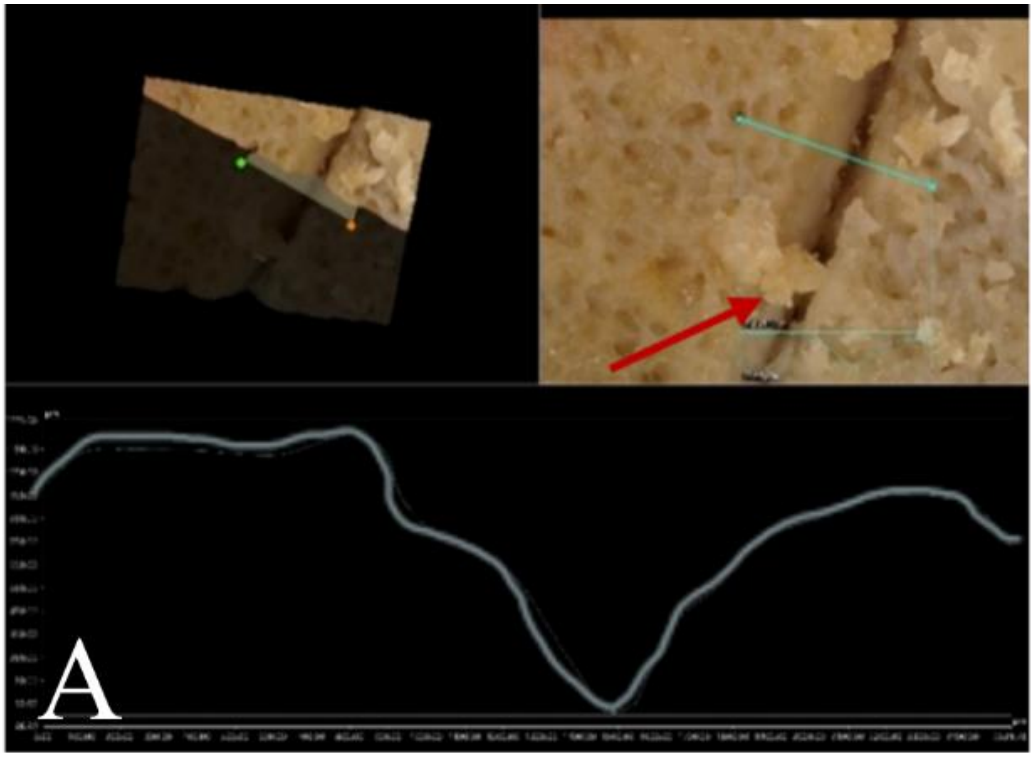
A

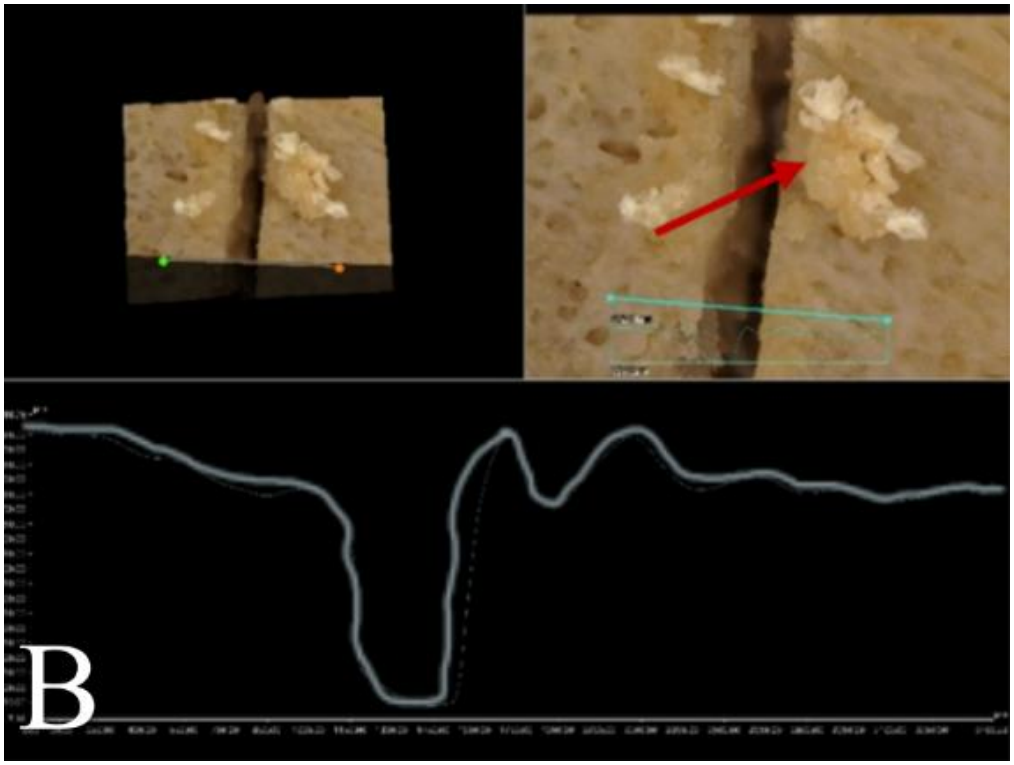
B

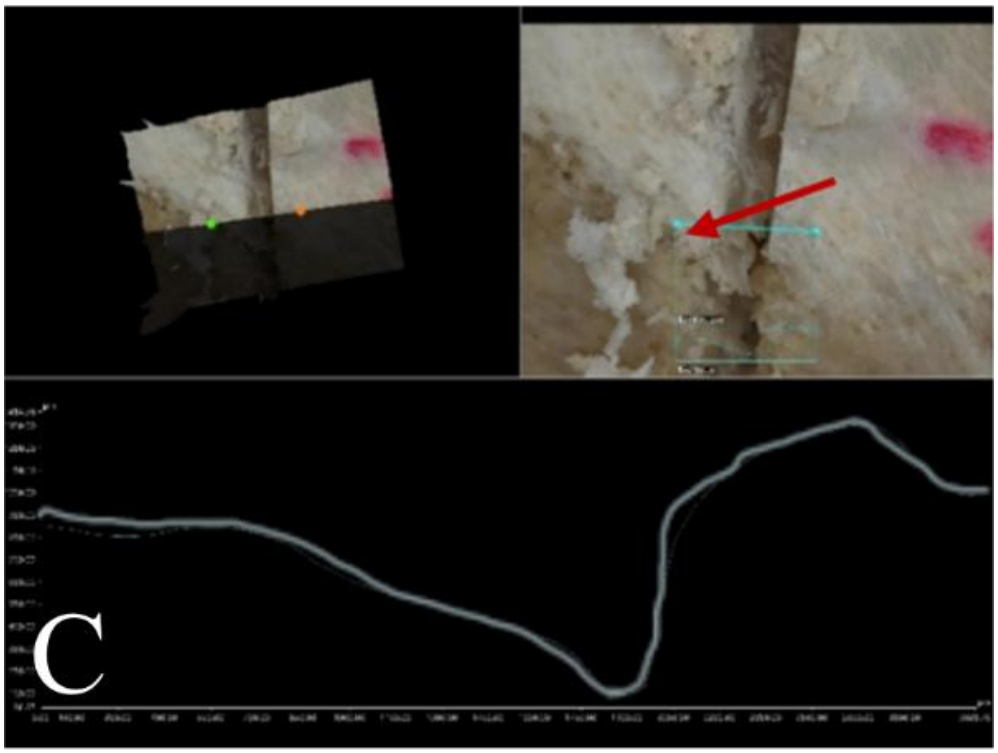

Figure 28 shows examples of cut marks produced on the scapula by a smooth-edged blade (A), serrated knife (B) and large serrated knife (C), with each highlighting clear examples of flaking, with large flakes present.

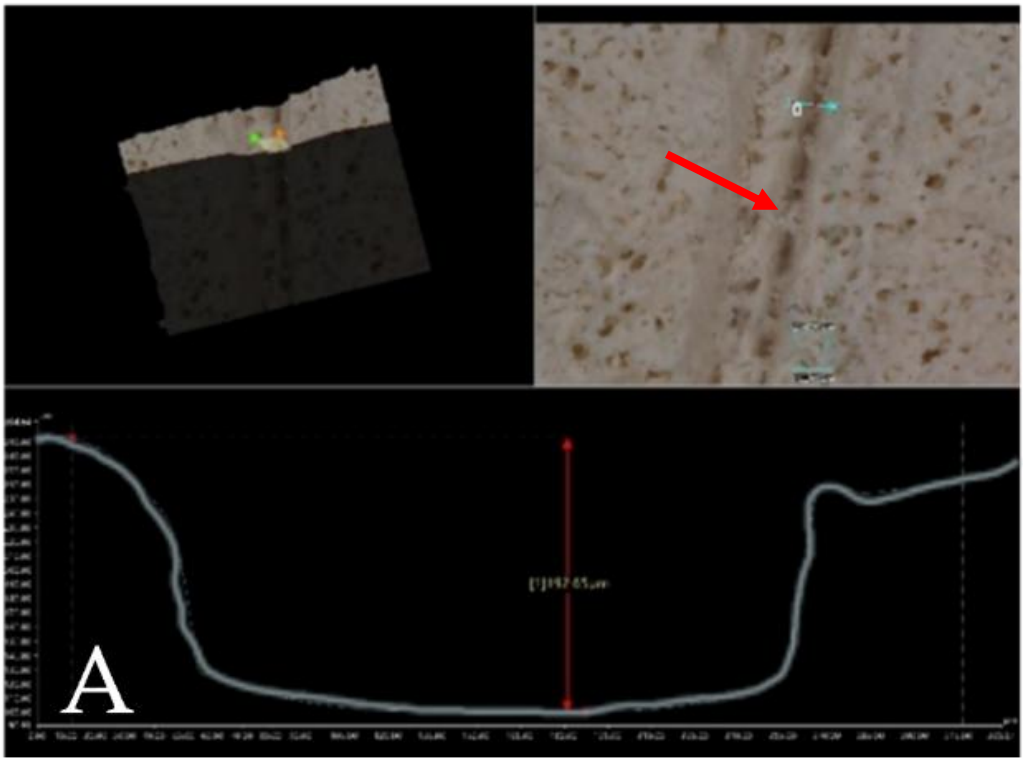
A

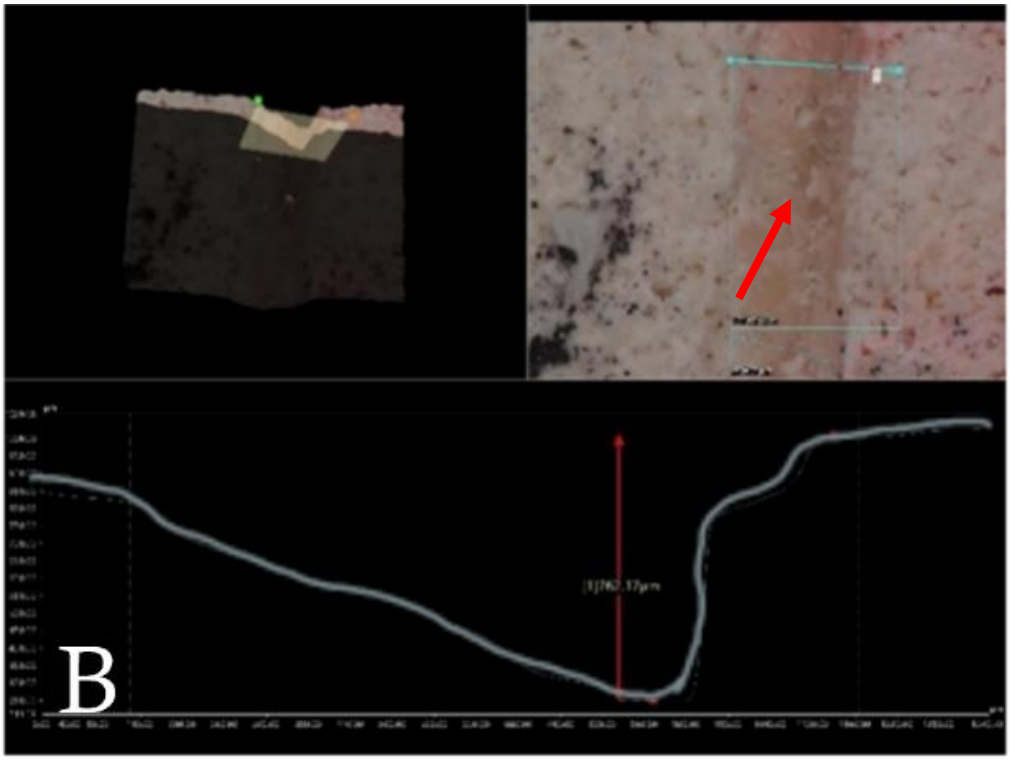
B

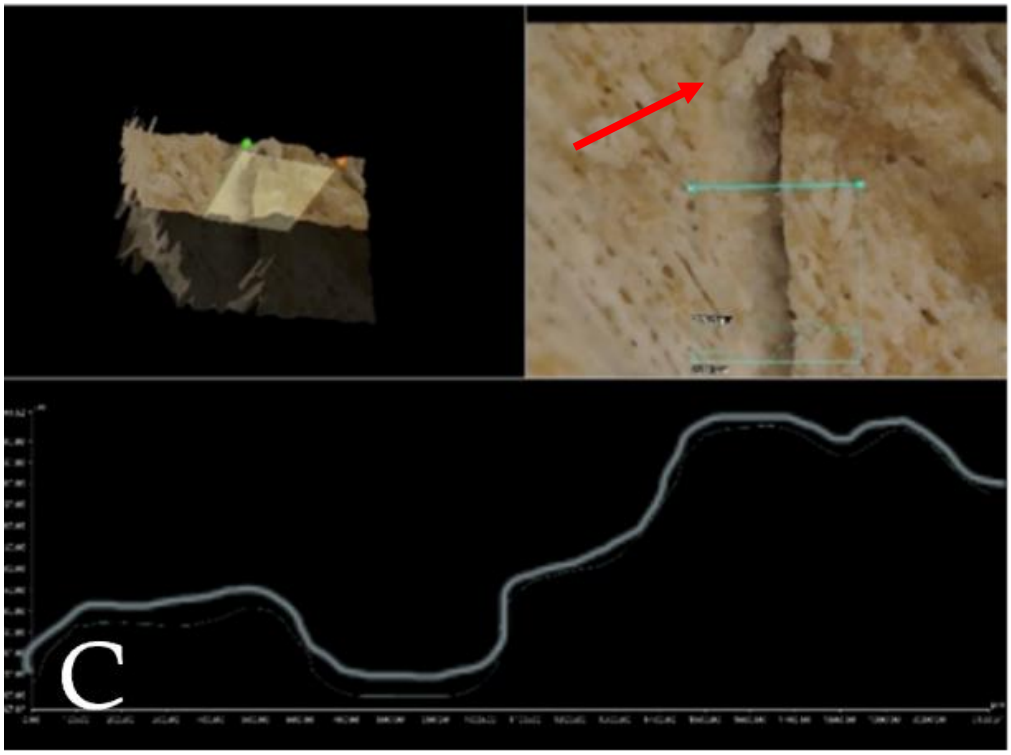

Figure 29 shows examples of cut marks produced on the frontal bone of a skull by a smooth-edged blade (A), serrated knife (B) and large serrated knife (C). Each cut exhibit examples of flaking.

4.4 Discussion

As seen in the results, there are clear statistical differences in the average volume of the cut mark when categorised by type of bone or knife used. This suggests, in a medicolegal situation where an assault has taken place, the cut mark produced may provide critical information to aid the investigation. This is also in accordance with the recent paper by Ghui et al (2023), attempting to differentiate cut marks between types of knives with a flowchart. Although the study found differences between serrated and non-serrated knives, the differences between serrated knives proved more difficult to decipher. In the present study however, the findings from serrated and larger serrated knives demonstrated a clear difference in the average size of the cut mark produced, in agreement with the findings of this study.

The statistical significance of the knife type in relation to the observed cut mark characteristics aligns with the findings of Thompson and Inglis (2009), who determined that serrated knives

produce distinct cut marks compared to non-serrated knives. They demonstrated that SEM analysis showed clear structural differences in cut marks, with serrated knives creating 'Y'-shaped incisions and non-serrated knives leaving 'T'-shaped incisions along the surface of the cut mark (Thompson and Inglis, 2009) see figure 22 for examples.

Cut mark analysis via the type of bone also provided statistically significant results with a p value of 0.001, notably below the p=0.05 threshold. This differentiation between the cut marks in each type of bone has been previously linked to the structure of the bone itself, i.e., cancellous or compact. Previous studies have found striations in the kerf wall of the cut marks depending on the type of bone used (Thompson and Inglis, 2009). The research found cancellous bone to provide clearer and more defined cut marks, although the conciseness of the kerf was found to cause more similarities than differences in the subtleties between serrated and non-serrated knives, the clear differences that have been produced can aid investigations significantly. Similarly to this present research, the cut marks produced in cancellous bones, such as the skull and scapula, resulted in a smoother and 'easier' cut, than compared to the more compact. Further comparison of cancellous vs compact bone cut marks also show notably more evidence of flaking and feathering.

Analysis of the sample characteristics revealed that approximately 24% exhibited signs of flaking, while another 24% displayed scoop defect-style cut marks. Most of the samples showing flaking were made with the serrated steak knife, while the remainder were caused by the large, serrated bread knife. This characteristic was most prevalent in the skull (77.8%) and femur (66.67%) samples.

Further analysis of the characteristics of the samples resulted in an observation of variability from the cut marks produced by the blade. As mentioned in table 16, there are multiple characteristics a kerf can possess, depending on the type of knife and bone involved. Primarily characteristics such as 'flaking' or 'feathering' would be expected in result of a serrated knife cut mark, due to the jagged line of the knifes edge. However, the results also found a clear deviation in the characteristics produced by the smooth-edged blade. Microscopic analysis found the blade cut marks met the criteria for seven of the eight characteristics, a high and unexpected variability for

one knife type. This could essentially be due to quality of the bone samples as they were collected from different locations, further work with different species remains may provide differing results for comparison. As it is porcine bone, the quality of the bone in this sense relates to the breeding, storage and preparation of the samples, however, in a forensic context, the quality of skeletal samples may relate more to identifiable characteristics of an individual such as age, lifestyle and disease/illness.

The use of a 3D microscope in this study enabled precise analysis of the cut mark morphology produced by various knives, consistent with findings from a study in 2018, by Courtenay et al. that compared cut marks, on bone from stone tools, using both 2D and 3D imaging platforms. The results indicated that while the 3D approach provided valid and reproducible results, it did not necessarily enhance accuracy (Courtenay et al., 2018). The use of 3D microscopy for skeletal analysis is a relatively new technique in forensic trauma analysis, offering various applications such as reconstructing the bone's surface in a virtual format, which allows for the collection of quantitative data on each cut mark, including characteristics like angles, flaking, and striations (Moretti, 2012).

Cut mark analysis is particularly relevant in violent crimes involving sharp force trauma, such as homicides, dismemberments, or assaults. The methods used in this study, particularly 3D microscopy, are relatively straightforward once samples are prepared, allowing for detailed analysis without excessive destructive testing. The ability to differentiate weapon types quickly can narrow investigative focus, for instance, linking an injury to a serrated bread knife rather than a smooth-edged kitchen knife. In forensic investigations, this analysis could help provide an insight into deciphering the type of weapon used if unknown, potential link to separate crimes through distinctive cut mark features, and provide information about when the cuts have been made, e.g., peri-/post-mortem.

Chapter 5

Thermal alterations to sharp force trauma

Chapter 5: How exposure to fire can alter sharp force injuries in porcine skeletal remains

5.1 Introduction

The analysis and identification of trauma are essential components of forensic investigations, as they help determine not only the cause of death but also the type of weapon involved and the manner in which an injury was inflicted. Traumatic injuries are generally classified according to the mechanism of force and the resulting characteristics of the wound. Broadly, three categories are recognised: blunt force, sharp force, and firearm trauma. Sharp force trauma, such as stab wounds, chop wounds, and incisions (Crowder et al., 2013), typically result from contact with a sharp-edged instrument capable of penetrating soft tissue. Chop wounds, inflicted by heavier tools such as axes or machetes, represent a combination of blunt and sharp force, as the weight of the instrument creates crushing abrasions while its edge produces deep lacerations. Incisions are precise, linear wounds produced by smooth, sharp blades such as scalpels, and are most commonly encountered in clinical or surgical contexts (Eze & Ojifinni, 2022).

In cases involving sharp force trauma, the resulting cut marks often display a characteristic V-shaped kerf. However, microscopic variations within these marks can offer crucial insights into the specific instrument used. These features include flaking, feathering, peeling or hinge fractures, micropeeling, microcurvature, exit notches, scoop defects, and chattering (McCardle & Stojanovski, 2018). Such details allow investigators to distinguish between different blade types and infer properties such as serration, sharpness, and direction of force.

The interpretation of trauma becomes more complex when skeletal remains have been exposed to fire. Burning causes both internal and external alterations, the most visually obvious being colour changes. As temperature increases, bone may transition from its natural off-white to black at temperatures below 400°C, dark grey around 600°C, light grey to white near 800°C, and finally calcined white above 900°C. These colour shifts reflect four progressive stages of thermal alteration: dehydration, pyrolysis, inversion, and fusion (Walternberger & Schutkowski, 2017). Dehydration at lower temperatures removes moisture and weakens the organic matrix, often

producing cracking. Pyrolysis involves the breakdown of organic components, generating gases, oils, and charcoal (Boslaugh, 2025). At higher temperatures, inversion increases the size of the bone's crystalline structures, while fusion—the final stage—leads to melting and coalescence of inorganic material, resulting in a brittle, porous, and structurally compromised residue (Thompson, 2004).

Understanding the interaction between sharp force trauma and thermal alteration is critical, particularly in cases where fire is intentionally used to obscure evidence. While many fire-related fatalities are accidental, some involve deliberate ignition aimed at destroying forensic traces, including homicidal injuries (Vachirawongsakorn et al., 2022). Examining how heat affects both skeletal tissue and pre-existing cut marks can therefore help forensic investigators avoid misinterpretation and improve the accuracy of trauma reconstruction. This research focuses on the combined analysis of sharp force trauma and thermal alteration to determine how high-temperature exposure affects the visibility, morphology, and interpretation of sharp force injuries on bone.

This study uses solely porcine samples and was inspired by a multitude of past investigations also favouring porcine bone in lieu of human samples. This is primarily due to the similar levels of soft tissue between both human and porcine samples, also the reactions when exposed to high temperatures and open flames, i.e., porosity, mineral levels and elasticity (Bonney, et al. 2020) allowing for the results to be applied to potential crime scenes.

Primarily for the thermal alterations, Agilent Attenuated Total Reflectance Fourier Transform Infrared (ATR-FTIR), and Malvern Panalytical, Epsilon 1 X-Ray Fluorescence (XRF) were used, prior to and post burning.

5.1.1 ATR-FTIR

ATR-FTIR provides an insight into the mineral content within a sample's composition. The technique provides an evaluation of the changes to a bone's mineral and matrix content (Paschalis, et al. 1996). For this study, the use of ATR-FTIR provides an understanding of the changes to organic materials within the bone sample, i,e., collagen and calcium levels. Additionally, this

method was also selected to evaluate the growth in hydroxyapatite crystalline structures and phosphate peaks.

5.1.2 X-Ray Fluorescence

The use of XRF in this study is to highlight the depletion of various minerals and elements in a bone sample when exposed to high temperatures. An XRF utilises incident x-ray beams that trigger secondary wavelengths to pass through either solid or powdered materials (Kristo, 2012). The XRF was also able to decipher additional elements in some of the samples, elements that had been essentially 'absorbed' during the burning process.

To analyse the samples portraying sharp force trauma, both Kubtec X-Ray and Keyence 3D microscopy were used, prior to and post burning.

5.1.3 3D Microscopy

Using a 3D microscope in this study has provided a detailed insight to the cut marks produced prior to and post burning. The 3D microscope provided clear images of the cut marks on each sample, with the potential of up to 500x magnification alongside a 3D recreation. Regarding forensic investigations, the use of a 3D microscope is used to analyse trace evidence as well as trauma, this includes evidence such as fibres, paint chips or soil samples (Carew, et al. 2021), Particularly for this study, the 3D microscope can recreate sharp force trauma cut marks thus bringing to light characteristics that may allude to identification of a weapon. This analysis technique was also used to highlight some of the structural changes to the samples due to the exposure to high temperatures, such as increases in porosity/dexterity, colour changes, and the beginning of calcination.

5.1.4 X-Ray

The use of an X-Ray is a common practice when analysing bone, particularly those with soft tissue intact. Favoured for its non-invasive and non-destructive approach, X-Ray analysis can provide clear images promptly with easy reproducibility (Alsulami, et al, 2022). Common

practice for the use of an X-Ray is to highlight trauma to a bone such as splinters or fractures or locating foreign objects that may have penetrated the soft tissue, other uses include alluding to the identification of an individual through specific characteristics i.e., age or sex (Alsulami, et al 2022). Specifically for this research, the appliance was favoured to highlight possible alterations to the sharp force trauma to the bone.

5.2 Method

5.2.1 Sample Selection and Preparation

A combination of fleshed (skull, thigh, leg) and defleshed (skull, mandible, tibia, fibula, femur, scapula, ilium) porcine bones was used, sourced from local butchers and abattoirs. Fleshed samples simulated realistic thermal responses at a crime scene, while defleshed samples were used to study thermal effects on sharp force trauma.

Defleshed samples were macerated using 50 ml/kg Persil non-bio detergent in boiling water, followed by careful removal of remaining tissue with scalpels, tongs, and spatulas. Visual inspection ensured bone integrity, with any damaged samples excluded (see Section 2.2.1).

5.2.2 Trauma Application

Three household knives were used: smooth-edged blade, serrated steak knife, and large serrated bread knife.

Defleshed bones: Three cuts per knife along the diaphysis (nine cuts per sample), serrated knives applied with pull motion, straight-edged blade with push.

Fleshed bones: Sharp force trauma applied with stabbing motion through flesh to contact bone.

5.2.3 Burning Protocols

Two open-flame approaches were used:

Garden incinerator: Galvanised steel chamber with charcoal or compressed wood (heat logs). Maximum temperatures: 617–625°C; burns <20 min.

Storage container: Simulated living room fire in high-strength Corten steel container, ignited via butane lighter and wastepaper bin. Temperatures: 612–623°C; burn duration 6–9.5 min. Used primarily for fleshed samples without trauma.

5.2.4 Analysis

5.2.4.1 ATR-FTIR/XRF

Defleshed samples were powdered for Agilent ATR-FTIR and Malvern Panalytical Epsilon 1 XRF analyses. Each sample was analysed three times with mean values calculated. XRF used a 5-min Omnian scan; ATR-FTIR was conducted in absorbance mode (4000–400 cm^{-1}). Control measurements were taken prior to burning for comparison (see Section 2.2.2.1 and 2.2.2.3).

5.2.4.2 X-Ray

Fleshed samples were imaged with a Kubtec Xpert X-Ray to visualise trauma to bone and surrounding tissue. Imaging parameters varied with sample size (20–90 kV / 20–180 μA).

5.2.4.3 3D Microscopy

Defleshed cut marks were examined with a Keyence 3D microscope to measure length, width, and depth, allowing calculation of conical volume:

$$V=\pi r^2 h/3$$

Magnification was adjusted to sample size: larger bones (tibia, fibula) ×40; smaller bones (ribs, vertebrae) ×80, maximum magnification ×80.

5.3 Results

Some samples did not withstand the burning process, specifically, the mandible and scapula were lost in the charcoal-based fire, while the skull was lost in the wood-based fire. As a result, certain before-and-after comparisons could not be completed. Overall, 25% of the samples were lost during burning, with a loss rate of 33.3% in the charcoal-based fire and 16.6% in the wood-based fire.

5.3.1 Thermal Alterations

5.3.1.1 3D Microscope

Structural images of each of the defleshed samples, before and after burning, show clear increases in the levels of porosity, with an increase in pore size. For example, in figure 30 (see arrows), the Fibula sample shows a tight knit structure prior to burning. However, the result of burning with wood as the fuel source has altered the sample into a much weaker structure, with a significant increase in pore size throughout. This sample also shows a change in colour to a charred dark grey with residual flecks of burned wood. Similarly for the Fibula sample burned with charcoal as the fuel source, a distinct increase in the number and size of pores can be seen, creating a much flakier and less dense structure overall. Similar changes to pore size and changes in colour can be seen in the remaining samples, throughout figures 30 and 31. Within each figure there are blank spaces, this represents the samples that did not survive the burning process and were destroyed with little to no specimen left to analyse, i.e., both the Mandible and Scapula samples did not survive the process when burned with charcoal, alike the skull sample when burned with wood.

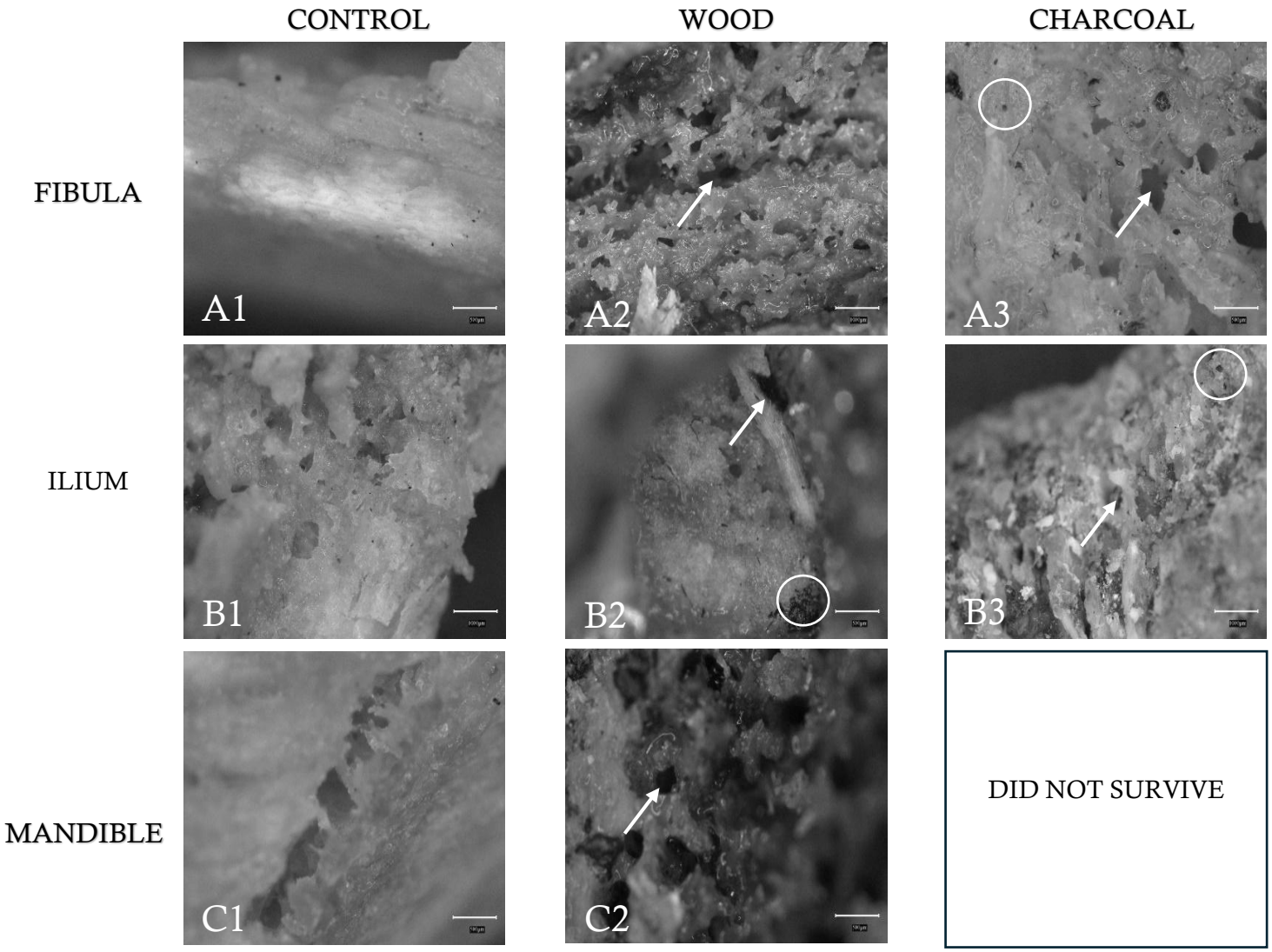

Figure 30 Structural images of each bone sample, Fibula(A1-3), Hip (Ilium)(B1-3), and Mandible(C1-2), before (control) and after being burned with either wood or charcoal. Blank spaces represent the samples that did not survive the burning process. Increased porosity is indicated by arrows throughout, with remaining 'flecks' from the ignition source circled.

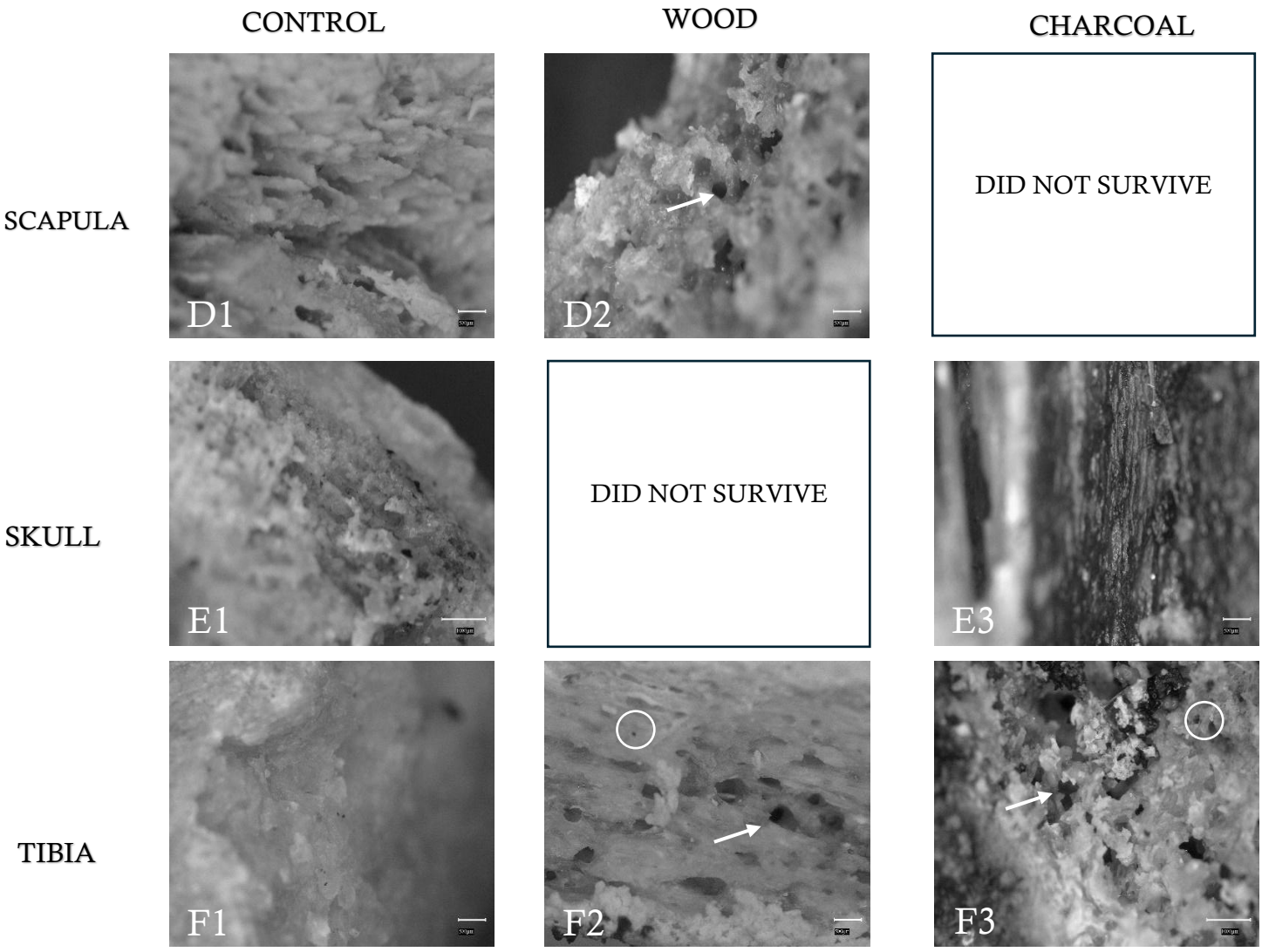

Figure 31 Structural images of each bone sample, Scapula (D1-D2), Skull (E1-E3), and Tibia (F1-F3), before (control) and after being burned with either wood or charcoal. Blank spaces represent the samples that did not survive the burning process. Increased porosity is indicated by arrows throughout, with remaining 'flecks' from the ignition source circled.

5.3.1.2 X-Ray

An example of the changes to the fleshed samples can be seen below in figure 32. The femur sample was placed in the storage container which reached a maximum temperature of 623°C. Figure 32A shows the strong structure of the bone with a low but notable level of remaining flesh. Sections lighter in colour note the change in section of the bone with the darker section towards the middle the diaphysis, and the lighter ends the more porous epiphysis. Darker shadows across the surface of the bone are indicative of the presence flesh on the sample, highlighted by red arrows in the figure.

Figure 32 B, there is a clear change in the colour of the bone. A much lighter colour throughout can be seen, with a reduction in size in the mid-diaphysis, measuring at 7.6cm prior to burning and 4.7cm post burning, a reduction of around 38%. The lighter colour overall indicates the start of calcination (blue arrows) in the sample. There is also a clear reduction in the level of flesh on the sample as the darker shadows have reduced throughout the image alongside a more defined outline of the varying sections of the sample, i.e., the diaphysis, proximal/distal epiphysis and cartilage.

Similarly in figure 33, a comparison of x-rays of a fleshed 'thigh' containing sections of a femur, tibia and fibula before (A) and after (B) being burned in the storage container that reached a maximum temperature of 612°C. As this sample was fully fleshed, there is a clear distinction between the bone and flesh in the image.

Once burned, figure 33B, there is a significant change in the colour in each of the bones, with a distinctive calcined white highlighted throughout (blue arrows). Similar to the femur sample, there is a reduction in size of the bone. Measurements of the diaphysis width of the femur before, 5.4cm, and after burning, 3.7cm, show a loss of 31%. This loss is slightly smaller than the previous femur sample and may be due to the higher level of flesh present initially. Also noted is a shift and almost separation of the tibia and fibula, this may be due to the reduction of flesh therefore reducing the structural integrity of the sample overall.

Alternatively, the skull sample in figure 34 was burned in the garden incinerator with wood as the fuel source. The intact skull had a strong layer of flesh present with only the ears removed. The flesh is indicated with red arrows to highlight the depth around the parietal and frontal bones, also to highlight the layer on the surface of the sample in the form of shadows. The width of the frontal bone measured at approximately 9.1cm before burning, and the body of the mandible measured 3.5cm.

Once burned the frontal bone reduced in size of around 25% measuring around 6.8cm. Similarly, the body of the mandible also reduced in size to 3.1cm, around 11% decrease. Alongside the other samples, there is a clear change in the colour of the bone with a much whiter colour overall once burned, this sample also shows strong indications of calcination of the bone, potentially due to low levels of flesh in various sections of a skull/head, i.e., above the zygomatic process also known as the cheekbones. The overall reduction in the levels of flesh is much more significant in this particular sample, with a strong decrease in the amount of flesh surrounding the parietal bone.

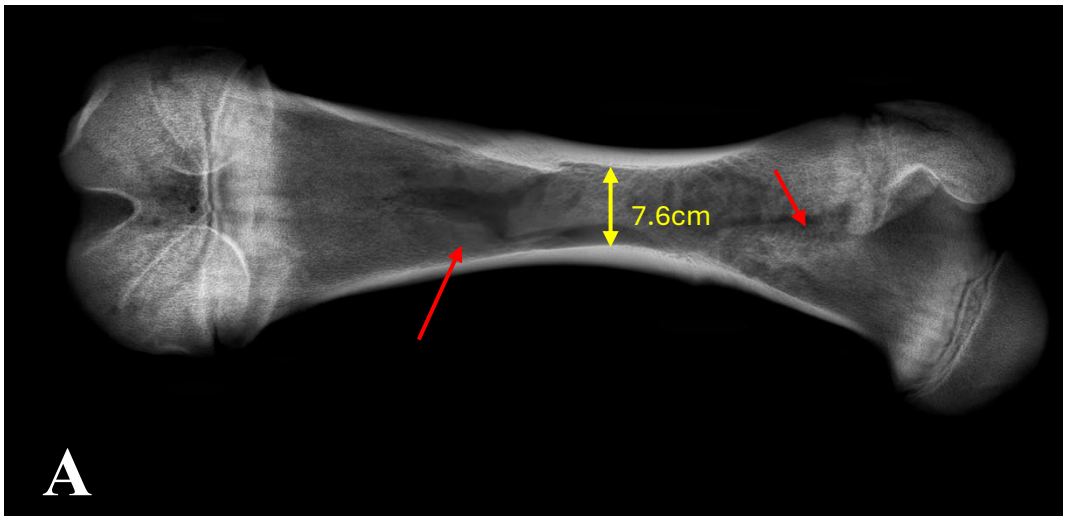

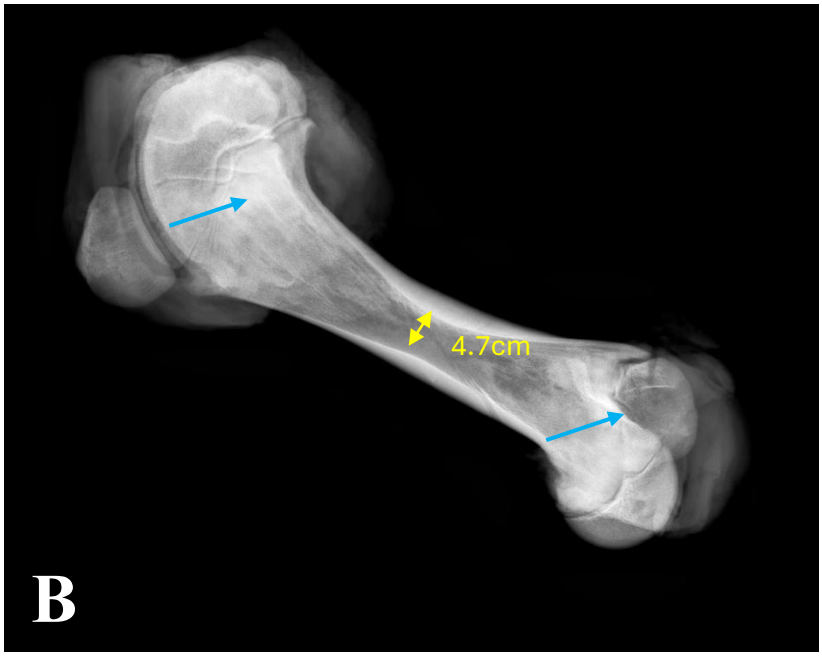

Figure 32 Comparison of femur samples in X-ray with flesh, indicated by red arrows, prior to burning (A), and after burning in storage container at 623°C (B). Clear differences in colour before and after with indications of the start of calcination in the lighter sections, highlighted by blue arrows. Reduction in size can also be seen, with a decrease in the width of the diaphysis. Also, reduction in level of flesh with clearer imaging of distal/proximal diaphysis compared to the previous image and lack of shadows across the surface.

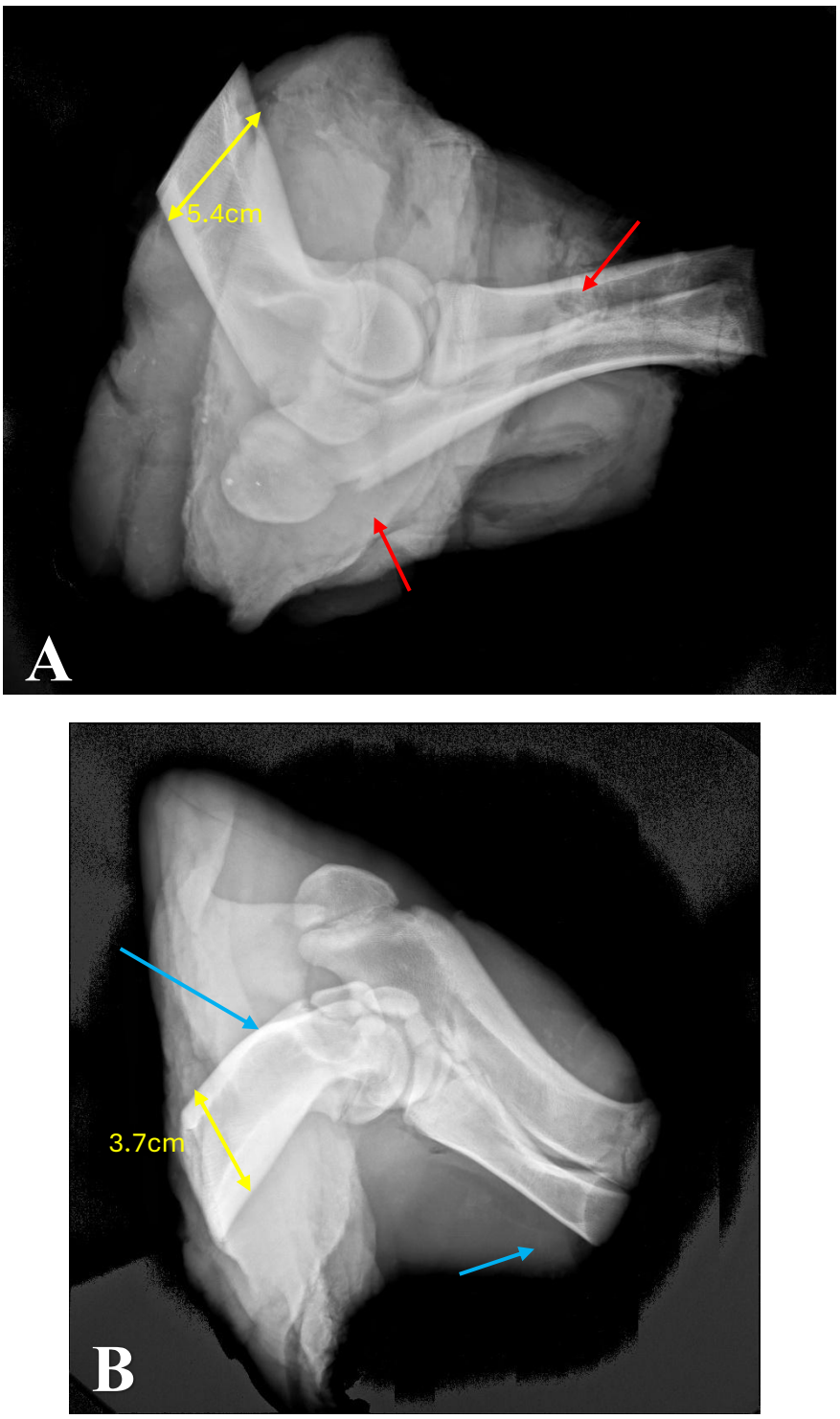

Figure 33 Comparison of thigh (femur/tibia/fibula) samples in X-ray with flesh, indicated by red arrows, prior to burning (A), and after burning in storage container at 623°C (B). Clear differences in colour before and after with indications of the start of calcination in the lighter sections, highlighted by blue arrows. Reduction in size can also be seen, with a decrease in the width of the diaphysis of the femur. Also, reduction in level of flesh with clearer imaging of distal/proximal diaphysis compared to the previous image and lack of shadows across the surface.

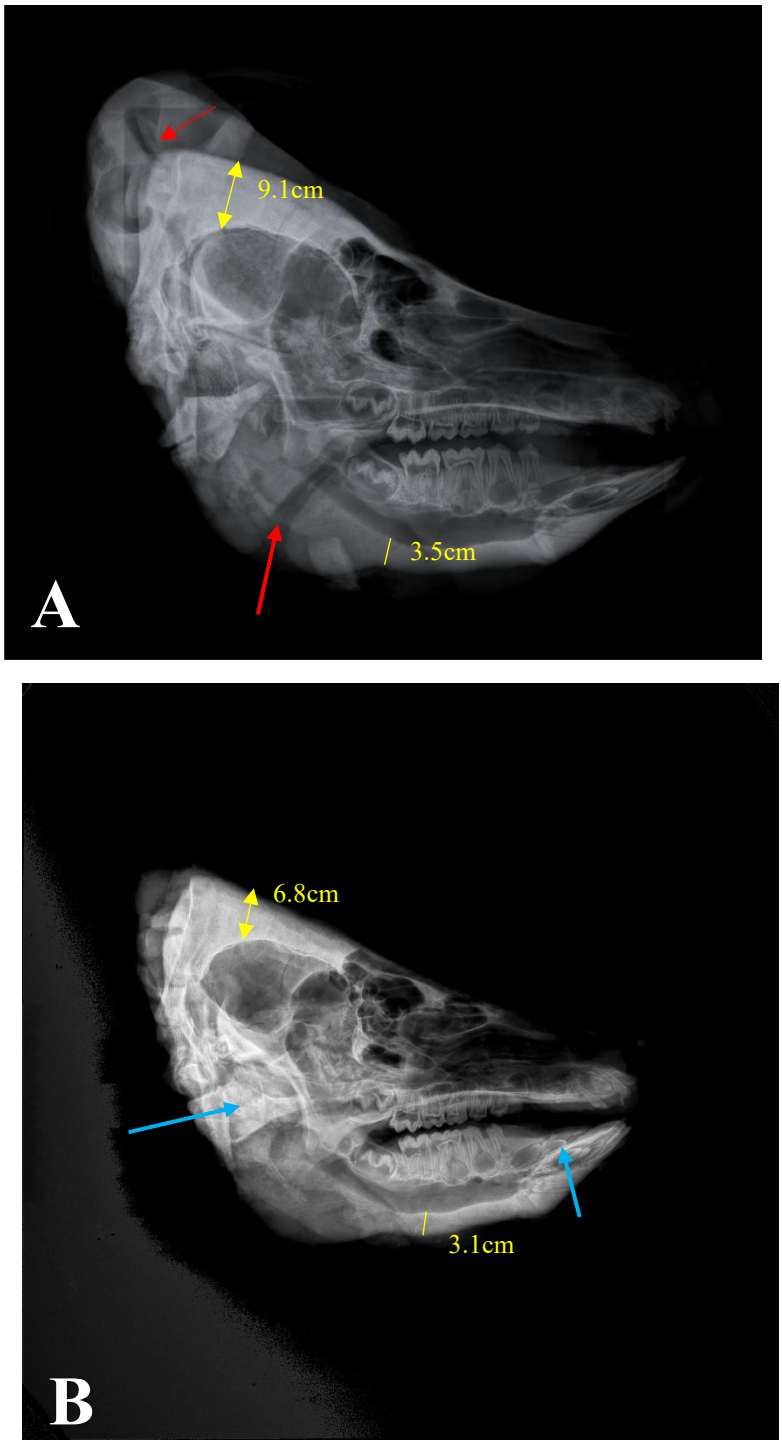

Figure 34 Comparison of skull sample in X-ray with flesh, indicated by red arrows, prior to burning (A), and after burning in garden incinerator with wood at 625°C (B). Indications of the start of calcination are highlighted by blue arrows in image B. There is a significant reduction in level of flesh with clearer imaging of the skull in the second image (B). Measurements of the frontal bone and body of the mandible show a reduction in size once exposed to the high temperature.

5.3.1.3 ATR-FTIR

Results from ATR-FTIR portrayed a significant loss in various minerals in the samples from each of the burning processes, figures 35 – 40. Each of the results are an accumulation of multiple readings to use the calculated average.

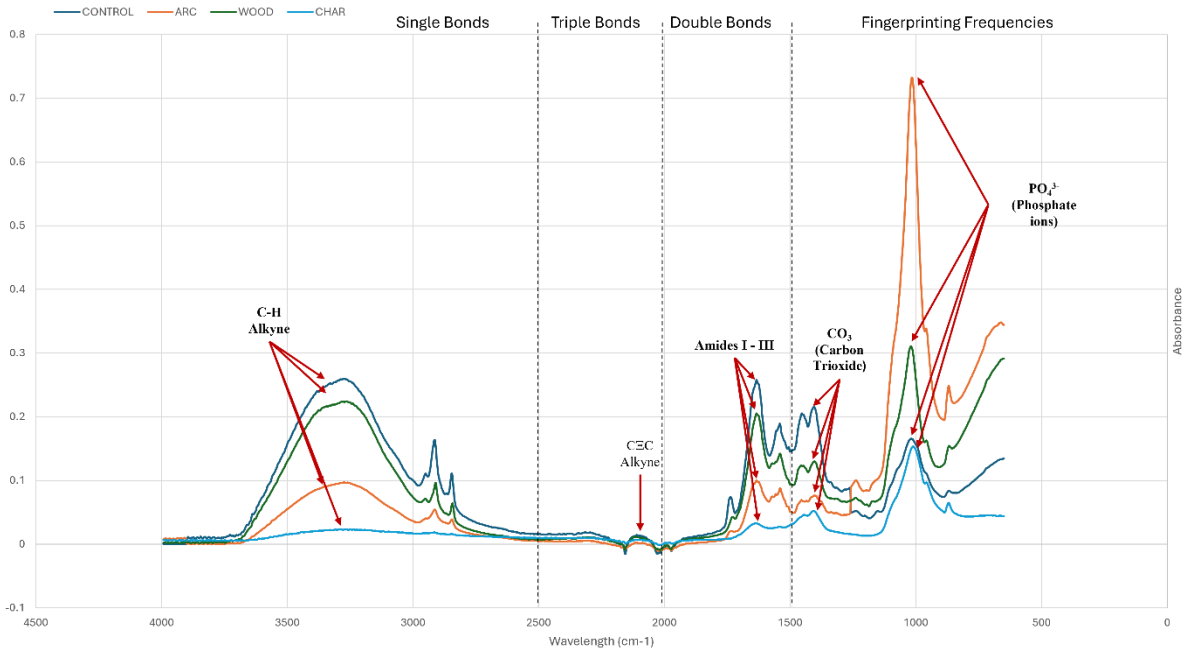

Figure 35 Fibula ATR-FTIR Spectra. Results show an increase in CO_3 and PO_4^{3-} between 1500cm^{-1} – 1000cm^{-1} once exposed to high temperatures, signifying a growth in hydroxyapatite crystalline structures. Decrease in Amide I – III levels indicate reduction in organic materials, at 1700cm^{-1} – 1500cm^{-1}.

Figure 35 shows each of the fibula samples for the control and burning methods. The fibula control sample shows an expected range of minerals within, such as Amides I-III, the presence of PO_4^{3-} and CO_3, however in much lower levels than when compared to the samples that have been exposed to high temperatures. The sample placed in the ARC shows a decrease in the level of Amides I-III, indicating a loss of organic materials e.g. collagen, at 1700cm^{-1} to 1500cm^{-1}. This sample also shows the strongest increases in CO_3 along with other compounds between 1600cm^{-1} - 1250cm^{-1}. A peak in PO_4^{3-} at 1000cm^{-1} signifies a growth in the size of hydroxyapatite crystalline structures. The sample placed in the wood-based fire shows a similar reaction, on a smaller scale. There is a decrease in those representing organic materials, Amides I-III /Collagen, at 1700cm^{-1} to

1500cm^{-1}, and an increase in the level of CO_3 and PO_4^{3-} between 1500cm^{-1} – 1000cm^{-1}. Unlike the previous samples, the sample placed in the charcoal-based fire shows little changes throughout the spectra, with an overall reduction in each of the compounds analysed. A sole increase in the levels of CO_3 as flesh remained on the sample prior to burning.

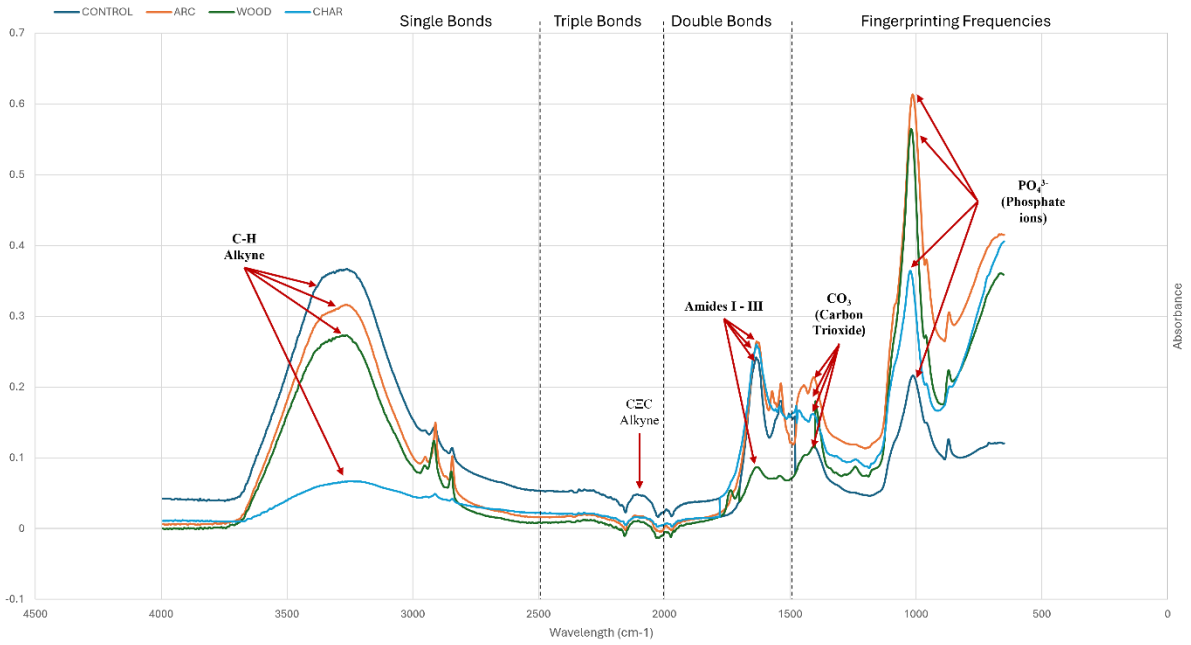

Figure 36 Ilium ATR-FTIR Spectra. Spectra shows significant decrease in recorded Alkyne levels at 3000cm^{-1} and 2700cm^{-1}, along with an expected decrease in Amide I-III levels 1600cm^{-1} – 1500cm^{-1}. Results also show an increase in PO_4^{3-} at 1000cm^{-1} and CO_3 at 1480cm^{-1} .

A pattern in each of the samples continues, with a significant peak in the level of PO43- in the ilium sample when burned in the ARC fire, this peak is portrayed at around 1000cm-1.The readings from the ilium sample placed in the wood-based fire also coincide with other samples showing a peak in CO3 and PO43- coupled with a decrease in organic materials, Amides I-III/Collagen. Slight peaks in C-H Alkyne at 2860cm-1 are representative of other organic materials remaining. The ilium sample placed in the charcoal-based fire shows the largest overall loss of organic materials, an almost complete loss of Amides I-III/Collagen between 1700cm-1 to 1500cm-1, the loss of organic materials is also highlighted by a reduction in the size of Alkyne peaks found at 2860cm-1 in the control sample. Similarly to other samples, there is a peak in the level of CO3 and PO43- identifying a growth in hydroxyapatite structures.

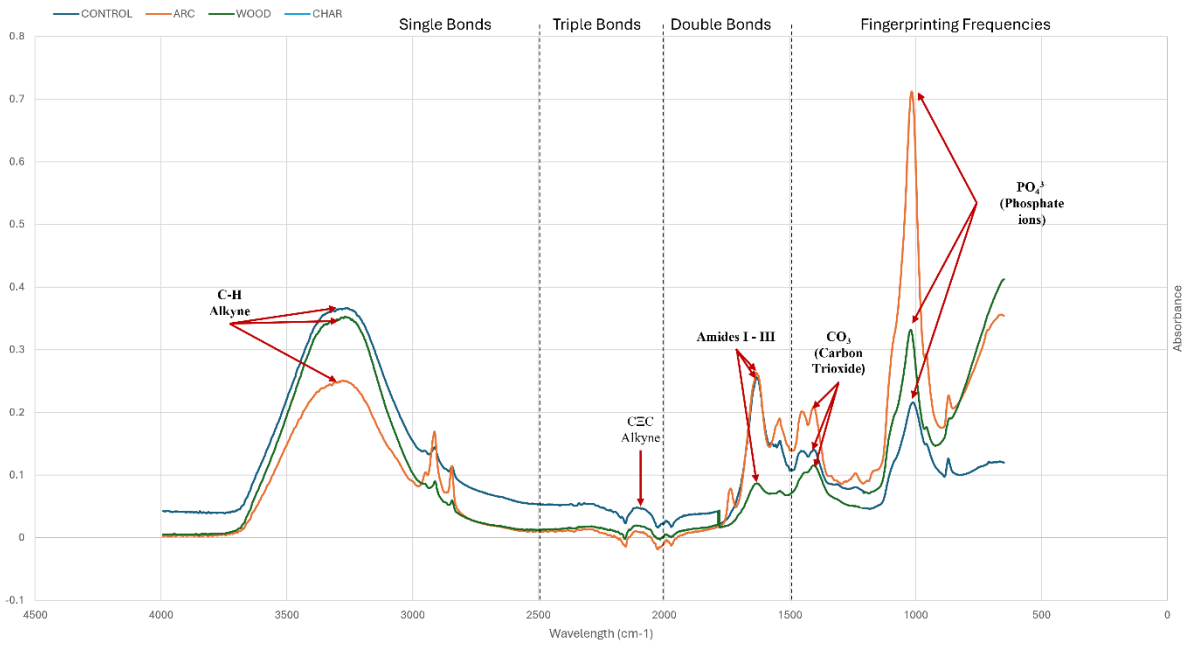

Figure 37 Mandible ATR-FTIR Spectra. Readings show a continued pattern of a peak in CO3 and PO43- between 1500cm-1 – 1000cm-1 after being exposed to high temperatures. A further continued pattern of decrease in Amides I-III between 1600cm-1 – 1500cm-1 highlighting the reduction in organic materials. The sample placed in the charcoal-based burning process did not survive.

The control mandible sample, in figure 37, continues to show the expected range of compounds within a fleshed sample. High readings of Amides I-III/collagen with lower levels of CO_3 and PO_4^{3-} than when compared to those that have been exposed to high temperatures. The sample placed in the ARC, again, shows the strongest peak of PO_4^{3-} at $1000cm^{-1}$ indicating the increase in hydroxyapatite crystalline structures. The wood-based sample shows only a slight decrease in the levels representing organic materials, with further levels of alkynes resulting in a similar way. The ARC sample also shows a higher increase than others in the level of CO_3, between $1500cm^{-1}$ – $1400cm^{-1}$, further indications of structural changes to -apatite crystals. The sample placed in the charcoal-based burning process did not survive.

When compared to the control, the scapula samples in figure 38 show a significant loss in the overall levels of Amides I-III when burned in the wood-based fire, between $1600cm^{-1}$ – $1500cm^{-1}$. The sample also shows a significant peak in the levels of PO_4^{3-} at $1000cm^{-1}$, an indication in the size of hydroxyapatite structures. There is a clear peak at a wavelength of $3200cm^{-1}$ representing C-H Alkyne, this presence may be indicative of remaining organic materials in the sample,

similarly for a secondary peak representing a C-H Alkyne at 2860cm^{-1}. A notable increase in the level of Carbon Trioxide, CO_3, between 1250cm^{-1} – 1500cm^{-1}, a contributor to -apatite structures, may also allude to the presence and size of hydroxyapatite crystalline structure due to the temperature. A scapula sample was not used in the ARC fire, and another did not survive the charcoal-based burning process, therefore there are no results for each.

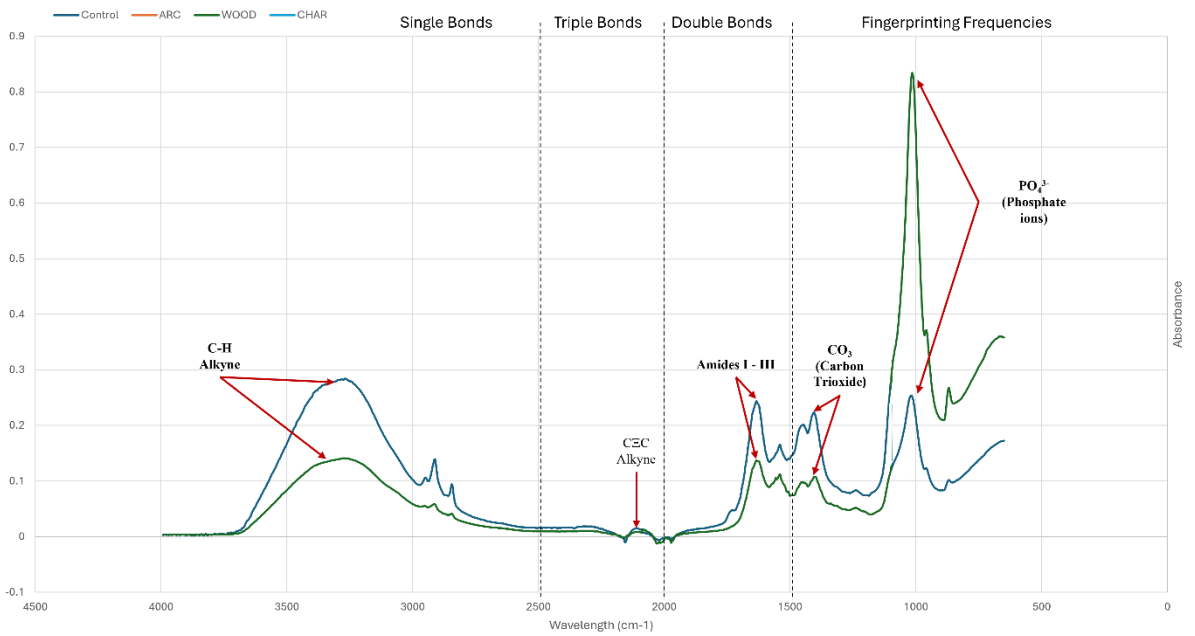

Figure 38 Scapula ATR-FTIR Spectra portraying a significant peak in the levels of PO43- at 1000cm-1 clear loss of Amides I-III between 1600cm-1 – 1500cm-1 and increased presence of CO3 at 1480cm-1 with an increase of C-H Alkyne at 3200cm-1 and 2860cm-1. A scapula sample was not used in the ARC fire, and another did not survive the charcoal-based burning process, therefore there are no results for each.

Similar to other samples, the skull sample, in figure 39, presented the strongest peak of PO_4^{3-} to be a result of the ARC fire. This sample also resulted in the strongest overall decrease in Amides I-III/Collagen, due to the charcoal-based fire, and presented no indications of remaining organic materials, as no further Alkynes were present. This sample also portrayed a similar level of CO_3 to that of the control. The skull samples exposed to charcoal provided results like other samples as there is a clear peak in PO_4^{3-} and CO_3 between 1500cm^{-1} – 1000cm^{-1}, continuing to indicate the size of the hydroxyapatite crystalline structures within the sample. The ARC sample, however, also

shows the presence of Alkynes, signifying remaining flesh after the sample has been burned. The sample placed in the wood-based burning process did not survive.

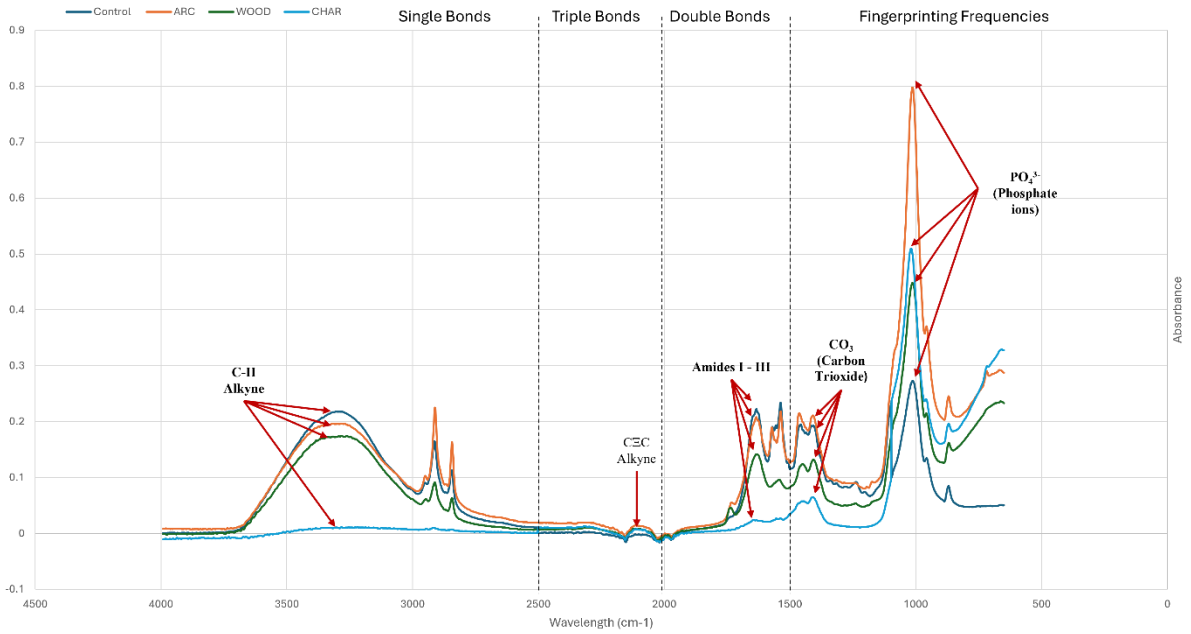

Figure 39 Skull ATR-FTIR Spectra. Clear peaks in the levels of PO_4^{3-} at 1000cm^{-1} and CO_3 at 1480cm^{-1} indicate a growth in hydroxyapatite crystalline structures. An overall decrease in Amide I-III levels portray a loss of organic materials, most significantly in the charcoal-based fire. A clear reduction in the level of C-H Alkyne is also an indication of remaining flesh once burned. The sample placed in the wood-based burning process did not survive.

In accordance with previous samples, the ARC results in figure 40 continues to show the highest peaks in both CO_3 and PO_4^{3-} between 1500cm^{-1} – 1000cm$^{-1.}$ This tibia sample also shows the strongest increase in Alkyne levels, between 3000cm^{-1} and 2700cm^{-1}, when compared to the control, the alkyne levels are indicative of a significant level of remaining organic material, alongside -apatite structures. As for the sample placed in the wood-based fire, there is a slight decrease in the levels of Amides I-III/Collagen due to the high temperatures, and an overall increase in the levels of CO_3 and PO_4^{3-} between 1500cm^{-1} – 1000cm^{-1}, however not as significant when compared to the ARC and charcoal samples. The tibia sample placed in the charcoal-based fire shows a complete depletion of Amides I-III/Collagen between 1700cm^{-1} – 1500cm^{-1}, the sample also shows a slight decrease in the levels of alkynes present in the control sample, furthering the reduction of organic materials in the results. The sample continues the pattern from previous

samples as there is a spike in the level of PO_4^{3-} at 1000cm^{-1}, representing the hydroxyapatite crystalline structures, coupled with an increase in the level of CO_3 around 1450cm^{-1}.

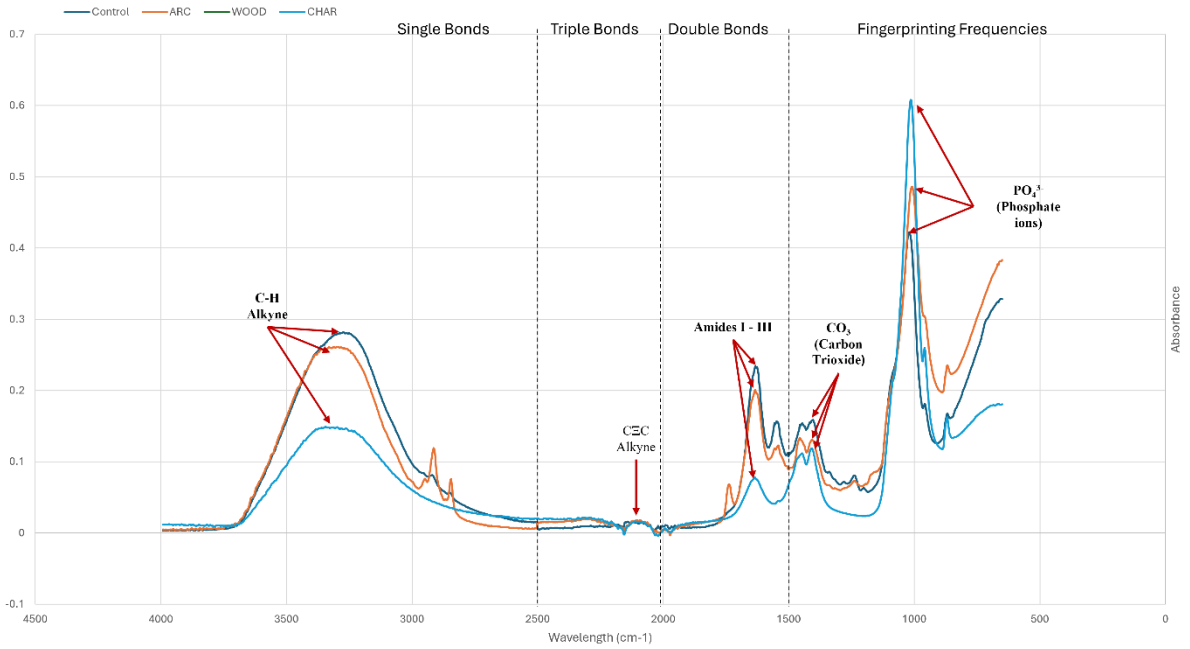

Figure 40 Tibia ATR-FTIR Spectra. Similar to other samples, the tibia results show a continuous peak in the levels of PO43- at 1000cm-1, particularly for the sample exposed to the charcoal-based fire. An overall decrease in Amide I-III levels signify loss of organic materials, alongside a decrease in both identified Alkynes, a further confirmation of reduction in remaining flesh.

5.3.4 Cut mark alterations

5.3.4.1 3D Microscope

The cut marks used in this research use both those demonstrated in chapter 4 with additional bone types.

The fibula samples exposed to the wood-based fire reduced in volume, with an overall loss of 74.5%. The cut mark produced by the large, serrated knife had the largest loss of around 83.4%, with the smooth-edged blade encountering a loss of 70.7% and the serrated knife a loss of 66%. Contrastingly to the samples exposed to the wood-based fire, the charcoal samples experiences

both loss and gain. The cut mark produced by the smooth-edged blade continued to lose 88% in volume, however, both serrated blades grew in volume, with the serrated blade almost tripling in volume by 178%, with the large, serrated knife growing by 109%.

The Ilium samples show more variation in the shapes of the cut marks depending on the knife used, particularly for the smooth-edged blade cuts. Each of the cuts vary in shape/size and show striations during the cuts. As for the serrated knife cut marks, there are similar characteristics with each of the cuts demonstrating an angle, the figure also depicts evidence of flaking in the first sample, along with all three of the cut marks produced by the large, serrated knife. Similarly, the large, serrated knife also depicts similar cuts throughout each sample, with likenesses between the cuts. Those placed in the wood-based fire varied in volume alterations, i.e., the smooth-edged blade cut mark reduced in volume by 10.43% along with the serrated knife cut mark that also reduced in volume at around 97.33%, whereas the cut mark created by the large, serrated knife increased in volume by 71.7%. Alternatively, the samples exposed to the charcoal base fire experienced more growth, as both the smooth-edged blade and the large, serrated knife cut marks grew by 20.86% and 11.96% respectively. As for the serrated knife cut mark, a reduction of 45% was seen.

When comparing the characteristics of the cut marks, on the mandible samples, via knife type, there are distinct similarities between each, for example, each of the cut marks produced by the smooth-edged blade show a similar shape along with evidence of flaking within the cut. The cut marks produced by both serrated knives show similarities in shape and angle, with similar levels of flaking as the smooth-edged cuts. The samples exposed to the wood-based fire created by the serrated knives each reduced in volume by an overall percentage of 87.96%, however, the cut mark produced by the smooth-edged blade, in fact, turned to a complete fracture. The mandible sample did not survive the charcoal burning process.

When comparing the scapula samples burned in the wood-based fire, the smooth-edge and serrated knife both experiences losses in volume of 14% and 90.2% respectively, however, the cut produced

by the large, serrated knife increased by 40.3%, more specifically in depth. The scapula sample did not survive the charcoal burning process.

The skull samples burned in the wood-based fire did not survive the burning process; however, those burned in the charcoal-based fire each decreased in volume with an overall average loss of 46.5%. The smooth-edged blade cut reduced by 88%, the serrated knife by 73.3%, the large, serrated cut by 39.69%.

The cut marks produced in the tibia samples, figure 41 – 43, show the most variance regarding shape and consistency. The cut marks created with the smooth-edged blade somewhat adhere to the 'v' shape that has been seen in previous samples, however there are alterations in some of the samples that create unexpected shapes. The cut marks produced by the serrated knife show clear signs of flaking along the kerf wall and minute levels of feathering at the edges. As for those created by the large, serrated knife, the cut marks overall show larger cuts with deeper damage. Both the smooth-edged blade and large, serrated knife tibia samples encountered losses in volume with the smooth edge cut losing 33.9% and the large, serrated losing 78.7%, however, the cut mark produced by the serrated knife increased in volume by 45%, particularly in width. Those exposed to the charcoal-based fire endured both losses and growth in volume. The cut produced by the smooth-edged blade lost a significant 85.69% in volume, whereas the cuts created by both serrate knives increased in volume, with an increase of 60% for the serrated knife cut and essentially doubling in volume for the large, serrated knife with 109% increase.

Figures 41 – 43 also show clear changes in colour depending on the fuel source. Throughout the samples burned with wood as a fuel source there is a distinct change in colour on the surface of the bone, with dark grey/black charring and residual materials or 'flecks' from the source itself, whilst still retaining a level of the bones original colour. As for the samples burned with charcoal, there is a clear and much more drastic change to the colour of the samples. Each of the samples have altered to a complete charred grey throughout, also with remaining material from the fuel source, and some distinct white components, possibly indicating the start of calcination. Images of other samples can be found in Appendix 3.

The average volume of the cut marks per bone type and via knife type can be seen in tables 24 and 25 below, with an overall comparison in figure 44, including a representation of the standard error for the samples.

Table 24 showing the average volume of a cut mark via bone type.

	Control	Wood	Charcoal
Fibula	2.34E+08	6.45E+07	1.85E+08
Ilium	1.91E+08	1.04E+08	1.53E+08
Mandible	1.06E+08	2.30E+08	-
Scapula	2.82E+08	1.27E+08	-
Skull	8.76E+07	-	4.84E+07
Tibia	1.48E+08	9.93E+07	3.61E+07

Table 25 showing the average volume of a cut mark via knife type.

	Control	Wood	Charcoal
Smooth	2.49E+08	3.04E+08	4.83E+07
Serrated	1.93E+08	2.40E+07	1.00E+08
Large, Serrated	8.28E+07	4.70E+07	1.18E+08

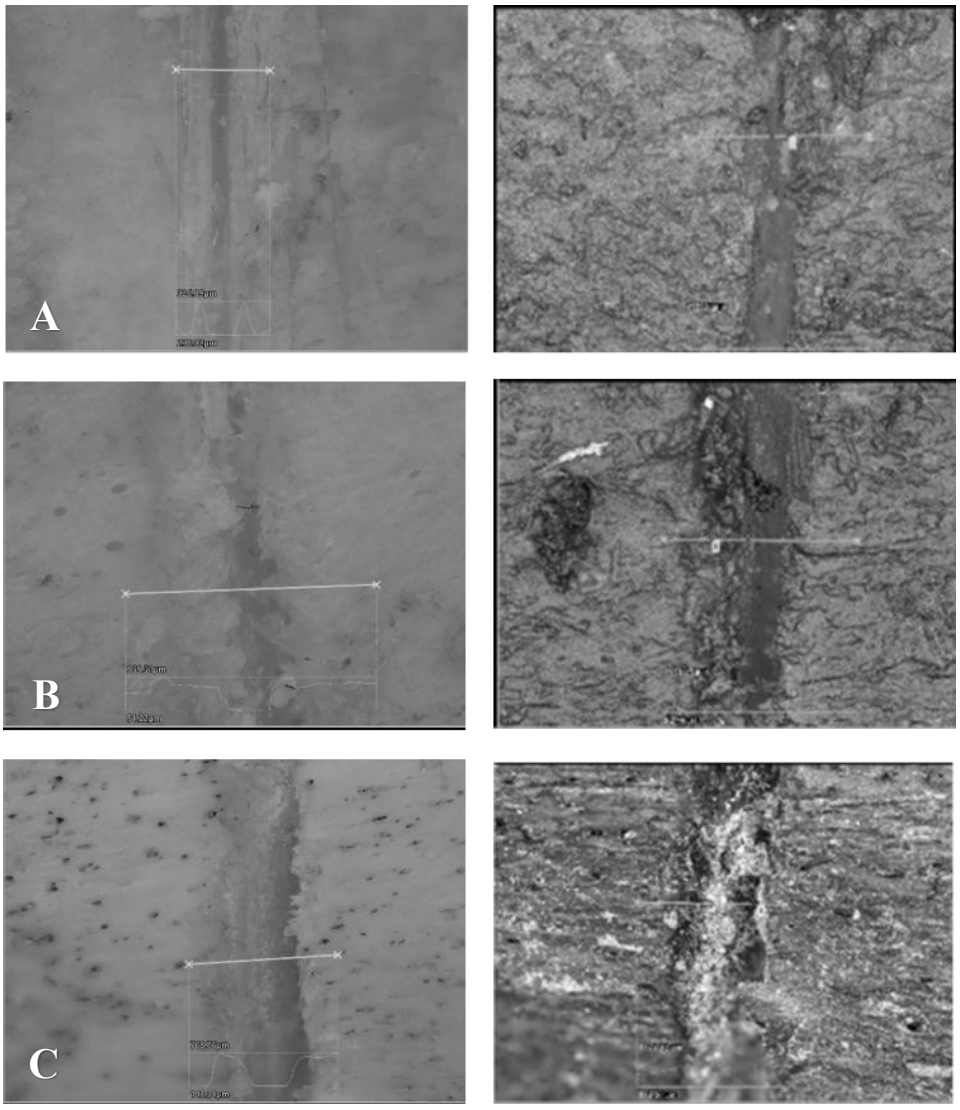

Figure 41 Tibia diaphysis cut marks prior to and post burning with wood-based fire. A represents the smooth-edged blade cut, B the serrated knife, and C the large, serrated knife.

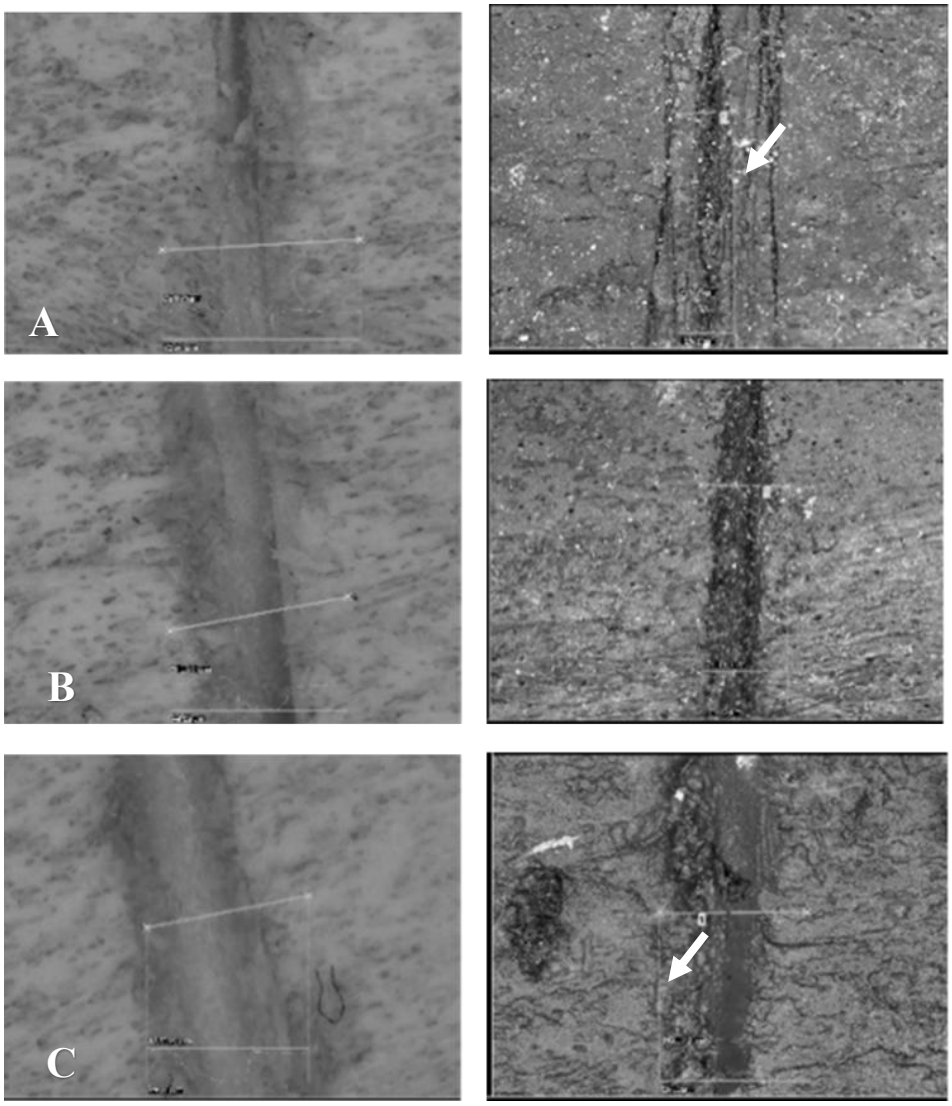

Figure 42 Tibia diaphysis cut marks prior to and post burning with charcoal-based fire. A represents the smooth-edged blade cut, B the serrated knife, and C the large, serrated knife. Arrows indicating white components, possibly the start of calcination.

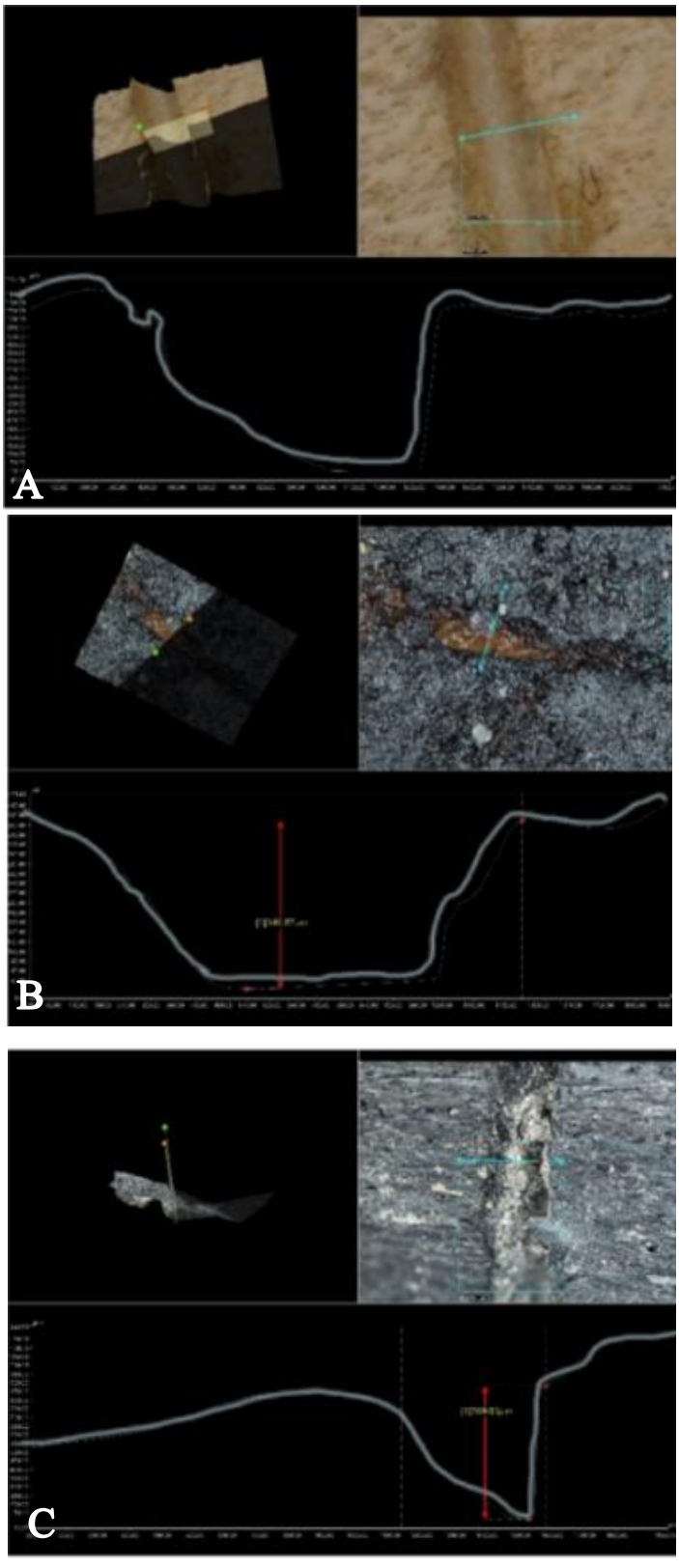

Figure 43 Examples of the 3D microscope images/measurements of Tibia cut marks prior to (A) and post burning (B/C). B represents the sample exposed to wood-based fire and C the charcoal-based fire

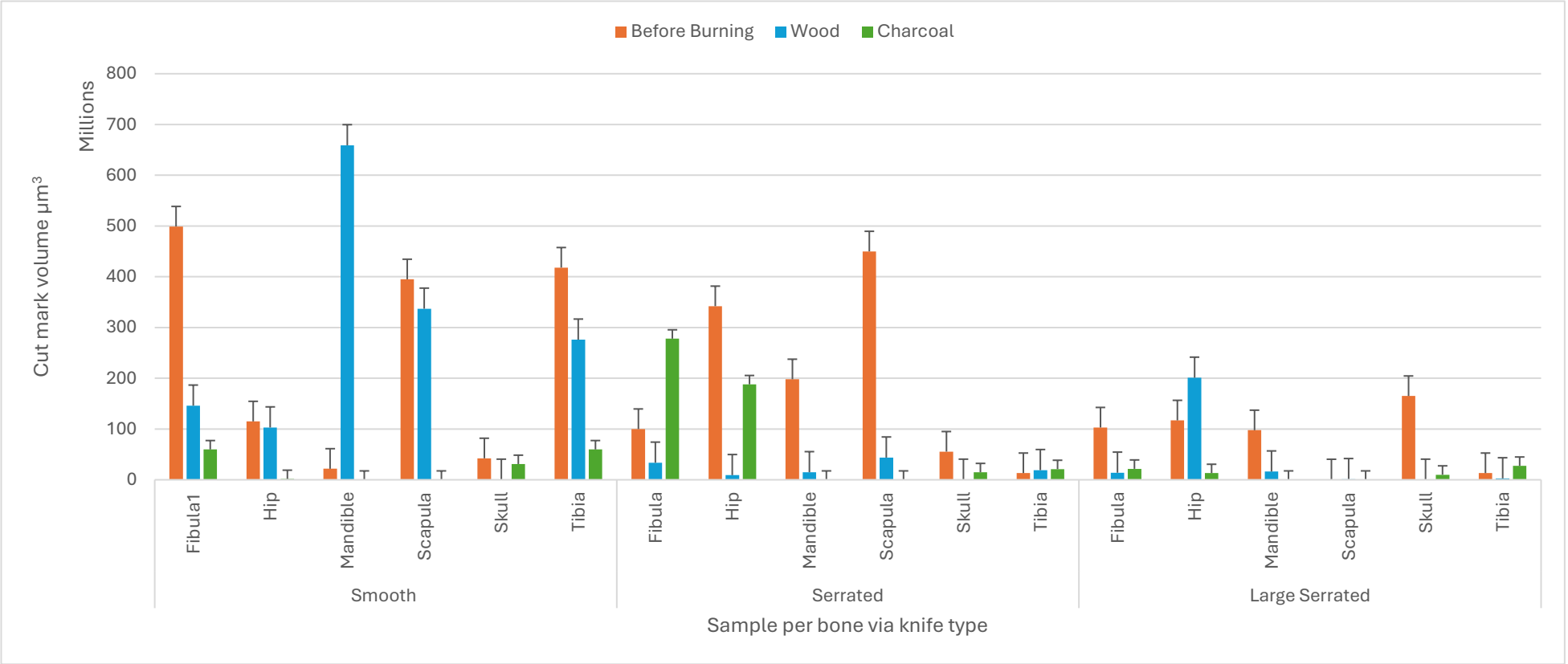

Figure 44 Comparison of cut marks before and after being exposed to wood and charcoal-based fire.

5.3.4.2 XRF

Some samples portrayed the addition of Iron (Fe) traces, possibly remaining from the knives use to create the cut marks however further investigations are needed.

Table 26 shows the results of the XRF analysis of the fibula samples. Throughout each burning method show a significant increase in the levels of Phosphorous and decrease in the levels of Calcium and Iron, each reaction due to the high temperatures. The samples also show the addition of other elements that were not present in the control sample. Neodymium and Bromine are both present in the ARC sample whereas only Neodymium is present in the remaining wood and charcoal samples.

Table 26: XRF results of Fibula samples. The results show an increase in Phosphorous, and a decrease in both Iron and Calcium. The sample also shows the addition of other elements, Neodymium and Bromine.

Element	**Control (%)**	**ARC (%)**	**Wood (%)**	**Charcoal (%)**
Phosphorous (P)	9.82	14.491	11.463	16.415
Calcium (Ca)	84.381	82.786	84.368	82.619
Iron (Fe)	0.905	0.409	0.226	0.052
Cerium (Ce)	-	-	-	-
Neodymium (Nd)	-	0.001	0.023	0.002
Bromine (Br)	-	0.016	-	-

The XRF results of each ilium sample, table 27, show an expected increase in the level of Phosphorous, once exposed to the high temperatures, along with a decreased Calcium and Iron. The addition of Bromine is also identified in the ARC sample.

Table 27: XRF results of ilium samples. An expected increase in the levels of Phosphorous, coupled with decreases in both Calcium and Iron levels. The sample from the ARC fire also recorded the addition of Bromine.

Element	**Control (%)**	**ARC (%)**	**Wood (%)**	**Charcoal (%)**
Phosphorous (P)	9.095	10.037	11.626	12.123

Calcium (Ca)	86.778	86.618	86.110	85.021
Iron (Fe)	0.461	0.276	0.126	0.341
Cerium (Ce)	-	-	-	-
Neodymium (Nd)	-	-	-	-
Bromine (Br)	-	0.012	-	-

Table 28 shows the XRF results for the mandible samples. The results show a continuous pattern of an increase in Phosphorous and decrease in Calcium. There is also the presence of additional elements in the results, this is related to the use of a butane cigarette lighter for the ignition in the ARC, as the sample shows recordings of Neodymium and Bromine, along with the wood fire sample having traces of Neodymium, also. The sample did not survive the charcoal-based fire therefore there are no results.

Table 28: XRF results of Mandible samples. Continuous pattern of an increase in Phosphorus and decrease in Calcium and Iron. Similar to other results, the addition of elements in both the ARC and wood-based fires are the results of the ignition source, Neodymium and Bromine. The mandible sample did not survive the charcoal-based fire therefore there are no results.

Element	**Control (%)**	**ARC (%)**	**Wood (%)**	**Charcoal (%)**
Phosphorous (P)	8.452	9.873	12.410	-
Calcium (Ca)	87.163	86.620	85.681	-
Iron (Fe)	0.715	0.297	0.054	-
Cerium (Ce)	-	-	-	-
Neodymium (Nd)	-	0.011	0.000	-
Bromine (Br)	-	0.015	-	-

Table 29 shows the XRF results for the scapula samples before and after being exposed to the wood-based fire. The sample exposed to the charcoal-based fire did not survive, and a scapula was not used for the ARC fire. The results show an expected increase in Phosphorous and decrease in

Calcium, however, there is also an increase in the Iron levels. This may be due to the application of trauma, as this sample had various cut marks applied from each type of knife in this study.

Table 29: XRF results of Scapula samples. Clear increase in the level of phosphorous and decrease in Calcium. A notable increase in the level of iron, potentially due to remaining element from the application of trauma. A scapula sample was not used in the ARC fire and did not survive the charcoal-based fire, therefore there are no results for either.

Element	**Control (%)**	**ARC (%)**	**Wood (%)**	**Charcoal (%)**
Phosphorous (P)	9.279	-	10.664	-
Calcium (Ca)	86.312	-	85.002	-
Iron (Fe)	0.243	-	0.253	-
Cerium (Ce)	-	-	-	-
Neodymium (Nd)	-	-	-	-
Bromine (Br)	-	-	-	-

The XRF results for each of the skull samples show an, expected, overall decrease in the levels of Calcium and Iron for each of the burning types. There is also a clear increase in the level of phosphorous throughout the samples, once exposed to high temperatures, this increase is particularly significant in the sample burned in the ARC fire, this sample also shows the addition of Bromine. Similarly, the sample burned in the charcoal-based fire also shows an additional element as traces of Neodymium. The skull sample did not survive the wood-based burning therefore there are no results.

Table 30: XRF results of Skull samples. Overall increase in levels of Phosphorus for remaining samples, with expected decrease in calcium levels due to heat. Two samples show additional elements, the ARC showing recordings of Bromine, and the charcoal sample showing traces of Neodymium. The skull sample did not survive the wood-based burning therefore there are no results.

Element	**Control (%)**	**ARC (%)**	**Wood (%)**	**Charcoal (%)**
Phosphorous (P)	14.67	17.285	-	15.663
Calcium (Ca)	86.945	86.786	-	83.409
Iron (Fe)	2.372	0.213	-	0.022

Cerium (Ce)	-	-	-	-
Neodymium (Nd)	-	-	-	0.000
Bromine (Br)	-	0.041	-	-

The results in the table 31, show indications of increased hydroxyapatite crystalline structures in the tibia sample, due to the increase in Phosphorous levels, particularly in the sample placed in the ARC fire. There is also the presence of Bromine in the sample retrieved from the ARC, alongside Neodymium. Both the wood and charcoal sample also show traces of Neodymium.

Table 31: XRF results of Tibia samples. Increase in levels of Phosphorous, indicative of hydroxyapatite crystalline structures increasing. Additional elements recorded in each of the burned samples, Bromine and Neodymium.

Element	**Control (%)**	**ARC (%)**	**Wood (%)**	**Charcoal (%)**
Phosphorous (P)	16.423	10.865	9.580	16.102
Calcium (Ca)	87.837	86.418	83.432	79.176
Iron (Fe)	0.905	0.108	0.157	0.056
Cerium (Ce)	-	-	-	-
Neodymium (Nd)	-	0.001	0.000	0.012
Bromine (Br)	-	0.014	-	-

5.3.4.3 Statistics

5.3.4.3.1 ANOVA

A series of two-way ANOVA tests, supplemented with t-tests, were conducted in SPSS to assess multiple hypotheses: (1) whether cut mark volume varies according to bone type, (2) whether it varies according to knife type, and (3) whether it is further influenced by exposure to different fire settings, either wood- or charcoal-based.

The two-way ANOVA comparing cut marks burned in wood-based fires yielded a p-value of 0.083. While this approaches significance, it remains above the 0.05 threshold, indicating only weak evidence against the null hypothesis and therefore not statistically significant. By contrast, the comparison of cut marks burned in charcoal-based fires produced a p-value of 0.034, which falls below the 0.05 threshold and therefore supports rejection of the null hypothesis. This result indicates a statistically significant effect of charcoal combustion on cut mark volume.

5.3.6.2 T-Test

Independent t-tests were also conducted to evaluate differences within specific sample groups. When comparing bone type, a slight but non-significant reduction in cut mark volume was observed in ilium samples following exposure to some of the higher temperatures ($p = 0.063$).

When grouped by fuel source, significant differences were identified. Cut marks exposed to charcoal-based fire saw statistically significant changes in volume ($p = 0.025$), and the comparison of pre- and post-burning values across fuel types found some significance ($p = 0.051$ [3.dp]).

Further tests by knife type revealed evidence of differential effects. Cut marks produced by the serrated knife showed changes in volume are trending towards significance ($p = 0.053$), suggesting that blade morphology may play a role in the thermal alteration of cut marks, although the result does not cross the determined 0.05 threshold.

The statistical tests are each in support of the hypotheses stated in 1.6.3, in which the exposure to heat will not only affect the morphology (fig 31 – 33 / 41 – 42) and macroscopic aspect of the samples (fig. 35 – 40), but also the sharp force trauma (fig. 43). Alternatively, the results in tables 24 – 25 show a clear reduction in size of each of the cut marks, rejecting the sub-hypothesis that exposure will obscure/mimic sharp force trauma thus complicating interpretation, although a change in size occurred, the cut marks remain distinguishable from heat-dependent alterations. This rejection therefore supports the final sub-hypothesis ‘the sequence of events, i.e., sharp force trauma before vs. after burning, will result in distinguishable morphological differences in bone

trauma patterns' as each of the cut marks remained distinguishable post-burning, including morphological changes.

5.4 Discussion

5.4.1 Thermal alterations

One of the primary alterations due to thermal exposure is the change in the colour of the bone. All of the samples in figures 41 - 43, show clear signs of a darker colour potentially indicative of the bones going through 'inversion' due to the temperatures reached 617°C/625°C. The process of inversion begins to take place once temperatures have exceeded 600°C (Marques, et al. 2018) and continues until in excess of 700°C in which the process of fusion takes over. Due to the remnants of fuel source, the colour changes are similar to organic char, an alteration that often begins at around 300°C. This is in accordance with studies that have found bones to progress through stages of colour change as temperature increases, with samples resulting in a calcined white once exceeding 800°C (Gallo, et al. 2025). However, a study has also found samples that may have been exposed to high temperatures such as 300°C - 400°C for a significantly longer period may result in a similar colour to those exposed to much higher temperatures, as the organic matter begins to break down and can continue to do so under the constant heat (Gallo, et al. 2025).

As seen throughout the XRF results, there is a continued pattern of increased Phosphorus once the samples have been exposed to high temperatures. Once burned, bone loses water and organic materials, i.e. collagen (Waterhouse, 2013). This concentrates the remaining inorganic minerals, including hydroxyapatite, which contains calcium and phosphate. Furthermore, the exposure of bone to high heats begins to transform the hydroxyapatite structures into a much more stable form and become crystalline, thus incorporating an increased number of phosphate ions therefore an increased number of phosphate/phosphorous (McKinnon, et al. 2020). Similar to this research, the temperatures necessary for this chemical alteration to occur is often more than 600°C,

therefore, the temperatures reached in each burning method, 600°C - 625°C, was expected to show said changes.

The identification of Cerium, Bromine, and Neodymium in the samples collected solely from the open flame fire and the garden incinerator suggests these elements were absorbed from the surrounding materials or the ignition source.

The ignition source for the open flame fire was a Butane cigarette lighter. Butane is a highly flammable hydrocarbon alkane (C_4H_{10}) commonly associated as a cause of accidental residential fires. Notably, Cerium, a lanthanide element, was detected in the open flame fire samples but not in those from the garden incinerator. This is consistent with its known presence in mischmetal alloys, often used in lighter flints to create sparks for ignition (Paul et al., 2017), confirming the role of the lighter in contributing Cerium to the fire environment.

Bromine (Br) detected in the open flame samples is indicative of flame-retardant materials in the surrounding environments, most likely household items such as upholstered furniture. This is expected given the residential context of the ARC fire scenario, which aimed to replicate real-life conditions. The results offer insight into the sample placement within the fire and the possible contents of the room prior to combustion, information that may prove useful in a medicolegal investigation. Neodymium (Nd), detected in trace amounts, may similarly reflect environmental contributions. Nd is commonly found in small electronic devices such as microphones and musical instruments (Royal Society of Chemistry, 2024). However, it's also possible that the detection of Neodymium is linked to the XRF analysis process itself, as specific types of glass are used in laser components within some XRF instruments. Both, Bromine and Neodymium were also found in samples from the garden incinerator, where no lighter was used and no obvious flame-retardant materials were present. This anomaly suggests that further investigation is needed to determine the source of these elements in the incinerator context

The samples that did not survive the burning process, Mandible and Scapula with charcoal, and Skull with wood, are some of the more porous of the samples. As higher temperatures increase the

levels of porosity within bone as it burns (S, et al. 2,022) the aforementioned samples have increased in porosity significantly, therefore resulting in a much weaker and more brittle structure. The sampled mentioned were either completely eviscerated by the fire or provided samples so small that they could not be analysed.

5.4.2 Cut mark alterations

As seen in the results there are detrimental alterations to the cut marks once burned. Most of the cut marks decreased in size due to the losses of remaining organic materials. However, the change in size also varies depending on the type of knife that was used and the type of bone affected. In the case of forensic investigations, this understanding is crucial as the changes to the original cut mark may result in a misinterpretation of what the weapon may have been, for example a cut produced by a large-serrated knife may be mistaken for one produced by a smaller serrated knife due to its reduction in size.

Most recently, a study, using ovine samples, focused on the topic of dismemberment and subsequent burning, at temperatures of 400°C, 600°C and 800°C, in an attempt to destroy evidence produced by saw marks (Chang, et al. 2024). The study found metric and morphic alterations to the pre-existing cut marks once burned however, those burned at 600°C were found to have significant alterations regarding the kerf width and expand notably. This finding relates to that of this study with alterations in the cut marks due to high temperatures (600°C), however due to the difference in sample source, i.e., ovine vs porcine, the appearance of complete fractures from the cut marks is still questioned.

The exposure to intense heat resulted in the cut mark increasing in size, as opposed to the expected decreasing. This alteration has been focused on in multiple studies to distinguish between pre-existing cut marks and fractures/breaks created by thermal exposure. A study composed in 2021 found similar reactions to cut marks when burned in regard to the morphological changes depending on the type of knife and bone affected. The research used 3 different knives, non-serrated, fine-serrated and coarse-serrated blades, to create cut marks in porcine ribs, specifically

wild boar, and exposed them to a maximum temperature of 850°C for around 30 minutes to achieve calcination (Vachirawongsakorn, et al. 2021). The results found the cut marks to remain recognisable without considerable alterations, however those produced by the coarse-serrated knife were most likely to have significant alterations. The study has similar results to that of this research as the resulting cut marks of the serrated knife had more significant morphological changes.

The use of a 3D microscope regarding trauma analysis is a relatively new approach within forensics. A study composed in 2024 focused on the use of Keyence VHX-2000 digital microscope to identify and distinguish between trauma-related and heat-related fractures in flat and irregular human bones, particularly after partial cremation. Researchers applied blunt or sharp force to five human skull tops (calottes) and five pelvis halves, then partially cremated them. They recorded 180 fractures using a high-resolution digital microscope and analysed them with 3D software, Geomagic Studio and Design X (Friedlander, et al. 2024). The 3D reconstructions allowed the researchers to analyse fracture shapes and curvature, aiding the differentiation between peri-mortem trauma and heat-induced fractures. While the main impact sites from blunt and sharp force trauma were clearly distinguishable, shallow or secondary trauma fractures were harder to tell apart from heat fractures. Ultimately, the study found that deep trauma fractures and heat fractures can be reliably differentiated using this 3D analysis method.

Further works for this study would replace the porcine bone with human bone samples for more realistic applications towards forensic investigations. This would also seek to include the analysis of blunt and firearm trauma, to gain a more varied insight into the various types of trauma that an individual can be exposed to and how the injuries may be thermally altered. This would also allow for the study to be repeated and therefore collect data for the samples that did not survive the previous burning methods.

Although the t-tests have varying significance, this may be improved by a larger sample size or repeated experiments.

Chapter 6

Discussion

6. Discussion

6.1 General Discussion

The focus for this research stemmed from the constant occurrence of fatalities resulting from both exposure to fire and/or sharp force trauma. In Europe, many deaths relating to residential fire, or similar, result in around 5000 a year (EFSA, 2025). More specifically in the United Kingdom, fire-related fatalities remain a significant concern, with approximately 269 deaths recorded in the year ending December 2023 (ONS, 2023). Notably, dwelling fires accounted for 72% of these fatalities, highlighting the critical need for effective prevention and response strategies (GOV.uk) Simultaneously, sharp force trauma continues to be a leading cause of homicide. In 2023, 46% of all homicides in England and Wales involved a sharp instrument, with kitchen knives being the most prevalent weapon (Handlos, et al. 2023). This trend highlights the urgency of understanding the dynamics of such injuries to inform both preventive measures and investigative practices.

The combination of each cause of death, fire exposure and sharp force trauma, presents unique challenges in forensic science analysis. The effects of high temperatures on bone can obscure and alter the characteristics of sharp force injuries, complicating the identification of the weapon used. Therefore, this research sought to bridge the gap in forensic methodologies by systematically investigating how thermal exposure influences the presentation and interpretation of sharp force trauma.

This research investigated how heat alters porcine bone to better understand burned skeletal remains at crime scenes, including factors such as fuel source and temperature. It also examined sharp force trauma to identify distinct injury patterns, potential weapons, and the circumstances of death. Finally, it explored how thermal exposure affects sharp force injuries, providing insights into both weapon identification and events surrounding death. The discussion covers three results chapters, thermal alterations (Chapter 3), sharp force trauma (Chapter 4), and their combined effects (Chapter 5), in relation to existing literature. As previously mentioned, porcine bone was employed throughout this study as a substitute for human bone. This selection was primarily driven by the availability and efficiency of sample collection in the initial stages of the research.

Bonney et al. (2020) demonstrated that porcine bone closely mirrors human bone in its elasticity, porosity, and microstructural organisation, supporting its suitability as a potential substitute. Similarly, Bonney et al. (2021) reported comparable fracture mechanics and mineral density profiles between porcine and human bone, further validating its relevance and relatability in investigations involving remains.

Along with the type of sample chose, the preparation of the samples was also taken into significant consideration as multiple were either boiled through the process of maceration and/or frozen for storage. The effects of boiling the samples were considered particularly as the temperature of the water can result in macroscopic and microstructural changes, such as increased porosity, lighter in colour and a loss of hydration, possibly affecting the outcome of the further exposure to high temperatures of fire (Bosch, et al. 2011).

Similarly, the effects of freezing the samples for storage in a -20°C freezer were also taken into consideration. Noted changes to a bone microstructure such as osteocyte disappearance, and collagen disorganisation may affect the results from the applied trauma and high heats (Jeromelj, et al. 2025). The use of freezing bone samples at this temperature is a common preservation method and is generally effective in morphological, biomechanical, and DNA preservation methods, with little to no negative effects (Pajnic, et al. 2025).

6.2 Thermal Alterations to Porcine Bone

Chapter 3 provides an in depth and comprehensive understanding of the morphological and structural changes to bone when exposed to various temperatures, and how each change may differ or alter further as the temperatures increase. This knowledge is crucial as recognising changes in colour, structural density, and microscopic features, such as increases in hydroxyapatite crystal size, provides valuable insight into what may have occurred at a crime scene. By identifying these alterations, investigators can determine characteristics of the fire, such as its maximum temperature, which in turn helps narrow down potential fuel sources and assess whether the fire was accidental or deliberately set.

The changes observed in the current study are consistent with findings from several other studies of a similar nature (Galloway et al., 2024). When all bones are exposed to temperatures ranging from 300°C to 900°C, alterations in colour, porosity, and fragility are most evident, while additional observations extend the knowledge of associated changes, such as mineral changes and crystallinity levels (Krap, et al. 2019).

Once exposed to various temperatures, the colours of a bone range from standard off-white/yellow (#E3DAC9) through shades of grey (#828282) and charred black (#364S4F) to calcined white (#FFFFFF). Similar studies have confirmed the pattern in which a bone sample may go through when exposed to high temperatures. For instance, a review of multiple studies by Galloway, Pope, and Juarez (2024) stated that whilst a bone may follow the expected pattern when burned in a controlled environment, similar to the colours shows in figure 13 (section 3.3.1), those burned in lesser controlled and more realistic conditions, whilst still reaching similar temperatures of 600°C – 650°C, are more likely to remain in a charred state due to the surrounding materials and fuel source, also seen in figures 41 – 43 (section 5.3.4.1) (Galloway, et al. 2024).

Areas for discussion have included the approach of how a colour may be assessed and identified. Previously used approaches included the Munsell Colour Chart (1984), originally created for determining the colour of soil samples and focused on the Hue, Chroma and Value of a samples colour. However, the approach was later discontinued when assessing burned bone due to its dependency on human perceived assessment, therefore open to subjective interpretation (Devlin, et al. 2015). Galloways review concluded, although controlled environments can provide a basic knowledge of how a bone may alter under increasing temperatures, similar to those of this study in the muffle furnace (see chapter 3), a more realistic burning scenario of a forensic context, i.e. lesser controlled/ open flame fires, has further aspects to take into consideration that will affect the alterations. Some external factors of the fire, an individual's anatomy, and the thermal conduction of the surrounding heat into the skeletal structures (Galloway, et al. 2024). Therefore, the colour of the bone can help towards determining the temperature of a fire but as part of an amalgamation of collected information and not a sole determinator. Although burned with

different fuel sources, the results in chapter 5 are also in agreement with these findings, regardless of the type of bone. The resulting colours of the samples, burned between 612°C – 625°C, show a grey/black charred colour, similar to that of the sample burned at 600°C in the muffle furnace in chapter 3.

Porosity and mineral changes are a combined change when bone is exposed to higher temperatures. The changes to bones mineral levels experience significant increase and decreases. As expected, most minerals, e.g. Calcium, decrease due to the temperature and dehydration, however, those associated with Hydroxyapatite Crystalline structures tend to increase, including Phosphorus. Once fires exceed 500°C, the crystalline profile of a bone begins to change (McKinnon, et al. 2020) this suggests decalcination of the sample along with an increase in hydroxyapatite crystalline structures. The increase in said crystalline structures also implies an increase in porosity, due to the hexagonal and almost honeycomb-like shape of the crystalline structure (Khalid & Chaudry, 2020). Similar to the results found in this research, a study composed in 2019 highlighted the primary changes to bones mineral content due to exposure to high temperatures. The research composed by Hoesel, et al. 2019 found changes began to occur as low as 200°C, in which, changes to proteins and lipids were observed, this continued through higher temperatures showing complete loss of lipids by 300°C, other transformations of minerals, i.e. collagen and other compounds, continues until temperatures reach around 600°C. Temperatures in excess of 600°C observe more significant changes to the bones mineral content, this is where the majority of the organic material within the bone is lost, leading to a 'reorganisation' of the remaining minerals, i.e. -apatite structures, and carbonate ions, in order to create space for hydroxyl ions thus creating the larger hydroxyapatite crystalline structures (Hoesel, et al. 2019). Further research into the solubility of various bone minerals, due to the reduction in higher temperatures alongside an increase in dehydration, found minerals like collagen and hydroxyapatite structures are in fact not water soluble due to complex structures, i.e., collagen contains a triple helix structure and is therefore insoluble to water (Al Hajj, et al. 2024).

The primary analytical techniques for this chapter include the use of Agilent Attenuated Total Reflectance Fourier Transform Infrared (ATR-FTIR) and Malvern Panalytical, Epsilon 1 X-Ray Fluorescence (XRF). The use of ATR-FTIR was initially applied to analysing burned skeletal remains by Thompson, et al. in 2009. The analysis provided insight on the crystallinity index, the quantity ratio in the bone regarding hydroxyapatite crystalline structures, and to understand thermal alterations to other minerals within the bone sample once exposed to high temperatures. The initial application found the use of ATR-FTIR to provide reliable measurement results regarding the crystallinity index. The study also found hydroxyapatite structural growth stabilises once 700°C has been reached (Thompson, et al. 2009), similar to the results of this present study. Further studies with a similar focus have since confirmed the initial findings (Ozdemir, et al. 2022, Marques, et al. 2021, and Legan, et al. 2020), with ATR-FTIR becoming a regular analytical technique in forensic investigations, thus supporting the use of this analytical technique for this research.

The use of X-Ray Fluorescence (XRF) was introduced to develop a method of analysis with a more chemical based analysis as opposed to the previously used morphological based approach (Rosa, et al. 2022). The use of XRF is limited to dry bone analysis, i.e., without flesh (Ricardo, et al. 2024). This provides a more focused result of the bone contents without interfering flesh levels; however, this also requires the removal of flesh which may in turn produce further complication, e.g. boiling the bone could damage the integrity of the bone, or residual elements from the materials used to remove the flesh, or remaining flesh itself, may be detected. The use of this analytical technique for the current study supports the idea that, overall, the use of XRF analysis was decidedly an appropriate method of analysis of chemical variations and elemental data for dry bone, particularly due to it being a non-destructive technique (Ricardoet al. 2024).

The detection of cerium (Ce), bromine (Br), and neodymium (Nd) exclusively in the open-flame and garden-incinerator samples in chapter 5 represents a novel contribution to the understanding of elemental absorption in thermally altered bone. The presence of Ce in the open-flame scenario can be attributed to the use of a butane lighter, where mischmetal alloys in lighter flints provide a

plausible source. Its absence in the garden-incinerator and muffle furnace samples reinforces the interpretation that Ce is introduced directly via the ignition source, as a lighter was not used in either scenario, marking the first reported case of this element in burned bone with potential forensic applications in reconstructing ignition methods. Similarly, the detection of Br in the open-flame samples is consistent with the inclusion of brominated flame retardants in household furnishings, materials commonly encountered in residential fires. This finding constitutes the first observation of Br in burned bone and highlights its value in providing contextual information on the environment of combustion, with potential use in differentiating between accidental and deliberate fire scenarios. Nd was detected in both open-flame and garden-incinerator samples, with possible sources including household electronics or, alternatively, contamination from the XRF system itself, where Nd-bearing glasses are used. Although the precise origin of Nd remains inconclusive, its detection highlights the importance of considering both environmental and instrumental contributions when interpreting elemental data. Collectively, these findings extend current knowledge by demonstrating that trace elements such as Ce, Br, and Nd may be incorporated into bone under specific burning conditions, thereby offering new approaches for forensic reconstruction of fires and contributing to the wider discourse on post-mortem diagenesis in thermally altered remains.

6.3 Sharp Force Trauma Analysis on Porcine Bone

Chapter 4 focuses on sharp force trauma to bone. This focuses on the current mortality rates regarding sharp force trauma related deaths, a look at how cut marks produced by sharp force trauma have varying characteristics e.g. flaking or feathering, and finally, how different types of knives can produce varying cut marks, and if the weapon can be determined from the cut marks characteristics. The means of this study is to understand how cut marks produced by different weapons may differ in characteristics, and whether said characteristics are able to not only differentiate between the cut itself but also whether they are significantly different enough to help towards identifying the weapon used. The results of this study can be applied to forensic investigations where death due to sharp force trauma has occurred with an undetermined weapon,

which once understood, can bring to light the circumstances around the death and provide further information as to what may have happened.

The identification of cut marks focuses, primarily, on the morphology of the cut itself, i.e., the shape, size, depth, and presence of striations or micro-fractures along the kerf wall (Braun, et al 2016). The positioning of the cut mark regarding the bone affected can have an effect on the production of the cut (Braun, et al 2016), however, most cut marks are generally produced with either a V or U-shape, thus inferring the type of tool used (& Soligo, 2008), see figure 22 for details. In a more historical approach by Bello & Soligo (2008), the morphology of a cut mark has been used to differentiate the tools used, and the materials they are made from, i.e. stone vs metal tools and, has since been implemented for current forensic investigations to identify weapons related to medicolegal situations (Bello & Soligo, 2008). The differentiation between a cut mark producing either a V or U shape is related to either the weapon used or the application of the cut (Krasinski, 2018). A V-shaped cut mark is determined to be the result of sharp/single-edged weapon, i.e., a knife or sword, whereas a U-shaped cut mark is often the result of trauma more closely related to blunt force, i.e., trampling or some chop wounds, depending on the size and dullness of the axe, as demonstrated in figure 21 (Krasinski, 2018, Okaluk & Greenfield, 2022).

Further identifying characteristics such as flaking, feathering etc. (see chapter 4) have been identified as distinguishing morphologies of various weapons. McCardle & Stojanovski (2018) were able to differentiate various weapons, more specifically when creating chop wounds, via the presence of characteristics such as microcurvature or an exit notch, seemingly related to a wound produced by a katana sword, whereas injuries produced by a machete, a more commonly found tool in forensic sharp force trauma investigations, found characteristics such as micropeeling, chattering and a scoop defect to be present. As for traits such as flaking or feathering, the study found their appearance to be more scarce and less related to one particular weapon when creating chop wounds and more to the process of sharp force trauma as a whole (McCardle & Stojanovski, 2018). However, in contrary to the findings of McCardle & Stojanovski (2018), and consistent with the results of this research, an investigation completed by Ghui, et al. (2024) found the presence of

flaking and feathering to be one of the most distinctive traits when analysing cut marks produced by serrated and microserrated knives. The results of this study were able to define a methodological approach to determining a cut mark in bone using a flowchart depending on the prevalent characteristics (See chapter 4) (Ghui, et al. 2024).

A standard approach to analysis sharp force trauma is the use of X-Ray. The use of an X-Ray provides non-invasive images of fleshed covered bone can allow an insight into some morphological aspects of a sharp force trauma injury, i.e., size, depth, and the presence of striations (Garvin, et al. 2016). That being said, recent technological advances have overtaken the use of X-Ray analysis, with approaches such as micro-CT and Lodox providing clearer and more accurate scans when compared to X-Ray (Spies, et al. 2022). Spies and collaborators (2022) labelled X-Ray a 'last resort' in sharp force trauma identification due to its lack of sensitivity on all trauma injuries applied, with its highest detection resulting in 46.5% for chop wounds, whereas micro-CT and Lodox, a low-dose, full body scan, each detected 60% and over (Spies, et al. 2022).

A more recent advancement into the analysis of cut marks, and utilised in this thesis, is the use of 3D microscopy, as seen in chapters 4 & 5. The use of this technique allows for precise analysis of small surfaces at high magnification with clear images and 3 dimensional recreations (Moretti, et al. 2015). First applied to a forensic context in 2012 by Boschin and Crezzini, the use of a 3D microscope was found to capture images of a bone surface to apply to taphonomic analysis, along with morphological and metrical data of a cut marks measurements. The study focused on more anthropological aspects with the intentions of applying the findings to differentiate between tools and their materials, e.g. stone or metal (Boschin & Crezzini, 2012), however, the transferrable approach can be applied to that of forensic investigations, as the cut mark can be deeply analysed to gain data on the morphological aspects i.e., size, shape, width and depth. This data can then be used to calculate the essential volume of a cut mark for differentiation between tools/weapons used, as seen in this thesis. Also similar to this thesis, more recent research has demonstrated the practicality of implementing 3D microscopy into the analysis of cut marks as a standardised approach along with further confirmation of its use for tool/weapon differentiation. Bello & Soglio

(2008) noted this technique could provide accurate results for the topography of cut marks with the potential to apply the findings to behavioural patterns, which in a forensic sense can lead to the events surrounding the time in which the trauma was received, i.e., a potential altercation or unmitigated attack. The study's results portrayed quantifying parameters of cut mark micromorphology with differentiating characteristics, however determining traits for varying patterns such carcass processing or butchery would require a comparative archive of data (Bello & Soglio, 2008), also correlating with the results of this thesis in chapters 4 & 5, in which differentiation between types of knives can be seen in the calculated volumes of each cut mark.

6.4 Thermal Alterations to Sharp Force Trauma on Porcine Bone

Chapter 5 of this thesis integrates the findings from chapters 3 and 4 to examine how sharp force trauma may be affected when bone is exposed to various temperatures. By applying the thermal alteration methods established in chapters 1 and 2, it was possible to assess whether observed changes were due to the burning process itself or the presence of trauma. Using a consistent burning protocol provided a baseline understanding of thermally induced changes in bone, allowing for the identification and analysis of any anomalies. Additionally, incorporating the insights from chapter two regarding the characteristics of cut marks and the influence of different tools or weapons helped contextualise these changes. This combined approach offers valuable insight into what forensic analysts might encounter when investigating burned skeletal remains that exhibit signs of sharp force trauma. Forensic investigations of this nature will need to understand previously mentioned aspects, such as characteristics of fire and how it may have started, but also whether the sharp force trauma determined was an injury or a cause of death with further burning as an attempt to eliminate the evidence. The research in this thesis found burned cut marks to still be identifiable, with volumetric calculations still possible. The before and after calculations of the burned cut marks provide an idea of how cut marks may alter depending on the bone type affected and how the fire burned, i.e., fuel source and maximum temperature. This is similar to that of Vachirawongsakorn, et al. (2022) as the study focused on cut marks in porcine ribs, created with serrated and non-serrated knives. Results found 72% of the marks were still

identifiable. However significant changes to length and width of each cut mark were also observed, this was also determined to differentiate depending on the type of knife used (Vachirawongsakorn, et al. 2022). Similar to this thesis in which, although each of the surviving cut marks were identifiable, variations to the conical volume of each depending on the knife used, bone type affected, and fuel source used in the fire, were observed, with some significance being identified when using charcoal as a fuel source, $p=0.025$, or when creating the cut marks with the large serrated knife, $p=0.046$. More recently, a study focusing on thermal alterations to saw marks in a forensic sense of 'hiding evidence' used saws to produce marks on ovine bones found distinctive characteristics were still able to be observed at varying temperatures, however this was ultimately deemed a 'temperature dependent' impact as varying temperatures resulted in varying results (Chang, et al. 2024). One of the most significant findings was the increase to kerf width and decrease to kerf depth once temperatures ranged between 600°C - 800°C, similar to the temperatures used in this study.

Ultimately the intent behind this thesis is to apply to forensic investigations with an idea of creating or attributing to a standardised approach of burned skeletal remains analysis with the inclusion of sharp force trauma injuries. This also includes the ability to understand the thermal changes to different types of bones depending on the fuel source or temperature reached, to identify cut marks and the differing characteristics depending on the weapon used, and ultimately a combination of both, to understand and identify the thermal changes to sharp force trauma, as each may be a factor in forensic investigations. This approach can also contribute to forensic investigations as a Standard Operating Procedure when analysing burned skeletal remains. This also includes a factor of 'reverse engineering' to reconstruct events, i.e., analysis can aid in identifying the individual, determining the cause of death, establishing the origin of the fire, and discerning the type of weapon used.

6.5 Limitations

The primary limitations of this research are associated with the availability and consistency of materials. Samples were locally sourced from abattoirs and butchers; however, as some suppliers

ceased trading during the course of the study, the acquisition of further material was hindered. This interruption resulted in inconsistencies in both the quality and quantity of bone types available for analysis.

The burning methods used in this study provided sufficiently controlled conditions to limit experimental variability. Nonetheless, such conditions do not fully replicate the complex and uncontrolled dynamics of real fire scenarios. To gain more realistic results, future investigations should therefore use less regulated burning environments that more closely mimic natural fire behaviour.

Further analytical limitations arose from the inability to use the muffle furnace with fleshed samples, which contributed additional inconsistencies to the dataset. Future research of this nature should seek to establish a more reliable and consistent source of materials, alongside experimental conditions that balance control with realistic fire behaviour in order to better simulate real fire scenarios.

Despite the advantages offered by the analytical techniques used in this study, each method presents inherent limitations that must be considered when interpreting results. ATR-FTIR analysis is primarily limited by its surface sensitivity, as infrared radiation typically penetrates only a few microns into a sample, restricting analysis to surface-level composition (Al-Amin, et al. 2025). Additionally, the presence of water can significantly interfere with infrared absorption, which is particularly problematic when analysing bone samples that have been frozen for preservation prior to analysis (Eurofins, 2025). X-ray imaging provides non-destructive and rapid assessment of bone quality; however, it requires a high level of operator training to ensure clear and accurate image production, particularly when residual soft tissue is present, as organic materials do not image as effectively as bone (Akhter & Recker, 2021). Furthermore, although risks are minimal when appropriate safety procedures are followed, radiation exposure remains a consideration. Similarly, X-ray fluorescence (XRF) analysis may fail to detect certain elements, making repeatability essential to ensure data reliability, and also presents a low risk of radiation exposure without adequate training (Padilla-Alvarez, 2009). Finally, 3D micro-imaging

techniques are highly dependent on sample preparation and storage conditions, as previously frozen and thawed bone samples may retain water or ice, leading to blurred images and compromised image quality.

Complimentary Techniques

Scanning Electron Microscopy with Energy Dispersive Spectroscopy (SEM-EDS)

Scanning Electron Microscopy coupled with Energy Dispersive Spectroscopy (SEM-EDS) is a high-resolution analytical technique used to examine surface morphology and elemental composition at the micro- to nanoscale. SEM functions by scanning a focused electron beam across the sample surface, generating detailed images through electron–matter interactions, while EDS detects characteristic X-rays emitted from the sample to identify and semi-quantify elemental composition (Goldstein et al., 2018). In forensic bone analysis, SEM-EDS is particularly valuable for identifying micro-damage associated with sharp force trauma, heat-induced cracking, and mineral phase alterations, as well as mapping elemental changes at trauma margins following thermal exposure (Thompson, 2015; Baier et al., 2021).

Raman Spectroscopy

Raman spectroscopy is a non-destructive vibrational spectroscopic technique that provides molecular-level information on the chemical composition and structural organisation of materials. The technique relies on the scattering of monochromatic laser light, producing spectra that correspond to specific molecular bonds and crystalline structures (Smith and Dent, 2019). In bone analysis, Raman spectroscopy is particularly effective for assessing changes in mineral crystallinity, carbonate substitution, and the organic–inorganic ratio, making it well suited for evaluating heat-induced alterations (Pasteris et al., 2014; Sa et al., 2017). Its high spatial resolution enables targeted analysis of specific regions, such as cut mark edges or fracture surfaces, complementing ATR-FTIR data.

Micro-Computed Tomography (Micro-CT)

Micro-computed tomography (Micro-CT) is a non-destructive three-dimensional imaging technique that enables high-resolution visualisation of internal structures within a sample. The method uses X-rays to generate multiple radiographic projections that are reconstructed into volumetric datasets, allowing detailed assessment of internal morphology without physical sectioning (Stock, 2008). In the analysis of skeletal remains, Micro-CT is particularly valuable for identifying internal fracture patterns, trauma propagation pathways, and heat-induced structural changes such as increased porosity and micro-cracking (Kahlon et al., 2019; Viner et al., 2020). This technique provides critical insight into trauma sequencing and structural integrity, complementing surface-based imaging methods such as microscopy and radiography.

6.6 Future Research

Further work for this thesis would see each experiment, particularly chapter 5, repeated for statistical improvement. Taking into consideration each results chapter, further work could be applied to chapter 3 to better understand the thermal alterations to bone by including a more varied selection of bones or bones or segmental body parts i.e., a complete section of a skeleton, both fleshed/defleshed for results more consistent with the findings of a crime scene. This would also include more varied temperatures, matching those used in the muffle furnace samples, for a better understanding and observation of the thermal alterations to bone in a more realistic setting as opposed to the controlled environment of a muffle furnace. Further work for chapter 4 would look to include more varied tools/weapons to create differentiating sharp force injuries alongside cut marks, e.g. chop wounds. This inclusion would help to provide a better understanding of the injuries that can be obtained from different weapons and how different bone types may react. Finally, for chapter 5, this would include each of the previously mentioned additions, as this chapter is an amalgamation of chapter 3 and 4. Chapter 5 would see each new aspect for further analysis of how more varied temperatures affect sharp force trauma, particularly from a wider selection of weapons.

An overall additional approach would be to take into consideration the effects of incomplete combustion. Incomplete combustion is the result of insufficient oxygen levels during combustion,

caused by either extinguishing or smothering a fire, therefore resulting in increased levels of carbon dioxide and an interrupted chemical process (Speight, 2011). The effects of incomplete combustion have been found to interfere with changes to colour of bone due to the presence of unburnt compounds, such as carbon (Krap, et al. 2019). As mentioned in chapter 3, the colour of a bone once burned can be used to speculate the maximum temperature a fire may have reached which can then allude to potential fuel sources, however, a change to the expected colour could lead to a misinterpretation of the surface layer changes (Krap, et al. 2017). The effects of complete combustion may also increase the presence of heat related fractures (Schmidt & Uhlig, 2012), a change to the bones morphological structure that must be taken into consideration if analysing thermal alterations to skeletal trauma.

6.7 Concluding comments

This research has highlighted the complex interplay between thermal exposure and sharp force trauma in skeletal remains. Through systematic experimentation and analysis, it has been demonstrated that varying temperatures can significantly alter the morphological and chemical characteristics of bone, thereby complicating the interpretation of traumatic injuries in forensic investigations.

The findings emphasise the necessity for forensic analysts to adopt a standardised approach when assessing burned skeletal remains. Such an approach should incorporate a range of analytical techniques, and a comprehensive understanding of how different fuel sources and temperatures affect bone, as this knowledge provides critical context for reconstructing the circumstances of fire events. Further, this study has shown that sharp force trauma injuries can be differentiated not only by the type of weapon used, but also by the visual and volumetric characteristics of cut marks. The use of calculated conical volumes to assess cut depth and width offers a more robust method for distinguishing between trauma types. Moreover, the application of high temperatures to bone with pre-existing trauma has been shown to induce morphological alterations to cut marks, reinforcing the need for standardised protocols when evaluating burned skeletal remains with trauma.

A key novel contribution of this thesis lies in the detection of cerium (Ce), bromine (Br), and neodymium (Nd) in thermally altered bone. These trace elements were observed exclusively in the open-flame and garden-incinerator scenarios, with significant forensic implications. The identification of Ce in open-flame samples, related to the use of butane lighters containing mischmetal alloy, marks the first reported instance of this element in burned bone, offering a potential means of reconstructing ignition methods. Similarly, the detection of Br, likely from brominated flame retardants in household furnishings, represents the first evidence of this element in burned bone and provides a novel starting point for contextualising the surrounding materials and placement of the remains, with potential to distinguish between accidental and deliberate fire scenarios. Nd, while of uncertain origin, was detected in both open-flame and garden-incinerator contexts, highlighting the necessity of accounting for both environmental contributions and potential instrumental contamination in elemental analysis. Collectively, these findings extend current knowledge by demonstrating that trace elements can be incorporated into bone under specific burning conditions, offering new approaches for forensic fire reconstruction and contributing to broader discussions of post-mortem diagenesis in thermally altered remains.

As forensic science continues to evolve, the integration of the findings presented in this thesis will enhance the accuracy and reliability of trauma and fire reconstructions. By combining controlled and less-controlled experimental data with novel elemental insights, this research advances methodological approaches for interpreting burned human remains, both with and without sharp force trauma, and ultimately contributes to the pursuit of justice in forensic investigations.

References

Adejumo, B.A. and Obasa, P.A. (2020) *Development of a muffle furnace*, *Journal of Science, Technology, Mathematics and Education (JOSTMED)*, 16(2), pp.94–103. Available at: https://journal.futminna.edu.ng/index.php/jostmed/issue/download/120/719

Ahlawat, B. (2021) *Burned bones as important forensic evidence: a review*, *Journal of Forensic Research*, 12(9). doi:10.35248/2157-7145.21.12.641. (Available at a journal repository) — this review summarises the four stages of heat-induced transformation: dehydration, decomposition, inversion, and fusion of bone following exposure to fire.

Alkhuder, K. (2022). Attenuated Total reflection-Fourier Transform Infrared spectroscopy: a Universal Analytical Technique with Promising Applications in Forensic Analyses. International Journal of Legal Medicine, 136(6), pp.1717–1736. doi:https://doi.org/10.1007/s00414-022-02882-2.

Alsulami, A. and Alfarsi, Y. (2022) '"The Use of X-Rays in Forensic Science: A Review of Applications and Recent Advances"', Migration Letters , 19(1741–8984).

Angin, S., Simsek, I.E. and Bilgic, E. (2020) 'Chapter 6 - Architecture of bone tissue and its adaptation to pathological conditions', in Comparative kinesiology of the human body: Normal and pathological conditions. London, United Kingdom: Academic Press, pp. 71–90.

Al Hajj, W., Salla, M., Krayem, M., Khaled, S., Hassan, H.F. and El Khatib, S. (2024). Hydrolysed collagen: Exploring its applications in the food and beverage industries and assessing its impact on human health – A comprehensive review. Heliyon, [online] 10(16), p.e36433. doi:https://doi.org/10.1016/j.heliyon.2024.e36433.

Anthrax (2022) Mayo Clinic. Available at: https://www.mayoclinic.org/diseasesconditions/anthrax/symptoms-causes/syc-20356203 (Accessed: 09 June 2023).

Arzi, B. et al. (2020) '2 - Maxillofacial bone healing', in Oral and maxillofacial surgery in dogs and cats. 2nd edn. St. Louis, MO: Elsevier, pp. 6–13.

Auer, J.A., Lopliez, M. and Markel, M. (2019) 'Chapter 74 - Bone Biology and Fracture Healing', in Equine surgery. 4th edn. St. Louis (Missouri): Elsevier, pp. 1025–1040.

Babrauskas, V. 2022, 'Ignition of gases, vapours, and liquids by hot surfaces', *Fire Technology*, vol. 58, pp. 281–310.ga

Baier, W., Norman, D.G., Donnelly, M.J. and Williams, M.A. (2021). Forensic 3D Printing from micro-CT for Court use- Process Validation. Forensic Science International, 318, p.110560. doi:https://doi.org/10.1016/j.forsciint.2020.110560.

Bailey, J.A., Wang, Y.S., van der Goot, F.R.W. & Gerretsen, R.R.R. (2011) *Statistical analysis of kerf mark measurements in bone*. Forensic Science, Medicine and Pathology, 7(1), pp. 53–62. doi:10.1007/s12024-010-9185-6.

Bassi, A. et al. (2016) '5 - Bone tissue regeneration', in Electrospinning for tissue regeneration. WOODHEAD, pp. 93–110. 151

Battisti, A.S., Haftel, A. and Murphy-Lavoie, H.M. (2023) *Barotrauma*, StatPearls [Internet]. Treasure Island (FL): StatPearls Publishing. Available at: https://www.ncbi.nlm.nih.gov/books/NBK482348/

Becker, P. (2014) "Chapter 4 - Our Disturbances, Disruptions and Disasters in a Dynamic World," in Sustainability Science: Managing Risk and resilience for sustainable development. Amsterdam: Elsevier, pp. 57–117.

Bello, S.M. and Soligo, C. (2008). A new method for the quantitative analysis of cutmark micromorphology. Journal of Archaeological Science, 35(6), pp.1542–1552. doi:https://doi.org/10.1016/j.jas.2007.10.018.

Ben Amar, I., Roudjane, M., Griguer, H., Miled, A. & Messaddeq, Y. 2022, 'The effect of particle size and water content on XRF measurements of phosphate slurry', *Scientific Reports*, vol. 12, article no. 17823, doi:10.1038/s41598-022-21392-0

Betts, J.G. et al. (2022) Anatomy and physiology, 2E Vol 2. Houston, TX: OpenStax, Rice University.

Bilezikian, J.P. et al. (2020) 'Chapter 14 - Bone Matrix Proteoglycans and Glycoproteins', in Principles of Bone Biology. 2nd edn. London, United Kingdom: Elsevier/Academic Press, pp. 225–237.

Bilezikian, J.P. et al. (2020) 'Chapter 4 - Carbohydrates', in Principles of Bone Biology. London, United Kingdom: Elsevier/Academic Press, pp. 77–103.

Blázquez, E. and Thorn, C. (2010) *Fires and explosions*, *Anaesthesia & Intensive Care Medicine*, 11(11), pp.455–457. doi:10.1016/j.mpaic.2010.08.007. Available at: https://www.sciencedirect.com/science/article/abs/pii/S1472029910002043 Blanco, A. and Blanco, G. (2022) 'Chapter 4 - Carbohydrates', in medical biochemistry. London: Elsevier, AP, Academic Press, pp. 77–103.

Blitterswvig, B.C.A. et al. (2023) 'Chapter 16 - Cartilage and bone regeneration', in Tissue engineering. 3rd edn. Amsterdam: Academic Press, pp. 533–583.

Bloise, N. and Visai, L. (2022) *Skeletal system*, in *Bioprinting for skeletal tissue regeneration: from current trends to future promises*. Elsevier. Available at: https://www.sciencedirect.com/science/article/pii/B978032385430600008X

Blosa, M., Sonntag, M., Carsten Jäger, Weigel, S., Seeger, J., Frischknecht, R., Seidenbecher, C.I., Matthews, R.T., Arendt, T., Rübsamen, R. and Morawski, M. (2015). The extracellular matrix molecule brevican is an integral component of the machinery mediating fast synaptic transmission at the calyx of Held. The Journal of Physiology, 593(19), pp.4341–4360. doi:https://doi.org/10.1113/jp270849.

Bonewald, L.F., Kneissel, M. and Johnson, M. (2013) *Preface: the osteocyte*, *Bone*, 54(2), p.181. doi:10.1016/j.bone.2013.02.018. Available at: https://pubmed.ncbi.nlm.nih.gov/23486185/

Bonney, H. and Goodman, A. (2020). Validity of the Use of Porcine Bone in Forensic Cut Mark Studies. Journal of Forensic Sciences, 66(1), pp.278–284. doi:https://doi.org/10.1111/1556-4029.14599. 152

Bosch, P., Alemán, I., Moreno-Castilla, C. & Botella, M. (2011) *Boiled versus unboiled: a study on Neolithic and contemporary human bones*. Journal of Archaeological Science, 38(10), pp. 2561–2570. doi:10.1016/j.jas.2011.04.019.

Boschin, F. and Crezzini, J. (2011). Morphometrical Analysis on Cut Marks Using a 3D Digital Microscope. International Journal of Osteoarchaeology, 22(5), pp.549–562. doi:https://doi.org/10.1002/oa.1272.

Boslaugh, S.E. (2019). Pyrolysis | Chemical Reaction. In: Encyclopaedia Britannica. [online] Available at: https://www.britannica.com/science/pyrolysis.

Braun, D.R., Pante, M. and Archer, W. (2016). Cut marks on bone surfaces: influences on variation in the form of traces of ancient behaviour. Interface Focus, 6(3), p.20160006. doi:https://doi.org/10.1098/rsfs.2016.0006.

Bretaud, S, Guillon, E., Karppinen, S.-M., Pihlajaniemi, T. and Ruggiero, F. (2020). Collagen XV, a multifaceted multiplexin present across tissues and species. Matrix biology plus, [online] 6-7(100023), pp.100023–100023. doi:https://doi.org/10.1016/j.mbplus.2020.100023.

Bryden, D.W., Tilghman, J.I. and Hinds, S.R. (2019). Blast-Related Traumatic Brain Injury: Current Concepts and Research Considerations. Journal of Experimental Neuroscience, [online] 13(13), p.117906951987221. doi:https://doi.org/10.1177/1179069519872213.

Byard, R. and Payne-James, J. (2016) 'Injury, fatal and nonfatal: Sharp and cutting-edge wounds', in Encyclopaedia of forensic and legal medicine. 2nd edn. Amsterdam: Elsevier, pp. 244–256.

Carew, R.M., French, J. and Morgan, R.M. (2021) '3D forensic science: A new field integrating 3D imaging and 3D printing in Crime Reconstruction', Forensic Science International: Synergy, 3, p. 100205. doi:10.1016/j.fsisyn.2021.100205.

Carroll, E. & Squires, K. (2020) 'Burning by numbers: A pilot study using quantitative petrography in the analysis of heat-induced alteration in burned bone', *International Journal of Osteoarchaeology*, 30, pp. 1-9. doi: 10.1002/oa.2902.

CDC (2009). American College of Emergency Physicians. [online] www.acep.org. Available at: https://www.acep.org/imports/clinical-and-practice-management/resources/ems-and- 153 disaster-preparedness/disaster-preparedness-grant-projects/cdc---blast-injury/cdc-blastinjury-fact-sheets/crush-injury-and-crush-syndrome.

Chakrabarty, A. and Cagin, T. (2016) *Fire and related process safety concepts*, in *Multiscale Modeling for Process Safety Applications*. Elsevier, pp. 5-110. Available at: https://www.sciencedirect.com/science/article/pii/B9780123969750000024

Chang, E.K., Abrahams, S. and Mole, C.G. (2024) 'Hiding the evidence: Preliminary investigation of heat-induced alterations to pre-existing saw Mark Trauma', Forensic Science International, 361, p. 112142. doi:10.1016/j.forsciint.2024.112142.

Cheremisinoff, N.P. and Rosenfeld, P.E. (2010) 'Sources of air emissions from Pulp and Paper Mills', Handbook of Pollution Prevention and Cleaner Production, pp. 179–259. doi:10.1016/b978-0-08-096446-1.10006-1.

Christensen, A., Passalacqua, N. and Bartelink, E. (2014) 'Chapter 2 - Human Osteology and Odontology', in Forensic anthropology: Current methods and practice. 2nd edn. San Diego, CA: Academic Press, pp. 19–53.

Clark, H, GOV.UK (2023). Fire and Rescue Incident statistics: England, Year Ending June 2022. [online] GOV.UK. Available at: https://www.gov.uk/government/statistics/fire-andrescue-incident-statistics-england-year-ending-june-2022/fire-and-rescue-incidentstatistics-england-year-ending-june-2022.

Clarke, B. (2008). Normal Bone Anatomy and Physiology. Clinical Journal of the American Society of Nephrology, 3(Supplement 3), pp.S131–S139.

Clemente, M.A., La Tegola, L., Mattera, M. and Guglielmi, G. (2017). Forensic Radiology: an Update. Journal of the Belgian Society of Radiology, [online] 101(S2). doi:https://doi.org/10.5334/jbr-btr.1420.

Cleveland Clinic (2022). Cartilage: What It Is, Function & Types. [online] Cleveland Clinic. Available at: https://my.clevelandclinic.org/health/body/23173-cartilage.

Cleveland Clinic (2022). Bone Fractures. [online] Cleveland Clinic. Available at: https://my.clevelandclinic.org/health/diseases/15241-bone-fractures. 154

Cohen–Jonathan, E., Bernhard, E.J. and McKenna, W.G. (1999). How Does Radiation Kill cells? Current Opinion in Chemical Biology, 3(1), pp.77–83. doi:https://doi.org/10.1016/s1367-5931(99)80014-3.

Collins, C. et al. (2019) 'Bone Micro- and Nanomechanics', in Encyclopaedia of Biomedical Engineering. Chapel Hill, NC: University of North Carolina, pp. 22–44.

Coneva, I. and Mullerova, J. (2018) *Definition of fire processes*, in *18th International Multidisciplinary Scientific GeoConference SGEM 2018*. 18th International Multidisciplinary Scientific GeoConference SGEM, 02–08 July 2018, Sofia, Bulgaria, pp.293–300. doi:10.5593/sgem2018/5.2/S20.039. Available at: https://www.sgem.org/index.php/component/jresearch/?view=publication&task=show&id=1465

Courtenay, L.A., Maté-González, M.A., Aramendi, J., Yravedra, J., González-Aguilera, D. & Domínguez-Rodrigo, M. (2018) *Testing accuracy in 2D and 3D geometric morphometric methods for cut mark identification and classification*. PeerJ, 6, e5133. doi:10.7717/peerj.5133.

Creager, M.A., Beckman, J.A. and Loscalzo, J. (2020) 'Chapter 3 - Vascular Smooth Muscle', in Vascular medicine: A companion to braunwald's heart disease. 2nd edn. Philadelphia, PA: Elsevier, pp. 25–42.

Crowder, C., Rainwater, C.W. and Fridie, J.S. (2013). Microscopic Analysis of Sharp Force Trauma in Bone and Cartilage: A Validation Study, Journal of Forensic Sciences, 58(5), pp.1119–1126. doi:https://doi.org/10.1111/1556-4029.12180.

Daniels, M.P. (2012). The Role of Agrin in Synaptic development, Plasticity and Signalling in the Central Nervous System. Neurochemistry International, 61(6), pp.848–853. doi:https://doi.org/10.1016/j.neuint.2012.02.028.

Devlin, J. and Herrmann, N. (2018) 'Chapter 6 - Bone Colour', in The Analysis of Burned Human Remains. 2nd edn. Academic Press, pp. 119–138.

Dokov, W. (2009). Assessment of Risk Factors for Death in Electrical Injury. Burns, 35(1), pp.114–117. doi:https://doi.org/10.1016/j.burns.2008.05.005.

Ellobody, E. (2023) 'Nonlinear material behaviour of the bridge components', Finite Element Analysis and Design of Steel and Steel concrete Composite Bridges, pp. 53–118. doi:10.1016/b978-0-443-18995-1.00001-3.

Eriksson, A. and Lindahl, T. (2019). Mechanisms of DNA repair and bone health. *International Journal of Molecular Sciences*, 20(15), p.3732. doi:10.3390/ijms20153732.

Eurofins (2023). FTIR (Fourier Transform Infrared Spectroscopy) Laboratory Services. [online] EAG Laboratories. Available at: https://www.eag.com/techniques/spectroscopy/fourier-transform-infraredspectroscopy-ftir/. 155

Eze, U. and Ojifinni, K. (2022). Trauma Forensics in Blunt and Sharp Force Injuries. Journal of the West African College of Surgeons, 12(4), pp.94–101.

F Faissner, A., Heck, N., Dobbertin, A. and Garwood, J. (2022). DSD-1-Proteoglycan/Phosphacan and Receptor Protein Tyrosine Phosphatase-Beta Isoforms during Development and Regeneration of Neural Tissues. [online] Nih.gov. Available at: https://www.ncbi.nlm.nih.gov/books/NBK6484/ [Accessed 20 Jun. 2025].

Fakhlaei, R. et al. (2024) 'Application, challenges and future prospects of recent nondestructive techniques based on the electromagnetic spectrum in food quality and safety', Food Chemistry, 441, p. 138402. doi:10.1016/j.foodchem.2024.138402.

Fan, R., Hao, Y., Liu, X., Kang, J., Hu, J., Mao, R., Liu, R., Zhu, N., Xu, M. and Li, Y. (2021). Native Collagen II Relieves Bone Impairment through Improving Inflammation and Oxidative Stress in Ageing db/db Mice. Molecules, 26(16), p.4942. doi:https://doi.org/10.3390/molecules26164942.

Feldman, D., J Wesley Pike and S, J. (2011). Vitamin D. Amsterdam ; Boston: Academic Press.

Feng, X. (2009). Chemical and Biochemical Basis of Cell-Bone Matrix Interaction in Health and Disease. Current Chemical Biology, 3(2), pp.189–196. doi:https://doi.org/10.2174/2212796810903020189.

Ferner, R.E. (2008) *Post-mortem clinical pharmacology*, *British Journal of Clinical Pharmacology*, available at: https://pubmed.ncbi.nlm.nih.gov/18637886/

Figueiredo, M., Fernando, A., Martins, G., Freitas, J., Judas, F. and Figueiredo, H. (2010) *Effect of the calcination temperature on the composition and microstructure of hydroxyapatite derived from human and animal bone*, Ceramics International, 36(8), pp. 2383–2393. doi:10.1016/j.ceramint.2010.07.016.

Filmus J, Capurro M, Rast J. Glypicans. Genome Biol. 2008;9(5):224. doi: 10.1186/gb2008-9-5-224. Epub 2008 May 22. PMID: 18505598; PMCID: PMC2441458.

Fischer, R.S., Wu, Y., Kanchanawong, P., Shroff, H. and Waterman, C.M. (2011). Microscopy in 3D: a biologist's toolbox. Trends in Cell Biology, 21(12), pp.682–691. doi:https://doi.org/10.1016/j.tcb.2011.09.008. 156

Florencio-Silva, R., Sasso, G.R. da S., Sasso-Cerri, E., Simões, M.J. and Cerri, P.S. (2015). Biology of Bone Tissue: Structure, Function, and Factors That Influence Bone Cells. BioMed Research International, 2015(421746), pp.1–17. doi:https://doi.org/10.1155/2015/421746.

Floyd, A.E. et al. (2007) 'Chapter 2 - Functional Anatomy of the Equine Digit: Determining Function from Structure', in Equine podiatry. 2nd edn. St. Louis (Mo.): Saunders, pp. 35–41.

Fowler, K.A., Dahlberg, L.L., Haileyesus, T. and Annest, J.L. (2015) *Firearm injuries in the United States: prevalence, public health burden, and implications for prevention. Preventive Medicine*, 79, pp.5–14. Available at: https://www.ncbi.nlm.nih.gov/pmc/articles/PMC4700838/

Franz-Odendaal, T.A., Hall, B.K. and Witten, P.E. (2005) 'Buried alive: How osteoblasts become osteocytes', Developmental Dynamics, 235(1), pp. 176–190. doi:10.1002/dvdy.20603.

Friedlander, H. et al. (2024) 'An innovative way to use 3d modelling on burnt bone to differentiate heat fractures from blunt and sharp force trauma', WIREs Forensic Science, 6(5). doi:10.1002/wfs2.1525.

Fritz, S., Chaitow, L. and Hymel, G.M. (2008) 'CHAPTER 6 - Review of Pertinent Anatomy and Physiology', in Clinical massage in the healthcare setting. 3rd edn. St. Louis, MO: Mosby, pp. 140–195.

Gallo, G., Fyhrie, M., Paine, C., Ushakov, S.V., Izuho, M., Gunchinsuren, B., Zwyns, N. and Navrotsky, A. (2021). Characterization of structural changes in modern and archaeological burnt bone: Implications for differential preservation bias. PLOS ONE, 16(7), p.e0254529. doi:https://doi.org/10.1371/journal.pone.0254529.

Galloway, A., Pope, E. and Juarez, C. (2024) 'Bone colour changes and interpretation of the temperature/duration of fire exposure to human remains in the forensic context', WIREs Forensic Science, 6(4). doi:10.1002/wfs2.1517.

Garantziotis, S. and Savani, R.C. (2019). Hyaluronan biology: a Complex Balancing Act of structure, function, Location and Context. Matrix Biology, 78-79, pp.1–10. doi:https://doi.org/10.1016/j.matbio.2019.02.002. 157

Garche, J. and Brandt, K. (2022) "Chapter 12 - Li-Secondary Battery: Damage Control Author links open overlay panel," in Electrochemical Power Sources: Fundamentals, systems, and applications-. S.l., Ulm: ELSEVIER, pp. 507–629.

Garnero, P. (2015). The Role of Collagen Organization on the Properties of Bone. Calcified Tissue International, 97(3), pp.229–240. doi:https://doi.org/10.1007/s00223-015-9996-2.

Garvin, H.M. and Stock, M.K. (2016). The Utility of Advanced Imaging in Forensic Anthropology. Academic Forensic Pathology, [online] 6(3), pp.499–516. doi:https://doi.org/10.23907/2016.050.

Gerrard, N. (2022). Grenfell: Five Things That Have Changed Five Years on (and Some That haven't) - Construction Management. [online] Construction Management. Available at: https://constructionmanagement.co.uk/grenfell-five-things-that-have-changed-fiveyears-on-and-some-that-havent [Accessed 20 Jun. 2025].

Gheisari, H., Karamian, E. and Abdellahi, M. (2015) 'A novel hydroxyapatite – hardystonite nanocomposite ceramic', Ceramics International, 41(4), pp. 5967–5975. doi:10.1016/j.ceramint.2015.01.033.

Ghui, M, Eliopoulous, C, and Borrini, M. (2023). Citation. Sage Journals, [online] 64(3). doi:https://doi.org/10.1177/00258024231198912. 66. Gitto, L. and Arunkumar, P. (2021). Sharp Force Injuries. [online] www.pathologyoutlines.com. Available at: https://www.pathologyoutlines.com/topic/autopsysharpforce.html.

Gitto, L. and Stoppacher, R. (2021). Gunshot Wounds. [online] www.pathologyoutlines.com. Available at: https://www.pathologyoutlines.com/topic/forensicsgunshotwounds.html.

Goldstein, J.I., Newbury, D.E., Joy, D.C., Ritchie, N.W.M., Scott, J.H.J. and Joy, D.C. (2018) *Scanning Electron Microscopy and X-ray Microanalysis*. 4th edn. New York: Springer.

González-Morelo, K.J., Vega-Sagardía, M. and Garrido, D. (2020). Molecular Insights into O-Linked Glycan Utilization by Gut Microbes. Frontiers in Microbiology, 11(11). doi:https://doi.org/10.3389/fmicb.2020.591568.

Groarke, R., Vijayaraghavan, R.K., Powell, D., Rennie, A. and Brabazon, D. (2021). 18 - Powder characterization—methods, standards, and state of the art. [online] ScienceDirect. Available at: https://www.sciencedirect.com/science/article/abs/pii/B9780128240908000068.

Grujicic, B. (2003) *Bones of the human body: Overview and anatomy*. Kenhub. Available at: https://www.kenhub.com/en/library/anatomy/how-many-bones-can-you-find-in-the-human-body

Gubbiotti, M.A., Neill, T. and Iozzo, R.V. (2017). A Current View of Perlecan in Physiology and pathology: a Mosaic of Functions. Matrix biology : journal of the International Society for Matrix Biology, [online] 57-58, pp.285–298. doi:https://doi.org/10.1016/j.matbio.2016.09.003.

Haddad, L.M., Winchester, J.F., Shannon, M.W., Borron, S.W., Burns, M. and Linden, C. (2007). Haddad and Winchester's clinical management of poisoning and drug overdose. Philadelphia: Saunders/Elsevier.

Hagen, B.C. and Meyer, A.K. (2021) *From smoldering to flaming fire: Different modes of transition*, *Fire Safety Journal*, 121, p.103292. doi:10.1016/j.firesaf.2021.103292. Available at: https://www.sciencedirect.com/science/article/pii/S0379711221000199

Hammerli, J., Hermann, J., Tollan, P. and Naab, F. (2021). Measuring in Situ CO2 and H2O in Apatite via ATR-FTIR. Contributions to Mineralogy and Petrology, 176(12). doi:https://doi.org/10.1007/s00410-021-01858-6.

Handlos, P., Švecová, T., Vrtková, A., et al. (2023) *Review of patterns in homicides by sharp force: one institution's experience*. Forensic Science, Medicine and Pathology, 19, pp. 525–533. doi:10.1007/s12024-023-00576-8.

Heljasvaara, R., Aikio, M., Ruotsalainen, H. and Pihlajaniemi, T. (2017). Collagen XVIII in Tissue Homeostasis and Dysregulation — Lessons Learned from Model Organisms and Human Patients. Matrix Biology

Helmenstine, A.M. 2024, *Flame Temperatures Table for Different Fuels*, *ThoughtCo*, 19 May 2024, viewed 13 January 2026, https://www.thoughtco.com/flame-temperatures-table-607307y, 57-58, pp.55–75. doi:https://doi.org/10.1016/j.matbio.2016.10.002.

Hilenski, L.L. and Griendling, K.K. (2013) *Syndecans as coreceptors in signal transduction*, in Braunwald's Heart Disease: A Companion to Braunwald's Heart Disease. 2nd edn. Elsevier. Available at: https://www.sciencedirect.com/topics/medicine-and-dentistry/syndecan

Hiraoka, Y., Sedat, J.W. and Agard, D.A. (1990) 'Determination of three-dimensional imaging properties of a light microscope system. partial confocal behaviour in epifluorescence microscopy', Biophysical Journal, 57(2), pp. 325–333. doi:10.1016/s0006- 3495(90)82534-0. 159

Hochberg, M.C. et al. (2023) in Rheumatology. 6th edn. Philadelphia, PA: Elsevier, pp. 1014–1020.

Hoesel, A., Reidsma, F.H., van Os, B.J.H., Megens, L. and Braadbaart, F. (2019). Combusted bone: Physical and chemical changes of bone during laboratory simulated heating under oxidising conditions and their relevance for the study of ancient fire use. Journal of Archaeological Science: Reports, 28, p.102033. doi:https://doi.org/10.1016/j.jasrep.2019.102033.

Houck, M.M. and Siegel, J.A. (2015). Fundamentals of Forensic Science. 3rd ed. Amsterdam ; Boston: Elsevier/Academic Press.

HSE (2019). Electrical Injuries - Electrical Safety at Work. [online] Hse.gov.uk. Available at: https://www.hse.gov.uk/electricity/injuries.htm.

Iozzo, R.V. and Schaefer, L. (2015) 'Proteoglycan form and function: A comprehensive nomenclature of Proteoglycans', Matrix Biology, 42, pp. 11–55. doi:10.1016/j.matbio.2015.02.003.

Jeong, J., Kim, J.H., Shim, J.H. et al. Bioactive calcium phosphate materials and applications in bone regeneration. Biomatter Res 23, 4 (2019). https://doi.org/10.1186/s40824-018-0149-3

Jeromelj, T., Leskovar, T. & Zupanič Pajnič, I. (2025) *The impact of storage conditions on DNA preservation in human skeletal remains: a comparison of freshly excavated samples and those stored for 12 years in a museum depot*. Genes, 16(1), 78. doi:10.3390/genes16010078

Jorolemon, M.R., Lopez, R.A. and Krywko, D.M. (2023). Blast Injuries. [online] PubMed. Available at: https://pubmed.ncbi.nlm.nih.gov/28613664/.

Kasem, M.A. et al. (2020) 'Investigating Egyptian archaeological bone diagenesis using ATR-FTIR micro spectroscopy', Journal of Radiation Research and Applied Sciences, 13(1), pp. 515–527. doi:10.1080/16878507.2020.1752480.

Kattla, J.J., Struwe, W.B., Doherty, M., Adamczyk, B., Saldova, R., Rudd, P.M. and Campbell, M.P. (2011) *Protein glycosylation*, in *Industrial Biotechnology and Commodity Products*, 2nd edn, Elsevier, pp.467–486. Available at: https://www.sciencedirect.com/science/article/pii/B9780080885049002300

Kahlon, B., Wescott, D.J. and Baumer, T.G. (2019) The application of micro-CT in forensic anthropology, *Journal of Forensic Sciences*, 64(6), pp.1660–1670.

Keeley, J.E. (2009) "Fire intensity, fire severity and burn severity: A brief review and suggested usage," International Journal of Wildland Fire, 18(1), p. 116. Available at: https://doi.org/10.1071/wf07049. 160

Keshav Tumram, N. (2020). Bone Abrasions Due to the Dragging Force of a Moving vehicle: Two Unusual Case Reports. Archives of Forensic Medicine and Criminology, 70(4), pp.251–256. doi:https://doi.org/10.5114/amsik.2020.104583.

Khalid, H. and Aqif Anwar Chaudhry (2020). Basics of hydroxyapatite—structure, synthesis, properties, and clinical applications. pp.85–115. doi:https://doi.org/10.1016/b978-0-08-102834-6.00004-5. 86. KIANI, C., CHEN, L., WU, Y.J., YEE, A.J. and YANG, B.B. (2002). Structure

and function of aggrecan. Cell Research, 12(1), pp.19–32. doi:https://doi.org/10.1038/sj.cr.7290106.

Kim, J.-M. et al. (2020) 'Osteoblast-osteoclast communication and bone homeostasis', Cells, 9(9), p. 2073. doi:10.3390/cells9092073.

Kohli, R. & Mittal, K.L. (eds) 2012, *Developments in Surface Contamination and Cleaning: Detection, Characterization and Analysis of Contaminants*, Elsevier, Amsterdam.

Krap, T., Ruijter, J.M., Nota, K., Karel, J., Burgers, A.L., Aalders, M.C.G., Oostra, R.-J. and Duijst, W. (2019). Colourimetric analysis of thermally altered human bone samples. Scientific Reports, [online] 9(1). doi:https://doi.org/10.1038/s41598-019-45420-8.

Krasinski, K.E. (2018). Multivariate Evaluation of Criteria for Differentiating Cut Marks Created from Steel and Lithic Implements. Quaternary International, 466, pp.145–156. doi:https://doi.org/10.1016/j.quaint.2016.04.025.

Kristo, M.J. 2012, 'X-Ray Fluorescence Analysis', in M.F. L'Annunziata (ed.), *Handbook of Radioactivity Analysis*, 3rd edn, Academic Press, Oxford.

Latahir, A. Z., Wai, C. K., Yaacob, S. F. F. S., Rahim, R. A. & Abdul Rahim, R. (2025) *Exploring the elemental detection on portable XRF vs SEM-EDX in household alloy materials analysis*. Microchemical Journal, 213, p. 113667. doi:10.1016/j.microc.2025.113667

Lebon, M., Reiche, I., Gallet, X., Bellot-Gurlet, L. and Zazzo, A. (2016). Rapid Quantification of Bone Collagen Content by ATR-FTIR Spectroscopy. Radiocarbon, 58(1), pp.131–145. doi:https://doi.org/10.1017/rdc.2015.11.

Legan, L., Leskovar, T., Č rešnar, M., Cavalli, F., Innocenti, D. and Ropret, P. (2019). Non-invasive reflection FTIR characterization of archaeological burnt bones: Reference database and case studies. Journal of Cultural Heritage. doi:https://doi.org/10.1016/j.culher.2019.07.006. 161

Li, N., Spetz, M.R. and Ho, M. (2020). The Role of Glypicans in Cancer Progression and Therapy. Journal of Histochemistry & Cytochemistry, 12(68), p.002215542093370. doi:https://doi.org/10.1369/0022155420933709.

LibreTexts (2013). Coordination Chemistry. [online] Chemistry LibreTexts. Available at: https://chem.libretexts.org/Bookshelves/Inorganic_Chemistry/Supplemental_Modules _and_Websites_(Inorganic_Chemistry)/Coordination_Chemistry.

Lin, X., Patil, S., Gao, Y.-G. and Qian, A. (2020). The Bone Extracellular Matrix in Bone Formation and Regeneration. Frontiers in Pharmacology, 11(757). doi:https://doi.org/10.3389/fphar.2020.00757.

Liu, Z., Wang, F. and Chen, X. (2008). Integrin αvβ3-targeted Cancer Therapy. Drug Development Research, [online] 69(6), pp.329–339. doi:https://doi.org/10.1002/ddr.20265.

Logan, C. , McColl, S. (2024), 'Temperature Related Alterations to Mineral Levels and Crystalline Structure in Porcine Long Bone: Intense Heat vs. Open Flame', World Academy of Science, Engineering and Technology, Open Science Index 205, International Journal of Medical and Health Sciences, 18(1), 10 - 16.

Lotze, M.T. and Thomson, A.W. (2010). Natural Killer Cells : Basic Science and Clinical Application. Amsterdam ; Boston: Elsevier/Academic Press.

Love, J.C. (2019). Sharp Force Trauma Analysis in Bone and cartilage: a Literature Review. Forensic Science International, 299(119-127), pp.119–127. doi:https://doi.org/10.1016/j.forsciint.2019.03.035.

Luo, Y. and Amromanoh, O. (2021). Bone Organic-Inorganic Phase Ratio Is a Fundamental Determinant of Bone Material Quality. Applied Bionics and Biomechanics, [online] 2021, p.e4928396. doi:https://doi.org/10.1155/2021/4928396.

Mamede, A.P., Gonçalves, D., Marques, M.P.M. and Batista de Carvalho, L.A.E. (2017) *Burned bones tell their own stories: A review of methodological approaches to assess heat-induced diagenesis*. *Applied Spectroscopy Reviews*, 53(5), pp.1–33. doi:10.1080/05704928.2017.1400442.

Marcus, R. and Bonewald, L. (2021). Chapter 7 - Osteocytes. [online] ScienceDirect. Available at: https://www.sciencedirect.com/science/article/abs/pii/B9780128130735000071.

Marques, M.P.M., Batista de Carvalho, L.A.E., Gonçalves, D., Cunha, E. and Parker, S.F. (2021). The impact of moderate heating on human bones: an infrared and 162 neutron spectroscopy study. Royal Society Open Science, 8(10). doi:https://doi.org/10.1098/rsos.210774.

Mattsson, K. et al. (2024) 'Nanoplastics in aquatic environments—sources, sampling techniques, and identification methods', Microplastic Contamination in Aquatic Environments, pp. 381–397. doi:10.1016/b978-0-443-15332-7.00003-x.

Maynard, R.L. and Downes, N. (2019) 'Chapter 3 - Introduction to the Skeleton: Bone, Cartilage and Joints', in Anatomy and histology of the laboratory rat in Toxicology and Biomedical Research. 1st edn. London: Academic Press, pp. 11–22.

McCardle, P. and Stojanovski, E. (2018), Identifying Differences Between Cut Marks Made on Bone by a Machete and Katana: A Pilot Study. J Forensic Sci, 63: 1813- 1818. https://doi.org/10.1111/1556-4029.13754

McGonagle, D. and Benjamin, M. (2015) *Ultrasound of the ankle and foot* in *Clinical Ultrasound*. 3rd edn. Elsevier. (Chapter discussing enthesis and relation to bone/cartilage anatomy). Available at: https://www.sciencedirect.com/science/article/pii/B9780323091381001236

Mckinnon, M., Henneberg, M. and Higgins, D. (2021). A review of the current understanding of burned bone as a source of DNA for human identification. Science & Justice, [online] 61(4), pp.332–338. doi:https://doi.org/10.1016/j.scijus.2021.03.006.

MD, R.G. (2023) Bones, Kenhub. Available at: https://www.kenhub.com/en/library/anatomy/bones (Accessed: 15 September 2023).

MERCK (2023) Review of O-linked glycoproteins. Available at: https://www.sigmaaldrich.com/GB/en/technical-documents/technical-article/proteinbiology/protein-labeling-and-modification/o-glycans (Accessed: 16 September 2023).

Mizutari, K. (2019) Blast-induced hearing loss, Journal of Zhejiang University. Science. B. Available at: https://www.ncbi.nlm.nih.gov/pmc/articles/PMC6380998/

Moo-Young, M. et al. (2019) '3.41 - Protein Glycosylation', in Comprehensive biotechnology. 3rd edn. Amsterdam, Netherlands: Elsevier, pp. 501–520.

Moretti, E., Arrighi, S., Boschin, F., Crezzini, J., Aureli, D. and Ronchitelli, A. (2015). Using 3D Microscopy to Analyse Experimental Cut Marks on Animal Bones 163 Produced with Different Stone Tools. Ethnobiology Letters, 6(2), pp.267–275. doi:https://doi.org/10.14237/ebl.6.2.2015.349.

Morley, M.G. et al. (2010) 'Blast eye injuries: A review for First Responders', Disaster Medicine and Public Health Preparedness, 4(2), pp. 154–160. doi:10.1001/dmp.v4n2.hra10003.

Morrison, K. (2023) *Flat bones: Definition, examples, diagram, and structure*. Healthline. Available at: https://www.healthline.com/health/flat-bones

Muchatuta , N. and Sale, S. (2007) 'Fires and explosions', in Anaesthesia & Intensive Care Medicine. 11th edn. Glasgow: Medicine Publishing, pp. 457–460. Available at: https://www.sciencedirect.com/science/article/abs/pii/S1472029907002147#sec5.

Muller, M.E. (1990) The comprehensive classification of fractures of Long Bones Vol 642. 3rd edn. Berlin: Springer-Verlag.

Murakami, T. 2022, '3 - Biotribology of natural joints', in *Biotribology of Natural and Artificial Joints: Reducing Wear through Material Selection and Geometric Design*, 1st edn, Elsevier, pp. 81–149.Murphy, C. & Barnes, J. 2006, *Fire Dynamics and Combustible Gases*, 1st edn, Fire Science Press, London

Nahian, A. and Chauhan, P.R. (2020). Histology, Periosteum and Endosteum. [online] PubMed. Available at: https://www.ncbi.nlm.nih.gov/books/NBK557584/.

Naomi, R., Ridzuan, P.M. and Bahari, H. (2021). Current Insights into Collagen Type I. Polymers, [online] 13(16). doi:https://doi.org/10.3390/polym13162642.

New Jersey Department of Health (2007). Right to Know Hazardous Substance Fact Sheet. [online] Available at: https://www.nj.gov/health/eoh/rtkweb/documents/fs/0106.pdf.

NIH (2018) Structure of bone tissue, Structure of Bone Tissue | SEER Training. Available at: https://training.seer.cancer.gov/anatomy/skeletal/tissue.html (Accessed: 04 December 2023). 164

NIH (2018) Classification of Bones, Classification of Bones | SEER Training. Available at: https://training.seer.cancer.gov/anatomy/skeletal/classification.html (Accessed: 16 September 2023).

Nishio, Y., Yoshioka, H., Noguchi, T., Kanematsu, M., Ando, T., Hase, Y. and Hayakawa, T. (2015). Fire Spread Caused by Combustible Facades in Japan. Fire Technology, 52(4), pp.1081–1106. doi:https://doi.org/10.1007/s10694-015-0535-5.

Oftadeh, R. et al. (2015b) 'Biomechanics and mechanobiology of Trabecular Bone: A Review', Journal of Biomechanical Engineering, 137(1). doi:10.1115/1.4029176.

Okaluk, T.R. and Greenfield, H.J. (2022). Macroscopic Chop Mark Identification on Archaeological Bone: An Experimental Study of Chipped Stone, Ground Stone, Copper, and Bronze Axe Heads on Bone. Quaternary, [online] 5(1), p.15. doi:https://doi.org/10.3390/quat5010015.

Olszta, M.J. et al. (2007) 'Bone structure and Formation: A new perspective', Materials Science and Engineering: R: Reports, 58(3–5), pp. 77–116. doi:10.1016/j.mser.2007.05.001.

OpenStaxCollege (2013). Bone Classification. [online] Hawaii.edu. Available at: https://pressbooks-dev.oer.hawaii.edu/anatomyandphysiology/chapter/boneclassification [Accessed 20 Jun. 2025].

Padilla-Alvarez, R. (2009) ' Methodology, advantages and limitations of in-situ XRF measurements (including overview of applications)', Joint ICTP/IAEA Advanced School on in-situ X-ray Fluorescence and Gamma Ray Spectrometry, 2064(5).

Pajnič, I. Z., Leskovar, T. & Zupanič Pajnič, I. (2025) *How to store the bone powder left after extraction for future analysis*. Forensic Science International, 369, 112436. doi:10.1016/j.forsciint.2025.112436.

Palmer, T. (2007) '16 - Extraction and Purification of Enzymes', in P. Bonner (ed.) Enzymes. 2nd edn. Nottingham: Woodhead, pp. 293–314.

Panda, S., Biswas, C.K. and Paul, S. (2021) 'A comprehensive review on the preparation and application of calcium hydroxyapatite: A special focus on atomic doping 165 methods for bone tissue engineering', Ceramics International, 47(20), pp. 28122–28144. doi:10.1016/j.ceramint.2021.07.100.

Parvizi, J. and Kim, G.K. (2010) 'Chapter 163 - Osteoclasts', in High-yield orthopaedics. W B Saunders Company, pp. 337–339.

Paschalis, E.P., Mendelsohn, R. and Boskey, A.L. (2011). Infrared Assessment of Bone Quality: A Review. Clinical Orthopaedics & Related Research, 469(8), pp.2170–2178. doi:https://doi.org/10.1007/s11999-010-1751-4.

Pasieczna-Patkowska, S., *et al.* 2025, *Application of Fourier Transform Infrared Spectroscopy …*, *Molecules*, 30(3), pp. 684. doi:10.3390/1420-3049/30/3/684.

Pasteris, J.D., Wopenka, B., Valsami-Jones, E. and Rogers, K.D. (2014) Bone and tooth mineralization studied by Raman spectroscopy, *Journal of Raman Spectroscopy*, 45(6), pp.510–527.

Pepe, A. et al. (2023) ‘Chapter 13 0- Blast Injuries’, in Current therapy of trauma and Surgical Critical Care. 1st edn. S.l.: ELSEVIER - HEALTH SCIENCE, pp. 73–77.

Ponzetti, M. and Rucci, N. (2021). Osteoblast Differentiation and Signalling: Established Concepts and Emerging Topics. International Journal of Molecular Sciences, 22(13), p.6651. doi:https://doi.org/10.3390/ijms22136651.

Rades, S., Hodoroaba, V.-D., Salge, T., Wirth, T., Lobera, M. P., Labrador, R. H., Natte, K., Behnke, T., Gross, T. & Unger, W. E. S. (2014) *High-resolution imaging with SEM/T-SEM, EDX and SAM as a combined methodical approach for morphological and elemental analyses of single engineered nanoparticles*. RSC Advances, 4(91), pp. 49577–49587. doi:10.1039/C4RA05092D

Rein, G. (2009) *Smouldering Combustion Phenomena in Science and Technology*, *International Review of Chemical Engineering*, 1(1), pp.3–18. Available at: http://hdl.handle.net/1842/2678

Ricardo A.M.P. Gomes, Ana Luisa Santos and Catarino, L. (2024). Elemental analysis using portable X-ray fluorescence: Guidelines for the study of dry human bone. International journal of paleopathology, 44, pp.85–89. doi:https://doi.org/10.1016/j.ijpp.2023.12.004.

Robinson (2022) Chemical Burns: Causes, symptoms, treatment, prevention, care, WebMD. Available at: https://www.webmd.com/first-aid/chemical-burns (Accessed: 08 December 2023).

Rod Brouhard, E.-P. (2023) The four types of bone, Verywell Health. Available at: https://www.verywellhealth.com/the-four-types-of-bone-4771778 (Accessed: 15 September 2023).

Rosa, J. et al. (2022) ‘Chemical Trace XRF analysis to detect sharp force trauma in fresh and burned bone’, Science & Justice, 62(5), pp. 484–493. doi:10.1016/j.scijus.2022.07.007. 166

Rosa, J., Batista de Carvalho, L.A.E., Ferreira, M.T., Gonçalves, D., Marques, M.P.M. and Gil, F.P.S.C. (2022). Chemical trace XRF analysis to detect sharp force trauma in fresh and burned bone. Science & Justice, [online] 62(5), pp.484–493. doi:https://doi.org/10.1016/j.scijus.2022.07.007.

Ross, F.P. (2011) *Chapter 18 – Osteoclasts*, in *Vitamin D (Third Edition)*. Elsevier. Available at: https://www.sciencedirect.com/science/chapter/abs/pii/B9780123819789100186

Sa, H. and Ahmed, S. (2023) *FTIR spectrum analysis to predict the crystalline and amorphous phases of hydroxyapatite: a comparison of vibrational motion to reflection*. RSC Advances, 13, pp.14625–14630. doi:10.1039/D3RA02580B.

Sa, Y., Wang, M., Deng, Y. and Zhang, Y. (2017) Evaluation of crystallinity changes in calcium phosphate using FTIR and Raman spectroscopy, *Spectrochimica Acta Part A: Molecular and Biomolecular Spectroscopy*, 173, pp.35–42.

Scaggion, C, Dal Sasso, G , Nodari, L, Pagani, L., Carrara, N., Zotti, A., Tommaso Banzato, Donatella Usai, Pasqualetto, L., Giulia Gadioli and Artioli, G. (2024a). An FTIR-based model for the diagenetic alteration of archaeological bones. Journal of archaeological science, 161, pp.105900–105900. doi:https://doi.org/10.1016/j.jas.2023.105900.

Samaritans (2019). Suicide facts for journalists. [online] Samaritans. Available at: https://www.samaritans.org/about-samaritans/media-guidelines/suicide-factsjournalists/.

Schiffer, D., Mellai, M., Boldorini, R., Bisogno, I., Grifoni, S., Corona, C., Bertero, L., Cassoni, P., Casalone, C. and Annovazzi, L. (2018). The Significance of Chondroitin Sulfate Proteoglycan 4 (CSPG4) in Human Gliomas. International Journal of Molecular Sciences, 19(9), p.2724. doi:https://doi.org/10.3390/ijms19092724.

Schultz (2008), Eric M. et al. "Investigation of Deflagration to Detonation Transition for Application to Pulse Detonation Engine Ignition Systems." .

Schmidt, C.W. & Uhlig, R. (2012) *Light microscopy of microfractures in burned bone*. In: L. Bell (ed.), *Methods in Molecular Biology: Bone and Cartilage Histology and Imaging* (vol. 915), New York, NY: Springer, pp. 227–234. doi:10.1007/978-1-61779-977-8_13.

Seibel, M.J. et al. (2006) 'CHAPTER 1 - Structure, Biosynthesis and Gene Regulation of Collagens in Cartilage a nd Bone', in Dynamics of bone and cartilage metabolism. San Diego: Academic Press, pp. 3–40.

Seladi-Schulman, J. (2018) Flat bones: Definition, examples, diagram, and Structure, Healthline. Available at: https://www.healthline.com/health/flat-bones (Accessed: 16 September 2023). 167

Shehata, T.P. and Krap, T. (2024). An overview of the heat-induced changes of the chemical composition of bone from fresh to calcined. International Journal of Legal Medicine, 138(3), pp.1039–1053. doi:https://doi.org/10.1007/s00414-024-03160-z.

Sheik, Z, Painter, K (2007). Smoke Inhalation. [online] WebMD. Available at: https://www.webmd.com/lung/smoke_inhalation_treatment_firstaid.htm.

Shenoy, Ravikiran & Pillai, Anand. (2017). Biology of fracture healing - an overview. Journal of Trauma and Orthopaedics. 5. 48-51.

Sherbet, G.V. (2014) '3 - Growth Factors in Differentiation and Morphogenesis', in Growth factors and their receptors in cell differentiation, cancer and cancer therapy. 2nd edn. Saint Louis: Elsevier Science, pp. 7–54.

Shrestha, R., Kanchan, T. and Krishan, K. (2023). Gunshot Wounds Forensic Pathology. [online] PubMed. Available at: https://www.ncbi.nlm.nih.gov/books/NBK556119/.

Simon, L.V., Lopez, R.A. and King, K.C. (2023). Blunt force trauma. [online] PubMed. Available at: https://www.ncbi.nlm.nih.gov/books/NBK470338/.

Smith, E. and Dent, G. (2019) *Modern Raman Spectroscopy: A Practical Approach*. 2nd edn. Chichester: Wiley.

Song, G., Rossi René M. and Mandal, S. (2017) "2 - Fires and thermal environments," in Thermal protective clothing for firefighters. Iowa, Iowa: Elsevier Science, pp. 5–15.

Souza, P., Lopes, H.B., Oliveira, F.S., Weffort, D., Freitas, G.P., Adolpho, L.F., Fernandes, R.R., Rosa, A.L. and Marcio Mateus Beloti (2021). The extracellular matrix protein Agrin is expressed by osteoblasts and contributes to their differentiation. Cell and Tissue Research, 386(2), pp.335–347. doi:https://doi.org/10.1007/s00441-021-03494-9.

Speight, J. G. (2011) *Combustion of hydrocarbons*. In: *Handbook of Industrial Hydrocarbon Processes*. 2nd edn. Cambridge, UK: Gulf Professional Publishing, pp. 421–463. doi:10.1016/B978-0-12-809923-0.00010-2.

Spies, A.J., Steyn, M., Prince, D.N. and Brits, D. (2022). Radiological Detection of Sharp Force Skeletal trauma: an Evaluation of the Sensitivity of Lodox in Comparison to CT and X-ray. International Journal of Legal Medicine, 136(5), pp.1417–1430. doi:https://doi.org/10.1007/s00414-022-02845-7. 168

Stauffer, É. (2020) 'Interpol review of Fire Investigation 2016–2019', Forensic Science International: Synergy, 2, pp. 368–381. doi:10.1016/j.fsisyn.2020.01.005.

Stock, S.R. (2008) *MicroComputed Tomography: Methodology and Applications*. Boca Raton: CRC Press.

Su, Z., Kishida, S., Tsubota, S., Sakamoto, K., Cao, D., Shinichi Kiyonari, Ohira, M., Takehiko Kamijo, Narita, A., Xu, Y., Takahashi, Y. and Kenji Kadomatsu (2017). Neurocan, an extracellular chondroitin sulfate proteoglycan, stimulates neuroblastoma cells to promote malignant phenotypes. Oncotarget, 8(63), pp.106296–106310. doi:https://doi.org/10.18632/oncotarget.22435.

Suzuki, G., Kida, A., Sakai, S. & Takigami, H. 2009, 'Existence state of bromine as an indicator of the source of brominated flame retardants in indoor dust', *Environmental Science & Technology*, vol. 43, no. 5, pp. 1437–1442, doi:10.1021/es802599d.

Team, E.W. (2020). Ammonium Nitrate (CHEBI:63038). [online] Ebi.ac.uk. Available at: https://www.ebi.ac.uk/chebi/searchId.do?chebiId=CHEBI%3A63038 [Accessed 20 Jun. 2025].

Thomas, E.L. et al. (2013) 'Whole body fat: Content and distribution', Progress in Nuclear Magnetic Resonance Spectroscopy, 73, pp. 56–80. doi:10.1016/j.pnmrs.2013.04.001.

Thompson, T.J.U. (2004) 'Recent advances in the study of burned bone and their implications for forensic anthropology', Forensic Science International, 146. doi:10.1016/j.forsciint.2004.09.063.

Thompson, T.J.U., Gauthier, M. and Islam, M. (2009). The application of a new method of Fourier Transform Infrared Spectroscopy to the analysis of burned bone. Journal of Archaeological Science, 36(3), pp.910–914. doi:https://doi.org/10.1016/j.jas.2008.11.013.

Thompson, T.J.U. (2015) Heat-induced dimensional changes in bone and their implications for forensic analysis, *Journal of Forensic Sciences*, 60(2), pp.418–425.

Tian, Y. and Zhang, H. (2013). Characterization of disease-associated N-linked glycoproteins. PROTEOMICS, 13(3-4), pp.504–511. doi:https://doi.org/10.1002/pmic.201200333.

Unal.S et al. (2021) '9 - Bone structure and formation: A new perspective', in Bioceramics: From Macro to nanoscale. 2nd edn. Amsterdam: Elsevier, pp. 175–193.

University of Birmingham (2024). Physics A level revision resource: Introduction to Young's Modulus. [online] University of Birmingham. Available at: 169 https://www.birmingham.ac.uk/study/undergraduate/schools-and-colleges/post-16/alevel-stem-resources/youngs-modulus.

Vachirawongsakorn, V., Márquez-Grant, N. and Painter, J. (2022) 'Survival of sharp force trauma in burnt bones: Effects of environmental factors', International Journal of Legal Medicine, 137(3), pp. 809–823. doi:10.1007/s00414-022-02916-9.

Vachirawongsakorn, V., Painter, J. and Márquez-Grant, N. (2021). Knife cut marks inflicted by different blade types and the changes induced by heat: a dimensional and morphological study. International Journal of Legal Medicine, 136(1). doi:https://doi.org/10.1007/s00414-021-02726-5.

Veenstra, A., Kerkhoff, W., Oostra, R.J. and Galtés, I. (2022) *Gunshot trauma in human long bones: towards practical diagnostic guidance for forensic anthropologists*. *Forensic Science, Medicine and Pathology*, 18(3), pp.359–367. doi:10.1007/s12024-022-00479-0. Available at: https://pubmed.ncbi.nlm.nih.gov/35451712/

Viner, M.D., Robson Brown, K.A. and Stewart, A. (2020) The use of micro-CT for trauma analysis in skeletal remains, *Forensic Science International*, 314, 110389.

Wagner, N.J. (ed.) (2021) *Organic Petrography and Geochemistry of Dispersed Organic Matter*, in Encyclopedia of Geology (Second Edition). Elsevier, pp.546-553

Waltenberger, L. and Schutkowski, H. (2017) 'Effects of heat on cut Mark Characteristics', Forensic Science International, 271, pp. 49–58. doi:10.1016/j.forsciint.2016.12.018.

Wang, X. et al. (2019) 'Chapter 1 - Natural Bone Tissue and Its Biomimetic', in Mineralized collagen bone graft substitutes. Duxford: Elsevier, WP, Woodhead Publishing, pp. 1–22.

Waterhouse, K. (2013) 'The effect of victim age on burnt bone fragmentation: Implications for remains recovery', Forensic Science International, 231(1–3). doi:10.1016/j.forsciint.2013.04.032.

Watkins, J. (2009) 'CHAPTER 4 - Connective tissues', in the pocket podiatry guide: Functional anatomy. 1st edn. Edinburgh: Churchill-Livingstone, pp. 107–156.

Watson, E.C. and Adams, R.H. (2018). Biology of Bone: The Vasculature of the Skeletal System. Cold Spring Harbor Perspectives in Medicine, [online] 8(7). doi:https://doi.org/10.1101/cshperspect.a031559. 170

Welsh, K.J., Kirkman, M.S. and Sacks, D.B. (2016). Role of Glycated Proteins in the Diagnosis and Management of Diabetes: Research Gaps and Future Directions. Diabetes Care, [online] 39(8), pp.1299–1306. doi:https://doi.org/10.2337/dc15-2727.

Wexler, P. and DuTeaux, S.B. (2014) 'Texas City Disaster', in Encyclopaedia of toxicology. 3rd edn. Amsterdam: Elsevier, Academic Press, pp. 519–520.

Wexler, P. and Kamrin, M.A. (2014). Encyclopaedia of Toxicology. 3rd ed. London ; San Diego, Ca: Elsevier/Academic Press.

Wexler, P., Fedoruk, M.J. and Hong, S. (2014) 'Musculoskeletal System', in Encyclopaedia of toxicology. 3rd edn. San Diego: Academic Press, pp. 403–406.

Wight, T.N. (2002). Versican: A Versatile Extracellular Matrix Proteoglycan in Cell Biology. Current Opinion in Cell Biology, 14(5), pp.617–623. doi:https://doi.org/10.1016/s0955-0674(02)00375-7.

WU, Y.J., PIERRE, D.P.L., WU, J., YEE, A.J. and YANG, B.B. (2005). The Interaction of Versican with Its Binding Partners. Cell Research, 15(7), pp.483–494. doi:https://doi.org/10.1038/sj.cr.7290318.

Yeung, A.Y. and Garg, R. (2022). Anatomy, Sesamoid Bones. [online] PubMed. Available at: https://www.ncbi.nlm.nih.gov/books/NBK578171/.

Zhu, W., Robey, Pa. and Boskey, A. (2010) 'CHAPTER 9 - The Regulatory Role of Matrix Proteins in Mineralization of Bone', in Fundamentals of osteoporosis. 3rd edn. Amsterdam: Academic (Osteoporosis), pp. 192–240.

Appendix

Appendix 1

X-Ray Fluorescence raw data

Appendix 1 A: XRF raw data for fibula in ARC and Wood/Charcoal based fires.

Charcoal

	P		**S**		**Cl**		**K**		**Ca**		**Ti**		**Fe**	
Ident	C	Unit	C	Unit	C	Unit	C	Unit	C	Unit	C	Unit	C	Unit
Fibula	16.415	%	0.077	%	0.171	%	0.424	%	82.619	%	0.024	%	0.052	%
	Zn		**Sr**		**Zr**		**Sn**		**Sm**		**Yb**		**Nd**	
	C	Unit	C	Unit	C	Unit	C	Unit	C	Unit	C	Unit	C	Unit
	0.074	%	0.116	%	0.001	%	0.022	%	0.001	%	0.005	%	0.002	%

Wood

	Si		**P**		**S**		**Cl**		**K**		**Ca**		**Ti**		**Fe**	
Ident	C	Unit	C	Unit	C	Unit	C	Unit	C	Unit	C	Unit	C	Unit	C	Unit
Fibula	0.268	%	11.463	%	0.368	%	2.305	%	0.524	%	84.368	%	0.051	%	0.226	%
	Zn		**Sr**		**Zr**		**Sn**		**Nd**		**Sn**		**Eu**		**Zn**	
	C	Unit	C	Unit	C	Unit	C	Unit	C	Unit	C	Unit	C	Unit	C	Unit
	0.163	%	0.197	%	0.002	%	0.044	%	0.023	%	0.018	%	0	%	0.163	%

ARC

	Si		**P**		**S**		**Cl**		**K**		**Ca**	
Ident	C	Unit	C	Unit	C	Unit	C	Unit	C	Unit	C	Unit
Fibula	0.549	%	14.491	%	0.958	%	1.405	%	1.176	%	82.786	%
	Ti		**V**		**Cr**		**Fe**		**Zn**		**Br**	
	C	Unit	C	Unit	C	Unit	C	Unit	C	Unit	C	Unit
	0.102	%	0.213	%	0.03	%	0.409	%	0.211	%	0.016	%

Appendix 1 B: XRF raw data for ilium in ARC and Wood/Charcoal based fires.

Charcoal

	Si		**P**		**S**		**Cl**		**K**		**Ca**		**Ti**		**V**	
Ident	C	Unit	C	Unit	C	Unit	C	Unit	C	Unit	C	Unit	C	Unit	C	Unit
ilium	0.666	%	12.123	%	0.23	%	0.332	%	0.926	%	85.021	%	0.127	%	0.001	%
	Mn		**Fe**		**Cu**		**Zn**		**Sr**		**Zr**		**Sn**		**Eu**	
	C	Unit	C	Unit	C	Unit	C	Unit	C	Unit	C	Unit	C	Unit	C	Unit
	0.01	%	0.341	%	0.008	%	0.112	%	0.081	%	0.003	%	0.018	%	0	%

Wood

	P		**S**		**Cl**		**K**		**Ca**		**Ti**	
Ident	C	Unit	C	Unit	C	Unit	C	Unit	C	Unit	C	Unit
ilium	11.626	%	0.233	%	0.524	%	1.041	%	86.11	%	0.02	%
	Fe		Zn		Sr		Zr		Sn			
	C	Unit	C	Unit	C	Unit	C	Unit	C	Unit		
	0.126	%	0.174	%	0.104	%	0.001	%	0.041	%		

ARC

	Si		**P**		**S**		**Cl**		**K**		**Ca**		**Ti**	
Ident	C	Unit	C	Unit	C	Unit	C	Unit	C	Unit	C	Unit	C	Unit
ilium	0.509	%	10.037	%	0.778	%	0.821	%	0.705	%	86.618	%	0.05	%
	V		**Cr**		**Fe**		**Zn**		**Br**		**Sr**			
	C	Unit	C	Unit	C	Unit	C	Unit	C	Unit	C	Unit		
	0.244	%	0.016	%	0.276	%	0.122	%	0.012	%	0.053	%		

Appendix 1 C: XRF raw data for Mandible in ARC and Wood based fires.

Wood

	P		**S**		**Cl**		**K**		**Ca**		**Ti**		**Fe**	
Ident	C	Unit	C	Unit	C	Unit	C	Unit	C	Unit	C	Unit	C	Unit
Mandible	12.41	%	0.237	%	0.751	%	0.587	%	85.681	%	0.005	%	0.054	%
	Zn		**Sr**		**Zr**		**Te**		**Sm**		**Eu**		**Nd**	
	C	Unit	C	Unit	C	Unit	C	Unit	C	Unit	C	Unit	C	Unit
	0.131	%	0.097	%	0.001	%	0.044	%	0.000	%	0.000	%	0.000	%

ARC

	Si		**P**		**S**		**Cl**		**K**		**Ca**		**Ti**		**Cr**
Ident	C	Unit	C	Unit	C	Unit	C	Unit	C	Unit	C	Unit	C	Unit	C
Mandible	0.496	%	9.837	%	0.776	%	0.953	%	0.74	%	86.62	%	0.047	%	0.014
	Mn		**Fe**		**Zn**		**Br**		**Nd**		**Sr**		**Eu**		
	C	Unit	C	Unit	C	Unit	C	Unit	C	Unit	C	Unit	C	Unit	
	0.011	%	0.297	%	0.133	%	0.015	%	0.011	%	0.06	%	0	%	

Appendix 1 D: XRF raw data for Scapula in the Wood based fire.

Wood

	Si		**P**		**S**		**Cl**		**K**		**Ca**		**Ti**
Ident	C	Unit	C	Unit	C	Unit	C	Unit	C	Unit	C	Unit	C
Scap	0.483	%	10.664	%	1.397	%	0.595	%	1.199	%	85.002	%	0.036
	Fe		**Zn**		**Sr**		**Zr**		**Sn**		**Re**		
	C	Unit	C	Unit	C	Unit	C	Unit	C	Unit	C	Unit	
	0.253	%	0.166	%	0.126	%	0.003	%	0.072	%	0.004	%	

Appendix 1 E: XRF raw data for Skull in ARC and Charcoal based fires.

Charcoal

	P		**S**		**Cl**		**K**		**Ca**		**Ti**	
Ident	C	Unit	C	Unit	C	Unit	C	Unit	C	Unit	C	Unit
Skull	15.663	%	0.167	%	0.224	%	0.313	%	83.409	%	0.014	%
	Fe		**Zn**		**Sr**		**Zr**		**Sn**		**Nd**	
	C	Unit	C	Unit	C	Unit	C	Unit	C	Unit	C	Unit
	0.022	%	0.098	%	0.066	%	0.001	%	0.024	%	0.000	%

ARC

	Si		**P**		**S**		**Cl**		**K**		**Ca**	
Ident	C	Unit	C	Unit	C	Unit	C	Unit	C	Unit	C	Unit
Skull	0.328	%	17.285	%	0.849	%	1.548	%	1.298	%	86.786	%
	Ti		**Fe**		**Zn**		**Br**		**Sr**		**Sn**	
	C	Unit	C	Unit	C	Unit	C	Unit	C	Unit	C	Unit
	0.058	%	0.213	%	0.244	%	0.041	%	0.074	%	0.07	%

Appendix 1 F: XRF raw data for Tibia in ARC and Wood/Charcoal based fires.

Charcoal

	P		**S**		**Cl**		**K**		**Ca**		**Ti**		**Fe**		**Zn**	
Ident	C	Unit	C	Unit	C	Unit	C	Unit	C	Unit	C	Unit	C	Unit	C	Unit
Tibia	16.102	%	0.154	%	3.757	%	0.497	%	79.176	%	0.015	%	0.056	%	0.077	%
	Br		**Sr**		**Zr**		**Sn**		**Nd**		**Ce**		**Sm**		**Yb**	
	C	Unit	C	Unit	C	Unit	C	Unit	C	Unit	C	Unit	C	Unit	C	Unit
	0.002	%	0.127	%	0.001	%	0.019	%	0.012	%	0.012	%	0	%	0.004	%

Wood

	Si		**P**		**S**		**Cl**		**K**		**Ca**	
Ident	C	Unit	C	Unit	C	Unit	C	Unit	C	Unit	C	Unit
Tibia	0.209	%	9.58	%	0.343	%	4.932	%	1.024	%	83.432	%
	Ti		**Fe**		**Zn**		**Sr**		**Zr**		**Nd**	
	C	Unit	C	Unit	C	Unit	C	Unit	C	Unit	C	Unit
	0.028	%	0.157	%	0.169	%	0.124	%	0.002	%	0.000	%

ARC

	Si		**P**		**S**		**Cl**		**K**		**Ca**		**Ti**	
Ident	C	Unit	C	Unit	C	Unit	C	Unit	C	Unit	C	Unit	C	Unit
Tibia	0.533	%	10.865	%	0.467	%	0.601	%	0.74	%	86.418	%	0.038	%
	V		**Fe**		**Zn**		**Br**		**Sr**		**Zr**		**Nd**	
	C	Unit	C	Unit	C	Unit	C	Unit	C	Unit	C	Unit	C	Unit
	0.007	%	0.108	%	0.135	%	0.014	%	0.076	%	0.001	%	0.001	%

Appendix 1 G: XRF raw data for Femur in muffle furnace control / 300°C / 450°C

	Si		**P**		**S**		**Cl**		**K**		**Ca**		**Ti**	
Ident	C	Unit	C	Unit	C	Unit	C	Unit	C	Unit	C	Unit	C	Unit
Femur	3.336	%	14.383	%	0.244	%	0.134	%	0.887	%	76.874	%	0.39	%
Control	**V**		**Mn**		**Fe**		**Zn**		**Sr**		**Zr**		**Sn**	
	C	Unit	C	Unit	C	Unit	C	Unit	C	Unit	C	Unit	C	Unit
	77.6	ppm	346	ppm	2.571	%	749	ppm	805.9	ppm	42.4	ppm	264	ppm
	Eu		**Re**		**Al**		**Cr**							
	C	Unit	C	Unit	C	Unit	C	Unit						
	3.9	ppm	16.4	ppm	0.942	%	88.6	ppm						

	P		**S**		**Cl**		**K**		**Ca**		**Ti**		**V**	
Ident	C	Unit	C	Unit	C	Unit	C	Unit	C	Unit	C	Unit	C	Unit
Femur	14.383	%	0.244	%	0.134	%	0.887	%	76.874	%	0.39	%	77.6	ppm
300°C	**Fe**		**Zn**		**Sr**		**Zr**		**Sn**		**Eu**		**Re**	
	C	Unit	C	Unit	C	Unit	C	Unit	C	Unit	C	Unit	C	Unit
	2.571	%	749	ppm	805.9	ppm	42.4	ppm	264	ppm	3.9	ppm	16.4	ppm

	P		**S**		**Cl**		**K**		**Ca**		**Ti**		**V**	
Ident	C	Unit	C	Unit	C	Unit	C	Unit	C	Unit	C	Unit	C	Unit
Femur	14.383	%	0.244	%	0.134	%	0.887	%	76.874	%	0.39	%	77.6	ppm
450°C	**Zn**		**Sr**		**Zr**		**Sn**		**Re**		**Sm**			
	C	Unit	C	Unit	C	Unit	C	Unit	C	Unit	C	Unit		
	749	ppm	805.9	ppm	42.4	ppm	264	ppm	16.4	ppm	0	ppm		

Appendix 1 G continued: XRF raw data for Femur in muffle furnace 600°C / 750°C / 900°C

	P		**S**		**Cl**		**K**		**Ca**		**Ti**		**Fe**	
Ident	C	Unit	C	Unit	C	Unit	C	Unit	C	Unit	C	Unit	C	Unit
Femur	14.383	%	0.244	%	0.134	%	0.887	%	76.874	%	0.39	%	2.571	ppm
600°C	**Zn**		**Sr**		**Zr**		**Re**		**Sm**					
	C	Unit	C	Unit	C	Unit	C	Unit	C	Unit				
	749	ppm	805.9	ppm	42.4	ppm	16.4	ppm	11.9	ppm				

	P		**S**		**Cl**		**K**		**Ca**		**Ti**		**Fe**	
Ident	C	Unit	C	Unit	C	Unit	C	Unit	C	Unit	C	Unit	C	Unit
Femur	18.104	%	631.8	ppm	0.214	%	0.213	%	81.192	%	105.5	ppm	536.9	ppm
750°C	**Zn**		**Sr**		**Zr**		**Sn**							
	C	Unit	C	Unit	C	Unit	C	Unit						
	753	ppm	406.2	ppm	12.1	ppm	191.1	ppm						

	P		**S**		**Cl**		**K**		**Ca**		**Ti**		**Fe**	
Ident	C	Unit	C	Unit	C	Unit	C	Unit	C	Unit	C	Unit	C	Unit
Femur	18.383	%	0.102	%	0.678	%			80.605	%	0	ppm	200.5	ppm
900°C	**Zn**		**Sr**		**Zr**		**Sn**		**Re**		**Te**		**Sm**	
	C	Unit	C	Unit	C	Unit	C	Unit	C	Unit	C	Unit	C	Unit
	699.6	ppm	0.101	%	14.9	ppm	178.1	ppm	14.9	ppm	198	ppm	14.3	ppm

Appendix 2
Further cut mark images
Femur, Scapula, and Skull

Appendix 2 A: *Cut marks produced on the diaphysis of a Femur by a smooth-edged blade, serrated knife and large serrated knife. A and C show signs of flaking due to the cut mark, whereas B shows signs of feathering along the kerf.*

Smooth-Edge Blade

Serrated Knife

Large Serrated Knife

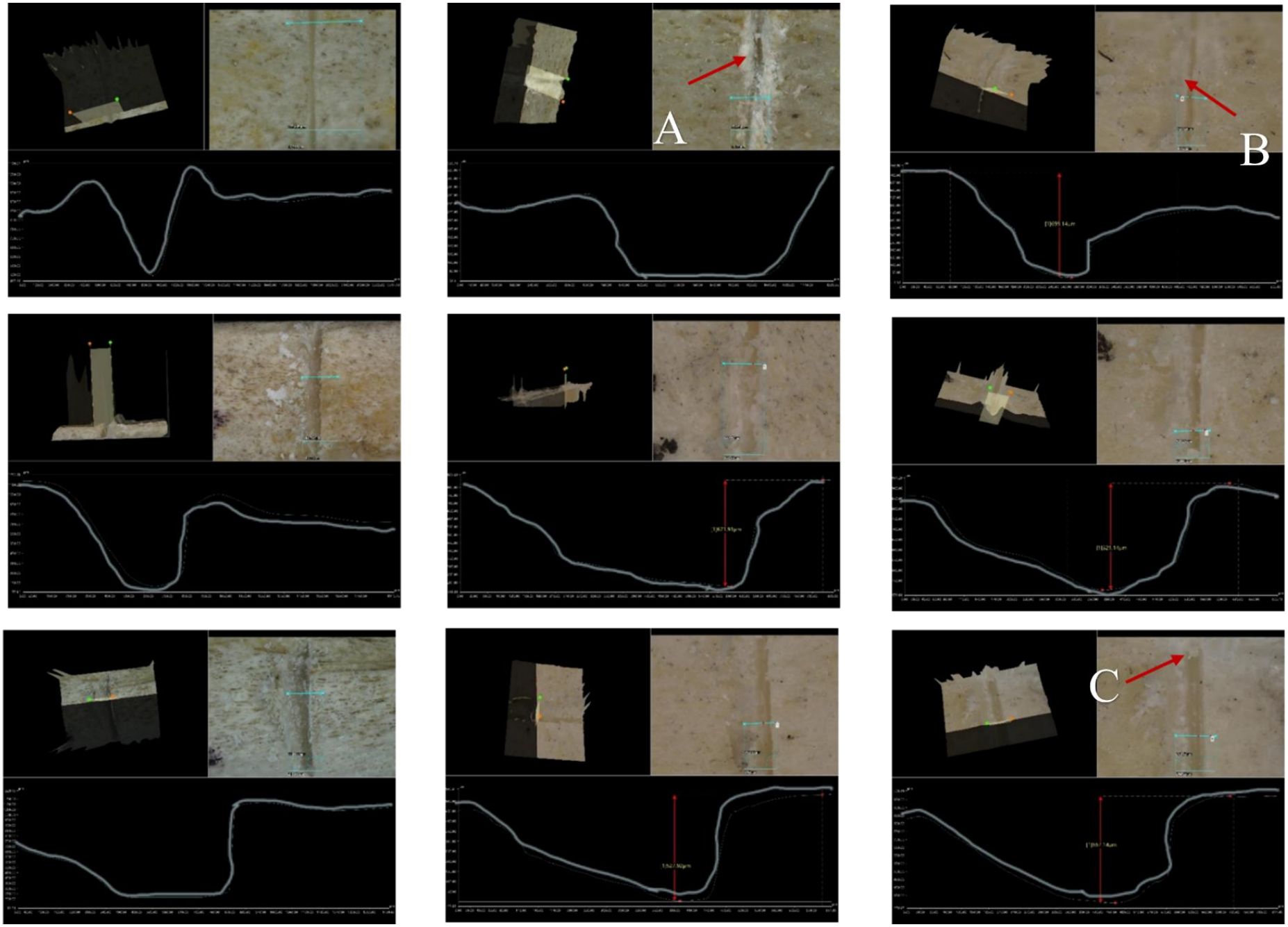

Appendix 2 B *Cut marks produced on the superior angle of a Scapula by a smooth-edged blade, serrated knife and large serrated knife. A – C each highlight strong examples of flaking, with large flakes present. D shows the presence of peeling, as the edge of the cut mark lifts away*

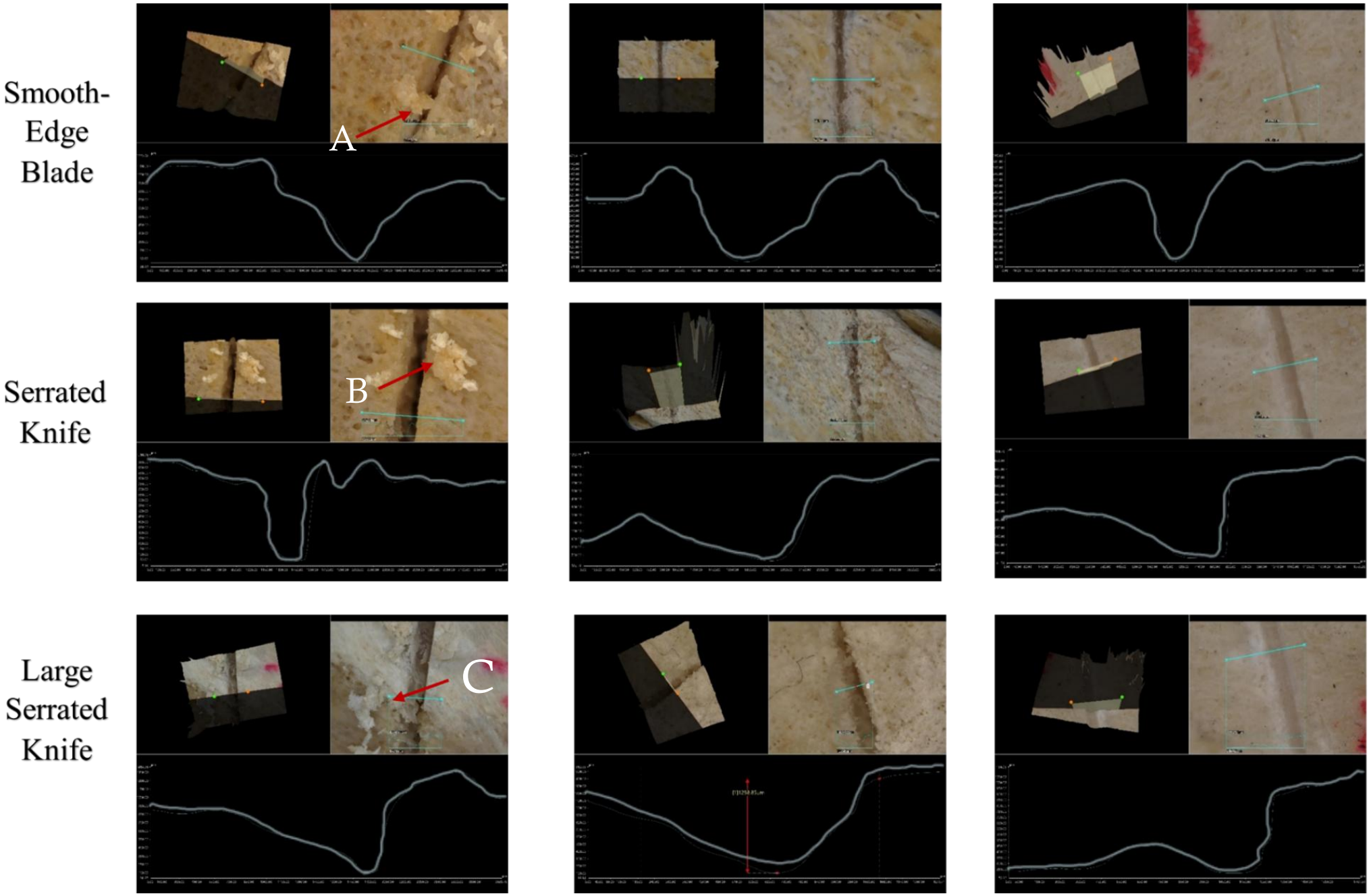

Appendix 2 C *Cut marks produced on the frontal bone of a skull by a smooth-edged blade, serrated knife and large serrated knife. A – C exhibit examples of flaking through the cut marks. D shows a clear example of a scoop defect towards the end of the cut*

.

Smooth-Edge Blade

Serrated Knife

Large Serrated Knife

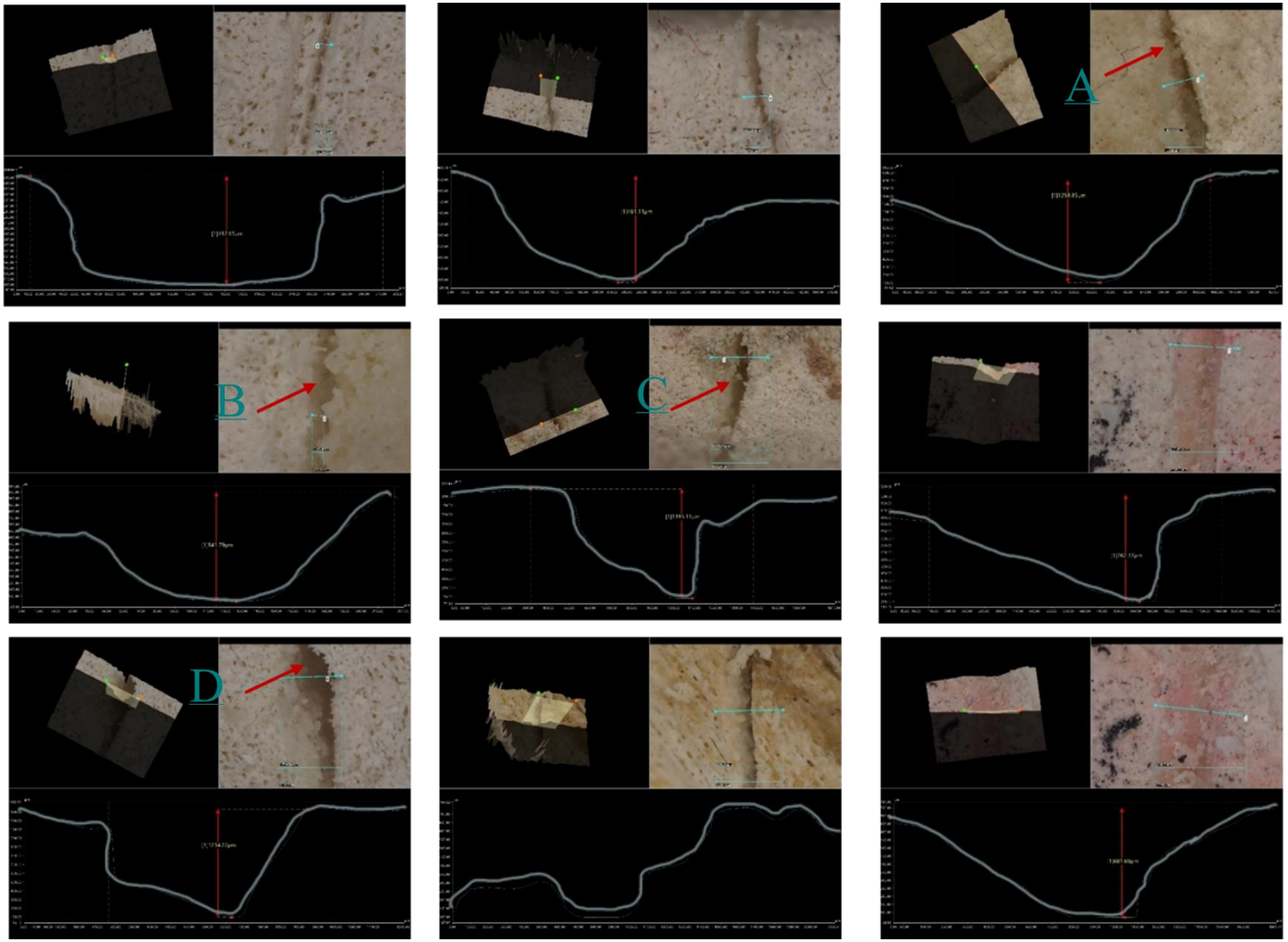

Appendix 3

Cut mark images before and after burning with 3D microscope measurements

Appendix 3 A *Cut marks produced on the diaphysis of a Fibula by a smooth-edged blade, serrated knife and large serrated knife before and after burning with either wood or charcoal as the fuel source.*

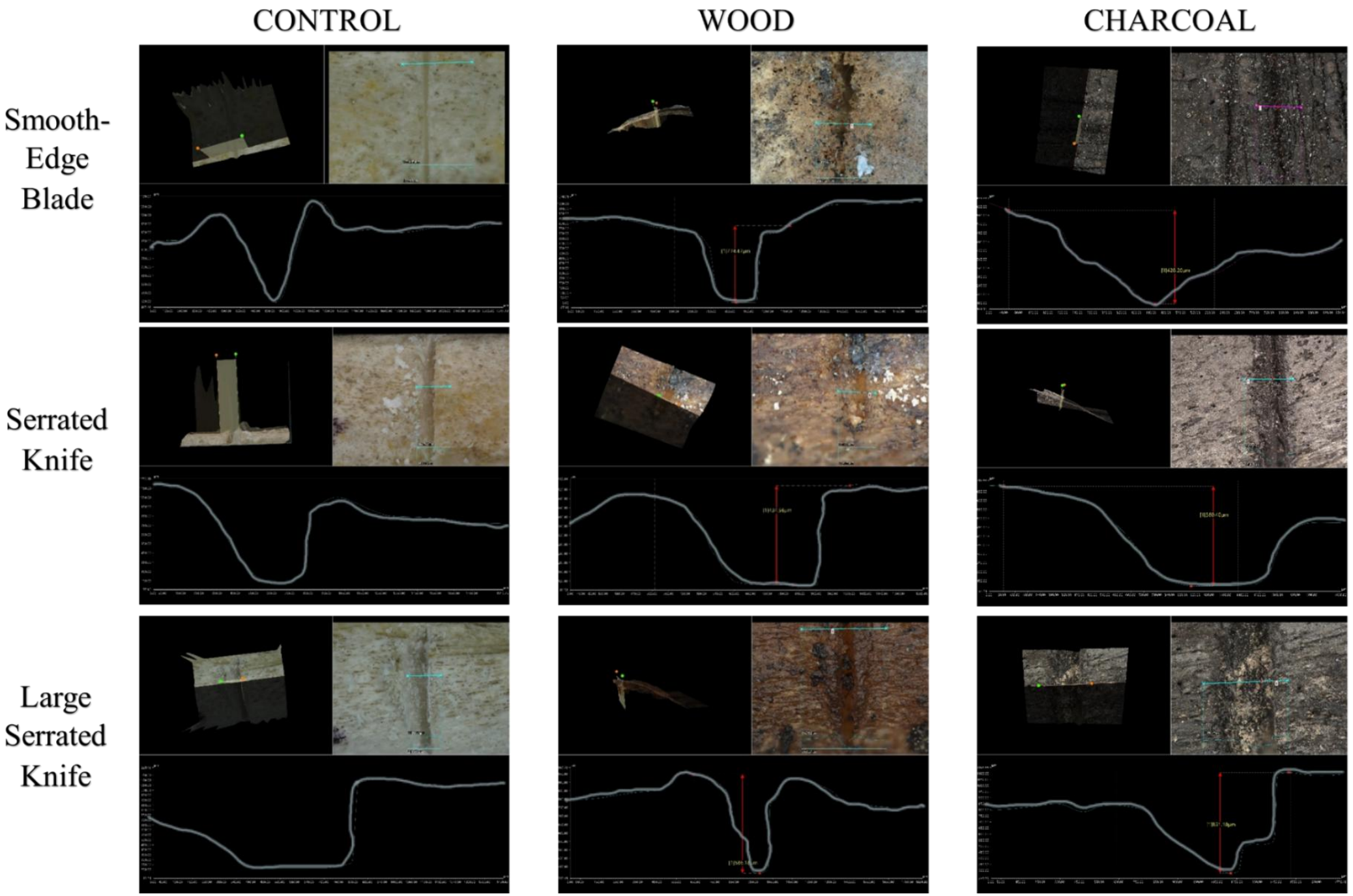

Appendix 3 B *Cut marks produced on the diaphysis of a Hip (Ilium) by a smooth-edged blade, serrated knife and large serrated knife. A and C both portray flaking in the cut mark. B also shows signs of flaking along with scoop defect qualities.*

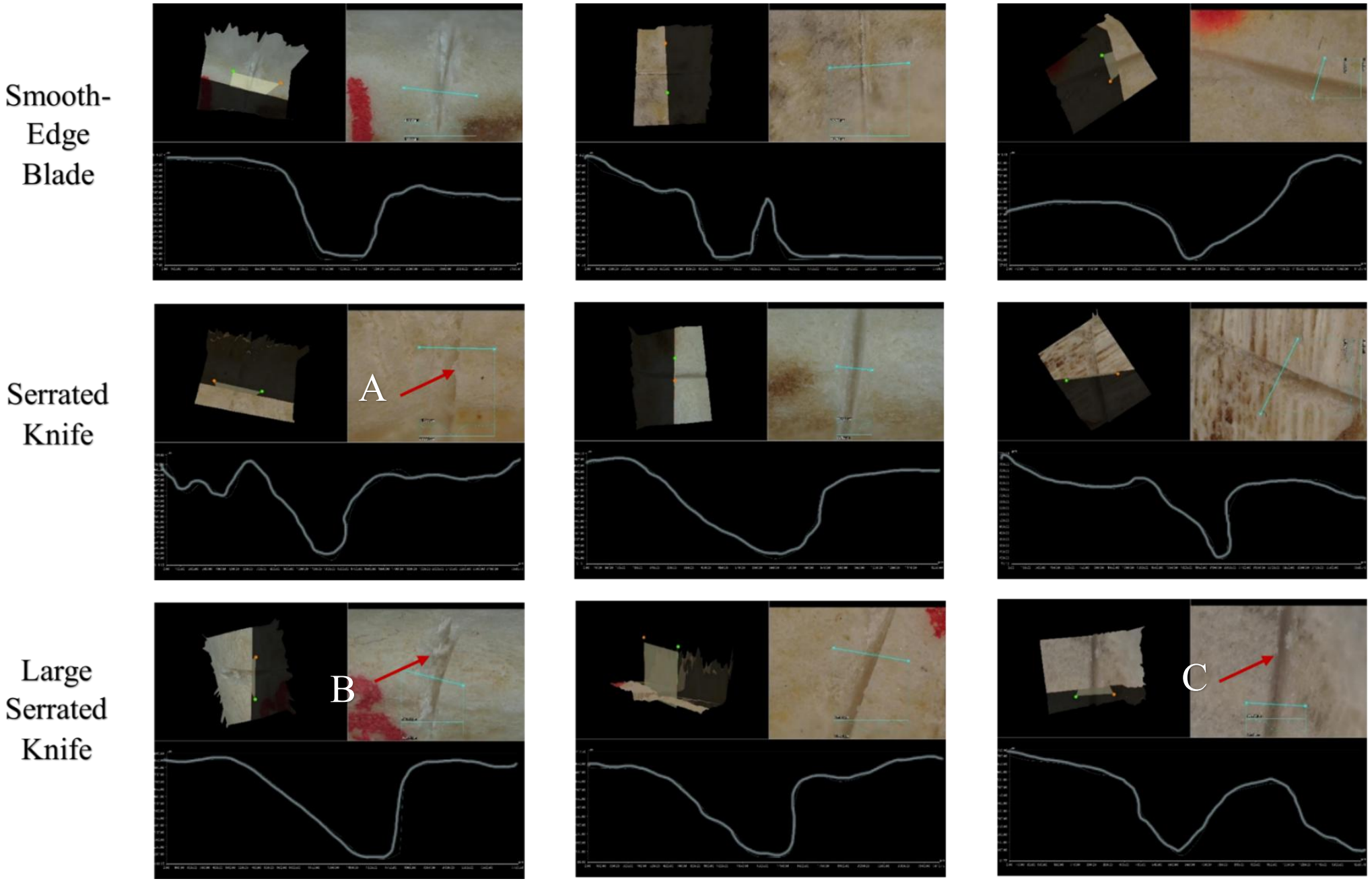

Appendix 3 C *Cut marks produced on the diaphysis of a Hip (Ilium) by a smooth-edged blade, serrated knife and large serrated knife before and after burning with either wood or charcoal as the fuel source.*

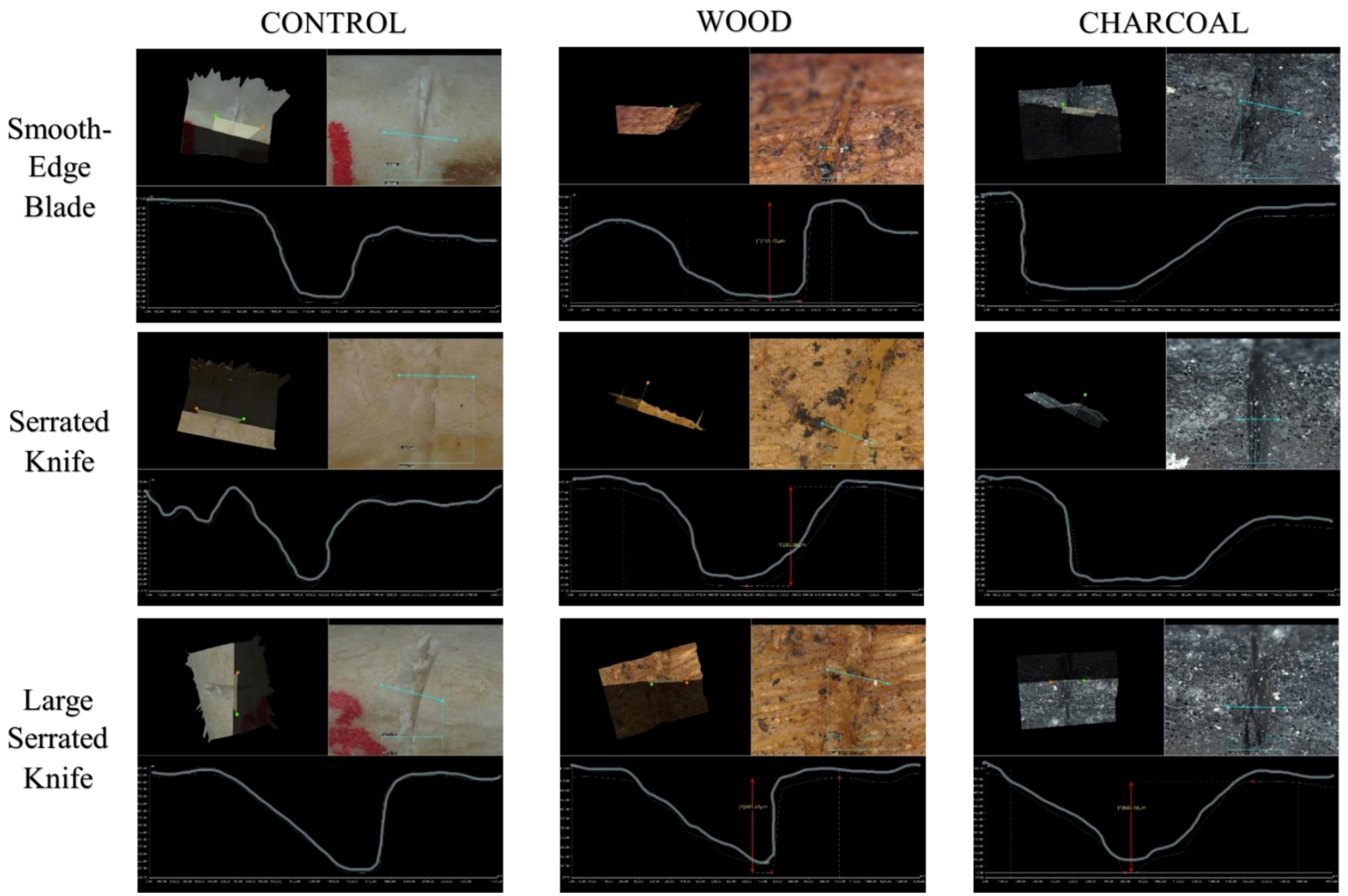

Appendix 3 D C*ut marks produced on the body of a Mandible by a smooth-edged blade, serrated knife and large serrated knife. A – D highlights varying levels of flaking in the cut marks, whereas E shows signs of chattering.*

Smooth-Edge Blade

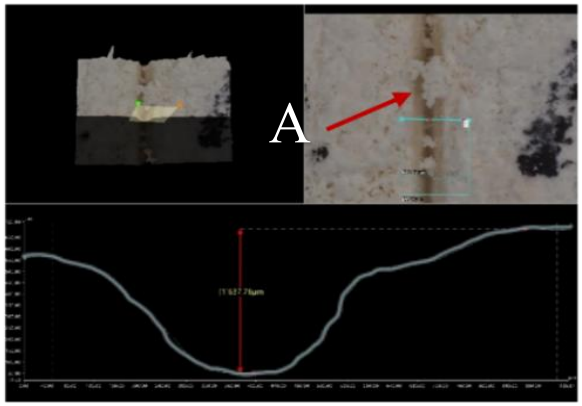

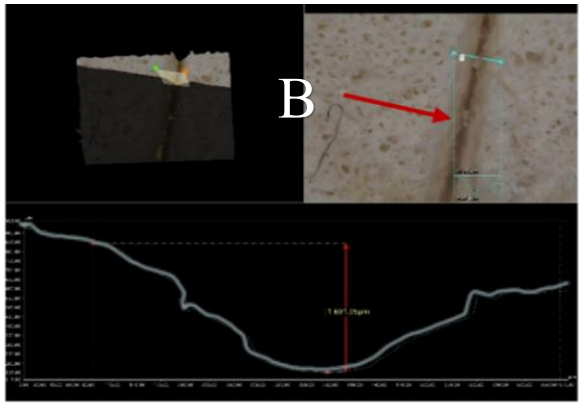

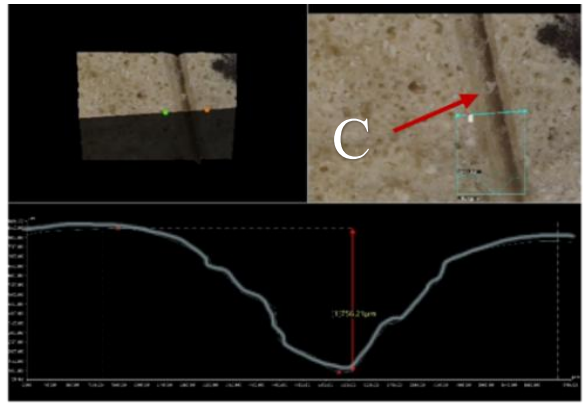

Serrated Knife

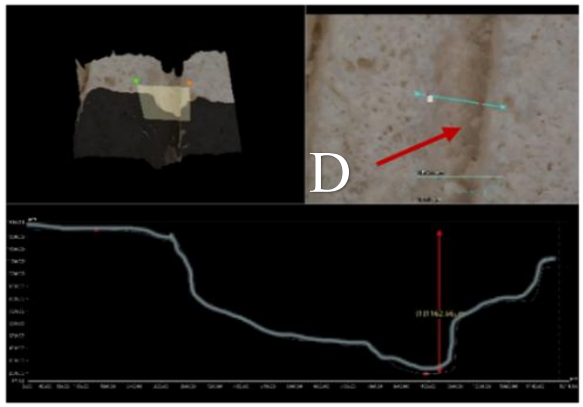

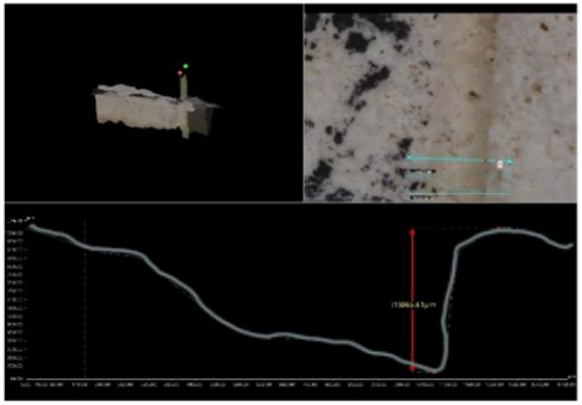

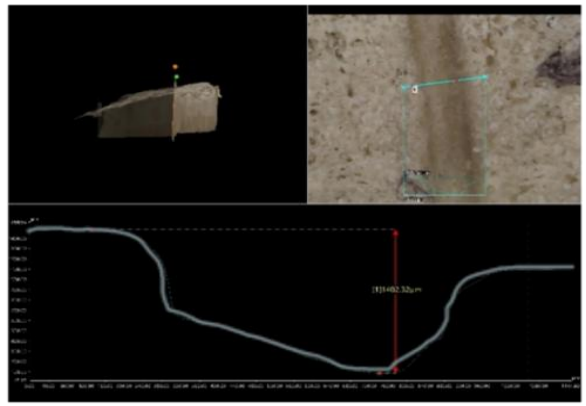

Large Serrated Knife

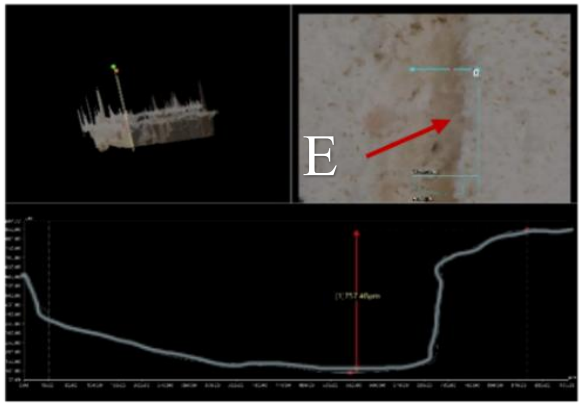

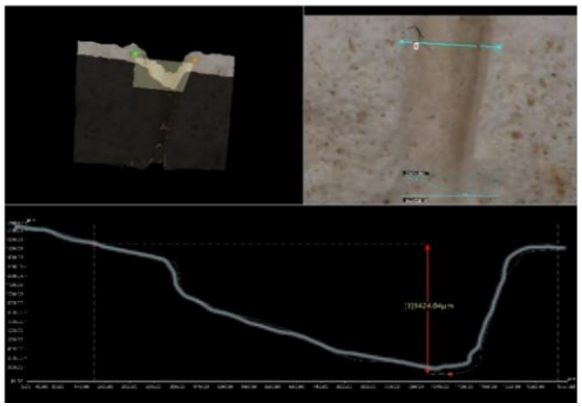

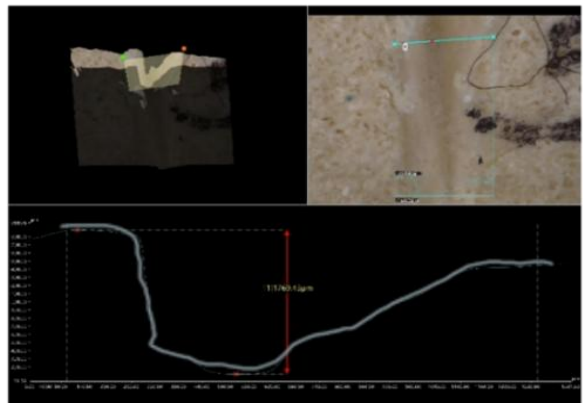

Appendix 3 E *Cut marks produced on the body of a Mandible by a smooth-edged blade, serrated knife and large serrated knife before and after burning with either wood or charcoal as the fuel source. Blank spaces represent the samples that did not survive the burning process.*

	CONTROL	WOOD	CHARCOAL
Smooth-Edge Blade	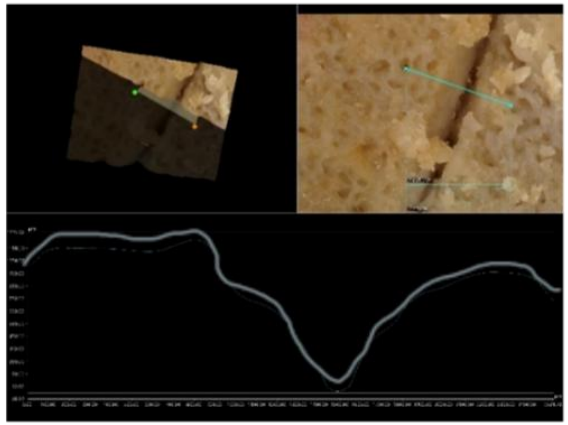	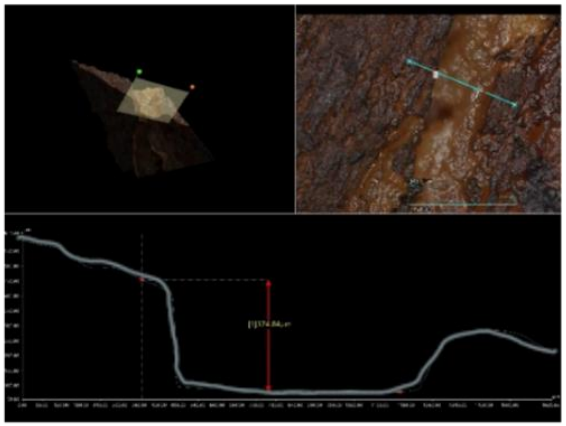	DID NOT SURVIVE
Serrated Knife	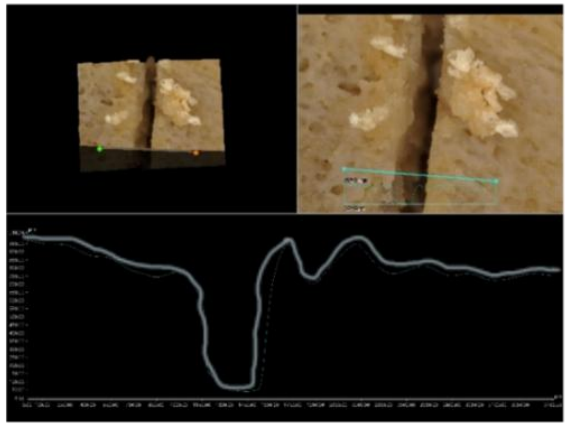	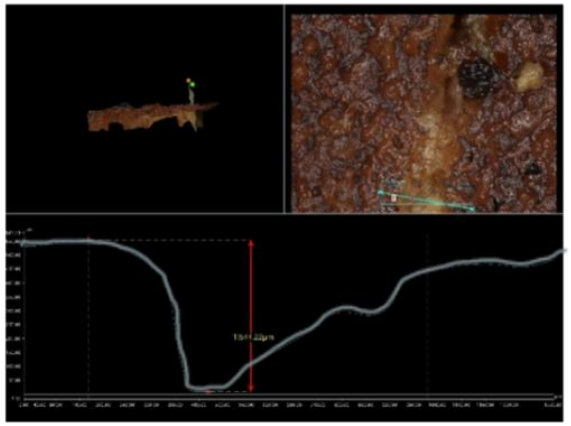	DID NOT SURVIVE
Large Serrated Knife	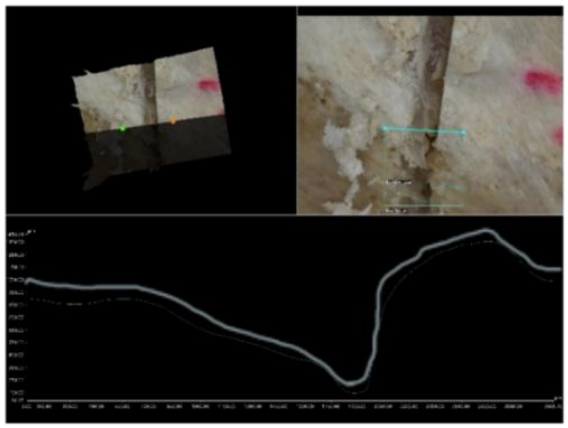	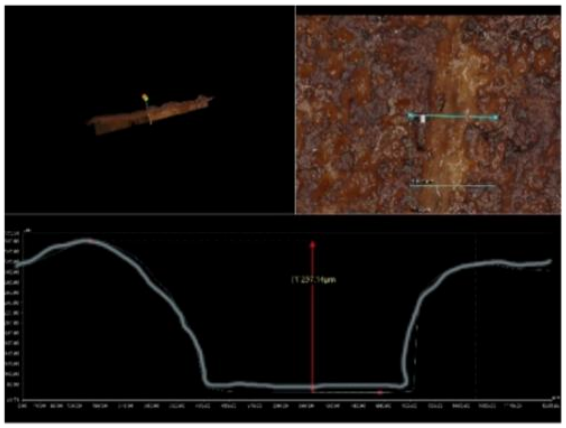	DID NOT SURVIVE

Appendix 3 F *Cut marks produced on the superior angle of a Scapula by a smooth-edged blade, serrated knife and large serrated knife before and after burning with either wood or charcoal as the fuel source. Blank spaces represent the samples that did not survive the burning process.*

	CONTROL	WOOD	CHARCOAL
Smooth-Edge Blade	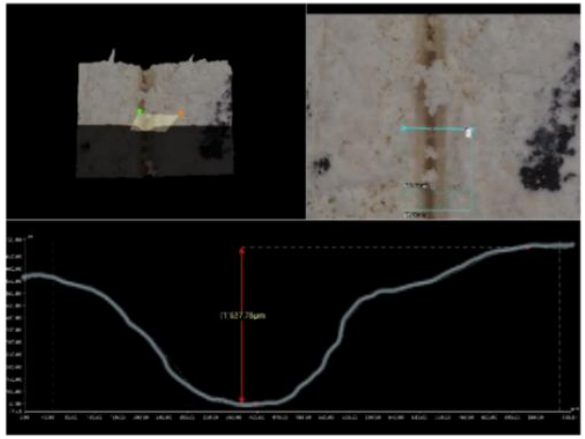	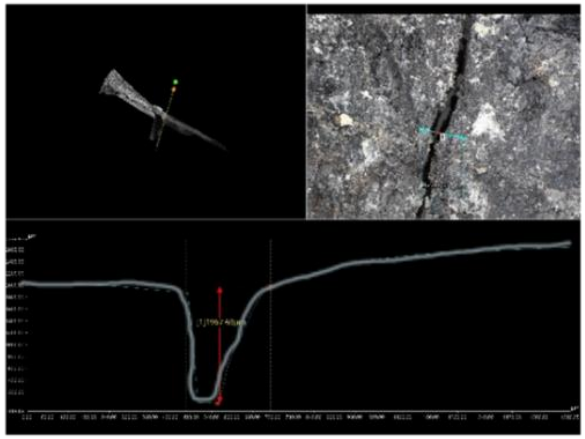	DID NOT SURVIVE
Serrated Knife	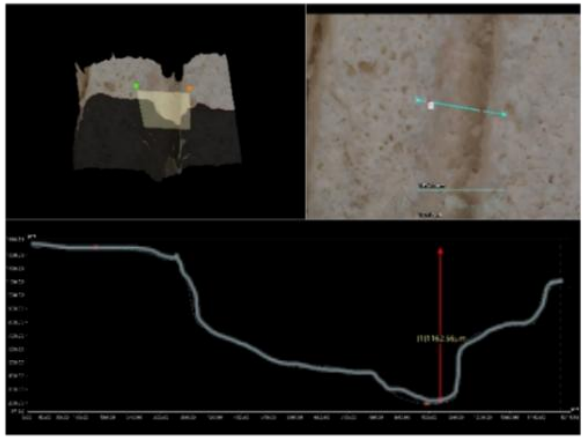	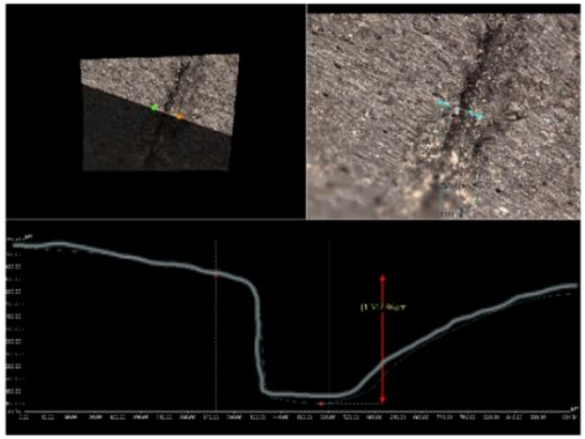	DID NOT SURVIVE
Large Serrated Knife	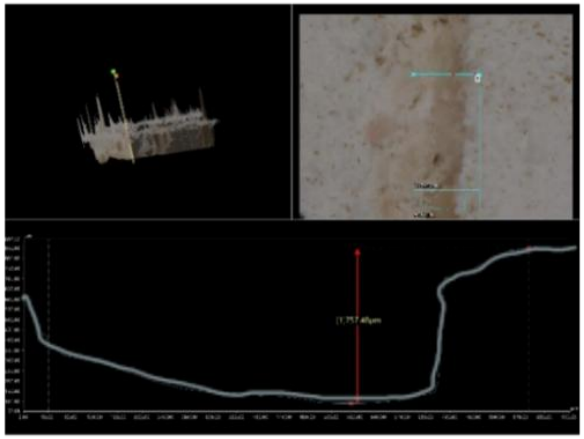	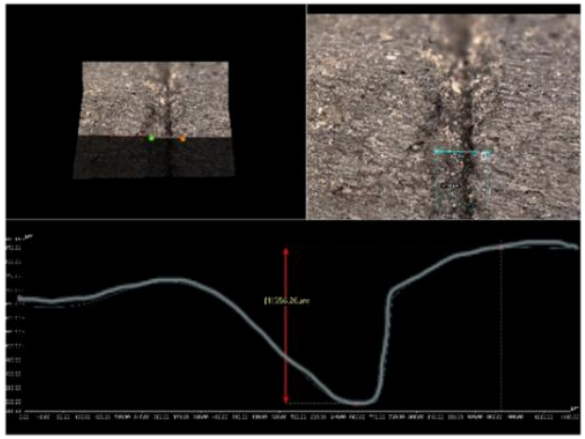	DID NOT SURVIVE

Appendix 3 G *Cut marks produced on the frontal bone of a Skull by a smooth-edged blade, serrated knife and large serrated knife before and after burning with either wood or charcoal as the fuel source. Blank spaces represent the samples that did not survive the burning process.*

	CONTROL	WOOD	CHARCOAL
Smooth-Edge Blade	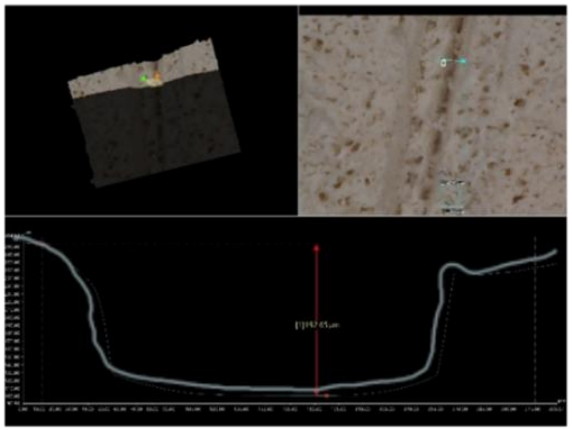	DID NOT SURVIVE	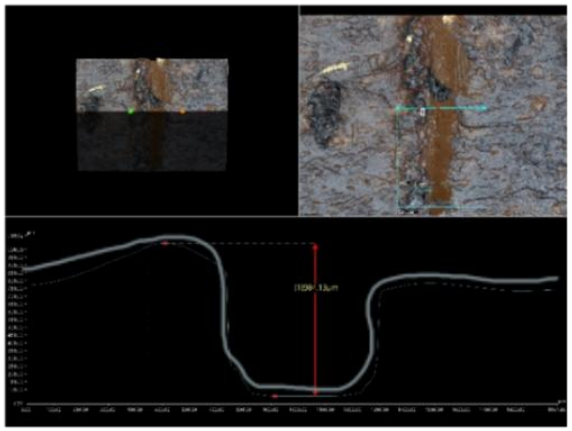
Serrated Knife	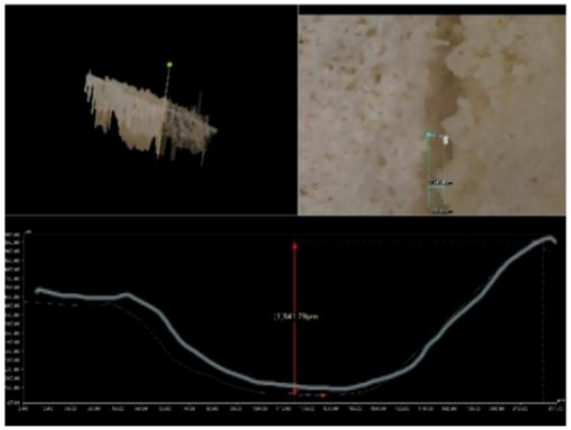	DID NOT SURVIVE	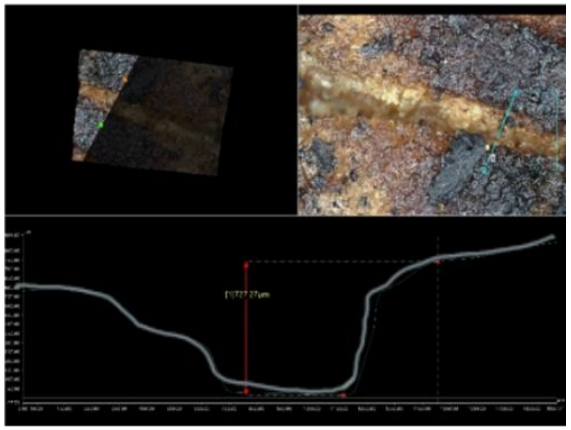
Large Serrated Knife	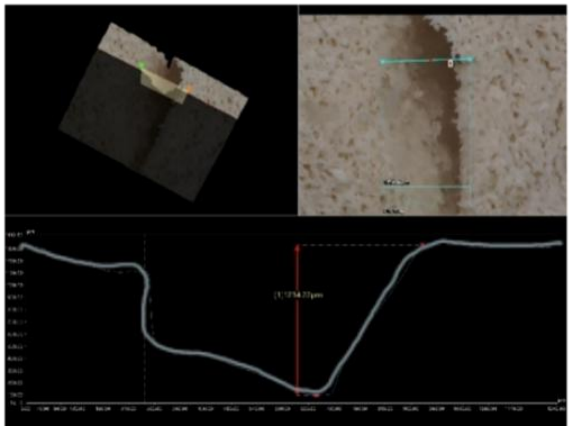	DID NOT SURVIVE	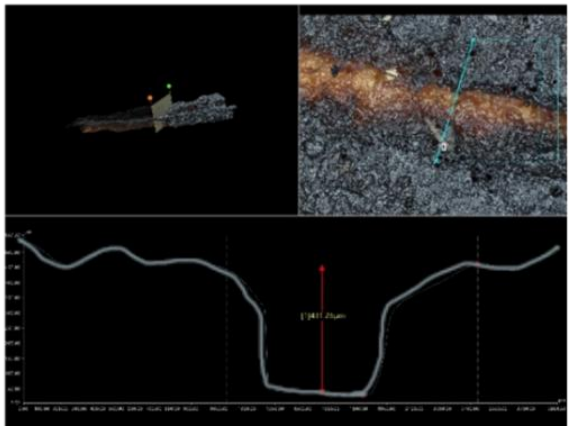

Appendix 4

Images of garden incinerator and storage container for burning

Appendix 4 A: *Image of storage container in early stages of fire spreading.*

Appendix 4 B: *Image of storage container during fire.*

Appendix 4 C: *Image of storage container and samples post burning.*

Appendix 4 B: *Image of garden incinerator in early stages of fire.*

Appendix 4 B: *Image of garden incinerator during fire.*

Appendix 4 F: *Image of garden incinerator samples post burning.*